



Universidade Federal do Rio de Janeiro
Centro de Ciências Matemáticas e da Natureza
Instituto de Química
Departamento de Bioquímica

**Evaluation of antitumoral activity of novel
dinuclear Cu^{2+} -complexes on tumorigenesis:
from the cytotoxic potential to the mechanism of
action**

Zeinab Ghasemishahrestani (Farzaneh)

**Rio de Janeiro
2020**

Zeinab Ghasemishahrestani (Farzaneh)

**Evaluation of antitumoral activity of novel
dinuclear Cu²⁺-complexes on tumorigenesis:
from the cytotoxic potential to the mechanism of
action**

Doctoral thesis presented to the Post-Graduate Program in Biochemistry (PPGBq) of the Institute of Chemistry (IQ) of the Federal University of Rio de Janeiro (UFRJ), as a requirement to obtain the title of Doctor of Science (Biochemistry).

Advisor: Marcos Dias Pereira

Co-advisor: André Souza Santos

**Rio de Janeiro
2020**

Approval Sheet

Zeinab Ghasemishahrestani (Farzaneh)

Evaluation of antitumoral activity of novel dinuclear Cu^{2+} -complexes on tumorigenesis: from the cytotoxic potential to the mechanism of action

Doctoral thesis submitted to the Post-Graduate Program in Biochemistry, Department of Biochemistry, Institute of Chemistry, Federal University of Rio de Janeiro - UFRJ, as part of the necessary requirements to obtain the title of Doctor of Science.

Approved by:

Marcos Dias Pereira, Doctor, IQ – UFRJ

André Luis Souza dos Santos, Doctor, IMPG – UFRJ

Gilberto Barbosa Domont, Doctor, IQ-UFRJ

Adriane Regina Todeschini, Doctor, IBCCF UFRJ

José Joao Mansure, Doctor, McGill University

Elizabeth Fidalgo Da Silva, Doctor, Windsor University

Ghasemishahrestani Zeinab (Farzaneh)

Evaluation of antitumoral activity of novel dinuclear Cu^{2+} -complexes on tumorigenesis: from the cytotoxic potential to the mechanism of action / Zeinab Ghasemishahrestani– Rio de Janeiro: UFRJ/2020.

Thesis (Doctorate in Sciences) - Federal University of Rio de Janeiro, Institute of Chemistry, Graduate Program in Biochemistry, Rio de Janeiro, 2020.

Advisor: Marcos Dias Pereira

Co-advisor: André Souza Santos

1. Cu^{+2} -complexes 2. Cytotoxicity 3. Intrinsic apoptosis 4. Antitumor metallodrug 5. Label-free proteomic I. Pereira Marcos Dias (Orient) II. Santos, André Luis Souza dos. (Co-orient.) III. Federal University of Rio de Janeiro Institute of Chemistry IV. Post-Graduate Program in Biochemistry

The present work was carried out at the Laboratory of Cytotoxicity and Genotoxicity (LaCiGen), Department of Biochemistry, Institute of Chemistry (IQ) and Laboratory for Advanced Studies of Microorganisms Emerging and Resistant (LEAMER), Department of General Microbiology, Institute of Microbiology Paulo de Góes (IMPG), Health Sciences Center (CCS), Federal University of Rio de Janeiro (UFRJ). under the guidance of Prof. Dr. Marcos Dias Pereira and Prof. Dr. André Luis Souza dos with the support of the CAPES– Coordenação de Aperfeiçoamento de Pessoal de Nível Superior.

Acknowledgement

اگر بازم به آتش افکنیدم، بال خواهم ساخت، پرواز خواهم کرد

"If you are thrown into the fire, make wings and fly with your mind"

Farzaneh

The present work denotes the end of a difficult journey full of challenges, overcoming, and reaching maturity. With all my heart full of joy and gratitude, I thank all those who were present in some way and played a role in the development and completion of this work. I am thankful of the financing granted by the development agencies, CAPES, FAPERJ and CNPQ, which was essential for the completion of this work.

I would like to begin by thanking my dear advisor, Professor Marcos Dias Pereira. I am very grateful for his consistent support and guidance during the running of this project. He has been a tremendous mentor for me. I would like to thank you for encouraging my research and for allowing me to grow as a research scientist. Your advice on both research as well as on my life have been priceless.

I would also like to thank my co-advisor, professor André Luis Souza dos Santos for his great advice and all the experience I had under his guidance. Thank you so much for your kindness and patience, in addition to excellent scientific contributions.

I was very lucky that I could participate in two different big groups of laboratories with two knowledgeable professors. The meetings and conversations were vital in inspiring me to think outside of the box, from many different perspectives in order to form a comprehensive and objective critique. Moreover, Prof. Marcos and Prof. André created a great peaceful environment for me, which led to the fruitful work. This is a great opportunity that an international student can have. I am very lucky to have you both in my life.

I would like to thank Prof. Nicolas Adrián Rey from the Pontifícia Universidade Católica do Rio de Janeiro (PUC-RJ) and his group for the synthesis of the compounds used in the present work.

Special thanks to prof. Gilberto Barbosa Domont and prof. Fábio Nogueira for their dedicated support and guidance and all dear friends in proteomic group specially Renata and Luiz.

I express my deepest gratitude to all members and former members of the Laboratory of Citotoxicity and Genotoxicity (LaCiGen) and Laboratory of advanced Study of Microorganisms

Emerging and Resistant (LEAMER). With special thanks to Prof. Marta Helena Branquinha (IM-PG-UFRJ) and many thanks to dear Dr. Simone Santiago Carvalho that co-supervised me in almost all my experiments.

Without a doubt, the collaborative spirit and excellent coexistence in the laboratory were decisive for the completion of this work. In particular, I am extremely grateful for friendships that I built during these years in the laboratory with all my dear friends that I'll never forget them in my life. Thank you so much for your kindness and endless exchanges of ideas!

This journey would not have been possible without the support of my dear friends, Mohammad Saadatmand, Denise Brito Reis, Mahan Mashoof and Carolina Martins Machado your kindness, advices and your friendship will be greatly appreciated. There are no words to convey my deepest gratitude and respect to you both!

A special thanks to my family. Words cannot express how grateful I am to my mother, and father Shahla Rostami and Sadegh Ghasemi, for all the effort dedicated to my personal and professional training and, mainly, for always believing in me and my dreams and for all of the sacrifices they've made to support me. I also thank my kind and lovely mother-in law, and father-in-law Fatemeh Partanian and Ali Khezri, their pure positive energy helped me and pushed me to strive towards my goal. Despite the distance, you have been and always will be, by my side with every step I take. Love you so much!

Finally, I would like to express my sincere appreciation to my beloved husband Hamidreza who spent many sleepless nights with me and was always my support in the moments when there was no one was there. I thank you for all your dedication and support during all these years. You have been a source of joy and comfort and your words of love and encouragement were essential for me to get here!

Abstract

Evaluation of antitumoral activity of novel binuclear Cu²⁺-complexes on tumorigenesis: from the cytotoxic potential to the mechanism of action

Zeinab Ghasemishahrestani

Supervisor: Marcos Dias Pereira

Co-adviser: André Luis Souza dos Santos

Abstract of the Doctoral thesis submitted to the Post-Graduate Program in Biochemistry, Institute of Chemistry, Federal University of Rio de Janeiro - UFRJ, as part of the requirements necessary to obtain the title of Doctor in Sciences - Biochemistry.

Cancer is a major cause of death worldwide. Current chemotherapy for cancer treatment associate with many side effects and tumor cells often become resistant to the drugs. Hence, development of chemotherapeutic strategies involving novel antitumor agents with increased efficacy and immunity has been the focus area of cancer treatment. The discovery of the antitumor properties of cisplatin in 1969 opened a new field in design and development of a new class of therapeutic drugs based on metal. The anticancer activities of Cu²⁺-complexes have been the focus of several researchers aiming to discover novel anticancer agents. In this study, we investigated the potential antitumor activity of two novel Cu²⁺-complexes, [Cu₂(μ-CH₃COO)(OH₂)(L₂)]· 1/2H₂O (R9) and [Cu₂(μ-OH)(OH₂)(HL₂)]ClO₄·2H₂O (R10), in different cancer cell lines MCF-7 (breast adenocarcinoma), A549 (lung carcinoma) and PC3 (prostate carcinoma). Both Cu²⁺-complexes showed great cytotoxic effects compared with the positive control cisplatin. The IC₅₀ (μM) values of R9 measured by the MTT assay in MCF-7, A549, PC3, was 1.01 ± 0.09, 1.01 ± 0.07 and 1.51 ± 0.06, respectively. On the other hand, MCF-7, A549, PC3 cell lines affected by R10 exhibited IC₅₀ (μM) of 1.27 ± 0.14, 1.23 ± 0.09 and 1.38 ± 0.16, respectively. MCF10A, the healthy breast epithelial cell line, after treatment with R9 and R10, showed the IC₅₀ (μM) of 8.19 ± 0.87 and 6.93 ± 0.96, respectively which is approximately 7-8 times more resistant than MCF-7, showing that Cu²⁺-complexes had a low toxicity to its relative non-cancerous cells. The pictures from invertor microscope gave us an idea of change in granularity that later proved by flow cytometry analysis which revealed the increase of granularity in both MCF-7 and A549 cell lines due to effect of R9 and R10 at IC₅₀ concentration (1.0 μM) about 2, 2.6, 1.5 and 1.4 times higher than the untreated cells, respectively. Cu²⁺-complexes at 1/2 IC₅₀, IC₅₀ and 2×IC₅₀ concentrations significantly reduced mitochondrial membrane potential (ΔΨ_m) and induced a high production of reactive oxygen species (ROS) in both MCF-7 and A549 cells measured through flow cytometry assay. The results of cell cycle arrest displayed the increase number of cells at Sub-G1 and concomitant decrease in G1,S and G2/M phases in both MCF-7 and A549 at IC₅₀ concentration of R9 and R10. Together with TUNEL assay, confirmed that both Cu²⁺-complexes induced DNA fragmentation in theses tumor cells where the percentage of cells with fragmented DNA induced by R9 and R10 at IC₅₀ concentration in MCF-7 and A549 were 3.5, 3.6, 2 and 2 times more than the untreated control, respectively that measured by flow cytometer. Moreover, the activation of caspase 9 exhibited that R9 and R10 treatment at IC₅₀ concentration induced cell death mainly through the intrinsic apoptosis pathway. Competition between Cu²⁺-complexes and PI for DNA binding revealed non-significant changes in percentage of fluorescent cells/fluorescence intensity as compared to control in both cell lines, assured that the compounds cannot bind to DNA as an intercalating agent. *In vivo* assay with *Galleria mellonella* showed that R9 presented a lower toxicity in comparison to cisplatin at the same concentration (50 mg/kg). The results of *G. mellonella* agreed with the LD₅₀ calculated in BALB/c mice treated with R9 and cisplatin. The results obtained in BALB/c mice is promising since the value of 71.6 mg/kg is much higher than the LD₅₀ of cisplatin, 6.6 mg/kg. The high value of

LD₅₀ means a small toxicity of Cu⁺²-complex. The Results obtained in the label-free proteomic analysis of differentially expressed proteins in breast cancer cells in response to R10 treatment revealed that, 118 proteins were significantly downregulated were linked to the 194 downregulated pathways and 49 proteins were upregulated that were defined 40 upregulated pathways. On the other side, in MCF-7 treated with cisplatin, 58 proteins were downregulated responsible for 105 pathways downregulated and 37 proteins were upregulated associated to the 47 pathways upregulated. Our results confirmed the difference of up/downregulated proteins expressed in R10-treated and cisplatin-treated cells that might be related to the possible different mechanism of action of R10 and cisplatin. Total 6 proteins related to the downregulation of apoptosis pathway in R10-treated cell include: lamin B1, NRAS, MAPK1, MAPK3, spectrin alpha, and calpain 2. Whereas, apoptosis inducing factor (AIFM1) was related to the upregulation of apoptosis. Moreover, MCF-7 cell death treated with R10 might occur by direct activation of apoptosis through AIF by down regulation of heat shock 70-kDa protein HSP70 together with downregulation of lamin that favor the entrance of AIF to the nucleus. The apoptosis may relate to the downregulation of RAS-ERK pathway via down regulation of ezrin, moesin and β 1-integrin (ITG β) which affect the activation of RAS, down regulate protein 14-3-3 ϵ , β and ζ (tyrosine 3- monooxygenase, tryptophan 5-mono-oxygenase) and reduce ERK1/2. Furthermore, the low expression of 14-3-3 ζ and dysregulation of CRM1/XPO1 (exportin 1) plus RAN GTPase, may sensitize cells to apoptosis. The downregulation of calpain, protein casein kinase, as well as catalytic (α 3, α 4) and regulatory (β 5) subunits of proteasome may activate apoptotic pathways for DNA degradation. In addition, down regulation of vacuolar ATPase (V-ATPase) may help in suppressing the growth and survival of tumor and together with the rate-limiting glycolytic enzyme pyruvate kinase may have great impact in glycolytic flux and force the cells through oxidative phosphorylation. Altogether, these results confirm that the Cu⁺²-complexes tested have a great potential as an antitumor metallodrug and is highly competitive with cisplatin chemotherapy drug.

Key words: Cu⁺²-complexes, cytotoxicity, intrinsic apoptosis, antitumor metallodrug, label-free proteomic.

List of figures

Figure 1. Pie charts present the distribution of cases and deaths for the 10 most common cancers in 2018 for both Sexes.....	2
Figure 2. The Estimated Number of cancer survivors in USA.....	3
Figure 3. Carcinogenesis phases: initiation, promotion, progression, and metastasis.....	4
Figure 4. Targeting cancer cells by changing ROS levels.....	7
Figure 5. The 10 hallmarks of cancer.....	9
Figure 6. The four phases of the cell cycle (G1, S, G2, and M), the non-cycling G0 state, and three well-known checkpoints.....	9
Figure 7. Cellular target of metal-based complexes anticancer agent.....	17
Figure 8. Cisplatin activation and DNA damage induction.....	23
Figure 9. Cisplatin can form covalent bonds with DNA.....	24
Figure 10. Schematic structures of H ₃ L1, R9 and R10.....	33
Figure 11. Analysis of the mitochondrial membrane potential using the fluorescent probe cationic JC-1 dye.....	36
Figure 12. Oxidation of H ₂ DCFDA by ROS.....	36
Figure 13. Different phases of cell cycle.....	37
Figure 14. Demonstration of fragmented DNA from apoptotic cells with the incorporation of fluorescein-labeled dUTP by the Tunel technique.....	39
Figure 15. Caspase-8 and -9 cleavage of the proluminogetic substrates containing LETD.....	40
Figure 16. Effect of R9 and R10 on viability of MCF-7, A549, PC3 and MCF10A.....	47
Figure 17. Change in morphology of MCF-7 and A549 cells after treatment with Cu ²⁺ -complexes.....	48
Figure 18. Cu ²⁺ -complexes, R9 and R10, increase cell granularity in MCF-7 and A549 cells....	49
Figure 19. Evaluation of mitochondrial membrane potential ($\Delta\Psi_m$) in MCF-7 cells treated with Cu ²⁺ -complexes R9 and R10.....	51

Figure 20. Evaluation of the mitochondrial membrane potential in A549 cells treated with Cu ²⁺ -complexes, R9 and R10.....	52
Figure 21. ROS production by MCF-7 cells treated with Cu ²⁺ -complexes, R9 and R10.....	54
Figure 22. ROS production by A549 cells treated with Cu ²⁺ -complexes, R9 and R10.....	55
Figure 23. Analysis of DNA fragmentation during treatment with Cu ²⁺ -complexes, R9 and R10 in MCF-7 cells.....	58
Figure 24. Analysis of DNA fragmentation during treatment with Cu ²⁺ -complexes, R9 and R10 in A549 cells.....	59
Figure 25. Induction of DNA fragmentation in MCF-7 cells treated with the Cu ²⁺ -complexes, R9 and R10 complexes.....	61
Figure 26. Induction of DNA fragmentation in A549 cells treated with the Cu ²⁺ -complexes, R9 and R10 complexes.....	61
Figure 27. Caspase 8 and 9 activities in the MCF7 and A549 cells after the treatment with the Cu ²⁺ -complexes, R9 and R10.....	63
Figure 28. Toxicity of Cu ²⁺ -complex R9 and cisplatin on <i>G. mellonella</i>	65
Figure 29. Determination of the Cu ²⁺ -complex R9 LD ₅₀ in BALB/c nude mice.....	66
Figure 30. Heat map showing differentially expressed proteins in breast cancer cells.....	68
Figure 31. Comparison of proteins altered by R10 and cisplatin treatments in MCF-7 cells.....	69
Figure 32. Analysis of differentially expressed proteins and their related pathways after R10-treated MCF-7 cells.....	72
Figure 33. Analysis of differentially expressed proteins and their related pathways after cisplatin-treated MCF-7 cells.....	74
Figure 34. Signaling cascade for inducing apoptosis in R10-treated MCF-7 cells.....	79
Figure 35. Signaling cascade for inducing apoptosis in cisplatin-treated MCF-7 cells.....	80
Figure 36. Comparison the expressed down/up-regulated proteins after R10/cisplatin treatment in MCF-7 cells.....	81
Figure 37. KEGG mapper analysis of common proteins expressed by R10 and cisplatin-treated MCF-7 cells.....	82
Figure 38. The most expressed proteins and their relative pathways in MCF-7 cells treated with R10.....	83
Figure 39. The effect of Cu ²⁺ -complexes in breast cancer cell signaling pathways.....	108

List of tables

Table 1. Some characteristics developed by tumor cells.....	8
Table 2. Different characteristics of cell cycle specific and nonspecific.....	13
Table 3. Cytotoxic chemotherapy agents that damage DNA, their mechanism of action, and the main types of damage that they cause.....	15
Table 4: Cytotoxicity effect of R9 and R10 on mammalian cell lines.....	47
Table 5. Competition between R9 and R10 with PI for DNA binding in MCF-7 and A549 cells..	64
Table 6. Total number of proteins, down/up-regulated proteins expressed after R10/cisplatin treatment of MCF-7 cells at 24 h identified and quantified by label-free analysis.....	67
Table 7. Proteins differentially expressed in related to the most down/up-regulated pathways after R10-treated MCF-7 cells that were analyzed by KEGG mapper.....	75
Table 8. Proteins differentially expressed in related to the most down/up-regulated pathways after cisplatin-treated MCF-7 cells that were analyzed by KEGG mapper.....	77

List of abbreviations

14-3-3 protein	3 tyrosine monooxygenase, 5 tryptophan monooxygenase
ACN	Acetonitrile CH ₃ CN
AIF	Apoptosis-inducing factor
ANOVA	Analysis of variance among group
Apaf-1	Apoptotic protease activating factor 1
APC/C	Anaphase-promoting complex/cyclosome
ATP	[(2R,3S,4R,5R)-5-(6-aminopurin-9-yl)-3,4-dihydroxyoxolan-2 yl] methoxy-hydroxyphosphoryl] phosphono hydrogen phosphate
ATP7A	ATPase P-type copper-transporting alpha
ATP7B	ATPase P-type copper-transporting beta
BALB/c	Albino mice
Bpy	Bipyridine
CCNS	Cell-cycle nonspecific antineoplastic agents
CCS	Cell cycle phase specific antineoplastic agents
Cdks	Cyclin-dependent kinases
Cisplatin	Cis-diamminedichloroplatinum (II)
CK	Casein kinase
CML	Chronic myeloid leukemia
COX-2	Cyclooxygenase-2
CRM1	Chromosomal maintenance 1
CT	Chymotrypsin
Ctr1	Copper transporter 1
Ctr2	Copper transporter 2
Cu/Zn-SOD	Superoxide dismutase [Cu-Zn]
Cyt c	cytochrome c
DCF	2',7'-dichlorofluorescein
DDA	Data dependent acquisition
DEP	Differentially expressed proteins

DMEM	Dulbecco's modified eagle's medium
DMSO	Dimethyl sulfoxide (CH ₃) ₂ SO
DNA	Deoxyribonucleic acid
DSBs	Double strand breaks
DTT	Dithiothreitol
EGF	Epidermal growth factor
EREG	Epiregulin
ERM	Ezrin-radixin-moesin
FBS	Fetal bovine serum
FCCP	Carbonyl cyanide-4-(trifluoromethoxy) phenylhydrazone
FDR	False discovery rate
FI	Fluorescence intensity
FL1	Green fluorescence intensity
FL3	Red fluorescence intensity
FOXO	Members of the class O of forkhead box transcription factors
GEF	Guanine nucleotide exchange factor
GRB2	Growth factor receptor-bound protein 2
H₂DCFDA	2',7'-dichlorofluorescein diacetate
H₂O₂	Hydrogen peroxide
HCD	Higher energy collision dissociation
HO·	Hydroxyl radical
HSP70	Heat shock 70-kDa protein
IAA	Iodoacetamide
IFNγ	Interferon γ
IκB	Inhibitor of NF- κ B
IL-1	Interleukin-1
JC-1	5,5',6,6'-tetrachloro1,1',3,3'-tetraethyl benzimidazolocarboyanine iodide
KEGG	Kyoto encyclopedia of genes and genomes
MAPK	Mitogen activated protein kinase
MAPKKK	MAP kinase kinase kinase

MATE1	Multidrug and toxin extrusion transporter 1
MDM2	Mouse double minute 2
MFI	Mean fluorescence intensity
MMP1	Matrix metalloproteinase 1
MMP2	Matrix metalloproteinase 2
MMPs	Metallo-proteinases
MnSOD	Manganese-dependent superoxide dismutase
MTT	3- (4,5-dimethylthiazol-2-yl)-2,5-diphenyltetrazolium bromide
NADPH	Nicotinamide adenine dinucleotide phosphate
NEMO	NF-kB essential modulator
NF-kB	Nuclear factor kappa B
NO	Nitrite oxide
NSAID	Nonsteroidal anti-inflammatory drug
NSP	Reactive nitrogen species
O²⁻	Superoxide
OCT2	Organic cation transporter 2
PDGF	Platelet-derived growth factor
PEP	Phosphoenolpyruvate
Phen	Phenanthroline
PI	Propidium iodide
PKC	Protein kinase C
PKM2	Pyruvate kinase muscle isozyme M2
PTP	Permeability transition pore
RAN GTPase	RAs-related nuclear protein
RLU	Relative light units
ROS	Reactive oxygen species
rTdT	Recombinant terminal deoxynucleotidyl transferase
RTK	Receptor tyrosine kinase
SBCCC	Schiff base copper coordinated compound
SCGE	Single cell gel electrophoresis

SOD	Superoxide dismutase
SOS	Son of sevenless
SSBs	Single strand breaks
SWI/SNF	Chromatin-remodeling complex
TCEP	Tris (2-carboxyethyl) phosphine
TEAB	Triethylammonium bicarbonate buffer
TFA	Trifluoroacetic acid
TGFβ	Insulin, transforming growth factor β
TLR	Toll-like-receptor
TNFα	Tumor necrosis factor alpha
TSCs	Thiosemicarbazones
TUNEL	Terminal deoxynucleotidyl transferase dUTP nick end labeling
UPP	Ubiquitin proteasome pathway
V-ATPase	Vacuolar ATPase
WHO	World health organization
XPO1	Exportin 1

List of contents

1. Introduction.....	1
1.1 Epidemiology of cancer, its global incidence, mortality and survival.....	1
1.2 Development and progression of cancer.....	3
1.3 Tumor characteristic.....	7
1.4 Classification of chemotherapy drugs related to their mechanism of action.....	12
1.4.1 Alkylating agents.....	13
1.4.2 Antimetabolites.....	14
1.4.3 Topoisomerase inhibitors.....	15
1.5 Metal-based complexes.....	15
1.5.1 Mechanism of action of metal complexes.....	18
1.5.1.1 Via ROS generation.....	18
1.5.1.2 Via DNA binding.....	20
1.5.1.3 Via Metallonucleases.....	21
1.6 Platinum-based complexes.....	22
1.7 Copper-based complexes.....	25
2. Justification.....	30
3. Objective.....	31
4. Materials and methods.....	32
4.1 Culture and maintain the Cells.....	32
4.2 Copper-based coordination compounds used in the study.....	32
4.3 Determination of R9 and R10 cytotoxicity.....	33
4.4 Assessment of cancer cell morphology.....	34
4.5 Evaluation of changes in mitochondrial membrane potential ($\Delta\Psi_m$).....	35
4.6 Evaluation of ROS production.....	36
4.7 Cell cycle analysis and DNA fragmentation.....	37
4.8 Induction of DNA fragmentation by TUNEL (apoptosis).....	38
4.9 Determination of caspase 8 and 9 activity.....	39
4.10 Competition of Cu^{+2} -complexes with PI on DNA binding.....	40

4.11 Evaluation of toxicity of R9 using animal models.....	40
4.11.1 Toxicity of R9 in <i>Galleria mellonella</i> model of study.....	40
4.11.2 Toxicity of R9 in in BALB/c mice.....	41
4.11.3 Statistical analysis.....	41
4.12 Analysis of differential expression of protein in breast cancer cells in response to R10 treatment.....	42
4.12.1 Sample preparation.....	42
4.12.2 Protein digestion.....	42
4.12.3 Analysis by mass spectrometry.....	43
4.12.4 Data analysis.....	43
5. Results.....	45
5.1 Cytotoxic activity of two binuclear Cu ²⁺ -complex on different cancer cells lines..	45
5.2 Assessment of cancer cell morphology.....	48
5.3 Evaluation of changes in mitochondrial membrane potential ($\Delta\Psi_m$).....	49
5.4 Evaluation of ROS production.....	52
5.5 Cell cycle analysis and DNA fragmentation.....	55
5.6 Induction of DNA fragmentation by TUNEL (apoptosis).....	59
5.7 Determination of caspase 8 and 9 activity.....	62
5.8 Competition between Cu ⁺² -complexes and PI for DNA binding.....	63
5.9 Evaluation of R9 toxicity using <i>in vivo</i> models.....	64
5.9.1 Toxicity of R9 in <i>Galleria mellonella</i> model of study.....	64
5.9.2 Toxicity of R9 in BALB/c nude mice.....	66
5.10 Analysis of differential expression of proteins in breast cancer cells in response to R10 treatment.....	66
6. Discussion.....	85
7. Conclusion.....	109
8. Perspective of the project.....	111
9. References.....	112
10. Attachments.....	136

1. Introduction

1.1 Epidemiology of cancer, its global incidence and mortality.

Cancer is predicted to be the leading cause of death and the only significant barrier to increasing life expectancy in any country in the 21st century. According to World Health Organization (WHO), in 2018, cancer was the second cause of death responsible for an estimated 9.6 million deaths. The incidence of cancer and death worldwide is growing rapidly. The reasons are complex, but reflect the aging and population growth, as well as changes in the prevalence and distribution of the main risk factors for cancer, some of which are associated with social and economic development (OMRAN *et al.*, 1971; NISHIHARA *et al.*, 2015; OGINO *et al.*, 2016).

With the rapid growth of population and aging around the world, the increase in cancer as a major cause of death is indicative of a significant reduction in the rate of mortality from stroke and cardiovascular disease in many countries (BRAY *et al.*, 2018). Cancer transition in emerging economies is more significant, while the rate of disease increases with changes in the characteristics of common cancers. A recurring observation is the ongoing displacement of infection-related and poverty-related cancers by those cancers that already are highly frequent in the most developed countries like Europe, North America, and high-income countries in Asia and Oceania (BRAY *et al.*, 2018; GERSTEN; WILMOTH, 2002). For both sexes combined, it is estimated that nearly one-half of the cases and over one-half of the cancer deaths in the world occurred in Asia in the year 2018, in part because close to 60% of the global population resides there (BRAY *et al.*, 2018).

Europe accounts for 23.4% of the total cancer cases and 20.3% of the cancer deaths, although it represents only 9% of the global population, followed by the Americans 21% of incidence and 14.4% of mortality worldwide. In contrast to other regions, the shares of cancer deaths in Asia (57.3%) and Africa (7.3%) are higher than the shares of incidence (48.4% and 5.8%, respectively) due to the different distribution of cancer types and higher case fatality rates in these regions (BRAY *et al.*, 2018).

Lung cancer is the most commonly diagnosed cancer (11.6% of the total cases) and the leading cause of cancer death (18.4% of the total cancer deaths), closely followed by female breast cancer (11.6%), and prostate cancer (7.1%) for incidence (Figure1) (DOGAN *et al.*, 2019, REBBECK *et al.*, 2017).

Among females, breast cancer is the most commonly diagnosed cancer and the leading cause of cancer death, followed by colorectal and lung cancer for incidence, and vice versa for mortality (BRINTON; GAUDET; GIERACH, 2017).

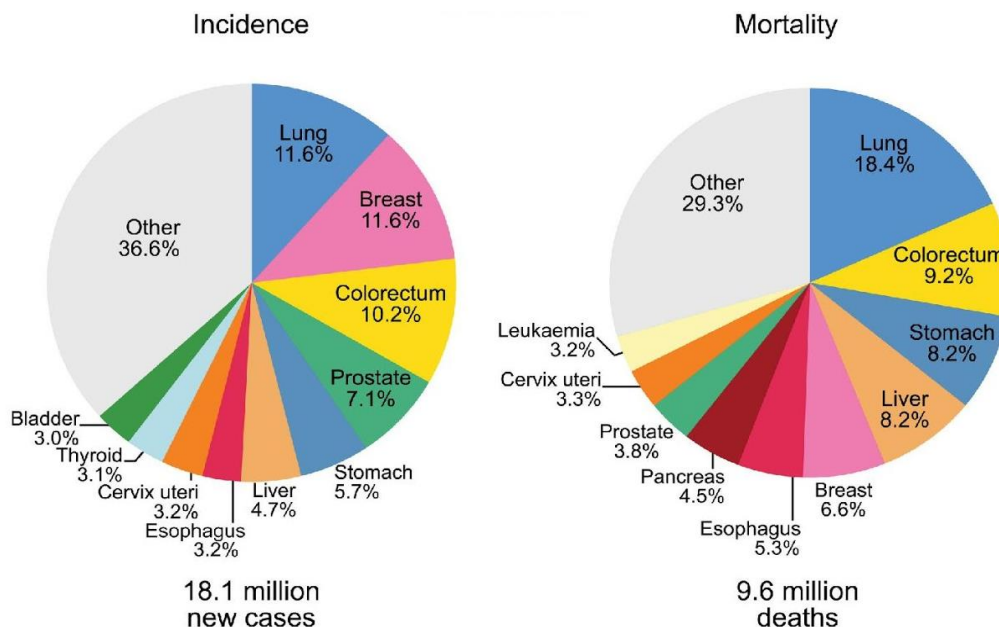


Figure 1. Pie charts present the distribution of cases and deaths for the 10 most common cancers in 2018 for both genders. The area of each pie chart reflects the proportion of the total number of cases or deaths (BRAY et al., 2018).

Despite the incidence and mortality, the number of cancer survivors continues to rise due to the advances in early detection and the variety of treatment such as surgery, chemotherapy, radiotherapy and immunotherapy. The number of cancer survivors in United State of America from 15.5 million on January 1, 2016 is projected to reach more than 20 million by January 1 in 2026 (MILLER, 2016). The three most prevalent cancers are prostate (3,306,760), colon and rectum (724,690), and melanoma (614,460) among males and breast (3,560,570), uterine corpus (757,190), and colon and rectum (727,350) among females. More than one half (56%) of survivors were diagnosed within the past 10 years, and almost one-half (47%) are aged 70 years or older (Figure 2) (MILLER, 2016).

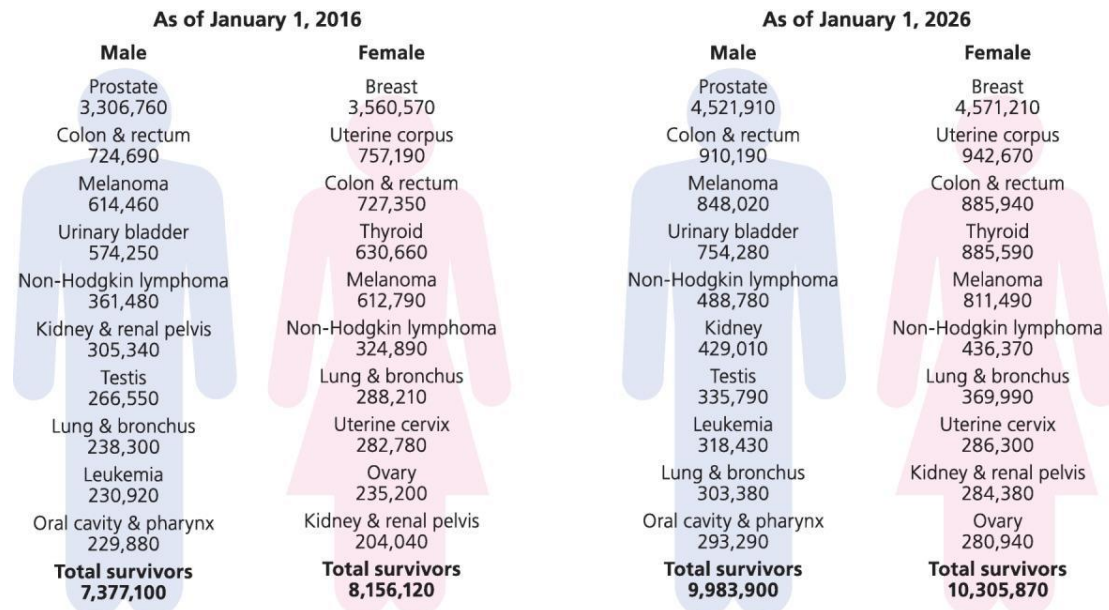


Figure 2. The estimated number of cancer survivors in USA.

Note: estimates for specific cancer types take into account the potential for a history of more than one cancer type (MILLER, 2016).

1.2 Development and progression of cancer.

The underlying causes of cancer development are the continual unregulated proliferation of cancer cells. A cancer cell grows and divides instead of responding appropriately to signals that control its behavior of normal cells, and indirectly, attacks on tissues, organs, and eventually spread throughout the body. The loss of overall growth control is the net result of abnormalities accumulated in multiple cell regulators and reflects the various aspects of cellular behavior, which differentiates cancer cells from their normal counterparts (BURRELL *et al.*, 2013, SAHAI, 2005).

At the cellular level, cancer development is a multi-stage process that involves initiation, promotion, progression, and metastasis stages (GRIVENNIKOV; GRETEN; KARIN, 2010; SINGH *et al.*, 2019; WU *et al.*, 2016b).

Initiation is the first step in cancer development and involves the alteration, change, or mutation of genes arising spontaneously or induced by exposure to a carcinogenic agent. Genetic alterations can result in deregulation of biochemical signaling pathways associated with cellular proliferation, survival and differentiation, which can be influenced by a number of factors, including the rate and type of carcinogenic metabolism and the response of the deoxyribonucleic acid (DNA) repair function. However, a single mutation does not give these cells the characteristics necessary to be considered carcinogenic (BOYLAND, 1985, SINGH *et al.*, 2019, TURAJLIC *et al.*, 2019). Unlike initiators, promoters do not covalently bind to macromolecules

or DNA within the cell but may bind to receptors on the cell surface affecting intracellular signaling pathways, which increase cell proliferation (KLAUNIG, 2000, PERERA *et al.*, 2016).

The promotion stage is considered relatively lengthy and reversible processes in which actively proliferating preneoplastic cells accumulate. In the promotion stage, the cell that underwent the initial mutation accumulates new mutations and metabolic alterations that allow it to be able to achieve uncontrolled growth, circumventing cell cycle control and programmed cell death (apoptosis) (DOU *et al.*, 2020; FEINBERG; KOLDOBSKIY; GÖNDÖR, 2016).

Progression is the phase between a premalignant lesion and the development of invasive cancer. Progression is the final stage of neoplastic transformation, where genetic and phenotypic changes and cell proliferation occur. This involves a fast increase in the tumor size, where the cells may undergo further mutations with invasive and metastatic potential. Tumor progression continues as additional mutations occur within cells of the tumor population (COOPER; HAUSMAN, 2007; FEINBERG; KOLDOBSKIY; GÖNDÖR, 2016). Some of these mutations transmit selective advantage to the cell, such as faster increased growth rate, tolerance, invasion, or metastasis, and consequently the generations of cells that have such a mutation thus become dominant within the tumor population. This process is called clonal selection, since a new clone of tumor cells has evolved based on its increased growth rate or other properties (such as survival, invasion, or metastasis) that give rise to a selective advantage. Clonal selection continues throughout tumor development, so tumors grow more rapidly and become increasingly malignant (COOPER; HAUSMAN, 2007; FEINBERG; KOLDOBSKIY; GÖNDÖR, 2016; GREAVES; MAL EY, 2012). The different carcinogenesis phases have shown in Figure 3.

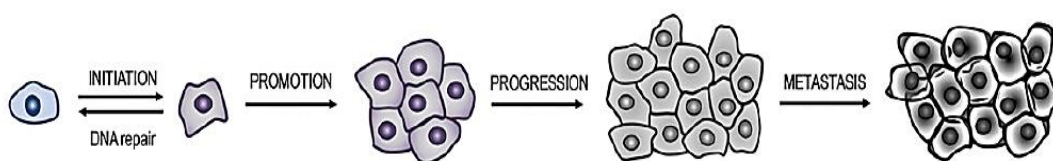


Figure 3. Carcinogenesis phases: initiation, promotion, progression, and metastasis. (SIDDIQUI *et al.*, 2015).

Radiation and many chemical carcinogens act by damaging DNA and inducing mutations. Some of the initiating agents chip in human cancers includes UV radiation (the major cause of skin cancer), carcinogenic chemicals in tobacco smoke, and aflatoxin (a potent liver carcinogen produced by some molds that contaminate improperly stored supplies of peanuts and other grains) (POIRIER; SANTELLA; WESTON, 2000; SHAMBERGER, 2018). The carcinogens in tobacco smoke (including benzoapyrene, dimethylnitrosamine, and nickel compounds) are the main causes of human cancer (ALEXANDROV *et al.*, 2016). In total, smoking is estimated to account

for roughly one-third of total cancer deaths (a significant complication for a carcinogenic agent) (ALEXANDROV *et al.*, 2016; MILLER, 2016; OLIVEIRA *et al.*, 2007), and 80 to 90% of lung cancers, as well as cancer in oral cavity, pharynx, larynx, esophagus, and other sites related to smoking (ALEXANDROV *et al.*, 2016). Other carcinogens contribute to cancer growth by stimulating cell proliferation instead of mutations. These compounds are referred to as tumor promoters. The phorbol esters a class of chemical compounds found in a variety of plants (ester derivatives of the tetracyclic diterpenoid phorbol) that stimulate cell proliferation by activating protein kinase C (PKC) are classic examples (LOU *et al.*, 2008, ROUX *et al.*, 2004). Hormones, especially estrogen, are important tumor promoters in the development of some human cancers. For example, the spread of uterine endometrial cells is stimulated by estrogen and excessive estrogen exposure is likely to increase a woman's endometrial cancer. In addition to chemicals and radiation, some viruses can also induce cancer (MORALES-SÁNCHEZ; FUENTES-PANANÁ, 2014 ; READ; DOUGLAS, 2014; TASHIRO; BRENNER, 2017). The common human cancers caused by viruses include liver cancer and cervical carcinoma, which make up 10 to 20% of worldwide cancer incidence (GRISCHKE; BRUCKER, 2019; LONDON; PETRICK; MCGLYNN, 2017).

Cancer cells are also able to escape the process of apoptosis (a kind of programmed cell death). As a result of uncontrolled growth, it is essential that vascularization (angiogenesis) of the tumor tissue occurs so that it is able to obtain nutrients and subsequently migrate and invade other healthy tissues, which characterizes the metastasis process (FOUAD; AANEI, 2017; HAN AHAN; WEINBERG, 2000).

The invaded tissues gradually lose their function that can lead to organ failure and in many cases death of the patient. Other metabolic alterations can be found commonly in tumor cells such as increased flow of glycolytic and pentose pathways, responsible for supplying the need for nutrients to generate adenosine triphosphate (ATP), nicotinamide adenine dinucleotide phosphate (NADPH) and carbon skeletons for nucleotide construction. All these components are geared towards the rapid growth and proliferation of cancer cells. The decrease in cellular respiration is another striking metabolic change that cells present for the onset and development of cancer. This phenotype probably occurs by the presence of defects in the electron transport chain and/or Krebs cycle (AYKINBURNS *et al.*, 2009), which results in the adaptive advantages of cancer cells for their rapid proliferation in an environment with less oxygen availability. In addition, solid tumor cells show an increase in the expression of lipid biosynthesis enzymes for the *de novo* synthesis of lipids to compose the plasma membranes and organelles of growing

cells (GATENBY; GILLIES, 2004). Changes in the mechanism of DNA repair, chromosomal instability, immune system evasion and changes in redox status are also common (APARICIO; BAE R; GAUTIER, 2014; JACKSON; BARTEK, 2009; SANDOVAL; ESTELLER, 2012).

Redox system is essential for the maintenance of cellular homeostasis. In physiological conditions, cells maintain redox balance through generation and elimination of reactive oxygen/nitrogen species (ROS/NSP). Superoxide ($O_2^{\cdot-}$), as an initial product of reduction of molecular oxygen (principal mechanism for ROS formation), results from the addition of a single electron to molecular oxygen. Superoxide can be rapidly dismutated by superoxide dismutase (SOD), yielding hydrogen peroxide H_2O_2 and O_2 . In the presence of reduced transition metals (e.g. Cu^{+2} , Fe^{+2} , Zn^{+2} , Mn^{+2}), H_2O_2 can be converted into the highly reactive hydroxyl radical HO^{\cdot} (DRÖGE, 2002).

Many complex mechanisms maintained the delicate balance between ROS generation and elimination, and impaired functioning of each of these mechanisms can lead to changes in cellular redox system. Redox homeostasis can be disrupted via an increase in ROS production and/or a decrease in ROS-scavenging capacity due to the exogenous stimuli or endogenous metabolic alterations resulting in an overall increase of intra cellular ROS levels, or oxidative stress that play important role in many pathological conditions such as cancer (LIGUORI et al., 2018; SCHIEBER; CHANDEL, 2014; VALKO et al., 2006). Under normal physiological conditions, ROS can incorporate reversibly into the structure of some macromolecules that play a critical role in regulating cellular function (SIES; JONES, 2007). However, under oxidative stress, excessive ROS attacks consistently lipids, proteins, and DNA, resulting in severe oxidative damage. Under oxidative stress condition, the non-enzymatic antioxidants (glutathione, ascorbic acid, α -tocopherol, carotenoids and phenolic compounds) are usually consumed and enzymatic antioxidants (superoxide dismutase, peroxidase and catalase) induced (IGHODARO; AKINLOYE, 2018; MIROŃCZUK-CHODAKOWSKA; WITKOWSKA; ZUJKO, 2018; WILLCOX; ASH; CATIGNANI, 2004). The intracellular oxidative balance is extremely important and is characterized by the control of ROS synthesis and the expression of antioxidant molecules. In cancer cells, this profile is inverted where even with an increase in the expression of the antioxidant system; it is not in a quantity capable of overlapping the high levels of ROS (KALYANARAMAN *et al.*, 2018).

Normal cells have lower amounts of both ROS and antioxidants than cancer cells. Thus, Loss of ROS or antioxidants causes only small changes in ROS homeostasis, then normal cells remain viable and functional. In contrast, cancer cells can be more susceptible to ROS level changes due to having higher amounts of these oxidant agents than the antioxidant counterparts.

Either treatment with antioxidants or prevention of ROS generation can cause cytostasis (inhibition of cell growth and multiplication) and possibly senescence, results in loss of sufficient ROS signaling to maintain growth and cause cancer specific oxidative cell death (Figure 4).

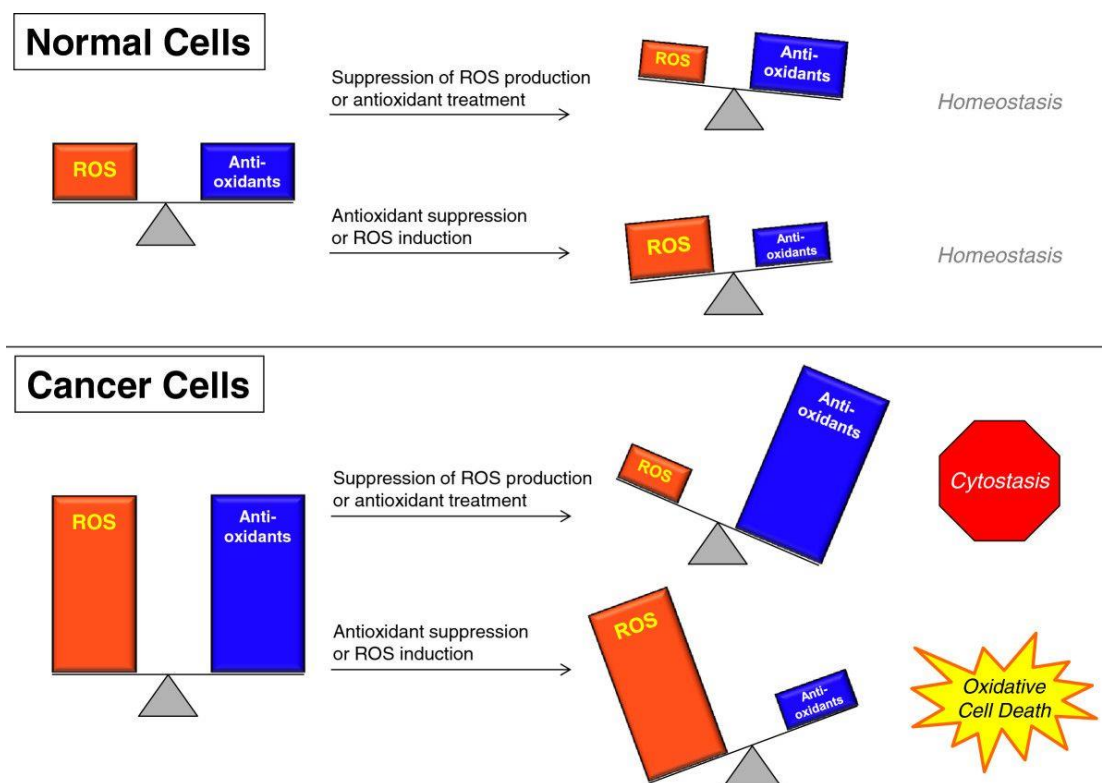


Figure 4. Targeting cancer cells by changing ROS levels (SULLIVAN; CHANDEL, 2014).

1.3 Tumor characteristics

Cancer cells showed morphological changes like variability in size and shape, increase in the ratio of nucleus/cytoplasm, nuclear number and size, changes in the size, morphology and functionality of mitochondria and formation of little differentiated cellular aggregates (BOTTONE *et al.*, 2013).

Increases in intracellular granularity have been observed during physiological processes that include senescence, apoptosis, and autophagy, making this phenotypic change a useful marker for identifying chemotherapeutic drug that induce cellular growth arrest or death (Table 1). The nature of cellular changes leading to increases in intracellular granularity is dependent on the agent and cell type under investigation. For example, growth arrest associated with increases in intracellular granularity may be produced by agents that induce cellular differentiation as observed with corticotropin-releasing hormone-induced keratinocyte differentiation (ZBYTE-

K *et al.*, 2005). They also can share some genetic and epigenetic changes like increase in oncogene and decrease in tumor suppressor genes, loss of proteins encoded by tumor suppressor genes for deletion or mutation, genetic instability and activation of genes capable of facilitating new mutations (Table 1) (TINHOFER *et al.*, 2014).

All cancer display acquisition of "immortality." Loss of growth inhibition dependent on contact or cell density, loss of cell cycle control and resistance to death by apoptosis, increased expression and secretion of growth factors and their receptors (Table 1).

Table 1. Some characteristics developed by tumor cells (TINHOFER *et al.*, 2014).

Morphological changes	Genetic and epigenetic exchanges	Changes in survival and growth properties
Changes and variability in cell size and shape	Increased expression of oncogene products	Acquisition of "immortality." Activation of telomerase
Increase in the ratio of nucleus/cytoplasm	Loss of proteins encoded by tumor suppressor genes, for deletion or mutation	Loss of growth inhibition dependent on contact or cell density. Stacked Growth
Increasing nuclear number and size	Changes in gene expression by changes in multiplication patterns of DNA	Less need for nutrients to survive and grow
Changes in the size, morphology and functionality of mitochondria	Genetic instability. Activation of genes capable of facilitating new mutations	Loss of cell cycle control and resistance to death by apoptosis
Formation of little differentiated cellular aggregates		Increased expression and secretion of growth factors and their receptors

In multiple stages of the carcinogenic process, each genetic variation is one of the benefits of tumor cells and, therefore, constituting hallmarks (characteristics) of cancer. These abilities acquired by tumor cells during tumor development favor their maintenance and are common to all types of cancers. Among them, we can highlight the proliferation signal, escape from growth suppressors, resistance to cell death, replicative immortality, angiogenesis induction, activation of invasion mechanisms, and metastasis (Figure 5) (HANAHAN; WEINBERG, 2011; MITTAL *et al.*, 2016).

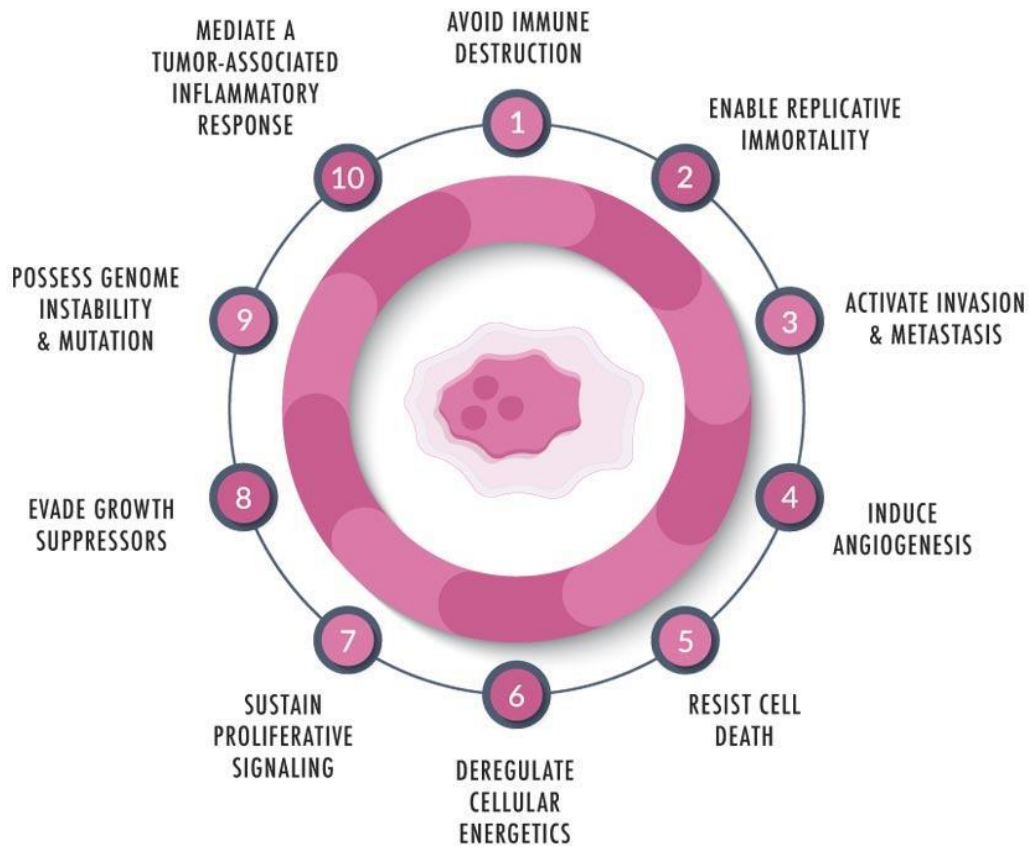


Figure 5. The 10 hallmarks of cancer (HANAHAH; WEINBERG, 2011).

Sustained proliferation signal and consequent loss of cell cycle control are fundamental and determinant characteristics of tumor formation. Cell cycle control or checkpoints play an important role in maintaining the fidelity and integrity of genome replication and repair. In the cell cycle there are three stages where the control points operate (TINHOFER *et al.*, 2014).

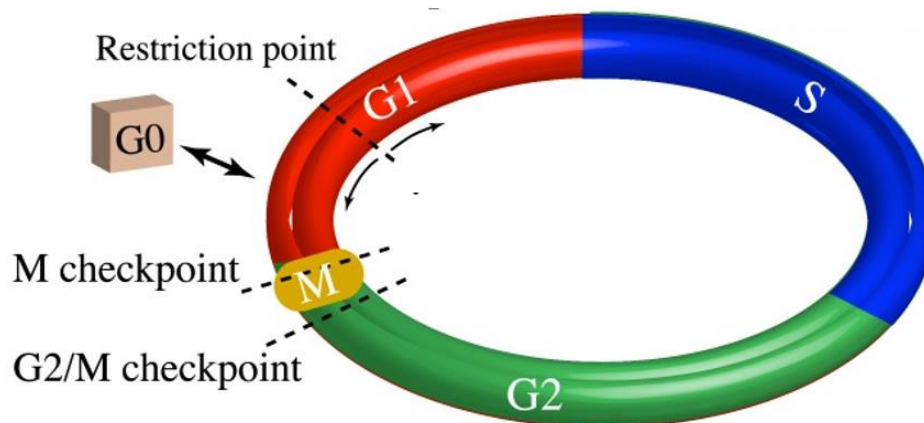


Figure 6. The four phases of the cell cycle (G1, S, G2, and M), the non-cycling G0 state, and three well-known checkpoints (JONES *et al.*, 2018).

The first control point is at the end of G1 phase and beginning of S phase. At this stage, the cell increases in size and have only one copy of their DNA. Cells in this stage synthesize proteins and increase in size and can remain in this stage for a long time (Figure 6). The replication occurs in the next phase, called S (synthesis), and allows the cell precisely to duplicate its chromosomes (HU *et al.*, 2013, TINHOFER *et al.*, 2014). After replicating the chromosomes, the G2 phase begins, preparing the cell for the M phase (mitosis), the phase where the increased stem cell finally divides in half to produce two cells, with the same number of chromosomes (TINHOFER *et al.*, 2014). Daughter cells immediately enter G1 phase and may restart the cell cycle or may temporarily or definitely stop the cycle (Figure 6) (CLARKE, 2017).

When the cell passes the first control point (G1/S), it has to replicate its DNA. The G2-M DNA damage checkpoint is an important cell cycle checkpoint, ensuring that cells do not initiate mitosis until damaged DNA or incompletely replicated DNA is sufficiently repaired after replication. Cells that have a defective G2-M checkpoint enter mitosis before repairing their DNA, leading to apoptosis or death by the help of gene suppressor p53 the so-called "guardian of the genome" (BURTON; KRIZHANOVSKY, 2014; ENGELAND, 2018; HU *et al.*, 2013). First, p53 stops the cell cycle at the G1 checkpoint by inhibiting the production of Cdks (cyclin-dependent kinases) that act as a control cell cycle transition. Second, inactivates DNA repair enzymes. In cases where damage is extremely irreversible, p53 triggers apoptosis, a cell death process (HU *et al.*, 2013, SARIN *et al.*, 2017). The third checkpoint occurs in metaphase (second stage of mitosis) and cell division only proceeds if the chromosomes are correctly attached to the spindle (BURTON; KRIZHANOVSKY, 2014).

Most tumor cells show loss of cell cycle control due to the mutations in genes responsible for this control, thus allowing cancer cells cross the restriction sites and divide, even that the conditions required for the cell division process are not fulfilled. Normal cells undergoing DNA damage remain in the G1 of the cycle in order to repair the damage before proceeding further of the cycle. However, cancer cells ignore the warning continue the cycle by duplicating the damaged DNA, thus leading to accumulation of mutations (KAR, 2016). Mutations in tumor cells lead them to ignore the signs of death and continue proliferating, increasing the chance of new mutations (POBEZINSKAYA; LIU, 2012). In this way, the transformed cells acquire immortal replicative ability indefinitely, whereas healthy human cells when cultured can double from 50 to 60 times, provided that the provision of nutrients and growth factors (ITO; HOUKIN, 2017; MAQSOOD *et al.*, 2013).

The most important core cell cycle regulators are proteins called cyclins (G1 cyclins, G1/S cyclins, S cyclins, and M cyclins). Binding of a cyclin activates Cdks, making it a functional enzyme and allowing it to modify target proteins. APC/C (anaphase-promoting complex/cyclosome) is a protein complex that causes M cyclins to be destroyed and, then starting anaphase (ALFIERI; ZHANG; BARFORD, 2017). In the early stages of tumor development, when usually less than two millimeters in diameter, the nutrition of the mass tumor occurs essentially by diffusion from neighboring tissues. As tumor grow, nutrition depends on the blood vessels that do not enter into degeneration and necrosis. In this way, the tumor cells induce the production of angiogenic factors to stimulate the formation of new blood vessels in order to supply its nutrient and oxygen needs (RAICA; CIMPEAN; RIBATTI, 2009; VIALARD; LARRIVÉE, 2017).

Angiogenesis is an essential process for development and dissemination of tumors and is directly related to tumor metastasis, because the new formed vessels serve as pathways for spreading cells to other outbreaks of colonization (RAICA; CIMPEAN; RIBATTI, 2009). Throughout the process of tumor progression, some cells acquire a more aggressive phenotype, which allows them to invade adjacent or far tissues. These more aggressive cells are often having different molecules like epiregulin (EREG), cyclooxygenase-2 (COX-2), matrix metalloproteinase 1 (MMP1), and matrix metalloproteinase 2 (MMP2) (promote extravasation and metastasis) (GUPTA *et al.*, 2007). expressed qualitatively and/or quantitatively compared to non-metastatic cells. These molecules are essential in the dissemination of metastatic tumors. Thus, the identification of genes and molecules that are associated with the process of metastasis is fundamental for the early diagnosis and elucidation of new therapeutic strategies (COGHLIN; MURRAY, 2010; FUHRMANN *et al.*, 2017).

The abilities of cancer cells reflect the characteristics of the entire population of a tumor, because the genetic changes that trigger the malignancy process should be in most tumor cells. However, at the stage of tumor progression, where genetic alteration accumulates, a cellular subpopulation can arise, and it identifies distinct variations that are distinct from other cells within tumor masses. Thus, the tumor cell population is heterogeneous, which means that not all cells share similar characteristics (BADVE, 2016; CASSIDY; BRUNA, 2017; PRASETYANTI; MEDEMA, 2017).

1.4 Classification of chemotherapy drugs related to their mechanism of action.

Chemotherapy targets the selective destruction of tumor preserving the healthy cells. Most chemotherapy drugs affect both cell population; however, due to the innumerable morphological and biochemical differences between them, the damage to malignant cells has to be larger than occur in healthy cells and tissues (JOHNSTONE *et al.*, 2016).

Antineoplastic drugs can be classified into three major classes: (i) cytotoxic drugs such as alkylating agents, platinum coordination (cisplatin, carboplatin, oxaliplatin), antimetabolites, microtubule damaging agents (vincristine, vinblastine, vinorelbine, paclitaxel, docetaxel), topoisomerase-2 inhibitor (etoposide), topoisomerase-1 inhibitor (topotecan, irinotecan), antimicrobials (actinomycin D, doxorubicin, daunorubicin, epirubicin, bleomycins, mitomycin and miscellaneous (hydroxyurea, L-asparaginase, tretinoin, arsenic trioxide); (ii) targeted drugs like tyrosine protein kinase inhibitors (imatinib, nilotinib), EGF receptor inhibitor (gefitinib, erlotinib), angiogenesis inhibitors (bevacizumab), proteasome inhibitor (bortezomib), unarmed monoclonal antibody (rituximab, trastuzumab), and (iii) hormonal drugs such as glucocorticoids (prednisolone), estrogens (fosfestrol, ethinylestradiol), selective estrogen receptor modulators (tamoxifen), selective estrogen receptor down-regulators (fulvestrant), aromatase inhibitors (letrozole, anastrozole), antiandrogen (flutamide), 5- α reductase inhibitor (finasteride), GnRH analogues (nafarelin, triptorelin), progestins (hydroxyprogesterone acetate).

Cytotoxic drugs can be classified according to how they affect cell cycle in tumor cells. Cell cycle phase specific antineoplastic agents (CCS) act on the particular phase. They are active against tumor cells that have a large portion of cells activity, and rapidly cycling. Fast cycling ensures that the cell passes through the phase vulnerable to the drug's effects (OZAWA *et al.*, 1989; SHERR; BARTEK, 2017; THU *et al.*, 2018). CCS acts at certain stages of the cell cycle, such as methotrexate (S phase), etoposide (G2 phase), and vincristine (M-phase). On the other hand, cell cycle nonspecific antineoplastic agents (CCNS) refer to a class of pharmaceuticals that act as antitumor agents at all or any phases of the cycle cross-link. Table 2 shows some differences between CCS and CCNS agents. Among the different classes of antitumor drugs most commonly clinically used, present a mechanism of cell cycle nonspecific action (DEFALCO; DE LUCA, 2010).

Table 2. Different characteristics of cell cycle specific and nonspecific (KATZUNG *et al.*, 2012).

Cell cycle specific agent (CCS)	Cell cycle nonspecific agent (CCNS)
Plant alkaloids and anti-metabolites	Alkylating agents and some natural products
Plant alkaloids G2-M phase DNA synthesis inhibitors S phase	Any phase of the cell cycle Cross linking and gene silencing
Only proliferating cells are killed	Both proliferating and resting cells are killed
Schedule dependent (Duration and timing rather than dose)	Dose dependent (Total dose rather than schedule)

Antineoplastic drugs can be divided based on their target. The target may be located in the tumor cell or in other elements that interact with the tumor cells (endothelium, extracellular matrix, immune system, host cells): (i) drugs directed against tumor DNA can act on DNA helix such as alkylating agents. They also may act on DNA-related proteins like topoisomerase I and II inhibitors, antimetabolites and ecteinascidin (HURLEY, 2002); (ii) drugs directed against tumor RNA, such as fluoropyrimidines and platinum compounds; however, they mainly act by binding to DNA (these molecules are directed against specific mRNAs, for instance, RNAs of bcl-2, myc, p53, mdm2, Her-2 and methyltransferase-1 have been targeted with these oligonucleotides (TOLCHER, 2001); (iii) drugs directed against proteins in the tumor cells, like monoclonal antibodies and small molecules, which are all very specific and their effect is cytostatic rather than cytotoxic and they can bind to membrane receptors or cytoplasmic proteins, and (iv) drugs acting on the endothelium and extracellular matrix, such most drugs acting in the matrix metalloproteinases (MMPs) that all of them have antiangiogenic effects.

We will further describe the cytotoxic drugs directed against tumor DNA that is showed in Table 3.

1.4.1 Alkylating agents

Alkylating agents are the oldest and most widely used antineoplastic agents, are known to act directly in DNA, and are not only active in the process of cell division. This class of antitumor affects the cells in all phases of cell cycle and is able to substitute an atom of hydrogen by an alkyl radical in a target molecule. They interact chemically with DNA preventing the

separation of the two DNA strands, a phenomenon that is fundamental for replication (KASTAN; BARTEK, 2004; SWIFT; GOLSTEYN, 2014).

Due to the low clinical efficacy of mono-chemotherapy, treatment of patients is usually associated with combination of other CCNS agents of the cell cycle. The main drugs used in this category include nitrogen mustard, busulfan, nitrosoureas, cisplatin and carboplatin (KASTAN; BARTEK, 2004). Alkylating agents capable of forming different types of intrastrand and cross-linking with the DNA are called bifunctional. However, those who are able to form cross-links are particularly more potent than intrastrand because the alkylation of two DNA filaments produced by bifunctional alkylating agents requires rather complex repair mechanisms (DRABLØS *et al.*, 2004; SOLL; SOBOL; MOSAMMAPARAST, 2017). Antitumor nitrogen mustards, such as bis(2-chloroethyl) methylamine (mechlorethamine), is one of the first alkylating agent with a long history of clinical application. The antitumor effects of nitrogen mustards are attributed to their ability to induce DNA-DNA and DNA-protein cross-links, which blocks DNA replication. Numerous derivatives of this compound such as chlorambucil, cyclophosphamide and ifosfamide still used as antitumor treatment (KONDO *et al.*, 2010; SOLL; SOBOL; MOSAMMAPARAST, 2017). Nitrogen mustards are bifunctional alkylating agents containing two N-(2-chloroethyl) groups that can spontaneously cyclize under physiological conditions. The resulting aziridinium ions are highly reactive and are capable of alkylating nucleophilic sites within DNA and proteins to form DNA-protein and DNA-DNA cross-links (RAJSKI; WILLIAMS, 1998). It has been established that the main molecular target of nitrogen mustards and other alkylating agents is the N-7 of guanine; N-1, N-3 of adenine and N-3 of cytosine may also be affected (HELLEDAY *et al.*, 2008, SINGH *et al.*, 2018).

1.4.2 Antimetabolites

Tumor cells are more susceptible to the various antimetabolic or structural analogues of nitrogenous bases, due to the metabolic difference compared to normal cells. In this way, the antimetabolite agents are responsible for biochemically blocking the synthesis of DNA and RNA; thus, they are restricted to the S phase of the cell cycle. Among the antimetabolites used clinically in the treatment of cancer, we can highlight methotrexate (folic acid analogue), purine analogs such as 6-mercaptopurine, thiguanine and, finally, the analogs of pyrimidines, 5-fluorouracil, azauridine and cytarabine (MASOOD *et al.*, 2016, TAKIMOTO *et al.*, 1999).

1.4.3 Topoisomerase inhibitors

Topoisomerases are essential proteins that during DNA replication and transcription, relieve torsional stress of DNA supercoiling by introducing transient nicks (POMMIER, 2006). There are two types of topoisomerases, topoisomerases I and II, which cause single strand breaks (SSBs) and double strand breaks (DSBs) within DNA molecule, respectively (WEINFELD *et al.*, 2011). Topoisomerases I and II are the targets of an increasing number of anticancer drugs that act to inhibit these enzymes by blocking the reaction that reseals the breaks in the DNA. Often the binding of the drug is reversible, but if a replication fork runs into the blocked topoisomerase, then a piece of the gapped DNA strand not bound by the topoisomerase could be released, creating a permanent breakage in the DNA that leads to cell death (POMMIER, 2006). Camptothecin widely used to treat colorectal, ovarian and lung cancer binds to DNA-topoisomerase I cleavage complexes, blocking religation of SSBs and resulting in the accumulation of transient SSBs (WEINFELD *et al.*, 2011). Concerning the use of topoisomerase II inhibitors, such as etoposide, commonly used to treat small cell lung and testicular cancer, a negative aspect is that their use has been related to the occurrence of secondary leukemia and other malignancies (GOKDUMAN, 2016; NITISS, 2009).

Table 3. Cytotoxic chemotherapy agents that damage DNA, their mechanism of action, and the main types of damage that they cause (SWIFT; GOLSTEYN, 2014).

Type of agent	Drug	Mechanism of action	DNA damage
Alkylating agents	Nitrogen mustards Nitrosoureas Temozolomide	Base alkylation- mono-functional DNA adducts Inter, intra and DNA-protein crosslinks	Block the replication machinery leading to strand breaks
Antimetabolites	5-Fluorouracil	Misincorporates into DNA Depletes dNTPs	Blocks the replication machinery leading to strand breaks
Topoisomerase inhibitor	Camptothecin Etoposide	Inhibit topoisomerase enzymes in complex with DNA	SSBs and DSBs

1.5 Metal-based complexes.

Therapeutic potential of metal-based complexes in cancer therapy has attracted a lot of interest mainly because metals exhibit unique characteristics, such as redox activity, variable coordination modes and reactivity toward the organic substrate (BRUIJNINCX; SADLER, 2008;

MUHAMMAD; GUO, 2014; NDAGI; MHLONGO; SOLIMAN, 2017). A metal complex consists of a central metal atom or ion that is bonded to one or more ligands, which are ions or molecules that contain one or more pairs of electrons that can be shared with the metal. A coordination complex whose center is a metal atom is called a metal complex (CHIVERS, 2005; MUHAMMAD; GUO, 2014).

Among metal-based drugs, the potential use of first row transition metal ions to act as anticancer agents has been investigated, mainly because their natural abundance, low price associated with the synthesis of their compounds and the natural presence of such metal ions in the body (CINI; BRADSHAW; WOODWARD, 2017; CRANS et al., 2018; DENOYER; CLATWORTHY; CATER, 2018). Transition or d-block metals have the d-orbitals partially filled and are included in groups III–XII of the periodic table, offering great advantages over common organic drugs, including a wide variety of coordination geometries and numbers, they can aggregate to a wide range of coordination geometries that give them unique shapes (CINI; BRADSHAW; WOODWARD, 2017). In the various accessible oxidation states available, many transition metals tend to undergo oxidation and reduction reactions (HAAS; FRANZ, 2010). The oxidation state of these metals is an important consideration in the design of the coordination compound. In biochemical redox catalysis, metal ions often serve to activate coordinated substrates and to participate in redox-active sites for charge accumulation. Metal complexes can aggregate to a wide range of coordination geometries that give them unique shapes. The bond length, bond angle and coordination site vary depending on the metal and its oxidation state. In addition to this, metal-based complexes can be structurally modified to a variety of distinct molecular species that confer a wide spectrum of coordination numbers and geometries, as well as kinetic properties that cannot be realized by conventional carbon-based compounds (BRUIJNINCX; SADLER, 2008; SALGA et al., 2012; SANTINI et al., 2014). Moreover, different forms of metal-ligand interaction exist; however, these interactions usually lead to the formation of complexes that are unique from those of individual ligands or metals. The thermodynamic and kinetic properties of metal-ligand interactions influence ligand exchange reactions (HAAS; FRANZ, 2010). The ability of metals to undergo this reaction offers a wide range of advantages to the metals to interact and coordinate with biological molecules (BRUIJNINCX; SADLER, 2008; VAN RIJT; SADLER, 2009; DENOYER; CLATWORTHY; CATER, 2018). Thus, the variety of mechanisms of action that metal-based complexes can offer is not the same as that of organic drugs.

Over the last century, the number of metal-based complexes used in medicine has increased significantly. From the group 11, elements such as copper (Cu), silver (Ag) and gold (Au)

have been known for centuries and their medicinal applications have been well reported (JUNG WIRTH *et al.*, 2011). Recent developments of Cu, Ag and Au metallodrugs have shown excellent potential as antitumor agents (LIANG *et al.*, 2017; MCGIVERN; AFSHARPOUR; MARMION, 2018; TIEKINK, 2008). Moreover, complexes of ruthenium and iron from group 8 have also shown remarkable antitumor activity with potent efficacy, low toxicity, less drug resistance, and are expected to become a new generation of clinical metal antitumor drugs (ABID; SHAMSI; AZAM, 2015; SOUTHAM *et al.*, 2017).

Amongst other metal group, bismuth directly affects *Helicobacter pylori* and gastric lymphoma; the effects of bismuth complexes of 6-mercaptopurine are promising (STEINBACH *et al.*, 1999). Several derivatives of vanadium show anti-proliferative activity, but their toxicity must be overcome (HANAUSKE *et al.*, 1987). The anti-proliferative effect of gallium could be related to its competition with the iron atom; in addition, a derivative appears to reverse the multidrug resistance (HEDLEY *et al.*, 1988). Rhodium, ruthenium, palladium, osmium and iridium are belong to the same group as platinum and they also presents interesting anti-cancer activity, but with the same nephrotoxicity (FRIK *et al.*, 2014; HOWARD; BEAR; KIMBALL, 1979; MA *et al.*, 2019; YANG *et al.*, 2017; ZHANG *et al.*, 2016).

Platinum complexes are now among the most widely used drugs for the treatment of cancer with four injectable Pt(II) compounds, cisplatin, carboplatin, oxaliplatin and nedaplatin approved for clinical use worldwide (DILRUBA; KALAYDA, 2016; JOHNSTONE; SUNTHARALINGAM; LIPPARD, 2016). Figure 7 outlines two main targets that are currently the focus of many research groups investigating the anticancer capabilities of metal-based complexes (GANESHPANDIAN *et al.*, 2014). The metal complexes can force the cancer cell go through apoptosis via ROS generation (figure 7). On the other hand, they can bind directly with DNA and RNA (metallo-interaction or metallo-insertion) led in DNA damage causing cell death (figure 7). Alternatively, they can inhibit the DNA repair enzymes (metallo-nucleases) resulting in hydrolytic and oxidative damage to DNA (figure 7) (JAYASEELAN *et al.*, 2016; YU; COWAN, 2018; ZHANG; SADLER, 2017a).

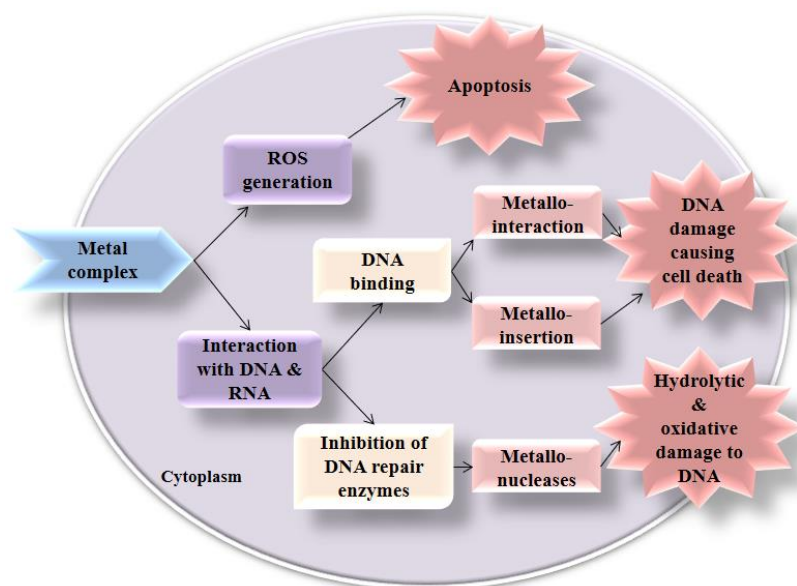


Figure 7. Cellular target of metal-based complexes anticancer agent.

1.5.1 Mechanisms of action of metal-based complexes.

1.5.1.1 Via ROS generation.

Reactive oxygen species are radicals, ions or molecules that have a single unpaired electron in their outermost shell of electrons. Among them, superoxide, hydrogen peroxide and hydroxyl radicals are the most well studied ROS in cancer. Intracellular active superoxide anions ($O_2^{\cdot-}$), hydrogen peroxide (H_2O_2), hydroxyl radicals ($\cdot OH$) and singlet oxygen (O_2) have the ability to induce lipid peroxidation, DNA damage, and depletion of the sulfhydryl groups, altered signal transduction pathways and calcium homeostasis (PANIERI; SANTORO, 2016; SZATROWSKI; NATHAN, 1991).

It has been suggested that the formation of ROS and the resultant oxidative stress play a major role in inflammation contributing to carcinogenesis. During chronic and acute inflammation, the $O_2^{\cdot-}$ is highly produced, the endogenous SOD can often become overwhelmed and unable to remove the excess amount of $O_2^{\cdot-}$, which can then promote a pro-inflammatory response. As SOD has been shown to be depleted in cancer cells, excess of $O_2^{\cdot-}$ can be metabolized into peroxynitrite ($OONO^{\cdot-}$) and the hydroperoxyl radical (HO_2) which play a role in tumor formation (O'CONNOR *et al.*, 2012).

ROS are produced as a byproduct of oxidative phosphorylation in mitochondria. Complexes I-IV and ATP synthase are located on the mitochondrial inner membrane of the electron transport chain. Approximately 80% of generated $O_2^{\cdot-}$ at complexes III and I is released into the intermembrane space of mitochondria whereas, 20% of this oxidant is released into the mitochondrial matrix (HAN; WILLIAMS; CADENAS, 2001; KUMARI *et al.*, 2018). Superoxide leak

into the cytoplasm through the mitochondrial permeability transition pore (MPTP) in the outer membrane of the mitochondrion and can be dismutated to H_2O_2 either by MnSOD, in the mitochondrial matrix or by Cu/ZnSOD in the cytosol (CROMPTON, 1999). Recent data suggest that H_2O_2 may cross-cellular membranes through specific members of the aquaporin family like aquaporin-8 (BIENERT *et al.*, 2007). In addition to the mitochondria, peroxisomes are other major sites of cellular ROS generation in which $\text{O}^{2\cdot-}$ and H_2O_2 are generated through xanthine oxidase in the peroxisomal matrix and the peroxisomal membranes (DEL RÍO *et al.*, 1992; DEL RÍO; LÓPEZ-HUERTAS, 2016).

Growth factors and cytokines can stimulate production of ROS in cancer. For example, an elevation of H_2O_2 and nitrite oxide NO levels were detected in tumor cells in response to interferon γ ($\text{IFN}\gamma$) and tumor necrosis factor alpha ($\text{TNF}\alpha$) (TIKU; LIESCH; ROBERTSON, 1990). Further, platelet-derived growth factor (PDGF), epidermal growth factor (EGF), insulin, transforming growth factor β ($\text{TGF}\beta$), interleukin-1 (IL-1), $\text{TNF}\alpha$, angiotensin and lysophosphatidic acid all induce the formation of $\text{O}^{2\cdot-}$ (BAE *et al.*, 1997, 2000; CAMPILLOS *et al.*, 2008; CERNANEC *et al.*, 2007; LIN *et al.*, 2013; ONYANGO, 2017; R.-M.; K.A., 2010; SUNDARESAN *et al.*, 1995). Activation of the small Rho GTPase K-RAS downstream of growth factors or its oncogenic mutation has been tightly associated with increased generation of superoxide and the incidence of various cancers (MINAMOTO; OUGOLKOV; MAI, 2002).

The higher levels of ROS can interfere nonspecifically with DNA, proteins, and lipids, which disrupt mitochondrial electron transfer chain resulting in the collapse of mitochondrial function and the threat of cell survival. Direct or indirect formation of ROS can lead to DNA damage (GALARIS; EVANGELOU, 2002). ROS have the ability to trigger apoptosis within cells through an apoptotic-signaling program. This is characterized by a number of features that ultimately breaks the cell down into a series of smaller units called apoptotic bodies that are phagocytized by adjacent cells (MATÉS; SÁNCHEZ-JIMÉNEZ, 2000). Due to the fact that cancer cells have increased ROS levels, they may selectively be more susceptible to the harmful effects of ROS increases. Increasing ROS production, especially in cancer cells, is likely to be difficult, although this is a proposed mechanism for several current chemotherapeutics function (ZOU *et al.*, 2017). Similarly, since cancer cells often increase the expression of antioxidant elements to maintain homeostasis, the promising approach is to inhibit antioxidants to expose cancer cells into endogenously ROS (GORRINI; HARRIS; MAK, 2013; SZNARKOWSKA *et al.*, 2017).

Beside ROS causal role in tumorigenesis, it can also be toxic to the cell and can potentially induce cancer cell death, cell cycle arrest and inhibit cancer progression. Therefore, cancer cells are dependent on maintaining the exact ROS levels that allow for pro-tumorigenic cell signaling without inducing cell death. The dependence of cancer cells on ROS homeostasis can be potentially applied to target them therapeutically. Chemotherapeutic drugs such as taxanes (e.g. paclitaxel), vinca alkaloids and anti-folates promote mitochondrial cell death through the release of cytochrome c and disrupt the mitochondrial electron transport chain, which leads to increased $O_2^{\cdot-}$ production (KAUFMANN; EARNSHAW, 2000; MOUDI *et al.*, 2013; RAMAWAT; MERILLON, 2008). Other chemotherapeutics like cisplatin, carboplatin and doxorubicin also significantly increase ROS, which is the basis of their antitumorigenic effect (CONKLIN, 2004, KOTAMRAJU, *et al.*, 2002). Briefly, cisplatin binds to the N7 reactive center on purine residues and as such can cause DNA damage in cancer cells, blocking cell division, increased ROS generation alters the mitochondrial membrane potential and damages the respiratory chain, which ultimately triggers the apoptotic process and resulting in apoptotic cell death (refer to section 1.6) (RYBAK *et al.*, 1999, VALKO *et al.*, 2006). Carboplatin second-generation platinum anticancer drug undergoes activation inside cells and forms reactive platinum complexes that cause the intra- and inter-strand cross-linkage of DNA molecules within the cell. This modifies the DNA structure and inhibits DNA synthesis. This may affect a cell in all the phases of its cycle. It has been reported that carboplatin could also induce oxidative stress to produce ROS, which in turn promoted apoptosis (CHENG *et al.*, 2008). Doxorubicin interacts with DNA by intercalation that caused prevention of macromolecule synthesis, ROS generation, DNA binding and cross-linkage and DNA damage by inhibition of the progression of topoisomerase II, an enzyme which relaxes supercoils in DNA for transcription and induction of apoptosis (GEWIRTZ, 1999; RENU *et al.*, 2018; TAKEMURA; FUJIWARA, 2007).

1.5.1.2 Via DNA binding.

DNA is considered the main target of many transition metal complexes. The availability of different coordination geometries allows for the synthesis of complexes with unique stereochemistry that can be used in DNA binding (BRUIJNINCX; SADLER, 2008; PAGES *et al.*, 2015). These complexes can interact with DNA through (a) covalent; b) non-covalent (electrostatic); (c) intercalation; (d) cleavage by oxidation; (e) cleavage by hydrolysis (BERGAMO; DYSON; SAVA, 2018; CAO *et al.*, 2017; DASARI; BERNARD TCHOUNWOU, 2014).

Most prevalent among covalent interactions with DNA are those involving coordination between metal ions and nucleophilic positions on the bases. Transition metal ions are capable

of coordinating also to the phosphate oxygen atoms. The ionic versus covalent character of these complexes clearly depends on the metal ions involved. Also of interest, but less common, are covalent interactions with the sugar moiety (CHANG; MEARES, 1982). The well-known and clinically used anticancer agent cisplatin is cytotoxic because of its ability to covalently bind DNA (MARKY, *et al.*, 1983). Non-covalently binding agents include (a) intercalators (b) groove-binding agents and (c) electrostatically binding agents/external binding agents.

Intercalation consists of the insertion of the compound between base pairs, thus unwinding the strands (KEENE; SMITH; COLLINS, 2009; MARKY *et al.*, 1983). Intercalators are characterized by having an extended planar aromatic structure (HURLEY, 2002). Intercalation can result in lengthens, stiffens and unwinds DNA where the degree of unwinding can vary depending on the intercalator (LERMAN, 1961). Barton *et al.* (1986) studied the metallo-intercalation of the sequence specific rhodium intercalator (BARTON, 1986). Δ - α -[Rh[(R,R)-Me2trien](phi)]³⁺, bound to a duplex octamer has been reported by Kielkopf *et al.* (2000) that target the sequence 5'-TGCA-3' through the involvement of both hydrogen bonding and methyl-methyl interactions in the DNA major groove (KIELKOPF, *et al.*, 2000, SONG, *et al.*, 2012). Groove binding involves direct interaction of the bound molecule with edges of base pairs in either of the major (G-C) or minor (A-T) grooves of the nucleic acids. It has been shown that copper-phenanthroline [Cu(phen)₂]²⁺ reversibly bound in the minor groove could cleave the DNA (SIGMAN, *et al.*, 1979). Draksharapu *et al.* (2015) showed the [Cu(dmbpy)(NO₃)₂] (dmbpy=4,4'-dimethyl-2,2'-bipyridine), [Cu(bpy)(N-O₃)₂] engage primarily through groove binding with st-DNA (DRAKSHARAPU, *et al.*, 2015).

In another study, mononuclear and dinuclear Cu²⁺-complexes with thiophenecarboxylic acid, [Cu(3-TCA)₂(2,2'-bpy)], [Cu(3-Me-2-TCA)₂(H₂O)(2,2'-bpy)], [Cu(5-Me-2-TCA)₂(H₂O)(2,2'-bpy)] and [Cu₂(2,5-TDCA)(DMF)₂(H₂O)₂(2,2'-bpy)₂] (ClO₄)₂ (where 3-TCA=3-thiophenecarboxylic acid; 3-Me-2-TCA=3-methyl-2-thiophenecarboxylic acid; 5-Me-2-TCA=5-methyl-2-thiophene carboxylic acid; 2,5-TDCA= thiophene-2,5-dicarboxylic acid; 2,2'-bpy=2,2'-bipyridyl; DMF= *N,N*-dimethylformamide), were reported that these compounds bind with DNA in minor groove binding (GURUDEVARU, *et al.*, 2018).

The electrostatic effects between cationic species and the negatively charged DNA phosphate backbone are ideal nonspecific interactions that might be important to enhance the binding of small molecules (LIPFERT, *et al.*, 2014).

Structural changes can result in functional changes such as transcription, replication, and DNA repair processes suppression (PAGES, *et al.*, 2015). The synthesis of transition metal

complexes and investigations of their interaction with DNA has been an active field of research. This is essential for applications in many areas, such as biological and medicinal (ARJMAND, *et al.*, 2012, USMAN, *et al.*, 2017).

1.5.1.3 Via Metallonucleases.

Nucleases are enzymes capable of catalyzing hydrolysis of nucleic acids by cleaving the phosphodiester bonds of nucleic acids. There are two major types of nucleases: exonucleases and endonucleases. Exonucleases are capable of removing nucleotides one at a time from a DNA molecule, whereas endonucleases work by cleaving the phosphodiester bonds within DNA molecule. DNA cleavage can be achieved through hydrolytic or oxidative mechanisms (RITTIÉ; PERBAL, 2008). Artificial metallonucleases have potential uses in gene regulation, mapping of protein and DNA interactions, probing of DNA specific structures and cancer therapy (WEST; MARNETT, 2006; WOLKENBERG; BOGER, 2002).

The building blocks of DNA and RNA are linked through phosphodiester functional groups and the hydrolytic cleavage can occur by enzymatic catalysts (nuclei) to break the strands (COWAN, 2001). Nucleophilic attack of water (or hydroxide) to the phosphodiester backbone of DNA give a five coordinate phosphate intermediate which is subsequently cleaved at either the P-O3' or P-O5' causing strand break and yielding the R-OH and R-O-PO₃H₂ terminus, that occur naturally as hydrolytic cleavage of DNA (HADJILIADIS; SLETTEN, 2009). The carboplatin and cisplatin exhibited DNA cleavage activity via a hydrolytic pathway in contrast to an oxidative pathway observed for the oxaliplatin analogues.

Copper-bis-phenanthroline complex ([Cu(phen)₂]²⁺) was the first copper based artificial nuclease reported in the literature (SIGMAN, *et al.*, 1979). Copper⁺²-complexes containing the sulfonamides sulfameter (smtrH) and sulfadimethoxine (sdmxH) and (NN)-bidentate ligands (2,2'-biyridine or 1,10-phenantroline) [Cu(smtr)₂(phen) and [Cu(sdmx)₂(phen)] has been reported by Nakahata *et al.* (2018) demonstrated nuclease activity by interaction with DNA via groove binding and intercalation (NAKAHATA, *et al.*, 2018).

The ternary Cu⁺²-Schiff base complexes derived from salicylaldehyde (sal) and amino acids and phen or bipyridine (bpy) as co-ligands, [Cu(sal-Gly)(bpy)], [Cu(sal-Gly)(phen)] developed by Correia *et al.* (2015) also presented nuclease activity (CORREIA, *et al.*, 2015).

1.6 Platinum-based complexes.

Within the research area of bioinorganic and medicinal chemistry, two main groups of compounds with antitumor activity have been investigated: a) platinum-based complexes e.g.

cisplatin and b) non-platinum-based complexes, e.g. titanium, iron, ruthenium, cobalt, copper, gold and gallium complexes.

The ability of cross-links DNA demonstrated by series of antitumor agents including platinum-based complexes. Among these compounds, we can highlight the cis-diamminedichloroplatinum (II) (cisplatin) that was discovered accidentally in 1965 as a compound with cytotoxic activity, and is widely used in the treatment of cancer (DASARI; BERNARD TCHOUNWOU, 2014). From this discovery, many analogues of cisplatin have been developed with the aim of improving and increase the chemotherapeutic ability. Cisplatin is a flat quadratic Pt(II) coordination compound with two ligands chlorides in *cis* position. Cisplatin is an important chemotherapeutic drug used in the therapy of a broad spectrum of human malignancies such as ovarian, testicular, head and neck, and lung cancer and it is effective against various types of cancers, including carcinomas, germ cell tumors, lymphomas, and sarcomas. It is generally accepted that DNA is the preferential cytotoxic target for cisplatin that bind preferentially the imidazole ring of the purines guanosine and adenosine forming monoadducts, intrastrand crosslinks, and interstrand crosslinks (RABIK; DOLAN, 2007). The first step for cisplatin to exert its toxic effects is to enter the cells. Several cell membrane transporters have been associated with cisplatin transport across the plasma membrane and across the cell. The copper transporter 1 (Ctr1) assigned to the SLC31A family has been demonstrated to mediate the cellular uptake of cisplatin (HOLZER, *et al.*, 2004, LARSON, *et al.*, 2009). The main function of copper transporter 2 (Ctr2, SLC31A2) deemed to reside in mediating the efflux of cisplatin from endosomes and lysosomes (BLAIR, *et al.*, 2011). Other copper transporters that have been implicated in cisplatin cellular handling are the P-type copper-transporting ATPases ATP7A and ATP7B. They both seem to transport platinum out of cells or into specific subcellular compartments (HOLZER, *et al.*, 2004, SAFAEI, *et al.*, 2012). The organic cation transporter 2 (OCT2) that mediate the transport of organic cations in or out of cells (CIARIMBOLI, *et al.*, 2005). Finally, the multidrug and toxin extrusion transporter 1 (MATE1) which may excrete platinum through urine and bile (OTSUKA, *et al.*, 2005, YONEZAWA, *et al.*, 2006).

When cisplatin entering the cell, two water molecules replace the two chlorides, producing the active form of cisplatin, which is able, to form adducts with proteins, RNA and DNA (KELLAND, 2007) (Figure 8).

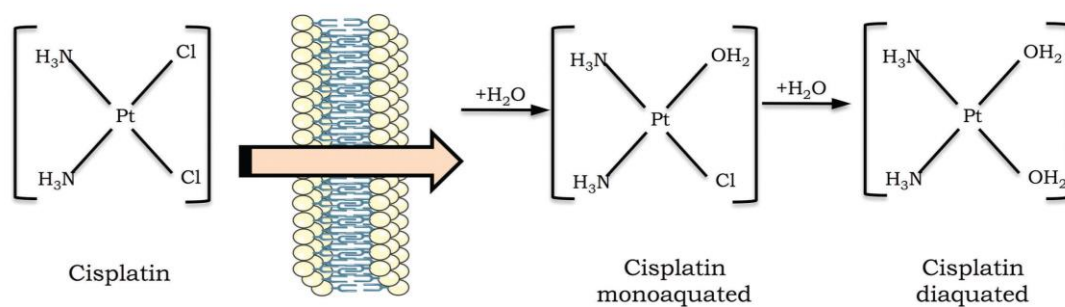


Figure 8. Cisplatin activation and DNA damage induction. The cisplatin activation process occurs by exchange of one or two of its chlorides for water molecules (monoaquated and diaquated, respectively) (KELLAND, 2007).

There are several possibilities of the binding sites for Pt from the bases, N1 of adenosine, N7 of adenosine and guanine, and N3 of cytosine. Like nitrogen mustards, cisplatin reacts preferentially with the N7 of the guanine residue forming a monoadduct and subsequently forming intra- and interstrand crosslinks. 1, 2-intrastrands are formed more frequently (65%) than 1, 3-intrastrands (25%) and 1, 2-interstrand structures that are formed to a lesser extent (3-5%) (Figure 9). Cross-linked bonds severely distort DNA double helix that finally leads to interruption of the cell cycle and/or leads to apoptosis (KELLAND, 2007, ROCHA, *et al.*, 2018).

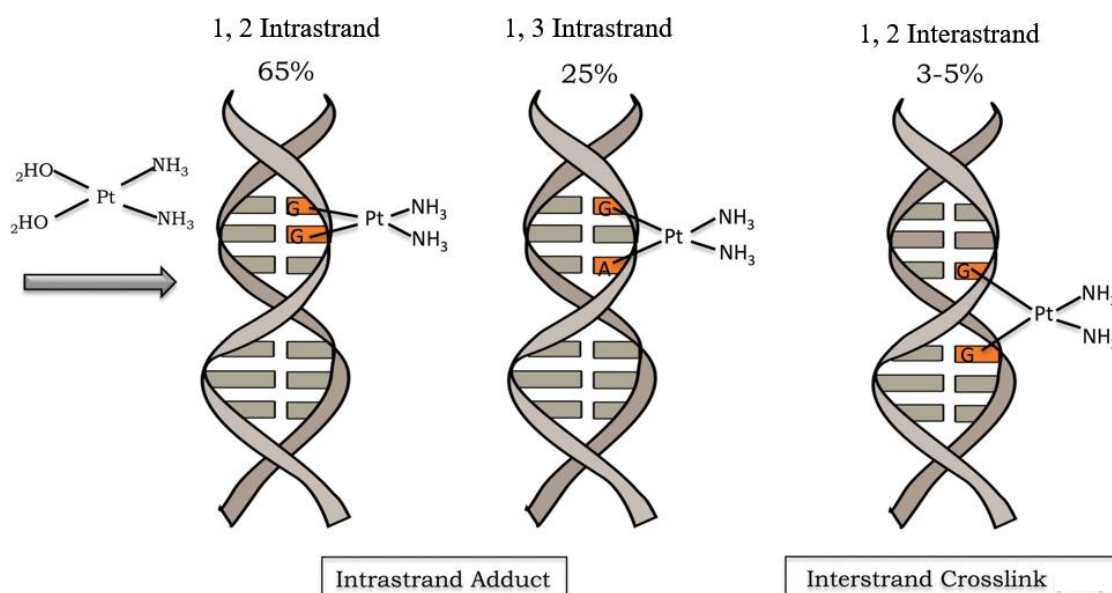


Figure 9. Cisplatin can form covalent bonds with DNA. The major DNA lesions are intrastrand DNA adducts and interstrand crosslinks. The percentages represent the frequency of each type of DNA damage induced by cisplatin (ROCHA, *et al.*, 2018).

Cisplatin and its analogues carboplatin and oxaliplatin has a mechanism of action similar to alkylating agents (KELLAND, 2007), it forms either monofunctional adducts or intra- and interstrand and DNA-protein crosslinks. Cisplatin causes severe side effects such as nephrotoxicity and is associated with resistance, especially in ovarian cancer (MAŁYSZKO, *et al.*, 2017). During therapy, resistance may be acquired or be intrinsic to the tumor due to the increased tolerance or repair of DNA damage, increased detoxification of cisplatin in the cytoplasm and decreased membrane transport into the cell. Carboplatin and oxaliplatin as analogues of cisplatin were introduced to overcome some of the resistance and side effects associated with cisplatin that both have the same mechanism of action as cisplatin but have different pharmacological properties (WOODS; TURCHI, 2013; ZAMBLE; LIPPARD, 1995). Side effects associated with the platinum drugs as well as tumor resistance limits their use clinically which has been further restricted by their poor solubility (1 mg/mL). However clinical success of cisplatin has not only led to the development of platinum-based drugs, but also other transition metals expecting more efficient in pharmacological, greater drug-to-patient survival, low clinical costs, less side effects and interacting with DNA differently, surpassing the inherent or acquired resistance to cisplatin (CHOVANEC, *et al.*, 2017, ELJACK, *et al.*, 2014).

1.7 Copper-based complexes.

Copper is an essential element for cell growth and development and is vital to proteins involved in many biological pathways such as mitochondrial respiration, and DNA synthesis. Copper complexes generally show an enhanced anti-proliferative activity (WANG, *et al.*, 2016). The cytotoxic effects of copper complexes based on the assumption that the study of endogenous copper may be less toxic to normal cells than cancer cells are (SANTINI, *et al.*, 2014).

Copper compounds act as anticancer agents where their modes of action differ to that of cisplatin and its counterparts and are active against platinum resistant cell lines (MASSIMILIANO DAIUTO, 2014). The properties of the copper coordination compounds are determined by the nature of the ligands and the donor atoms coordinated to the metal ion. The variety of accessible arrangements allows a wide choice of ligands and donor atoms (N, O, S, and halogens) (TISATO, *et al.*, 2010). The redox potential of the physiologically accessible $\text{Cu}^{1+}/\text{Cu}^{2+}$ (reduced cuprous/oxidized cupric) pair varies dramatically depending on the coordination environment, due to the type of donor, geometry, electronic and stereo effect of the substituent and chelation (MORO-OKA, 1999).

Cu^{2+} -complexes have been shown to possess a broader spectrum of antitumor activity and lower toxicity than platinum drugs and are suggested to be able to overcome inherited and/

or acquired resistance to cisplatin (DENOYER, *et al.*, 2018, SANTINI, *et al.*, 2014). Cu^{2+} -complexes can bind to DNA and act as chemical nucleases, capable of breaking the DNA molecule, leading to cell cycle disruption and apoptosis (RAMAN; SOBHA, 2012). DNA cleavage can occur by oxidation of the nucleobase, hydrolysis of the phosphate ester, or by the oxidation of deoxyribose sugar. Generally, the nuclease activity of Cu^{2+} -complexes is observed in the presence of oxidizing or reducing agents. This oxidative cleavage of DNA is believed to occur through Fenton chemistry, involving the generation of ROS ($\text{Cu}^+ + \text{H}_2\text{O}_2 \rightarrow \text{Cu}^{2+} + \text{OH}^- + \text{OH}\cdot$) (COLLIN, 2019, O'CONNOR, *et al.*, 2012). On the other hand, there are several Cu^{2+} -complexes capable of cleaving the DNA through a hydrolytic mechanism (MANIKANDAMATHAVAN, *et al.*, 2011, NUNES, *et al.*, 2015). In addition to DNA, other cellular components, such as topoisomerases or the proteasome, cyclooxygenases, and mitochondria are emerging as new targets of Cu^{2+} -complexes (BOODRAM, *et al.*, 2016, WILSON, *et al.*, 2016, ROCHFORD, *et al.*, 2020).

In recent years, several families of Cu^{2+} -complexes have been studied as potential antitumor agents. Cu^{2+} -complexes have been largely investigated as an alternative class of cancer therapeutics but to date, only two Cu^{2+} -complexes have reached phase I clinical trials (GALIN DOMURILLO, *et al.*, 2015). In contrast to Pt drugs, which covalently bind DNA nucleobases, copper derivatives predominantly form non-covalent interactions with DNA either via intercalation, electrostatic forces of attraction and/or major or minor groove binding (discussed in 1.6 section).

As noted earlier, Sigman *et al.*, Pioneered research in the late 1970s on Cu^{2+} -complexes as potential agents of chemical nuclease when they developed $[\text{Cu}(\text{phen})_2]^{2+}$ capable of inducing oxygen dependent DNA cleavage (SIGMAN, *et al.*, 1979). An extensive number of Cu-phen derivatives have since been investigated many of which exhibit potent anticancer activities.

There are numerous examples in the literature of Cu^{2+} -complexes with remarkable anticancer activity.

Mohammadizadeh *et al.* (2018) reported the synthesis of a novel Cu^{2+} -complex $[\text{Cu}(\text{L})(\text{phen})]$ which is (1,10-phenanthroline)[4-bromo-2-((5-chloro-2-hydroxyphenyl)imino) methyl]phenol]copper²⁺. Effect of $[\text{Cu}(\text{L})(\text{phen})]$ on MCF-7 and L929 (normal subcutaneous adipose tissue of mouse) cell line showed the IC_{50} value of 17 μM and 38 μM against MCF-7 and L929 cell line (breast and normal subcutaneous adipose tissue of mouse), respectively. IC_{50} values for MCF-7 were significantly lower than L929. This result showed that normal cells were less sensitive than cancerous cells to the complex. It means the $[\text{Cu}(\text{L})(\text{phen})]$ can selectively inhibit the growth of the MCF-7 cancerous cells. Furthermore, the cells were treated by IC_{50} of $[\text{Cu}(\text{L})$

(phen)] for 24 h and apoptosis were also tested by Annexin V-fluorescein isothiocyanate (FITC) and propidium iodide (PI). The results demonstrated that the [Cu(L)(phen)] complex triggered cell death via apoptosis compare to different Cu²⁺-complexes with mixed ligands especially, phen containing complexes (BRAVO-GÓMEZ, *et al.*, 2009, CORREIA, *et al.*, 2015, DEEGAN, *et al.*, 2007, DEVEREUX, *et al.*, 2006) that were reported to induce programmed cell death (apoptosis) in cervical and breast cancer cell lines (JAIVIDHYA, *et al.*, 2012), we could expect that [Cu(L)(phen)] complex possess the potential for development as an anticancer drug for human breast cancer (MOHAMMADIZADEH, *et al.*, 2018).

Among the Cu²⁺-complexes containing N and O-donor ligands, casiopeinas are the most representative Cu²⁺-complexes with antitumor potential, tested *in vitro* and *in vivo* models (CARVALLO-CHAIGNEAU *et al.*, 2008; RUIZ-AZUARA; E. BRAVO-GOMEZ, 2010). The casiopeinas are of the general formula [Cu (N-N) (O- O)] NO₃ or [Cu (N-N) (N-O)] NO₃, where N-N is a substituted aromatic diimine (1,10 -phenanthroline (phen) or 2,2'-bipyridine (bpy), N-O is an essential amino acid or peptide and OO is acetylacetonate or salicylaldehyde. The casiopeina [Cu(L)(acetylacetonate)]NO₃, with L=(4,4'-dimethyl-2, 2'-bipyridine), named casiopeina III, has been one of the most investigated prototypes of a wide series of similar complexes (BRAVO-GÓMEZ *et al.*, 2009). Casiopeina III showed promising *in vivo* activity against xenografts of HCT-15 colorectal cancer cells (CARVALLO-CHAIGNEAU *et al.*, 2008). The relative tumor volume of rats bearing HCT-15 cells showed slow growth, compared to control animals when treated with casiopeina III (6 mg/kg, every 4 days until 6 doses). In addition, treatment with casiopeina III resulted in cell death by induction of apoptosis. Unfortunately, histological analysis revealed a chronic, complex-induced irritative effect for peritoneal necrosis (CARVALLO-CHAIGNEAU *et al.*, 2008). The casiopeinas were explicitly designed to interact with genetic material, producing oxidation and DNA fragmentation, through the generation of ROS after copper reduction (SERMENT-GU-ERRERO , *et al.*, 2011). The synthetic study in casiopeina-like compounds has focused on the use of the phen ligand to generate an N6-donor ligand [2,9-bis(2',5'-diazahexanyl)-1,10-phenanthroline]. The corresponding complex was shown to be cytotoxic against HeLa (cervical cancer cell line) (IC₅₀ = 1.84 μM) (GARCÍA-RAMOS, *et al.*, 2012).

Schiff bases derived from an amino and carbonyl compound belong to an important class of ligands that coordinated to metal ions. The Schiff base coordinated with Cu²⁺-complexes shows the considerably high anticancer activities (CHAVIARA *et al.*, 2004; PONTIKI; HADJIPAVLOU-LITINA; CHAVIARA, 2008). Yan Xia *et al.* (2019) synthesized Schiff base copper coordinated compound SBCCC, considered its effect on human gastric cancer cell lines,

SGC 7901 and BGC823. The IC_{50} of SBCCC in SGC-7901 and BGC-823 cells was 1 μM , and compound induces apoptosis and causes cell cycle arrest at the G1 phase. SBCCC induces apoptosis via multiple pathways including inhibition of nuclear factor kappa B (NF- κ B), ROS production and autophagy (XIA, *et al.*, 2019). Maheswari *et al.* (2005) synthesized $[\text{Cu}^{2+}(\text{pyrimol})\text{Cl}]$ a Cu^{2+} -complex with a Schiff base as a ligand (Hpyrimol). The water soluble Cu^{2+} -complex, may catalytically bind the DNA, in the absence of reducing agents, by intercalating the planar structure of the complex in the DNA base pairs. This complex also showed high cytotoxicity in murine leukemia cells (L1210) cisplatin-sensitive and (L1210) cisplatin-resistant. As well as human ovarian carcinoma cells (A2780), cisplatin-sensitive and (A2780) cisplatin-resistant. The IC_{50} (μM) values for cell lines (L1210) cisplatin-sensitive, (A2780) cisplatin-sensitive and (A2780) cisplatin resistant illustrate 3.6 ± 0.2 , 3.4 ± 0.2 and 8.3 ± 0.6 , respectively that are in the range of that observed for IC_{50} (μM) of cisplatin 2.3 ± 0.3 , 2.3 ± 0.2 , 7.5 ± 0.2 . In addition, (L1210) cisplatin-resistant showed IC_{50} (μM) = 10.3 ± 0.3 , which is more active than IC_{50} (μM) of cisplatin 14.2 ± 0.2 (MAHESWARI, *et al.*, 2006). These results are promising for a potential clinical program because the activity of this Cu^{2+} -complex is comparable to that of cisplatin drug.

As the level of prostaglandin found in tumor cells is much higher than normal cells, the non-steroidal anti-inflammatory drugs (NSAIDS) coupled with active Cu^{2+} metal centers may play a combined role in the cytotoxic activity of these metal compounds (TAN, *et al.*, 2010). NSAIDS inhibit the action of prostaglandins by inhibiting cyclooxygenase (COX) activity of the enzyme prostaglandin G/H-synthase. The Cu^{2+} -complexes of salicylic acid $[\text{Cu}(\text{sal})(\text{phen})]$ and $[\text{Cu}(3\text{-MeOsal})(\text{phen})] \cdot \text{H}_2\text{O}$ {where 3-MeOsal=3-methoxysalicylic acid} reported by O'Connor *et al.* (2012) have shown significant cytotoxic activity against MCF-7, prostate (DU145), cisplatin resistant ovarian (SK-OV-3), and colon (HT29) cancer cell lines. The IC_{50} (μM) reported after 24 h treatment by $[\text{Cu}(\text{sal})(\text{phen})]$ described as 49.3 ± 2.1 in MCF-7, 7.8 ± 1.2 in DU145, 7.1 ± 0.5 in SK-OV-3 and 11.2 ± 2.1 in HT29. Moreover, the cells treated 24 h by $[\text{Cu}(3\text{-MeOsal})(\text{phen})] \cdot \text{H}_2\text{O}$ exhibited the IC_{50} (μM) of 47.5 ± 3.0 , 8.4 ± 0.9 , 9.2 ± 0.6 and 12.9 ± 3.4 in MCF-7, DU145, SK-OV-3 and HT29. In addition, the DNA studies concluded that the compounds have a high affinity for binding to DNA through an intercalation mode of binding and have the ability to induce relaxation of the supercoiled DNA (O'CONNOR, *et al.*, 2012). Similarly, the Cu^{2+} -complexes of piroxicam and meloxicam induced cytopathological changes, including DNA damages in HeLa and 8MGBA (glioma cancer cell line) treated cells and showed a significant decrease of their viability and proliferation (DYAKOVA, *et al.*, 2015).

Imidazo[1,2-a]pyridines have been reported as potential anticancer agents in the literature. Copper 6-bromo-N-cyclohexyl-2-(pyridin-2-yl)imidazo[1,2-a]pyridin-3-amine acetate (JD88), was synthesized by Dam et al. (2017) (DAM et al., 2017). Then, Leonie Harmse et al. (2019) reported the effect of this copper-imidazo[1,2-a]pyridines complex (JD88) showing high cytotoxicity effect against HT-29 cells with an IC_{50} value lower than 1 μ M. Treatment of HT-29 cells with the JD88 after 24 h resulted in fragmented nuclei suggestive of apoptotic cell death, which was confirmed by increased annexin V binding and caspase-3/7 activity. The Cu^{2+} -complex JD88, caused a loss of mitochondrial membrane potential and increased caspase-9 activity. The absence of caspase-8 activity indicated activation of the intrinsic apoptotic pathway (HARMSE, *et al.*, 2019).

Thiosemicarbazones (TSCs), and their copper derivatives, have been extensively studied mainly due to the potential applications as antitumor compounds. Pahontu et al. (2016) reported new Cu^{2+} -complexes, $[Cu(L)(H_2O)_2(OAc)]$, $[Cu(HL)(H_2O)_2(SO_4)]$, $[Cu(L)(H_2O)_2(NO_3)]$, $[Cu(L)(H_2O)_2(ClO_4)]$, $[Cu(L)_2(H_2O)_2]$, were synthesized from 8-ethyl-2-hydroxytricyclotridecan-13-one thiosemicarbazone (HL) with IC_{50} (μ M) of >10 , 1.6 ± 3 , 6.4 ± 5 , 6.5 ± 4 and 14.2 ± 3 , respectively, against HL-60 leukemia cells after 24h. The Cu^{2+} -complexes $[Cu(HL)(H_2O)_2(SO_4)]$, including the bidentate NS ligand and sulfato group, demonstrate an important cytotoxicity activity for HL-60 cells compared to the other and inhibit malignant HL-60 cell growth by IC_{50} of 1.6 μ M after 24 h (PAHONȚU, *et al.*, 2016). García et al reported the synthesis of $[Cu(PTSC)(ONO_2)]_n$ compound, (PTSC=pyridine-2-carbaldehydethiosemicarbazone) that showed IC_{50} (μ M) of 5.48 ± 0.79 exhibiting potent activity against the SW480 human colon carcinoma after 24 h (GARCÍA-TOJAL, *et al.*, 2018). The experimental results indicate that the TSCs and their copper derivatives could be candidates for further developments as potential anticancer drugs.

GAMA et al. (2011) synthesized three complexes of Cu^{2+} : chloro [N-(2-hydroxy benzyl-2-pyrazoloyl) imine] Cu^{+2} ; bis (-chloro) bis [N- (2-hydroxy-3, 5-dichloro benzyl-2-pyrazoloyl) imine] Cu^{+2} and; chloro [N- (2-hydroxy-3, 5-diiodo benzyl-2-pyrazoloyl) imine] Cu^{+2} . All of them exhibited moderate cytotoxicity after 24 h of incubation, in human tumor cell lines, prostate cancer (PC3) with IC_{50} (μ M) of 365 ± 51 , 196 ± 18 and 95 ± 40 , for 1, 2 and 3, respectively. For MCF-7 these three complexes showed an IC_{50} (μ M) of 247 ± 47 , 97 ± 22 and 78 ± 23 in chloro [N-(2-hydroxy benzyl-2-pyrazoloyl) imine] Cu^{+2} ; bis (-chloro) bis [N- (2-hydroxy-3, 5-dichloro-benzyl-2-pyrazoloyl) imine] Cu^{+2} and; chloro [N-(2-hydroxy-3, 5-diiodo benzyl-2-pyrazoloyl) imine] Cu^{+2} , respectively (GAMA, *et al.*, 2011).

2. Justification

Increasing life expectancy and modern living habits have led to cancer becoming the second leading cause of death from disease in the world. For this reason, this disease has become the focus of health surveillance in developed and developing countries. About 70% of cancer patients require chemotherapy treatment. Antitumor drugs commonly used in medical practice generally lack the ability to fight cancer cells without affecting normal tissues (ASLAM, *et al.*, 2014). As a result, it has a number of side effects and greatly weakens the body. Such organic weakness often leaves the body vulnerable to opportunistic diseases and may lead the patient to death. In addition, many tumor types are resistant to currently available treatments, which is one of the major obstacles to antitumor therapy (HAYES, 2004). In this context, a permanent search for more effective treatments becomes necessary. While many chemotherapeutic drugs are organic-based, the discovery of the anticancer properties of cisplatin by Barnett Rosenberg in 1965 and its subsequent introduction into the clinical stage as an anticancer agent in 1978, give rise to research into the use of metal-based drugs as an alternative class of anticancer agent (ROSENBERG, *et al.*, 1969). Based on the discovery of cisplatin's antitumor properties, studies around the development of new antineoplastic potential coordination compounds have been developed over the years. The use of essential metals in the synthesis of new compounds aims to achieve less toxicity to body tissues not affected by cancer. In addition, the use of combined chemotherapy is common in order to decrease the concentrations used and consequently the collateral damage caused.

Complexes of other transition metals are being actively explored as alternative classes of chemotherapeutics. While the copper complexes reported to date have demonstrated enormous potential as anticancer agents, there remains a need for a more systematic, targeted and multidisciplinary approach if a copper complex is to translate from academic research into the clinical setting.

3. Objective

The current study deals with the effects of two novel Cu^{+2} -complexes $[\text{Cu}_2(\mu\text{-CH}_3\text{COO})(\text{OH}_2)(\text{L}_2)] \cdot 1\frac{1}{2}\text{H}_2\text{O}$ (R9) and $[\text{Cu}_2(\mu\text{-OH})(\text{OH}_2)(\text{HL}_2)]\text{ClO}_4 \cdot 2\text{H}_2\text{O}$ (R10) in different cancer cell lines MCF-7, A549 and PC3. We studied the cytotoxicity and genotoxicity impact of R9 and R10 on cancer cells after 24 h of treatment to detect their mechanism of action.

Specific objectives:

- Evaluate the effects of Cu^{+2} -complexes on viability of cancer cell lines by MTT assay;
- Assess the morphology and granularity changed via light field microscope and flow cytometry assay;
- Evaluate mitochondrial membrane potential by spectrofluorimeter;
- Estimate intracellular ROS level via flow cytometry assay;
- Evaluate cell cycle arrest via flow cytometry assay;
- Evaluate activity of Caspase 8 and 9 through caspases kit by spectrofluorimeter;
- Evaluate DNA degradation via TUNEL assay;
- Assess the possibility of DNA binding by competition with propidium iodide;
- Assess antitumor activity *in vivo*;
 - Evaluate of toxicity of R9 in *Galleria mellonella*;
 - Evaluate of toxicity of R9 in in BALB/c mice;
- Analysis of differential protein expression of MCF-7 cells treated with R10 by proteomics;
- Obtain the proper mechanism action of novel Cu^{+2} -complex derivatives;

4. Materials and methods

4.1 Culture and maintain the Cells.

The human breast (MCF-7), lung (A549) and prostate (PC3) cancer cell lines were obtained from the Cell Bank of Hospital Universitário Clementino Fraga Filho, UFRJ, Brazil. Cells were maintained in DMEM (Dulbecco's Modified Eagle's Medium, Sigma-Aldrich), containing 4.5 g/L glucose, 0.32 g/L L-glutamine, and supplemented with 1.65 g/L sodium bicarbonate and penicillin-streptomycin (1%) (Gibco). DMEM was supplemented with 10% (v/v) FBS (fetal bovine serum; Gibco) in order to reduce the concentration of dimethyl sulfoxide (DMSO) below 1%. All solutions remained stable stored in the refrigerator at 4°C for the period of approximately 45 days or in the freezer from -25 to -5°C, for an indefinite period. Cells were cultured at 37°C in a humid atmosphere containing 5% CO₂. To avoid the use of aged cells, the culture medium was exchanged every 48 h with cells being trypsinized (trypsin 0.05%) and transferred to a new bottle or experimental plate when reaching 80% confluence. In all experiments, we used less than 20 passages of the cells (each tube of thawed cells was maintained for a maximum of 20 trypsinization). MCF10A cells (human mammary epithelial cell line) were cultured in DMEM /Ham's F-12 (GIBCO-Invitrogen, Carlsbad, CA) supplemented with 100 ng/mL cholera toxin, 20 ng/mL epidermal growth factor (EGF), 0.01 mg/mL insulin, 500 ng/mL hydrocortisone, and 5% chelex-treated horse serum. All of the growth factors were purchased from Sigma (St. Louis, MO, USA). MCF10A cells were subjected to no more than eight passages in culture when used in experiments.

4.2 Copper-based coordination compounds used in the study.

The non-symmetrical ligand *N*-isonicotinoyl-2-hydroxy-3-[(2-hydroxybenzyl)(2-pyridyl methyl)amino]methyl}-5-methyl benzaldehyde hydrazone (H₃L1) (Figure 10A), coordination compounds [Cu₂(μ-CH₃COO)(OH₂)(L₂)]·1½H₂O (R9) (Figure 10B) and [Cu₂(μ-OH)(OH₂)(HL₂)] ClO₄·2H₂O (R10) (Figure 10C), were synthesized by the group of Professor Nicolas Adrián Rey from the Pontifícia Universidade Católica do Rio de Janeiro (PUC-RJ) (RAFAELA DOS SANTOS MORAES; NICOLÁS ÁDRIAN REY, 2016). The chemotherapeutic drug cisplatin (Sigma, P4394-1G) was used as a positive control. Cisplatin was diluted directly into DMEM medium supplemented with 10% FBS plus penicillin-streptomycin and fresh solution prepared before each experiment. R9 and R10 compound where prepared in 100% DMSO and then diluted so

that final concentration did not exceed 1%. Stock solutions of compounds were made at a concentration of 1 mg/mL and stored in the refrigerator for up to 3 months. Doxorubicin and menadione were used as a control for determination of intracellular reactive oxygen species (ROS) and was diluted in DMEM medium, supplemented with 10% FBS plus penicillin-streptomycin, and fresh solution prepared before each experiment.

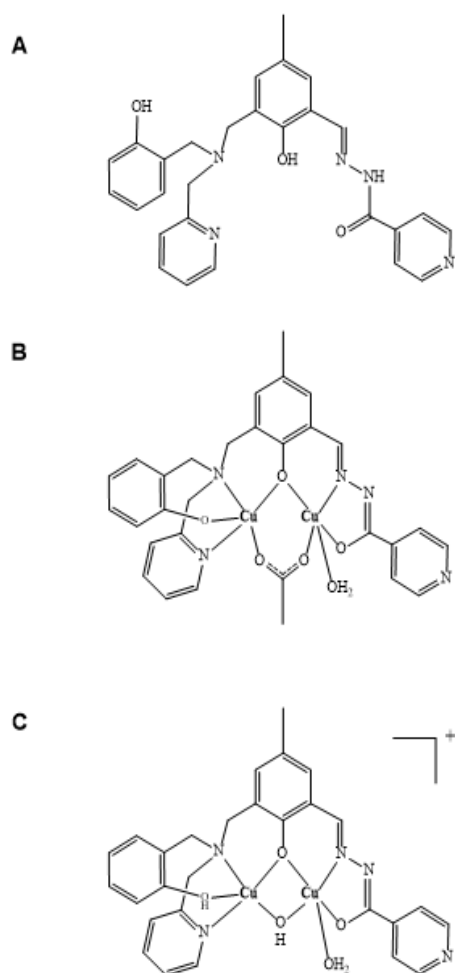


Figure 10. Schematic structures of H₃L1, R9 and R10. H₃L1 (A) ligand structure and structural proposals for complexes R9 (B) and R10 (C).

4.3 Determination of R9 and R10 cytotoxicity.

Cellular metabolic activity of MCF-7, A549 and PC3 was performed on the basis of the reduction of MTT (3-(4,5-dimethylthiazol-2-yl)-2,5-diphenyltetrazolium bromide, Sigma-Aldrich Co., St. Louis, MO, USA) to formazan crystals as described by (DENIZOT; LANG, 1986). The reaction of MTT reduction to formazan purple crystal is mediated by the enzyme mitochondrial succinate dehydrogenase. Cells (1.0×10^4 cells/well) were seeded in 96-well plates and cultured until confluence. In all experiments, the number of cells in the culture flasks was determined by counting in optical microscope using trypan blue. Cells were incubated at 37 °C and 5% CO₂ for 24 h. Then, the culture medium DMEM was replaced with fresh DMEM

medium supplemented with FBS (10% V/V) containing different concentrations of the complexes (0.5, 1, 1.5, 2, 2.5, 3 μ M) and the cisplatin positive control at the concentrations of 1, 5, 10, 15, 20, 30, 40 μ M. The H₃L1 ligand and copper chloride, used for the synthesis of the copper complexes, were also tested at the mentioned concentrations. The cytotoxicity of DMSO, used in the complex dilution, was evaluated at concentrations of 0.5 and 1%. After 24 h, cells were incubated with 100 μ L of a 0.5 mg/mL MTT solution in DMEM medium for 3 h. Cells were incubated in the dark for proper reduction of MTT and formation of formazan crystals. Thereafter, the formazan crystals were dissolved in DMSO (100 μ L/well), and the absorbance was measured at 570 nm using a microplate reader PowerWave HT (SpectraMax Gemini XPS 190, Molecular Devices, CA, USA). All treatment conditions were done in quadruplicate and absorbance values were expressed as percentage of viability when compared to cells without drug treatment. The IC₅₀ was defined as the concentration of the compounds required to reduce the viability of treated cells to 50 % in comparison to untreated control cells. The IC₅₀ (half maximal inhibitory concentration) was calculated by non-linear logarithmic regression using GraphPad Prism 7.0 software. Results were calculated from the mean \pm standard deviation of three independent experiments.

MCF10A cells (American Type Culture Collection, Manassas, VA) were cultured in DMEM/Ham's F-12 (GIBCO-Invitrogen, Carlsbad, CA) supplemented with 100 ng/mL cholera toxin, 20 ng/mL epidermal growth factor (EGF), 0.01 mg/mL insulin, 500 ng/mL hydrocortisone, and 5% chelex-treated horse serum. All of the growth factors were purchased from Sigma (St. Louis, MO, USA). MCF10A cells were subjected to no more than 10 passages in culture when used in experiments. Cells (1.0×10^4 cells/well) were seeded in 96-well plates and treated with different concentrations of the complexes R9 and R10 (0.5, 1, 2, 5, 10, 15 μ M) and the cisplatin positive control at the concentrations of (1, 5, 10, 15, 20, 30, 40 μ M). MTT assay was performed as previously described.

4.4 Assessment of cancer cell morphology.

To evaluate and detect some possible cell morphologic alterations, MCF-7 and A549 cells (5.0×10^5 cells/well) were seeded in 6 well plates and cultured in DMEM supplemented with 10% FBS for 24 h. Then, cells were treated with 1 μ M copper coordination compounds, R9 and R10. After 24 h, the morphological changes of the cells were obtained with the Eclipse E200 light field microscope (Nikon, Japan) and compared to control (untreated cells). Cell morphology was evaluated after cells trypsinization and wash step (2x) with PBS. The granularity was measured by fluorescence analysis on a flow cytometer (BD FACSCalibur™) where

10,000 events were counted per sample. Histograms were obtained using WinMDI software version 2.9. Side scatter and forward scatter of light refraction differentiate the size and granularity within the cell populations. The results obtained from mean fluorescence intensity of two parameters size (FSC) and complexity (granularity) (SSC).

4.5 Evaluation of changes in mitochondrial membrane potential ($\Delta\Psi_m$).

The loss of mitochondrial electrochemical potential gradient ($\Delta\Psi_m$) is known as an early event in apoptosis (SMILEY et al., 1991). Using the cationic, lipophilic dye, JC-1 (5,5',6,6'-tetrachloro1,1',3,3'-tetraethylbenzimidazolocarbo-cyanine iodide), facilitate the detection of changes in mitochondrial inner membrane electrochemical potential in living cells and therefore, is suitable for apoptotic cell detection. In normal cells, due to the electrochemical potential gradient, the dye concentrates in the mitochondrial matrix where it forms red fluorescent aggregates (J-aggregates) where the emission is 590 nm (red fluorescence). Any event that dissipates the mitochondrial membrane potential prevents the accumulation of JC-1 dye in the mitochondria and thus, the dye is dispersed throughout the entire cell leading to a shift from red (J-aggregates) to green fluorescence (JC-1 monomers), where the emission is 530 nm (green fluorescence) (Figure 11). Consequently, mitochondrial depolarization is shown by a decrease in the fluorescence intensity ratio (red/green). The MCF-7 and A549 cells were transferred to 6 well plates in a final volume of 2,000 μL per well, representing 5.0×10^5 cells per well. After 24 h, the cells were treated with R9 and R10 at the concentration of $\frac{1}{2}\times\text{IC}_{50}$, IC_{50} and $2\times\text{IC}_{50}$ (0.5, 1 and 2 μM) and cisplatin, as a standard chemotherapy drug, at a concentration of IC_{50} of cisplatin on MCF-7 (14 μM) and A549 (32 μM). After 24 h the cells were trypsinized and washed twice with PBS. The supernatant was discarded and the cells resuspended in reaction medium containing 125 mM sucrose, 65 mM KCl, 10 mM HEPES/ K^+ , pH 7.2, 2 mM Pi, 1 mM MgCl_2 , and 500 μM EGTA. In sequence, cells were incubated with 10 $\mu\text{g}/\text{mL}$ JC-1 for 30 min with readings every minute in a spectrofluorometer (SpectraMax Gemini XPS, Molecular Devices, CA, USA). Cells were incubated with carbonyl cyanide-4-(trifluoromethoxy) phenylhydrazone (FCCP) (1 μM), a mitochondrial protonophore, as a positive control of mitochondrial depolarization. After 30 min, to remove $\Delta\Psi_m$, FCCP (1 μM) was added to all systems (including control) of final concentration of 2 μM . The relative $\Delta\Psi_m$ value was obtained calculating the ratio between the reading at 590 nm and the reading at 530 nm (590:530 ratio). Histograms for measuring the loss of red fluorescence indicating cells with altered mitochondrial membrane potential were obtained using GraphPad Prism 7.0 software.

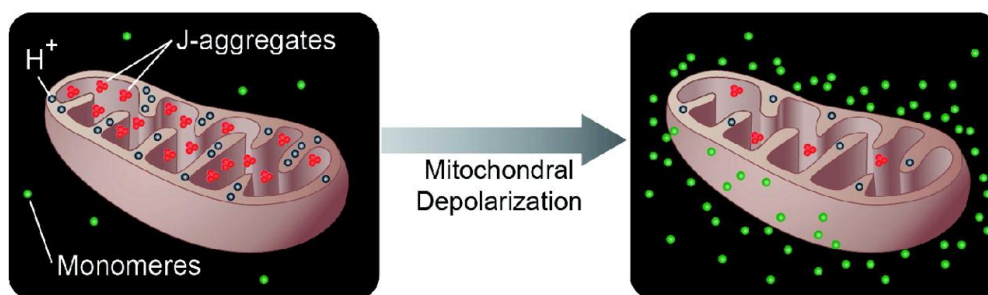


Figure 11. Analysis of the mitochondrial membrane potential using the fluorescent probe cationic JC-1 dye (SAKAMURU; ATTENE-RAMOS; XIA, 2016).

4.6 Evaluation of ROS production.

Analysis of the intracellular oxidation/ROS production was performed using the fluorescent probe, 2',7'-dichlorofluorescein diacetate (H₂DCFDA), as described by Wang and Yi, 2008 (WANG; YI, 2008). Cellular ROS levels can be measured in live cells by the conversion of H₂DCFDA to a fluorescent dye 2',7'-dichlorofluorescein (DCF) (Figure 12). The fluorescence generated is directly proportional to the amount of oxidized H₂DCFDA to DCF. Since the emission of the fluorescent dye is about 529 nm, it can be measured in the FL-1 green channel by flow cytometry. Cells (5.0×10^5 cells/well) of MCF-7 and A549 lineages were seeded in 6 well plates and grown in DMEM supplemented with 10% FBS for 24 h. After this period, cells were treated with the 0.5, 1 and 2 μ M R9 and R10. Doxorubicin (200 μ g/mL) and menadione (30 μ M) were used as a positive control. After 24 h, cells were trypsinized and washed twice with PBS. Cells were centrifuged for 5 min at 2,000 rpm and the pellet resuspended with 200 μ l of a 5 μ M solution of H₂DCFDA diluted in PBS and incubated for 30 min. Fluorescence measurement was performed on a flow cytometer (BD FACS Calibur™) where 10,000 events were counted per sample. Histograms were obtained using Flowing software version 2.5.1. The results were calculated based on side scatter of light refraction (SSC) versus green fluorescence intensity (FL1).

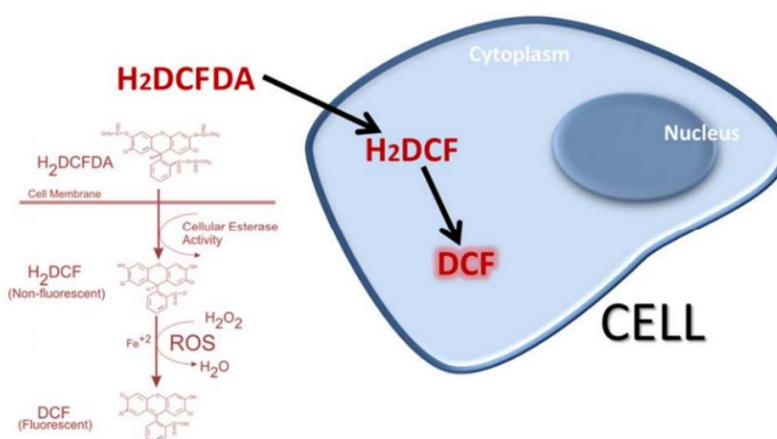


Figure 12. Oxidation of H₂DCFDA by ROS (adapted from AG scientific, [https://agscientific.Com /ros](https://agscientific.Com/ros)).

4.7 Cell cycle analysis and DNA fragmentation.

The DNA fragmentation in apoptotic cells translates into a low fluorescence intensity in Sub-G1 phase compared with cells in G1 phase of the cell cycle (NICOLETTI et al., 1991). The intensity of fluorescence captured by the flow cytometer is directly proportional to the amount of DNA in each cell phase (GONG; TRAGANOS; DARZYNKIEWICZ, 1994; NUNEZ, 2001). Thus, the highest proportion of cells in the G1 phase is characterized by the largest peak in the histogram graph. The S phase is characterized by DNA replication, does not form a well-defined peak and lies between the G1 and G2/M phase of the histogram. The G2/M phase represents twice the fluorescence intensity of the G0 phase, thus double of DNA in S phase before mitosis is complete. The Sub-G1 phase, which has a lower fluorescence intensity due to DNA fragmentation, is determinant for the identification of apoptotic cells (Figure 13).

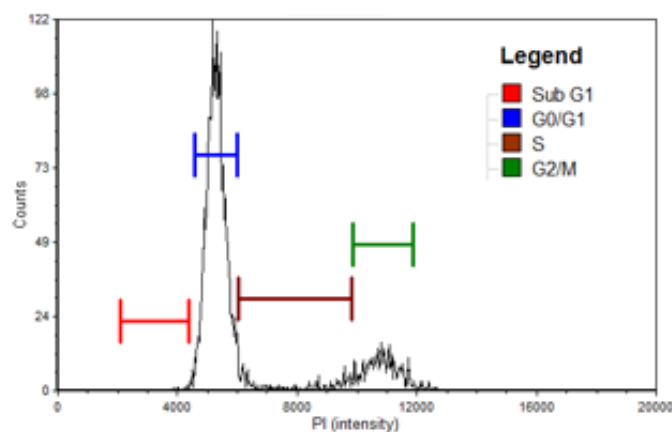


Figure 13. Different phases of cell cycle. Cell cycle analysis is used to determine the proportion of cells in each stage of the cell cycle for a given cell population based on variations in DNA content. Sub-G₁ population is indicated in red. G₀/G₁ population is in blue, S phase population is in brown, and G₂/M phase population is in green (adapted from <https://www.nexcelom.com/fluorescence-based-cell-cycle-analysis>).

In order to determine the changes on the cell cycle of MCF-7 and A549 cells induced by R9 and R10, cells were treated or not with Cu²⁺-complexes and incubated in the presence of propidium iodide PI prior to the analysis by flowcytometry. MCF-7 and A549 cells were transferred to 6 well plates at a concentration of 5.0×10^5 cells/well in a final volume of 2,000 μ L per well. After 24 h, after reaching confluence, the cells were treated with copper coordination compounds at concentrations of IC₅₀ (1 μ M) or cisplatin at the concentrations of 14 μ M (IC₅₀ of cisplatin on MCF-7 cell) and 32 μ M (IC₅₀ of cisplatin on A549 cell). After 24 h the cells were trypsinized and washed twice with PBS (phosphate buffered saline pH 7.4). The cells were resuspended in 0.5 mL of PI (100 mg/mL in PBS) containing RNase A (248 U/mL),

and the mixture was incubated for 20 min in the dark at room temperature. The fluorescence intensity of PI was analyzed with a FACS Calibur (BD Biosciences BD FACSCalibur™) flow cytometer where 10,000 events were counted per sample. Histograms and percentages of cells in Sub-G1 as well as G1, S and G2/M phases were obtained through Flowing software version 2.5.1. The graphs were plotted using GraphPad Prism 7.0 software.

4.8 Induction of DNA fragmentation by TUNEL (apoptosis).

Analysis of DNA fragmentation was performed using the TUNEL technique (Terminal deoxynucleotidyl transferase dUTP nick end labeling) using the Promega Fluorimetric Kit (G3250) according to (GAVRIELI; SHERMAN; BENSASSON, 1992; MURATORI et al., 2000). The methodology is based on the addition of fluorescein-labeled dUTP to the 3'ends of the fragmented DNA by the action of the enzyme rTdT (recombinant terminal deoxynucleotidyl transferase) (Figure 14). Cells from the MCF-7 and A549 were transferred to 6 well plates in a final volume of 2,000 μL /well, representing 5.0×10^5 cells/well. After 24 h, the cells were treated with the R9 and R10 at a concentration of IC_{50} (1 μM) and the IC_{50} of cisplatin on MCF-7 (14 μM) and A549 (32 μM). After additional 24 h the cells were trypsinized and washed twice with PBS. Then, cells were fixed with 1 mL of 4% paraformaldehyde in PBS for 20 min on ice, washed again with PBS and permeabilized during incubation with 70% ethanol for a period of at least 4 h and left at most one week on ice. Subsequently, the pellets were washed with PBS plus 5% FBS and resuspended in 8 μL of equilibration buffer for 5 min at room temperature. Cells were then incubated for 60 min in 200 mM potassium cacodylate, 25 mM Tris-HCl, 0.2 mM DTT, 0.25 mM BSA and 25 mM cobalt chloride buffer, 5 μL of the nucleotide mixture containing fluorescent dUTP (50 μM fluorescein-12-dUTP, 100 μM dATP, 10 mM Tris-HCl pH 7.6 and 1 mM EDTA) and 1 μL of the rTdT enzyme, the latter being substituted in the negative control by deionized H_2O . The reaction mixture was cautiously resuspended with the use of a micropipette every 15 min and 1 mL of 20 mM EDTA was added at the end. The mixture was vortexed gently and centrifuged at 3,000 rpm for 5 min. The pellet was washed twice with 0.1% Triton X-100 in PBS containing 5 mg/mL BSA and subsequently the cells were incubated with 200 μL of 10 $\mu\text{g}/\text{mL}$ propidium iodide (PI) and 200 $\mu\text{g}/\text{mL}$ RNase A. After 30 min at room temperature and protected from light, the samples were analyzed on a flow cytometer (BD FACSCalibur™) where 10,000 events were counted per sample. Histograms were obtained from the plot of red fluorescence intensity (FL3) versus green fluorescence intensity (FL1) using Flowing software version 2.5.1. The graphs were plotted using GraphPad Prism 7.0 software.

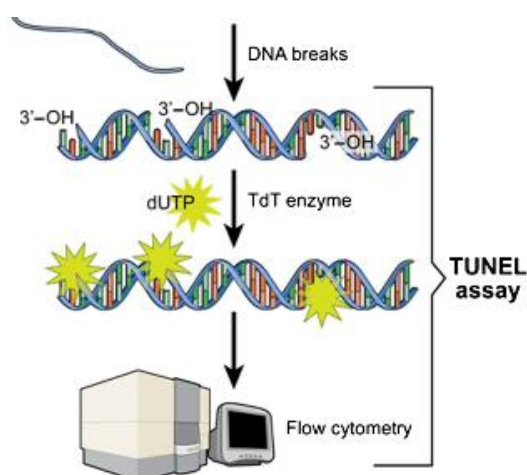


Figure 14. Demonstration of fragmented DNA from apoptotic cells with the incorporation of fluorescein-labeled dUTP by the TUNEL technique. The TUNEL technique is able to quantify the proportion of DNA fragments by binding to dUTP via TdT (MALVEZZI et al., 2014).

4.9 Determination of caspase 8 and 9 activity.

MCF-7 and A549 cells were transferred to 12-well plates at a final concentration of 2.5×10^5 cells/mL at a volume of 1,000 μ L/well (2.5×10^5 cells/well). After 24 h, cells were treated with the copper coordination compounds at a concentration of IC_{50} of cisplatin on MCF-7 (14 μ M) and A549 (32 μ M). After 24 h, cells were trypsinized and 2×10^4 cells were transferred to 96-well opaque white plate in a final volume of 50 μ L of Kit reagent (caspase-Glo® 8 assay, G8200 and caspase-Glo® 9 assay, G8210). The reaction mixture contains the substrate for caspase 8 (Z-LETD-aminoluciferin) or for caspase 9 (Z-LEHD-aminoluciferin) and luciferase enzyme. The MG-132 proteasome inhibitor that reduces the degradation of ubiquitin-conjugated proteins was also added to the reaction medium to decrease non-cell-specific reactions.

In this assay, In the absence of active caspase, the caspase substrates do not act as substrates for luciferase and thus produce no light. After the substrates have been cleaved by the corresponding caspase, aminoluciferin is released and can contribute to produce of light in a luminescence reaction (Figure 20). The resulting luminescent signal is directly proportional to the amount of caspase activity in the sample.

Fifty (50) μ L of DMEM medium plus 50 μ L of Kit reagent was used as the blank. The plates were read on the GloMax® 96 Microplate Luminometer (SpectraMax Gemini XPS, Molecular Devices, CA, USA company). Caspase activity was measured in luminescence units. The luminescence of each sample was measured in a plate-reading luminometer with parameters of 1-minute lag time and 0.5 second/well read time. The results were calculated from the signal

generated that is proportional to the amount of caspase activity present. The graphs were plotted using GraphPad Prism 7.0 software.

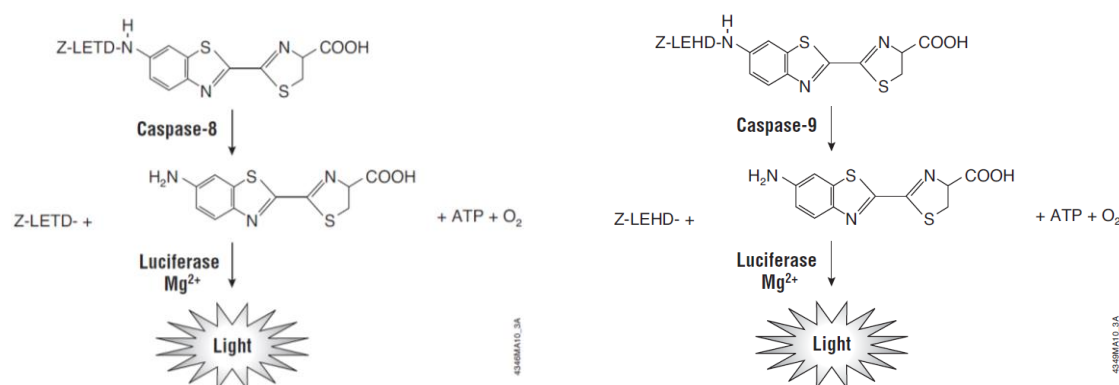


Figure 15. Caspase-8 and -9 cleavage of the pro-luminogenic substrates containing LETD/LEHD. Following caspase cleavage, a substrate for luciferase (aminoluciferin) is released, resulting in the production of light (adapted from www.promega.com.br).

4.10 Competition of Cu^{+2} -complexes with PI on DNA binding.

The DNA binding dyes can bind to the major or minor groove, may be AT or GC preferential, or may intercalate into the DNA strand itself. PI is an intercalator agent, wedges in between the base pairs in the DNA helix. In this assay, we use PI to assess the possibility of DNA binding of R9 & R10 in MCF-7 and A549 cell lines by competition with PI as an intercalating agent.

To perform this assay, MCF-7 and A549 cells (5.0×10^5 cells/well) were plated in 6-well plates. The experiments were carried out by adding of the PI (10 $\mu\text{g}/\text{mL}$) and IC_{50} concentration of R9/R10 (1 μM) to the cells. PI and each of compounds R9/R10 were added to the cells simultaneously. The cells were incubated at room temperature for 1 h. The procedure was repeated for 2 and 4 h to make sure if more incubation time has effect on binding process. Untreated cells were used as control. The fluorescence intensity of cells with PI and treated cells with PI plus R9 or R10, respectively, were measured by fluorimeter (SpectraMax Gemini XPS, Molecular Devices, CA, USA).

4.11 Evaluation of toxicity of R9 using animal models.

4.11.1 Toxicity of R9 in *Galleria mellonella* model of study.

After oviposition of great wax moths, the larvae of *G. mellonella* were obtained and maintained in the dark at 21°C with artificial diet (200 g wheat flour, 20 g wheat bran, 200 g wheat germ, 120 g beer yeast, 120 g honey, 120 g brown sugar, 400 g milk powder and 120 g

glycerol) in relative humidity $70\% \pm 10\%$ in an incubator without photoperiod. Larvae maintenance is performed periodically, in which all animals are removed from the old feed and placed into a clean box with fresh feed. To assess the cytotoxicity of R9 or cisplatin, larvae of *G. mellonella* were selected by similar size (15–20 mm), weight (approximately 200 mg) and absence of grey pigmentation. As a control, we also tested the cytotoxicity of DMSO 0.2% and DMEM in larvae of *G. mellonella*. Ten larvae were used for administration of 10 μ l of a 1 mg/mL (50 mg/kg of *G. mellonella*) of R9 or cisplatin by injection (25 μ l Hamilton syringe) into *G. mellonella* hemocoel (a body cavity that contains blood or hemolymph and functions as part of the circulatory system), via the last left pro leg. After injection, larvae were maintained in 90-mm glass dishes without artificial diet in the dark at 28°C. Survival was followed daily until 7 days and the number of larvae, pupae and wax moths were monitored until 20 days. The larvae of *G. mellonella* were considered dead when no reaction to touch was observed. Survival curve and statistics were designed using Graph Pad Prism 7 software.

4.11.2 Toxicity of R9 in BALB/c mice.

The experiments involving animals followed the welfare rules approved by the UENF Ethics and Research Committee with animals (CEUA protocol n° 349). The mice came from the UENF central animal farm, where they were confined in appropriate cages, accommodated in suitable facilities.

Toxicity was analyzed in six-week-old female BALB/c nude mice weighing approximately 20 g divided into 4 groups of 6 animals. The copper compound (R9) diluted in an excipient composed of PBS + DMSO (v/v = 23%) was inoculated intraperitoneally at concentrations of 0.8, 8 or 80 mg/kg animal. Animal mortality was verified every 24 h for 30 days. The LD₅₀ (lethal dose for 50% of mice) was calculated by nonlinear logarithmic regression analysis of the data using Graph Pad Prism 7 software.

4.11.3 Statistical analysis

The results obtained were calculated from a mean \pm standard deviation of at least 3 independent experiments. Statistical analysis was performed using GraphPad Prism version 7 software. One-way ANOVA test followed by Tukey: compare all pairs of columns or Dunnett: in order to compare the control (untreated) with the samples treated with the compounds statistical test was used for all experiments. Significant differences were considered as $P < 0.05$.

4.12 Analysis of differential expression of protein in breast cancer cells in response to R10 treatment.

The aim of proteomics used in this study was to identify the protein expression profile after treatment with R10 or cisplatin. Thus, we used proteomics to find whether a 24 h treatment with a coordination compound (e.g. R10) was able to produce a different protein expression profile in the breast cancer cell line MCF-7, compared with untreated or cisplatin-treated cells.

4.12.1 Sample preparation.

MCF-7 cells (1.0×10^6 cells/well) plated in 6 well plate was cultured under 37°C and 5% CO₂ for 24 h until confluence. Then, the culture medium DMEM was replaced with fresh DMEM medium supplemented with FBS (10% V/V) containing R10 at IC₅₀ concentration (1 μM). For comparison of protein expression profile, cells were also treated with cisplatin (14 μM). After 24 h of treatment, cells were detached from the substratum by the help of trypsin (trypsin 0.05%) (500 μl/well), then cells were collected in 1.5 mL tubes and washed 3 times with PBS (phosphate buffered saline pH 7.4). Finally, cells were maintained in 500 μl of PBS.

4.12.2 Protein digestion.

Cells were reconstituted in a mixture of 100 μl of 100 mM TEAB buffer (Triethylammonium bicarbonate buffer 1 M, pH 8.5 ± 0.1) containing 7 M urea and 2 M thiourea. Cells were disrupted by 3 cycles of 30 min freezing and 8 min of thaw in liquid nitrogen. Pellets were removed by centrifugation at 20,000 rcf for 30 minutes at 4°C and soluble proteins were transferred to fresh vials. Protein concentrations were determined using Qubit™ protein assay kit (Invitrogen) according to the manufacturer's instructions. One hundred micrograms (100 μg) of protein from each sample has taken and subjected to tryptic digestion protocol that included reduction of disulfide bonds in dithiothreitol (DTT) or (tris(2-carboxyethyl)phosphine) (TCEP) solution at a final concentration of 10 mM for 1 h at 30°C. Thiol groups were alkylated by incubating samples with iodoacetamide (IAA) solution at a final concentration of 40 mM for 1 h at room temperature in the dark. Trypsin was added at a 1:50 enzyme/protein (W/W) and digestion was carried out overnight at 37°C (16 h). The reaction was stopped by adding 10% trifluoroacetic acid (TFA) to give a final concentration of 0.1%.

For peptide cleaning, C18 spin columns were incubated with 200 μL 100% acetonitrile (ACN) for 15 min and centrifuge at 2,000 × g for 1 min. The same amount of ACN was added and the centrifugation step were repeated. Columns were equilibrated with 150 μL 0.1% TFA and centrifuged at 2,000 × g as above (this step was repeated three times). Then 75–150 μL of

each sample were added and centrifuged at 2,000 ×g as above. The columns were washed using 0.1% TFA and centrifuge at 2,000 ×g as above. The wash/centrifugation cycle were repeated three times.

The peptides were eluted in two successive steps into the same collection tube by adding 0.1% TFA/50% ACN and 0.1% TFA/70% ACN followed by centrifugation at 2,000 ×g as above. Then, the samples were dried during 4 h by vacuum centrifugation. Peptides were suspended in 30 µL of 20 mM TEAB (pH 8.5) and peptides were quantified using the Qubit 2 fluorometric assay to normalize peptide amounts in each condition (0.5 µg/mL). Each sample (0.5 µg/mL) was applied in conical vial subjected to individual analysis by LC-MS/MS analyses to protein identification and quantification.

4.12.3 Analysis by mass spectrometry.

The mixture of peptides was resuspended in 0.1% formic acid, quantified by Qubit™ protein assay kit (Invitrogen), and analyzed in triplicate using a nano- LC Proxeon EASY-nLC II coupled to a LTQ-OrbitrapVelos mass spectrometer (Thermo Scientific). Peptides (0.5 µg/mL) were loaded on to a pre-column (2 cm length, 200 µm inner diameter, packed in-house with ReproSilPur C18-AQ 5 µm resin – Dr. Maisch GmbH HPLC) and fractionated in a column (15 cm length, 75 µm inner diameter, packed in-house with ReproSilPur C18-AQ 3 µm resin – Dr. Maisch GmbH HPLC). Peptides was analyzed in technical triplicate after 3 h of gradient (5% to 40% B/167 min; 40% to 95% B/5 min; 95%B/8 min). NanoLC solvent A consisted of solvent A (95% H₂O / 5% acetonitrile (ACN) / 0.1% formic acid) and solvent B of (95% ACN / 5% H₂O / 0.1% formic acid). The full scan and MS/MS acquisition was made in a positive mode applying a data dependent acquisition (DDA). The operating parameters of the mass spectrometer were dynamic exclusion list of 90 s, spray voltage at 2.5 kV, no auxiliary gas flow and 235°C in the heated capillary. Full MS scan was acquired in 60,000 resolutions at m/z 400 in the Orbitrap analyzer. The 10 most intense ions were selected for fragmentation by Collision-Induced Dissociation (CID) with normalized collision energy of 30. MS² spectra were analyzed in the LTQ 30,000-signal threshold, and dynamic exclusion enabled for 30 s with a repeat count of 1.

4.12.4 Data analysis.

The data were analyzed with Proteome Discoverer 2.1. (Thermo Fischer, USA) using the Sequest^{HT} algorithm *Homo sapiens* database downloaded from UniProt in May 2019. Search parameters were full-tryptic hydrolysis, two missed cleavages, oxidation of methionine,

and n-terminal protein acetylation as variable and carbamidomethylation as fixed modifications, and a peptide and fragment tolerance of 10 ppm and 0.5 Da, respectively. For the processing workflow, we used the Percolator node for peptide -to-spectrum matches (PSM) validation and for setting up the false discovery rate (FDR). A cutoff score was established to accept an FDR <1%. Proteins were grouped according to the maximum parsimony approach. Protein quantification was based on the node Precursor Ion Area Detection using the sum of up to three peptide peak areas.

Comparative analyses were carried out with the program Venny 2.1 and Perseus (TYANOVA *et al.*, 2016). For the gene ontology, cellular component, biological processes, and molecular function of quantified proteins, we used the KEGG program, and Perseus (TYANOVA *et al.*, 2016; XING *et al.*, 2016). Proteins whose variation in abundance was statistically significant by student T-test, in KEGG program (Kyoto encyclopedia of genes and genomes) and GraphPad Prism 7.0 software were used for protein regulation pathways and protein-protein interaction analyses (OGATA *et al.*, 1999).

5. Results

5.1 Cytotoxic activity of two dinuclear Cu²⁺-complexes on different cancer cells lines.

In order to investigate the possible cytotoxic effects of Cu²⁺-complexes, the human cell lines representing the three high incidence cancer, lung, breast and prostate were selected for *in vitro* assay (DOGAN, 2019; REBBECK, 2017). The selected cell lines, MCF-7 (breast), A549 (lung) and PC3 (prostate), are also widely used as a model for the study of cytotoxicity of new drugs (FRANKLIN, 2018; RAZAK et al., 2019; RIBEIRO et al., 2020).

The cytotoxic activity of Cu²⁺-complexes was expressed as the half-maximal inhibitory concentration (IC₅₀). According to Figure 16 (A and B) we observed the decrease of cell survival after treatment of MCF-7, A549 and PC3 with different concentrations (0.5 to 3 μM) of R9 and R10 after 24 h. The cytotoxic activity of R9 and R10 was observed from 1 μM concentration and at the higher concentrations, whereas no detectable effect at the lowest concentration (0.5 μM) was observed. The survival of MCF10A cells, used as a control for non-cancer cell line, treated with different concentrations of Cu²⁺-complexes ranging from 0.5 to 15 μM at 24 h is illustrated in Figure 16C. Finally, in Figure 16D, we can observe the survival of MCF-7, A549, PC3 and MCF10A cells treated with cisplatin (5 to 50 μM) for 24 h. The IC₅₀ of Cu²⁺-complexes and cisplatin were calculated using the "Dose-response curves - Inhibition" equation and "log (inhibitor) vs. normalized response -- variable slope" with the aid of GraphPad Prism 7.0 software.

In Table 4, we can observe the IC₅₀ values of metal-based complexes for the A549, MCF-7, PC3 and MCF10A cell lines. As shown in the Table 4, we observe a very low IC₅₀ values, close to 1 μM of Cu²⁺-complexes being required to kill/disrupt half of metabolic activity of all three cancer cells, contrasting with the high IC₅₀ values found for cisplatin (13.74 ± 0.99, 31.74 ± 2.14 and 36.22 ± 0.44 in MCF-7, A545 and PC3, respectively). Cisplatin was used as standard metal-based complex (Pt²⁺-complex) and chemotherapeutic drug mostly employed in cancer chemotherapy. For the MCF-7, A549 and PC3 cell lines treated with R9 we observed an IC₅₀ (μM) of 1.01 ± 0.09, 1.02 ± 0.07 and 1.51 ± 0.06, respectively. On the other hand, MCF-7, A549 and PC3 cell lines exposed to R10 exhibited an IC₅₀ (μM) of 1.27 ± 0.14, 1.23 ± 0.09 and 1.38 ± 0.16, respectively. Indeed, both Cu²⁺-complexes showed a significant higher cytotoxic activity, almost 14, 32 and 36-times higher than cisplatin in MCF-7, A549 and PC3 cell lines, respectively. Therefore, these results show that the Cu²⁺-complexes have a promising anticancer potential compared to the chemotherapeutic drug, cisplatin. On the other hand, it is

interesting to note that MCF10A, healthy breast epithelial cells, as a control for non-cancer cell line after treatment with R9 and R10, showed the IC_{50} (μM) of 8.19 ± 0.87 and 6.93 ± 0.96 , respectively which is approximately 7-8 times more resistant than MCF-7. The latter result demonstrated the enhance activity of the R9 and R10 in cancer cells (MCF-7) if compared with the healthy breast epithelial cell line, MCF10A (Figure 16C, Table 4).

To make sure that the antitumor activity of the Cu^{2+} -complexes was actually caused by the complexes, we performed the same assay exposing cells with the ligand, $\text{H}_3\text{L1}$ alone or with the simple salt (copper chloride), both used for the synthesis of the complexes (Figure 10A and Table 4). As expected, none of these compounds was cytotoxic to the cells. Furthermore, since DMSO in high concentrations may be toxic to cells and it was used as a solvent for the dilution of Cu^{2+} -complexes in the concentration of 0.2%, we also tested its cytotoxicity. As expected, we did not observe any reduction on the cell viability (Table 4).

The results obtained from the MTT assay showed that Cu^{2+} -complexes, R9 and R10, had almost the same potential for antineoplastic activity against the types of cancer cell lines tested. Hence, subsequent analysis was performed only with the breast and lung cancer cell lines, exposed or not to Cu^{2+} -complexes or to the standard chemotherapeutic drug, cisplatin. The concentrations tested in the other analysis were based on the IC_{50} values obtained. We used Cu^{2+} -complexes with nearly close concentrations to IC_{50} ($1 \mu\text{M}$), the half of IC_{50} ($0.5 \mu\text{M}$) and 2 times of the IC_{50} ($2 \mu\text{M}$), furthermore, the cisplatin were used in its IC_{50} concentration of $14 \mu\text{M}$ and $32 \mu\text{M}$, in both cell lines MCF-7 and A549, respectively.

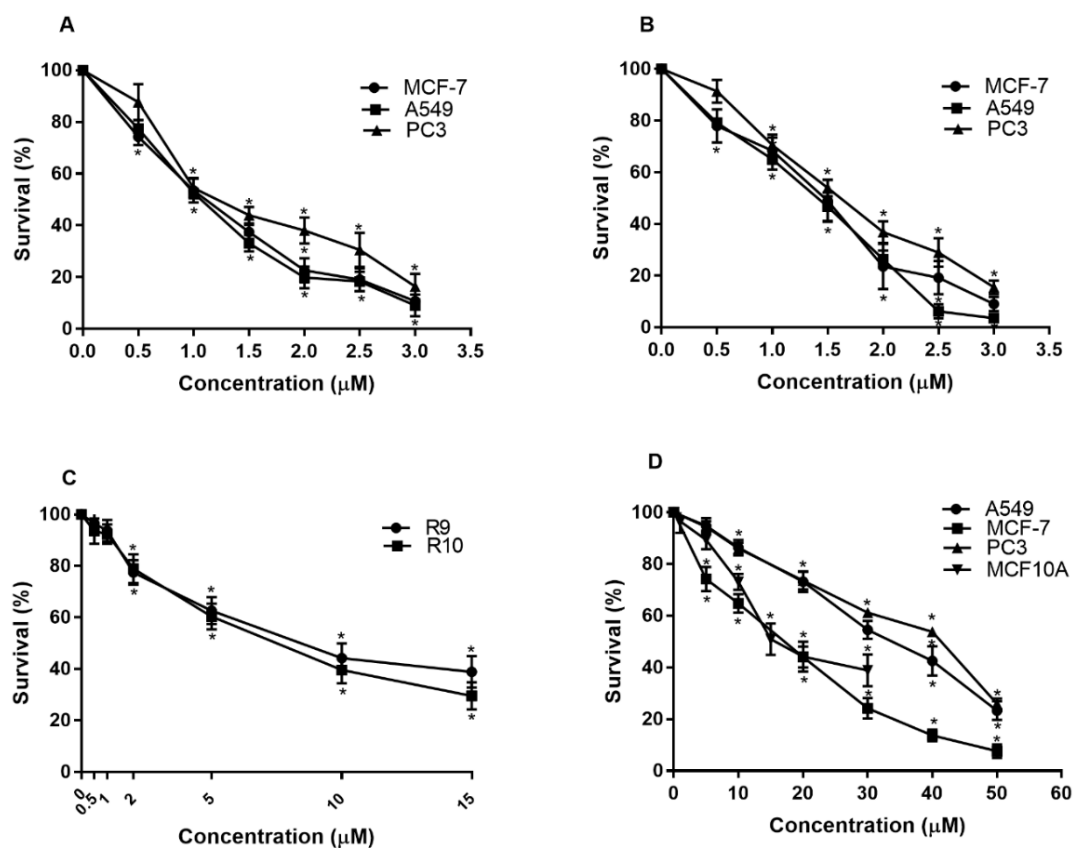


Figure 16. Effect of R9 and R10 on viability of MCF-7, A549, PC3 and MCF10A. MTT assay of MCF-7, A549 and PC3 cells treated with different concentrations of Cu^{2+} -complexes ranging from 0.5 to 3 μM during 24 h. (A) cell survival of MCF-7, A549 and PC3 cells treated with R9; (B) cell survival of MCF-7, A549 and PC3 cells treated with R10; (C) cell survival of MCF10A cells (control for non-cancer cell line) treated with different concentrations of Cu^{2+} -complexes (R9 and R10) ranging from 0.5-15 μM during 24 h, and; (D) cell survival of MCF-7, A549, PC3 and MCF10A cells treated with cisplatin ranging from 5-50 μM during 24 h. Survival curves were plotted with the aid of GraphPad Prism 7.0 software. Data are shown as relative cell survival (mean % \pm S.D bar) as compared with that in control (n = 3). * $p < 0.0001$ compared to control. All statistics were performed by one-way ANOVA using Dunnett.

Table 4: Cytotoxicity effect of R9 and R10 on mammalian cell lines.

Cell lines	IC_{50} (μM)					
	R9	R10	Cisplatin	$\text{H}_3\text{L1}$	$\text{Cu}(\text{ClO}_4)_2 \cdot 6\text{H}_2\text{O}$	DMSO
MCF-7 (Breast cancer)	1.01 ± 0.09	1.27 ± 0.14	13.74 ± 0.99	>100	>100	>100
A549 (Lung cancer)	1.01 ± 0.07	1.23 ± 0.09	31.74 ± 2.14	>100	>100	>100
PC3 (Prostate cancer)	1.51 ± 0.06	1.38 ± 0.16	36.22 ± 0.44	>100	>100	>100
MCF10A (mammary epithelial cell)	8.19 ± 0.87	6.93 ± 0.96	18.30 ± 1.39	–	–	–

IC_{50} values obtained after 24 h exposure of three different cancer cell lines, MCF-7, A549 and PC3, and non-cancer human mammary epithelial cell, MCF10A, to R9, R10, cisplatin, $\text{H}_3\text{L1}$ ligand and $\text{Cu}(\text{ClO}_4)_2 \cdot 6\text{H}_2\text{O}$.

5.2 Assessment of cancer cell morphology.

A simple observation on light microscopy corroborated the action of R9 and R10 to the probable cell alterations that can be indicative of cell death due to apoptosis. The treatment of MCF-7 and A549 cells with both R9 and R10 revealed some relevant morphological changes when compared to untreated cells (Figure 17). The population of attached cells in the control after 24 h is shown in Figures 17. For cells treated with R9 and R10 at IC_{50} concentration, we noted changes in the cell morphology after 24 hours of exposure, with cells detached from the well plate bottom and shrinkage appearance (Figure 17). The most significant alterations were rounding shape with swollen of cell body after treatment with both R9 and R10 (Figure 17).

We further analyzed the relative granularity of cells using flow cytometer. Side scatter (SSC) and forward scatter (FSC) of light refraction differentiate the granularity and size within the cell populations. Granularity was measured by mean of side scatter height using flow cytometry (Figure 18A). Illustrative dot plots of MCF-7 and A549 treated with R9 and R10 during 24 h obtained by FACS analysis showed the increase in cell population in y axis (side scatter height SSC), suggesting that treated cells are granulocytic and have a high side scatter of light refraction compare to the untreated cells (Figure 18A). According to Figure 18B, we can observe an increase in granularity of MCF-7 after treatment with R9 and R10. The granularity was 2 and 2.6 times higher than the untreated MCF-7 cells, respectively. Moreover, in A549 treated with R9 and R10, the increase in granularity was 1.5 and 1.4 times higher than that was observed by the untreated A549 cells, respectively. Our results revealed that Cu^{2+} -complexes affect granularity of MCF-7 and A549 cells (Figures 17 and 18B).

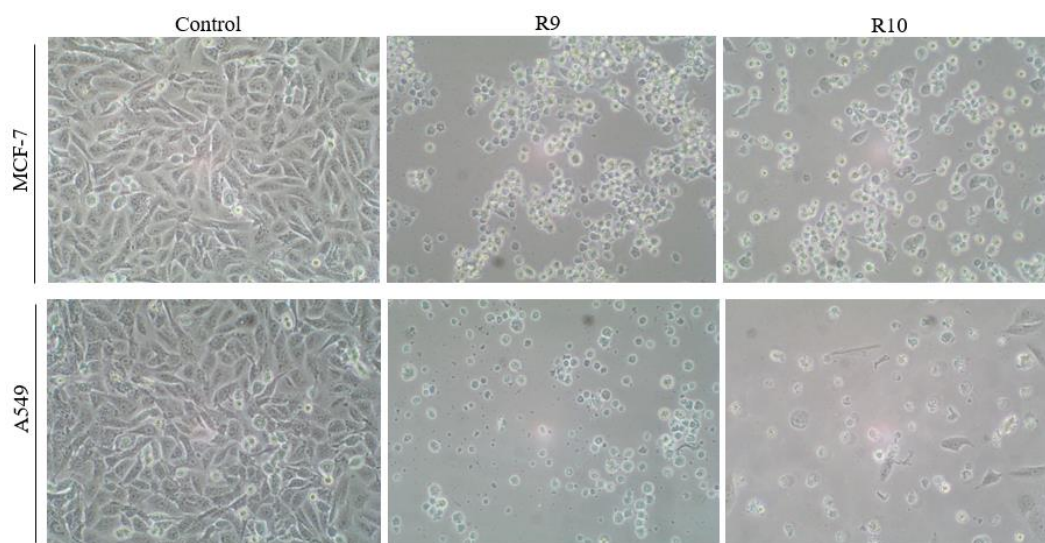


Figure 17. Change in morphology of MCF-7 and A549 cells after treatment with Cu^{2+} -complexes. Cells were treated with IC_{50} of both Cu^{2+} -complexes, and after 24 h pictures have been taken by NIKON Eclipse TS-100 inverted microscope. Data are represented as mean \pm S.D of at least 3 independent experiments (n=3).

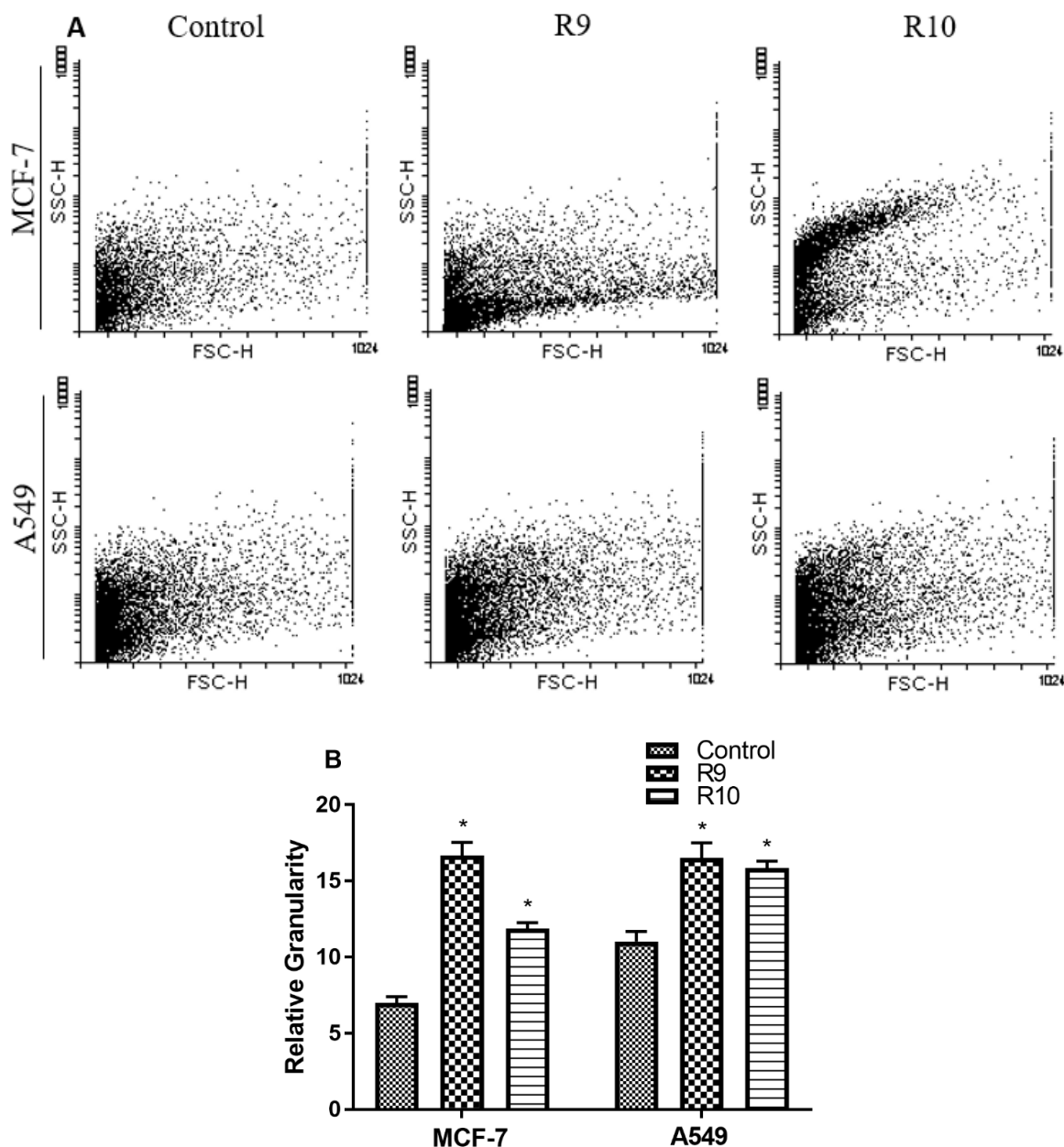


Figure 18. Cu^{2+} -complexes, R9 and R10, increase cell granularity in MCF-7 and A549 cells. MCF-7 and A549 cells were treated with IC_{50} values of Cu^{2+} -complexes for 24 h followed by flow cytometry analysis. (A) Plots of forward scatter (FSC) versus side scatter (SSC) are shown. (B) The bar diagram shows the mean in relative granularity of MCF-7 and A549. Data are represented as mean \pm S.D of at least 3 independent experiments ($n=3$). * $p<0.0001$ compared to control. All statistics were performed by one-way ANOVA using Dunnet.

5.3 Evaluation of changes in mitochondrial membrane potential ($\Delta\Psi_m$).

Detection of mitochondrial membrane potential changes can be followed by JC1 fluorophore staining. Our results show a downward trend of red fluorescence (J-aggregates) in both the MCF-7 and the A549 cancer cell lines treated with Cu^{2+} -complexes (Figure 19A and C, 20A and

C). The 24 h treatment of cells with R9 and R10 ensuing incubation for 30 minutes with fluorochrome JC1 demonstrated a significant reduction in $\Delta\Psi_m$ compared to untreated MCF-7 cells (Figure 19A and 19B) and in A549 cells (Figure 20A and 20B). After 34 min of reaction, 2 μM FCCP, the classical inhibitor of the mitochondrial function, was added to all systems in order to completely collapse the $\Delta\Psi_m$.

The results indicated a marked reduction in mitochondrial polarization of MCF-7 and A549 with both Cu^{2+} -complexes at the concentration of $\frac{1}{2}\times\text{IC}_{50}$, IC_{50} and $2\times\text{IC}_{50}$ (Figure 19A, 19B, 20A and 20B). Cisplatin also induced the reduction in mitochondrial membrane potential at IC_{50} concentration in MCF-7 and A549 (Figure 19B and 20B). The reduction caused by cisplatin was 2.65 times higher in MCF-7 cells than that of in A549 (Figure 19A and C, 20A and C). Nearly complete depolarization of the mitochondrial membrane potential occurred at concentrations of $2\times\text{IC}_{50}$ in MCF-7 (Figure 19A and B) and in A549 cells (20A and B). As expected, the addition of the classical inhibitor of the mitochondrial function reduced the mitochondrial membrane potential in all the systems (Figure 19A and C, 20A and C).

Treatment of the MCF-7 cells with both R9 and R10; result in mitochondrial depolarization via dose-dependent manner. Interestingly, both Cu^{2+} -complexes at IC_{50} concentration showed the same amount of reduction in mitochondrial membrane potential as cisplatin (3.7 times lower than the control), and the Cu^{2+} -complexes at $2\times\text{IC}_{50}$ concentration displayed the same reduction in $\Delta\Psi_m$ as the FCCP (5.8 times lower than the control) (Figure 19B, D). On the other hand, the decrease in $\Delta\Psi_m$ in A549 via treatment with both Cu^{2+} -complexes was even more interesting in comparison to cisplatin (Figure 20B, D). The Figure 20B and D showed that mitochondrial membrane depolarization occurred at IC_{50} concentration almost 2 times more than that of in control that is significantly higher than cisplatin (1.5 times higher than control) in both R9 and R10.

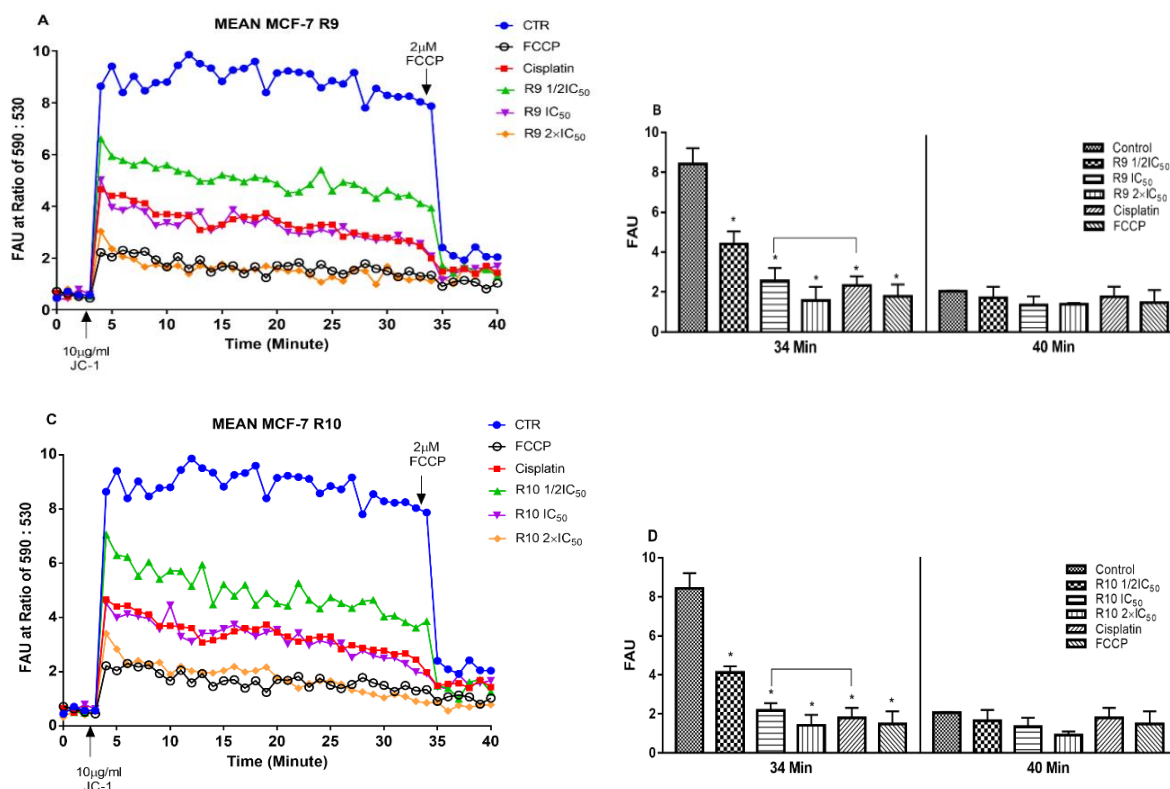


Figure 19. Evaluation of mitochondrial membrane potential ($\Delta\Psi_m$) in MCF-7 cells treated with Cu^{2+} -complexes R9 and R10. Graphical representation of the level of $\Delta\Psi_m$, expressed as fluorescence arbitrary units (FAU) in MCF-7 cells treated with R9 (A) and R10 (C). The arrow indicates the time point (34 min) at which the uncoupler FCCP (2 μM) was added to the reaction system to collapse $\Delta\Psi_m$. $\Delta\Psi_m$ values (expressed as FAU) shown in bar diagram before (34 min) and after (40 min) the addition of the uncoupler FCCP in MCF-7 cells treated with R9 (B) and R10 (D). P values were obtained comparing the control cells with the treated groups, and the * indicates that $P < 0.05$. Statistics were performed by one-way ANOVA using Tukey.

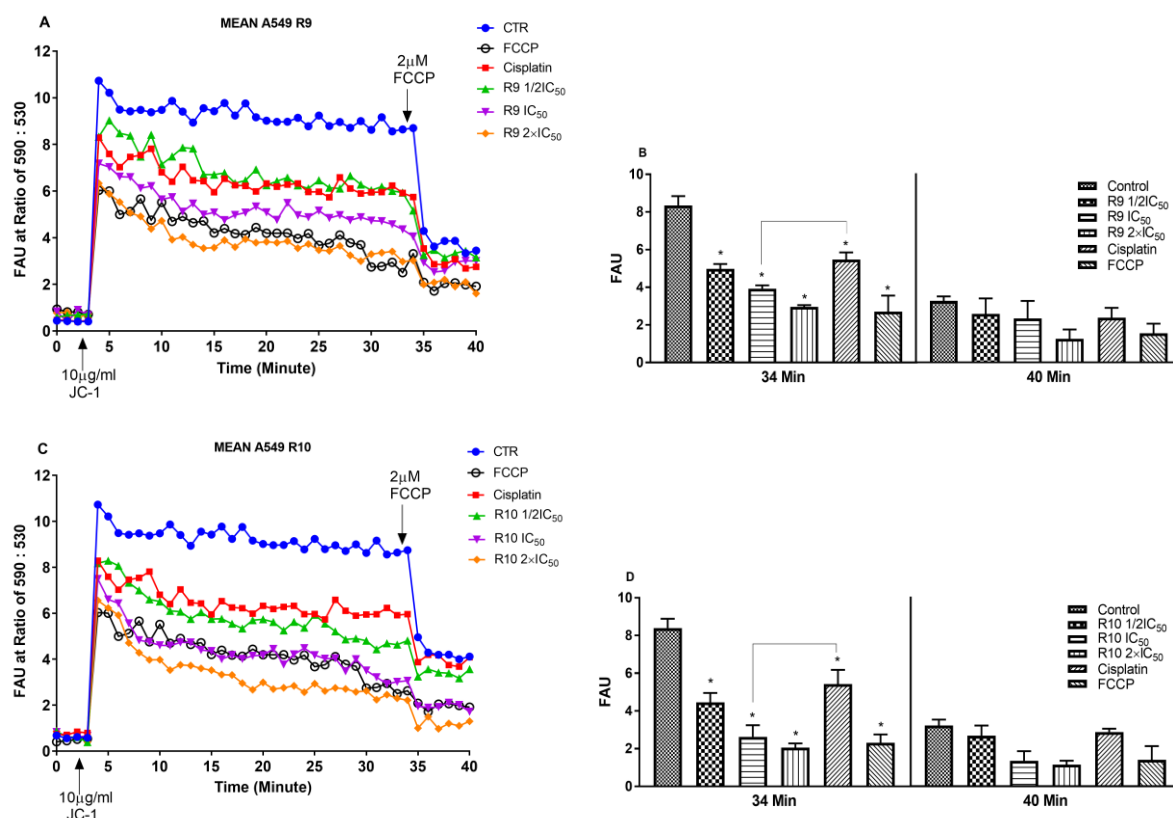


Figure 20. Evaluation of the mitochondrial membrane potential in A549 cells treated with Cu²⁺-complexes, R9 and R10. Graphical representation of the level of membrane mitochondrial potential, expressed as fluorescence arbitrary units (FAU), in A549 cells treated with R9 (A) and R10 (C). The arrow indicates the time point (34 min) at which the uncoupler FCCP (2 μ M) was added to the reaction system to collapse mitochondrial potential of cells. $\Delta\Psi_m$ values (expressed as FAU) shown in bar diagram before (34 min) and after (40 min) the addition of the uncoupler FCCP in A549 cells treated with R9 (B) and R10 (D). P values were obtained comparing the control cells with the treated groups, and the * indicates that $P < 0.05$. Statistics were performed by one-way ANOVA using Tukey.

5.4 Evaluation of ROS production.

Decreased mitochondrial dehydrogenase assessed by MTT and morphological changes in cells, as well as a decrease in mitochondrial membrane potential, may be associated with cell death due to apoptosis. Evaluation of mitochondrial membrane potential showed potential damage to mitochondria and as a result may increase ROS production. Since cells constantly generate ROS during aerobic metabolism, the maintenance of oxidative balance is very important for cells; the powerful antioxidant system of cells can control the level of ROS to bypass the overproduction of ROS. In this context, ROS and the oxidative damage are thought to play an important role in many human diseases including cancer (SULLIVAN; CHANDEL, 2014).

Quantification of intracellular oxidation can be easily accomplished by using the cell permeable fluorescent probe, 2'-7'-dichlorodihydrofluorescein diacetate (DCFH-DA), which when oxidized emits fluorescence and directly measures the redox state of a cell. The control

stands for the cells exposed to fluorescent probe but not Cu^{2+} -complexes, whereas the positive control was carried out with cells treated with doxorubicin and menadione to make sure that the assay was properly performed. The fluorescence intensity (FI) represented the percentage of ROS (ROS%), and the mean fluorescence intensity (MFI) displayed the amounts of ROS produced after the effect of Cu^{2+} -complexes, doxorubicin and menadione in cancer cell lines.

The FI to represent the percentage of ROS (ROS%), showed that the MCF-7 cell line underwent an increase in intracellular oxidation as a result of treatment with the $\frac{1}{2}\times\text{IC}_{50}$, IC_{50} and $2\times\text{IC}_{50}$ concentrations of R9, reaching about 1.8, 2.2 and 2.3 times higher than untreated cells, in MCF-7 respectively (Figure 21A). The obtained results for R10 showed that cells exposed to the same concentrations presented similar increase in ROS%; 1.8, 2.1 and 2.4 times higher than the untreated cells in MCF-7 (Figure 21B). On the other hand, the amounts of ROS produced (mean fluorescence intensity MFI) in MCF-7 by the effect of R9 and R10 at the concentrations of IC_{50} and $2\times\text{IC}_{50}$ were about (2 and 3.4) as well as (2 and 3.7) times higher than the control, respectively (Figure 21C and D). Our results of ROS% in A549 treated with R9 and R10 at the concentrations of $\frac{1}{2}\times\text{IC}_{50}$, IC_{50} and $2\times\text{IC}_{50}$ revealed an increase of 2.1, 2.8 and 3.5 times and 2.1, 2.7 and 3.5-times higher fluorescence intensity compared to the control, respectively (Figure 22A and B). However, the mean fluorescence intensity MFI of ROS amounts calculated (1.9, 3.7 and 4.2) and (2.4, 4.1 and 4.6) times higher than control in A549 treated with R9 and R10 at the concentrations of $\frac{1}{2}\times\text{IC}_{50}$, IC_{50} and $2\times\text{IC}_{50}$, respectively (Figure 22C and D).

It is clearly seen in Figures 21A and B as well as 22A and B that upon R9 and R10 treatment, even in lowest dose ($\frac{1}{2}\times\text{IC}_{50}$) the ROS generated cell percentage is increased in comparison to the control in both cell lines. In addition, our results suggest that Cu^{2+} -complexes treatment induced ROS production is dose-dependent (Figure 21A and B, 22A and B). The increase in the amount of ROS produced after R9 and R10 treatment was significant and dose-dependent in both cell lines (Figure 21C and D, 22C and D). Moreover, the amount of ROS produced after treatment in both cell lines was higher as compared to control except for $\frac{1}{2}\times\text{IC}_{50}$ of R9 and R10 in MCF-7 (Figure 21C and D). Results showed that the significant increase of ROS at IC_{50} concentration after treatment with both compounds in both cell lines in a dose dependent way.

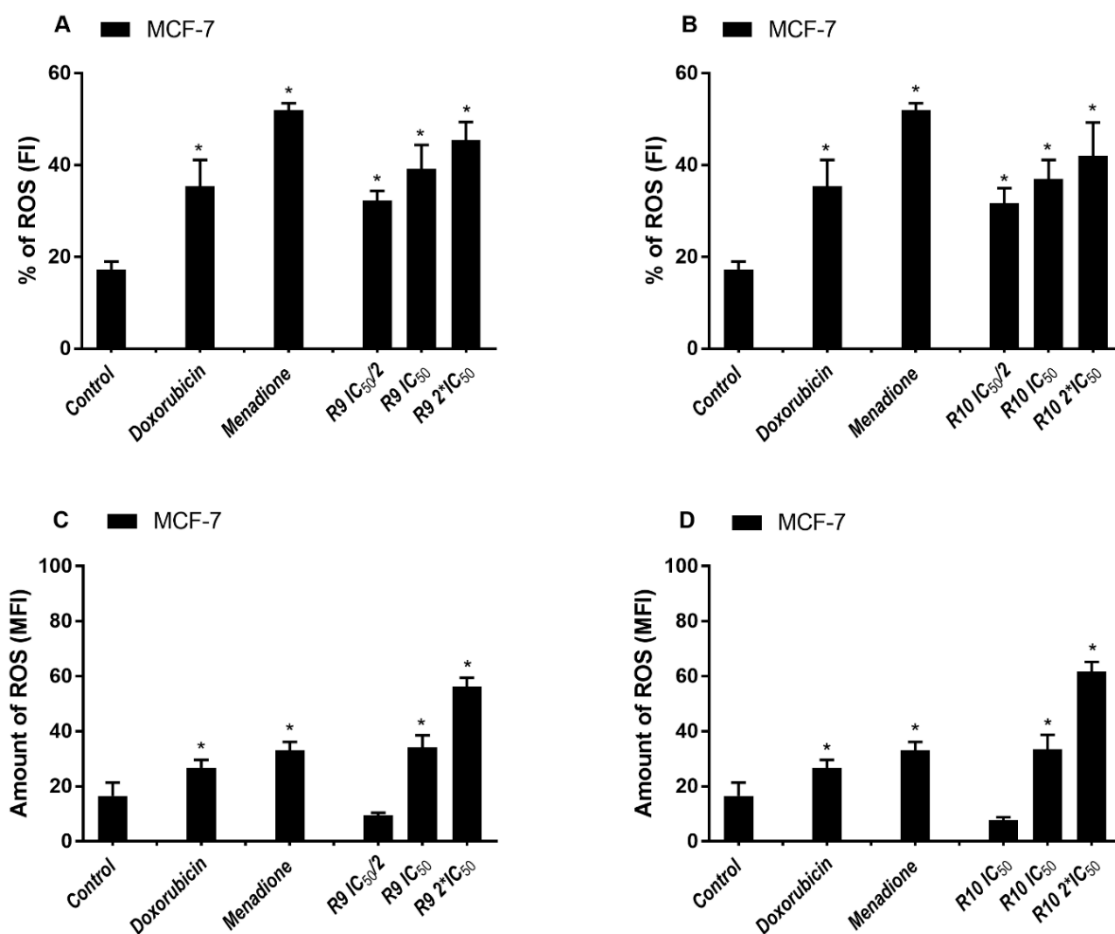


Figure 21. ROS production by MCF-7 cells treated with Cu²⁺-complexes, R9 and R10. Cells were treated for 24 hours in presence of $1/2 \times IC_{50}$, IC_{50} , $2 \times IC_{50}$ R9 (A and C) and R10 (B and D) or doxorubicin (200 μ g/mL) and menadione (30 μ M). Doxorubicin and menadione were used as positive control for ROS production. Fluorescent intensity of ROS% in MCF-7 cells treated with R9 and R10 is displayed in (A) and (B). The mean fluorescent intensity (the amount of ROS produced) in MCF-7 cells treated with R9 and R10 is displayed in (C) and (D). Mean \pm S.D of 3 independent experiments (n=3). *p<0.005, compared to control. All statistics were performed by one-way ANOVA using Tukey.

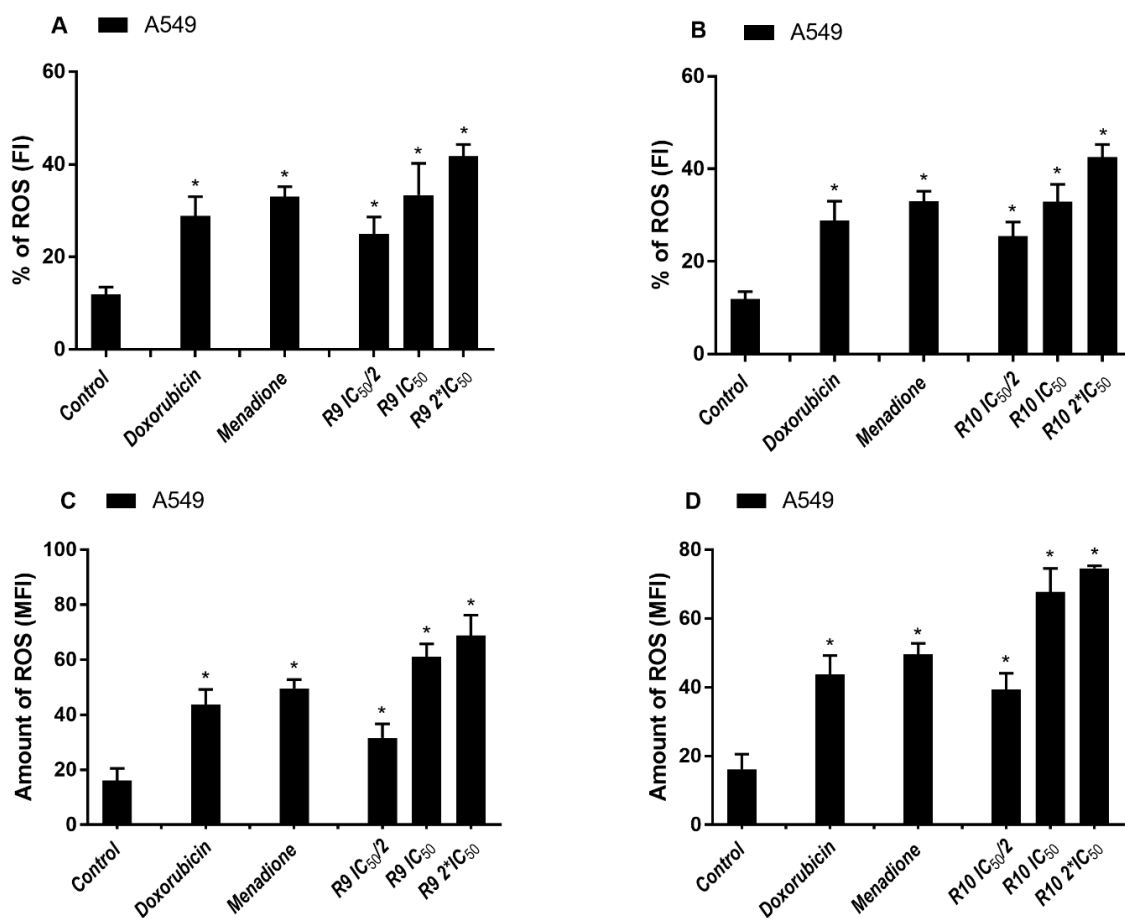


Figure 22. ROS production by A549 cells treated with Cu²⁺-complexes, R9 and R10. Cells were treated for 24 hours in presence of $\frac{1}{2}\times\text{IC}_{50}$, IC_{50} , $2\times\text{IC}_{50}$ R9 and R10 or doxorubicin (200 $\mu\text{g}/\text{mL}$) and menadione (30 μM) used as positive control. Results were obtained by flow cytometer as described in materials and methods. The bar diagram is displayed the fluorescent intensity of percent of ROS produced in A549 cells treated with R9 (A) and R10 (B), doxorubicin and menadione. The mean fluorescent intensity showed the amount of ROS produced in A549 cells treated with R9 (C) and R10 (D), doxorubicin and menadione. Mean \pm S.D of 3 independent experiments ($n=3$). * $p<0.005$, compared to control. All statistics were performed by one-way ANOVA using Tukey.

5.5 Cell cycle analysis and DNA fragmentation.

Cell cycle control or checkpoints play an important role in maintaining the fidelity and integrity of genome replication and repair. Regarding to DNA fragmentation, it may arise as a consequence of the process of apoptosis induced by the activation of caspase enzymes via an extrinsic and/or intrinsic signaling pathway. Furthermore, DNA fragmentation may also occur under conditions that directly cause DNA damage and therefore may stimulate the process of apoptosis through signaling pathways independent of caspase activation (FAVALORO et al., 2012; LIU; BALIGA, 2005).

In order to verify the DNA fragmentation occurred by the treatment of MCF-7 and A549 cells with both Cu^{+2} -complexes, we decided to evaluate the cell cycle phases as well as detection of cells with DNA content in Sub-G1 Phase. Cell-to-cell phases and cells with DNA fragmentation (Sub-G1) were analyzed with propidium iodide (PI). Figures 23(A-D) and 24(A-D) represent the distribution of MCF-7 and A549 cells into phase/point where fragmented DNA is detected (Sub-G1) after R9 and R10 treatments. Distribution of the cell cycle phases shown in the MCF-7 untreated cells (Figure 23A) and after treatment with cisplatin (Figure 23B), R9 (Figure 23C) and R10 (Figure 23D) at IC_{50} concentrations of each. The untreated control represented in A549 (Figure 24A), and after treatment with cisplatin (Figure 24B), R9 (Figure 24C) and R10 (Figure 24D) at IC_{50} concentrations. In comparison with the untreated control, the number of cells shift to the left (Sub-G1) was evident in both cancer cell lines in all treatments. Furthermore, the number of cells decreased in all cell cycle phases, G1, S and G2/M phases after R9 and R10 treatment in both cancer cell lines (Figures 23(A-D) and 24(A-D)).

Treatment of both cancer cell lines with R9 and R10 caused the DNA content distribution decreased and this phenomenon indicated that Cu^{+2} -complexes had an effect on cell cycle progression. After R9 and R10 exposure with MCF-7 cells, the cell population (cell percentage) increase in the Sub-G1 phase raised from 0.47% to 86.21% and 77.66%, respectively. The G1 phase decreased from 68.05% to 11.65% and 19.76%, the S phase decreased from 13.89% to 3.24% and 2.29% and G2/M decreased from 20.50% to 1.65% and 3.98% in MCF-7 cells treated with R9 and R10, respectively (Figure 23E and F). In contrast, A549 cells treated with R9 and R10, showed the increase in the percentage in Sub-G1 phase from 0.49% to 66.89% and 47.05%, respectively. Reduction in G1 phase occurred from 64.33% to 24.56% and 46.47%, reduction in S phase occurred from 13.89% to 2.29% and 3.57% and reduction in G2/M phase occurred from 20.50% to 3.98% and 1.91% in A549 cells treated with R9 and R10, respectively (Figure 24E and F).

In comparison with untreated cells, we observed a high induction of DNA fragmentation in Sub-G1 phase in MCF-7 cells after R9 and R10 treatment (277.4 and 165.2 times higher than the control) (Figure 23E and F). Whereas, in A549 the DNA fragmentation was 136.5 and 96 times higher than that of untreated cells (Figure 24E and F). Furthermore, Figure 23E displayed that the percentage of DNA in Sub-G1 phase in MCF-7 untreated cells change from 0.47% to 51.39% after treatment with cisplatin (Figure 23E and F). The G1, S and G2/M phase decreased from 68.05%, 8.13% and 18.97% to 41.83%, 3.11% and 3.17% in A549 cells treated with cisplatin, respectively. Whereas, in A549 cells treated with cisplatin the percentage of

DNA in Sub-G1 phase increased from 0.49% to 20.63% (Figure 24E and F). In addition, G1, S and G2/M phase decreased from 64.33%, 13.89% and 20.50% to 72.94%, 3.34% and 1.65% in cisplatin-treated A549 cells, respectively (Figure 24E and F). Therefore, cisplatin exposure induced DNA percentage in the Sub-G1 phase that is 109.3 and 42 times higher than in untreated cells in MCF-7 and A549 cells (Figure 23E and F, 24E and F).

At the IC_{50} concentration of R9 and R10, the levels of cells with DNA fragmentation and consequently apoptosis reaches more than 50% in both tested cell lines (Figure 23E and F, 24E and F) that is significantly higher than the DNA fragmentation induced by cisplatin. The comparison with cisplatin demonstrated the percentage of DNA in Sub-G1 phase showed 1.6 and 1.5 times more in MCF-7 treated R9 and R10, respectively and 3.2 and 2.2 times more in A549 treated R9 and R10, respectively (Figure 23E and F, 24E and F). Therefore, both Cu^{+2} -complexes demonstrated a significant greater capacity to induce DNA fragmentation.

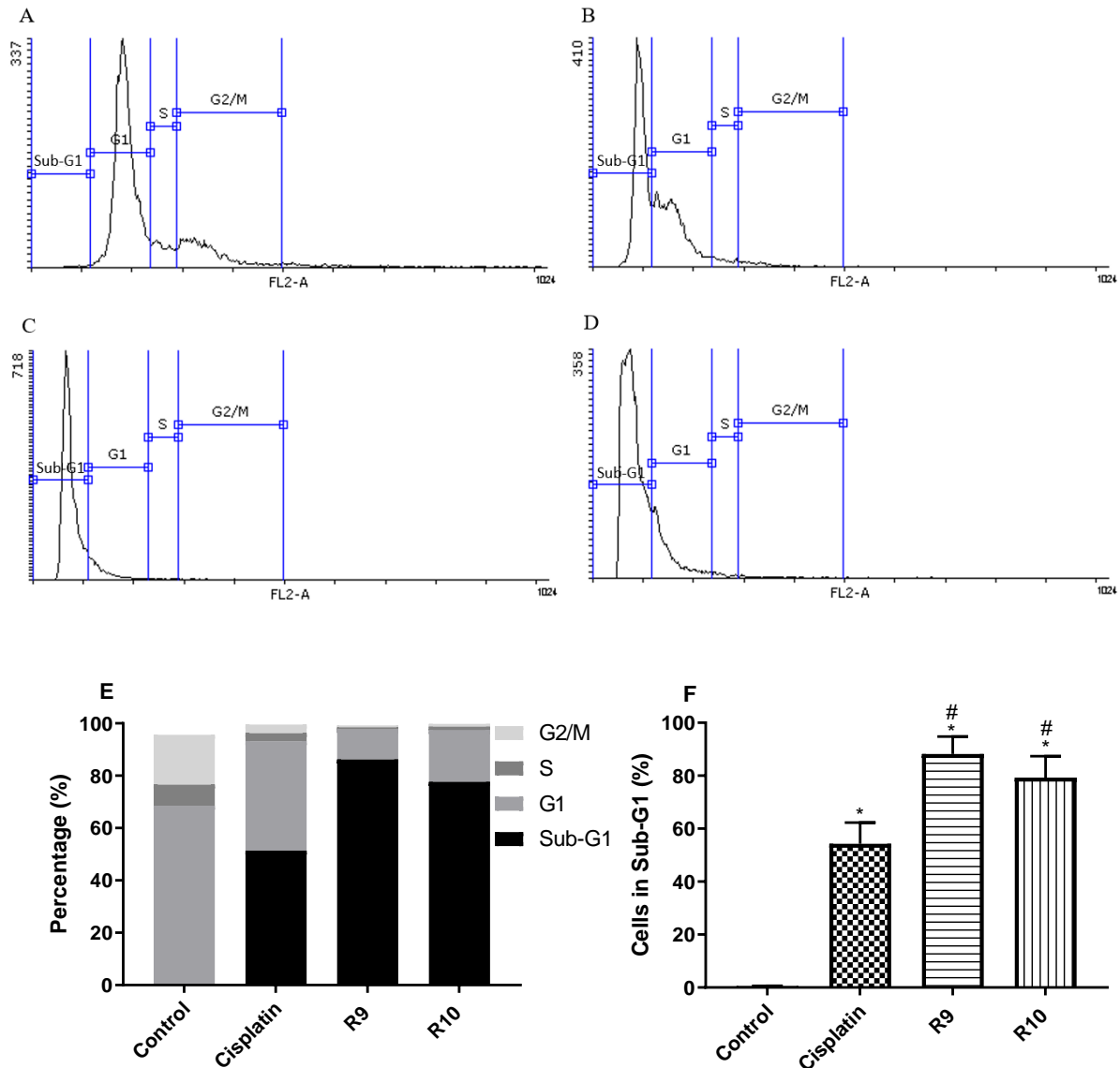


Figure 23. Analysis of DNA fragmentation during treatment with Cu^{2+} -complexes, R9 and R10 in MCF-7 cells. After treatment with Cu^{2+} -complexes or cisplatin, the cells were incubated with propidium iodide (10 $\mu\text{g}/\text{mL}$) containing 200 $\mu\text{g}/\text{mL}$ of RNase A. The amount of DNA was measured by flow cytometry. The distribution of the cells through phase/point (Sub-G0 or Sub-G1, G0/G1, S, G2/M) from left to right in MCF-7 untreated cells (A), cells treated with cisplatin (B), R9 (C) and R10 (D) at IC_{50} concentration. Quantification analysis of G0/G1, S and G2/M cell cycle from flow cytometry where the cell cycle percentages were derived from flow cytometric analysis of MCF-7 cells treated with R9 and R10 (1 μM) (F). The mean percentage of cells in Sub-G1 (E) is an indicative of cells in the process of apoptosis caused by treatments with Cu^{2+} -complexes or cisplatin. *Statistically different in relation to the untreated cells, $p < 0.0001$ #statistically different in relation to cisplatin $p < 0.0001$. Statistics were performed by two-way ANOVA using Dunnett.

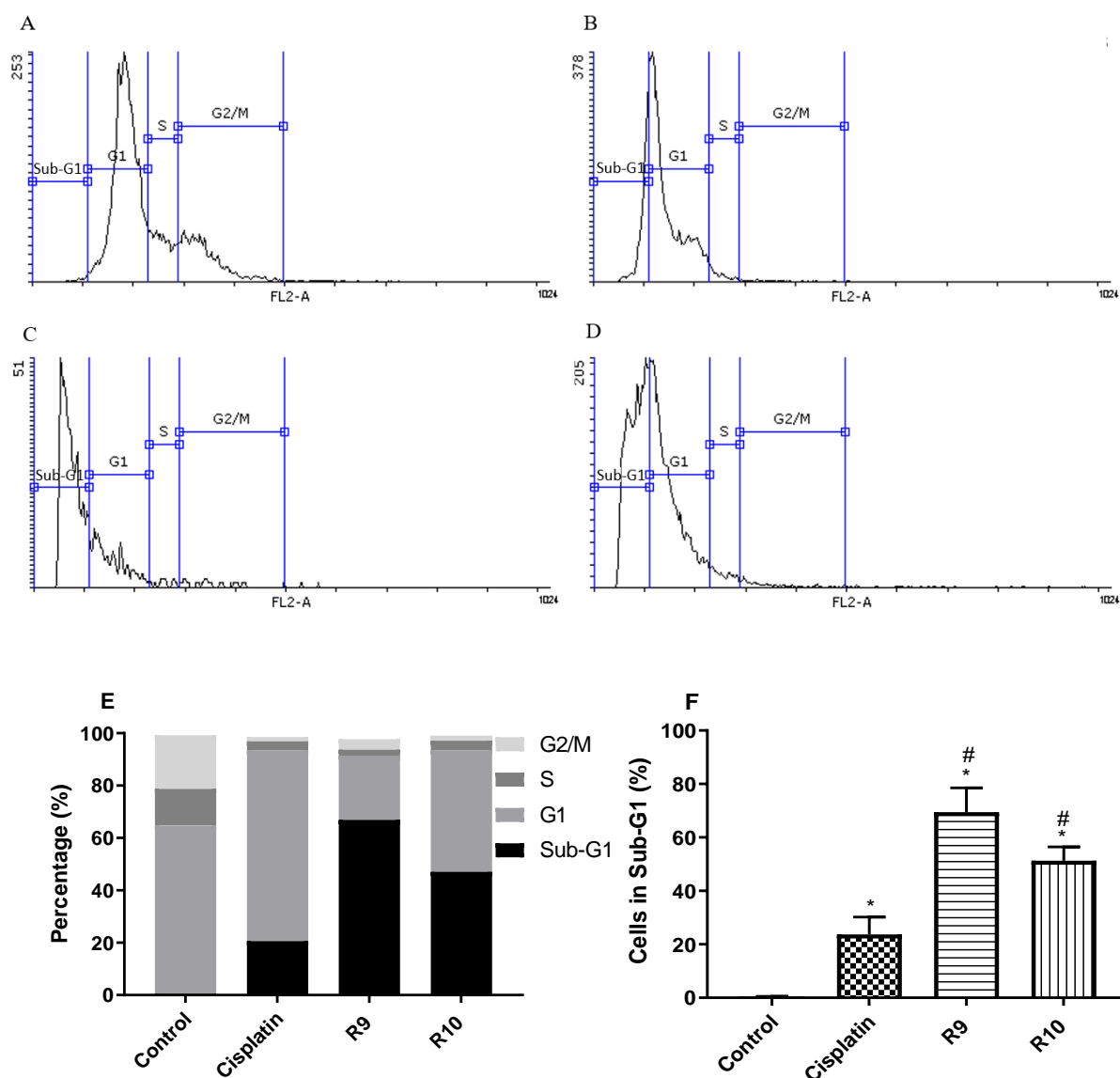


Figure 24. Analysis of DNA fragmentation during treatment with Cu^{2+} -complexes, R9 and R10 in A549 cells. After treatment with Cu^{2+} -complexes or cisplatin, the cells were incubated with propidium iodide (10 $\mu\text{g}/\text{mL}$) containing 200 $\mu\text{g}/\text{mL}$ of RNase A. The amount of DNA was measured by flow cytometry. The distribution of the cells through phase/point (Sub-G0 or Sub-G1, G0/G1, S, G2/M) from left to right in A549 untreated cells (A), cells treated with cisplatin (B), R9 (C) and R10 (D) at IC_{50} concentration. Quantification analysis of G0/G1, S and G2/M cell where the cell cycle percentages were derived from flow cytometry analysis of MCF-7 cells treated with R9 and R10 (1 μM) (F). Percentage of cells in Sub-G1 (E) as an indicative of cells in apoptosis caused by treatment with Cu^{2+} -complexes or cisplatin. *Statistically different in relation to the untreated cells, $p < 0.0001$ #statistically different in relation to cisplatin $p < 0.0001$. Statistics were performed by two-way ANOVA using Dunnett.

5.6 Induction of DNA fragmentation by TUNEL (apoptosis).

Although we observed an increase in the percentage of MCF-7 and A549 cells in Sub-G1 after Cu^{2+} -complexes treatment, we searched for an additional experiment to confirm the

occurrence of DNA fragmentation. Thus, we used the TUNEL technique to determine whether the cause of death could be a consequence of the apoptosis process. The results were analyzed through dot plots as shown in Figure 25A and 26A. The number of cells with DNA degradation can be showed by the red fluorescence intensity (FL3) (PI) versus green fluorescence intensity (FL1) (dUTP) where it is possible to verify the displacement of green fluorescence intensity in FL1-H. This is associated to the number of cells with DNA degradation that might be related to the apoptotic cells after treatment with Cu^{+2} -complexes and cisplatin in comparison to untreated cells. Figures 25A and 26A represent the induction of DNA fragmentation in both MCF-7 and A549 cell lines after Cu^{+2} -complexes and cisplatin at the IC_{50} concentration. It is shown that the population of cells with fragmented DNA that may be related to the apoptotic cells moved from the left to the right quadrant and has been detectable by green fluorescence intensity (FL1) in both treated cell lines (Figure 25A and 26A). Untreated MCF-7 and A549 cells showed 16.8% and 20.8% of cells with DNA degradation, respectively (Figure 25B and 26B). The treatment with the Cu^{+2} -complexes (R9 and R10) at the IC_{50} concentration prompted the increase in the percentage of cells with DNA degradation to 60.2% and 61.2% in MCF-7 and 43.6% and 45.3% in A549, respectively (Figure 25B, 26B). In comparison to the untreated cells, the percentage of DNA fragmentation induced by R9 and R10 in MCF-7 were 3.5 and 3.6 times higher than the control, respectively (Figure 25B). On the other hand, the R9 and R10 complexes induced about 2 times higher the percentage of DNA degraded cells compare to the control in A549 (Figure 26B). These results corroborate with detection of Sub-G1 cells. In both cell lines, Cu^{+2} -complexes and cisplatin showed almost the same amount of DNA degradation, which is different from those obtained in Sub-G1 analysis (Figure 25B, 26B).

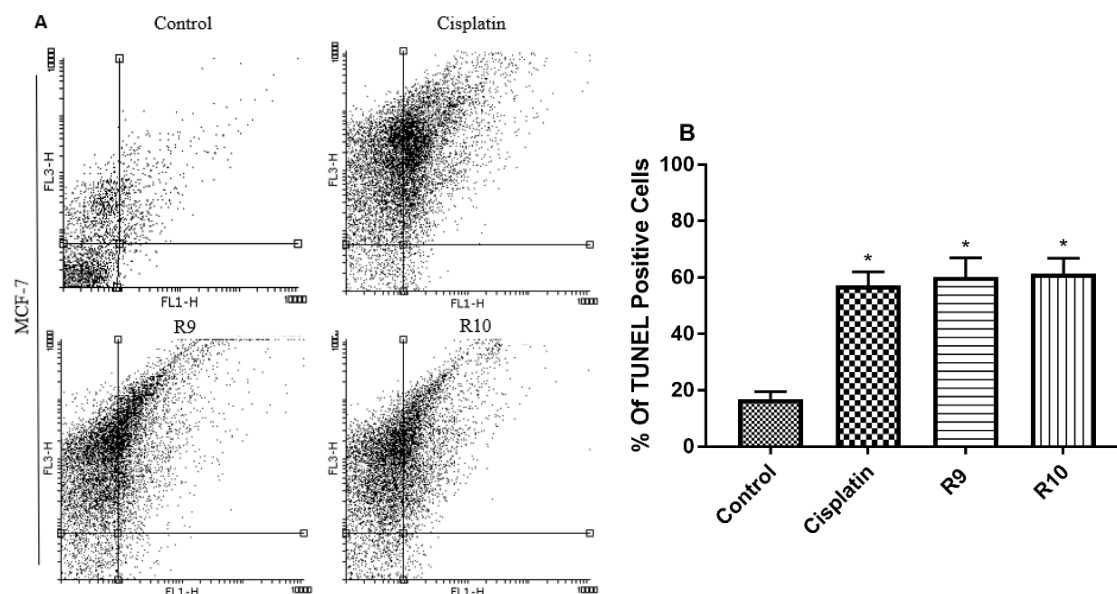


Figure 25. Induction of DNA fragmentation in MCF-7 cells treated with the Cu^{2+} -complexes, R9 and R10 complexes. The MCF-7 cells were treated with the IC_{50} concentrations of R9, R10 and cisplatin for 24 h at 37°C . At the end of the incubation period, the cells were washed, fixed with 4% paraformaldehyde and permeabilized with 70% ethanol and then used for TUNEL staining, for detecting DNA with the free OH'3 end. (A) is a representative image of histograms presenting the percentage of cells with DNA degradation in MCF-7 treated with R9, R10 and cisplatin. (B) is represented the mean percentage of TUNEL positive cells with DNA degradation. (*) difference statistically significant in relation to control, $p < 0.0001$. Statistics were performed by one-way ANOVA using Dunnet.

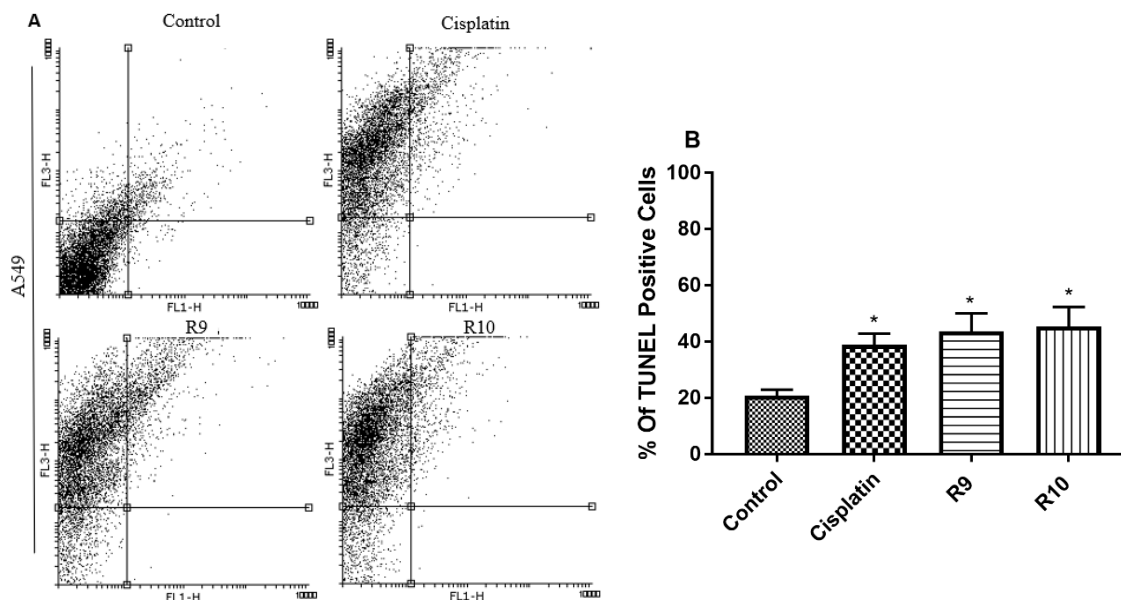


Figure 26. Induction of DNA fragmentation in A549 cells treated with the Cu^{2+} -complexes, R9 and R10 complexes. The A549 cells were treated with the IC_{50} concentrations of R9, R10 and cisplatin for 24 h at 37°C . At the end of the incubation period, the cells were washed, fixed with 4% paraformaldehyde and permeabilized with 70% ethanol and then used for marking with the TUNEL probe, for detecting DNA with the free OH'3 end. Panel A is the dot plots representative results of percentage of cells with DNA degradation in A549 treated with R9, R10, and cisplatin (A). Bar graph shows the percentage of cells with DNA degradation (B). (*) difference statistically significant in relation to control, $p < 0.0001$. Statistics were performed by one-way ANOVA using Dunnet.

5.7 Determination of caspase 8 and 9 activity.

Apoptosis cell death can occur by an extrinsic and/or intrinsic cellular signaling pathways with the consequent activation of specific caspases for each signaling pathway or even independently of the caspases. To verify which signaling pathway could be activated during treatment with the Cu^{2+} -complexes, we determined the activity of caspase 8 and 9 enzymes because activation of caspase 8/10 and caspase 9 occurs in the first stage of signaling by extrinsic and intrinsic pathways, respectively (COHEN, 1997). For this assay, MCF-7 and A549 cell lines were treated for 24 h with the IC_{50} concentration (1 μM) of the Cu^{2+} -complexes and cisplatin. According to the Figure 27A and C, we can observe that in both cancer lines, MCF-7 and A549, caspase 8 was not activated by the treatment with Cu^{2+} -complexes. On the other hand, when we analyzed the activity of caspase 9, we verified a significant increase in the activity of this enzyme (Figure 27B and D). The relative caspase 9 activity of untreated MCF-7 and A549 cells was 311.2 RLU (the number of relative light units). The relative caspase 9 activity calculated for MCF-7 cells treated with R9 and R10 reached to 684.4 RLU and 590.3 RLU, respectively. Thus, the treatment with Cu^{2+} -complexes showed a 2.2 and 1.9-fold increase in caspase 9 activity in comparison to untreated cells. Regarding to caspase 9 activity in A549 cells, the treatment with Cu^{2+} -complexes increased to 891.1 RLU and 802.7 RLU, respectively, it represented a 2.8 and 2.5-fold increase in caspase 9 activity (Figure 27B and D). Moreover, cisplatin-treated MCF-7 and A549 exhibited the relative caspase 9 activity of 785.4 RLU and 1241.8 RLU, respectively. Comparison of the active caspase 9 measured in cisplatin-treated MCF-7 and A549, revealed that the cisplatin showed non-significant difference compare to the R9 and R10-treated MCF-7 cells. However, in A549 cells, cisplatin displayed 1.5 times more relative caspase 9 activity compare to the R10-treated A549 cells.

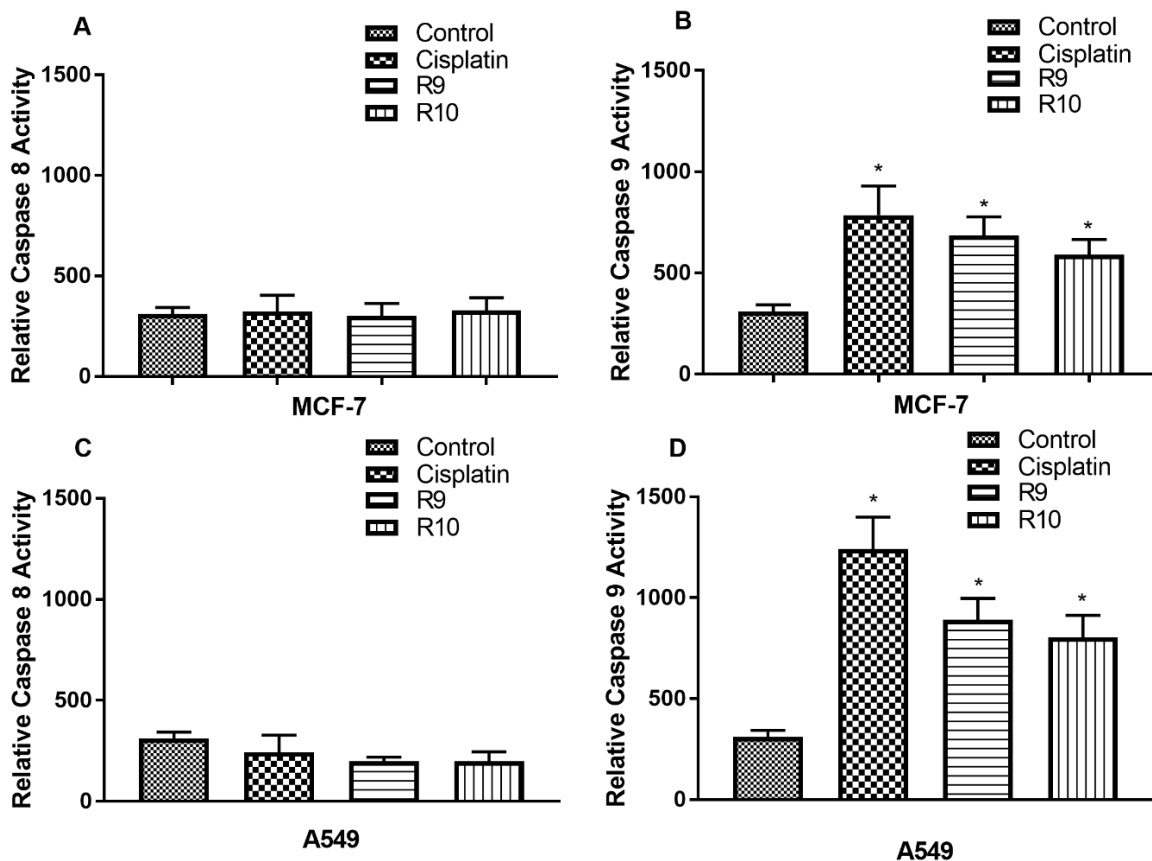


Figure 27. Caspase 8 and 9 activities in the MCF-7 and A549 cells after the treatment with the Cu^{+2} -complexes, R9 and R10. Cells were treated with Cu^{+2} -complexes at IC_{50} concentration or cisplatin at 32 μM and 14 μM in A549 and MCF-7 cell lines, respectively, for 24 h. A and B represent the relative activity of caspase 8 and caspase 9 in MCF-7 cells. C and D represent the relative caspase 8 and caspase 9 activity in A549 cells. The results represent the mean and standard deviation of at least three independent experiments. (*) statistically different in relation to control. $p^* < 0.003$ one-way ANOVA using Dunnet.

5.8 Competition between Cu^{+2} -complexes and PI for DNA binding.

Propidium iodide (PI) is a fluorescent intercalating agent that can bind between DNA bases with no sequence preference. In order to find whether both Cu^{2+} -complexes can bind to DNA as an intercalating agent, we performed the assay based on competition with PI. The MCF-7 or A549 cells treated only with PI was used as our control in this experiment. Results indicated that the percentage of fluorescent MCF-7 cells (%) treated with IC_{50} concentration of R9 and R10 was the same, 3.57%, showing no significant changes in comparison to untreated MCF-7 cells (3.3%). On the other hand, A549 treated with IC_{50} concentration of R9 and R10, represented the fluorescent cells percentage of 1.35% and 1.32%, respectively where there was no significant difference compared to the untreated cells (1.34%) (Table 5). In both cell lines treated

with Cu²⁺-complexes we could not see any significant changes in % of fluorescent cells/fluorescence intensity as compared to control. These results confirm that Cu²⁺-complexes cannot bind to DNA as an intercalating agent.

Table 5. Competition between R9 and R10 with PI for DNA binding in MCF-7 and A549 cells.

Systems	Concentration of Cu ²⁺ -complexes (μM)	Fluorescence intensity	% of fluorescent cells
MCF-7 cells	-	18.54 \pm 0.08	0.29 \pm 0.08
MCF-7 cells + PI	-	73.39 \pm 0.09	3.30 \pm 0.08
MCF-7 cells + R9 + PI	1	77.53 \pm 0.75	3.57 \pm 1.41
MCF-7 cells + R10 + PI	1	80.10 \pm 1.43	3.75 \pm 1.13
A549 cells	-	33.23 \pm 0.06	1.65 \pm 0.07
A549 cells + PI	-	84.56 \pm 0.05	1.34 \pm 0.07
A549 + R9 + PI	1	86.89 \pm 1.07	1.35 \pm 1.06
A549 + R10 + PI	1	85.63 \pm 1.61	1.32 \pm 1.17

5.9 Evaluation of R9 toxicity using *in vivo* models.

5.9.1 Toxicity of R9 in *Galleria mellonella* model of study.

The larvae of the greater wax moth have been shown to be an excellent model organism, convenient and inexpensive that replaces the use of small mammals for *in vivo* toxicity experiments. Toxicity was carried out by injecting R9 or cisplatin at 1 mg/mL (50 mg/kg of *G. mellonella*) dose, as well as DMEM and DMSO 0.2%. After injection, the survival of larvae was evaluated up to 7 days in the dark. Analysis of the representative survival curve of *G. mellonella* larvae treated with DMSO and DMEM did not show any change in the percentage of survival as compared to the untreated larvae (Figure 28).

It was observed that, after R9 treatment, the survival rate decreased in 10%, only at the 5th day and continued on day 6th to 20% reaching 30% at the 7th day (Figure 28A). On the other hand, the treatment with cisplatin promoted the reduction in the percentage of larvae survival in 20, 50, 60 and 70% after 3rd, 4th, 5th, 6th and 7th days, respectively (Figure 28A). The results clearly showed that at the same dose of cisplatin, the R9 complex was much more well tolerated presenting lower toxicity (30% of larvae death) in comparison to cisplatin the (70% larvae death); until day 7th R9 represented 2.3 times less toxicity than cisplatin (Figure 28A). We further monitored the number of animals in the larvae, pupae and wax moth life cycle (Figure 28B, C and D). We observed that while by day 11th no larvae remained in cisplatin-treated

group, the same happened only at day 14th in R9-treated group, which was very close to ultimate loss of larvae in the control group (day 15th) (Figure 28B). The insect at pupae stage is in its inactive immature form between larvae and adult. Conversion of larvae to pupae in the control group started at day 5th and reached to the highest number of animals (90%) at day 14th (Figure 28C). This conversion occurred in both R9 and cisplatin treatment on day 9th. While in former group it reached 70% on day 14th, in cisplatin group the conversion from larvae to pupae reached at 30% on day 12th continuing unchanged until day 20 (Figure 28C). Figure 28D show that in control at day 14th, pupae started to differentiate to wax moths (adults) from 10% and reached to 100% until the day 20th. In R9-treated group the conversion from pupae to wax moth occurred on day 15th from 10% and reached to 70% on day 20th. Moreover, in cisplatin none of pupae converted to wax moth (Figure 28D) revealing that cisplatin is highly toxic for *G. mellonella*. Regarding to R9, in comparison to cisplatin, it seems that *G. mellonella* well tolerate this Cu²⁺-complex.

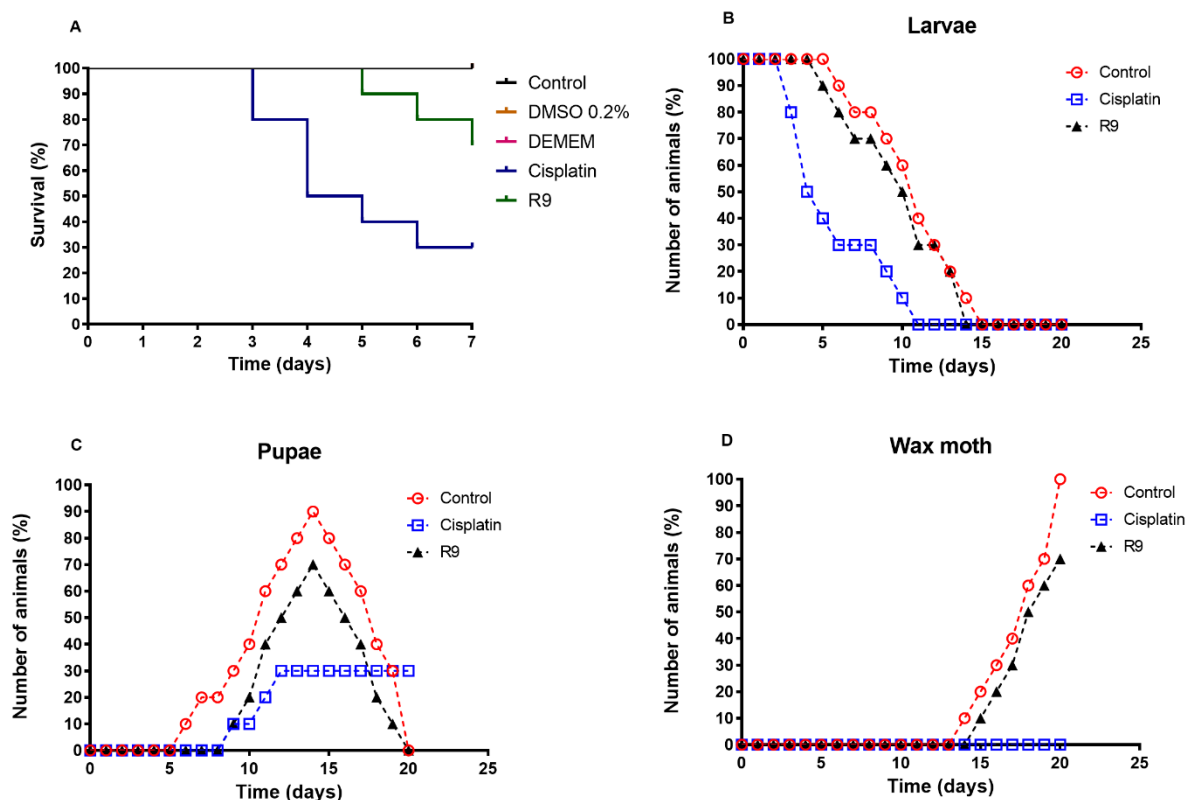


Figure 28. Toxicity of Cu²⁺-complex R9 and cisplatin on *G. mellonella*. Percentage of *G. mellonella* survival after exposure to 1 mg/mL of R9 or the clinical antitumor drug cisplatin over the period of 7 days (A). The control groups constituted in a group harboring untreated *G. mellonella*. Percentage of number of *G. mellonella* larvae after exposures to 1 mg/mL of R9 or cisplatin (B). Percentage of number of pupae (C) and percent of number of wax moth (D) after 20 days. Experimental groups were composed of 10 larvae, and the experiments were carried out in triplicates. The log-rank test was used to compare the survival rates; **p < 0.01 and *p < 0.05.

5.9.2 Toxicity of R9 in BALB/c nude mice.

Since we observed reduced toxicity of R9 to *Galleria mellonella*, we further analyzed the toxicity of this Cu^{2+} -complexes to BALB/c mice. For the *in vivo* toxicity test, female BALB/c nude mice were used. The approximately 20 g animals were divided into groups of 4 and treated with the Cu^{2+} -complex, R9, at dose of 0.8, 8 or 80 mg/kg for 30 days. By calculating nonlinear logarithmic regression, the toxicity curve was converted to a LD_{50} (Lethal Dose for 50 % of mice) value of 71.6 mg/kg (Figure 29). This experiment didn't finish and we have to repeat it again with more concentrations between 8 and 80 mg/kg to obtain a legitimate curve to calculate the proper LD_{50} .

The value found is 10.5 times higher than the LD_{50} of cisplatin (6.6 mg/kg) (ASTON et al., 2017), which means a much lower toxicity to the living organism. These results corroborate the IC_{50} values found in MCF10A indicating that the Cu^{2+} -complex R9 has a targeted activity to tumor cells, less damaging healthy cells.

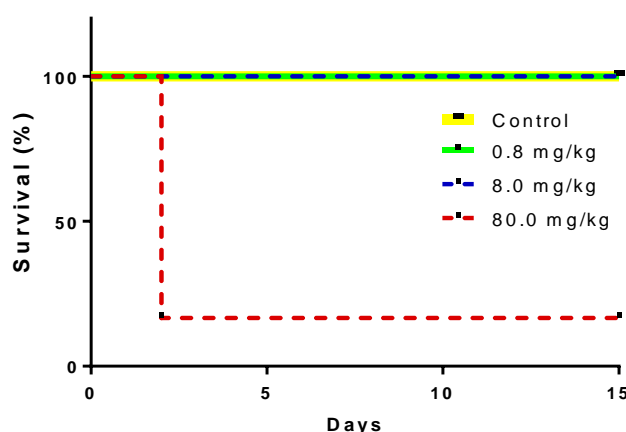


Figure 29. Determination the LD_{50} of Cu^{2+} -complex R9 in BALB/c nude mice. Mice weighing approximately 20 g were randomly divided into groups of 4 and subjected to treatment with 0.8, 8 or 80 mg of the Cu^{2+} -complex R9, per kg of the animal's weight. Survival of animals was monitored over 30 days and expressed as percentage of survival.

5.10 Analysis of differential expression of proteins in breast cancer cells in response to R10 treatment.

Our strategy consisted of deciphering differentially expressed proteins after treatment with R10 and cisplatin in comparison to untreated cells. Label-free-based quantitative proteomics were employed to identify differentially expressed proteins, which are expressed after R10 and cisplatin treatments.

In the proteomics analysis, we identified a total of 1,098 proteins from all systems tested: R10-treated, cisplatin-treated and untreated cells. 167 in R10- treated cells were differentially expressed proteins (DEP) recognized where 118 proteins were significantly downregulated and 49 proteins were upregulated. Moreover, 95 DEP in cisplatin-treated cells were founded which, 58 proteins were downregulated and 37 proteins were upregulated. All these proteins were identified with significant variation in their relative abundance by student T-test (p-value < 0.05) via Perseus software (Table 6).

Table 6. Total number of proteins, down/upregulated proteins expressed after R10/cisplatin treatment of MCF-7 cells at 24 h identified and quantified by label-free analysis.

	Proteins	Differentially expressed proteins R10-treated (p-value<0.05)	Differentially expressed proteins cisplatin-treated (p-value<0.05)
Label-free analysis	1,098	167	95
Downregulated proteins	-	118	58
Upregulated proteins	-	49	37

The 167 DEP by treatment with R10 and 95 proteins dysregulated via treatment with cisplatin were presented in the form of heatmap to visualize the trend of variation in the proteins profile of cells (Figure 30A and B). The Heat map illustrating the differentially expressed proteins (significantly up/downregulated) found in cells treated with R10/cisplatin. The complete list of protein analyzed comparing the systems treated or not with R10 and cisplatin was summarized in supplementary file (Attachment 1 and 2) where the selection criteria for up- and down-regulated proteins, gene name and GO biological process name included, besides p-value and/q-value < 0.05, ($n \geq 3$).

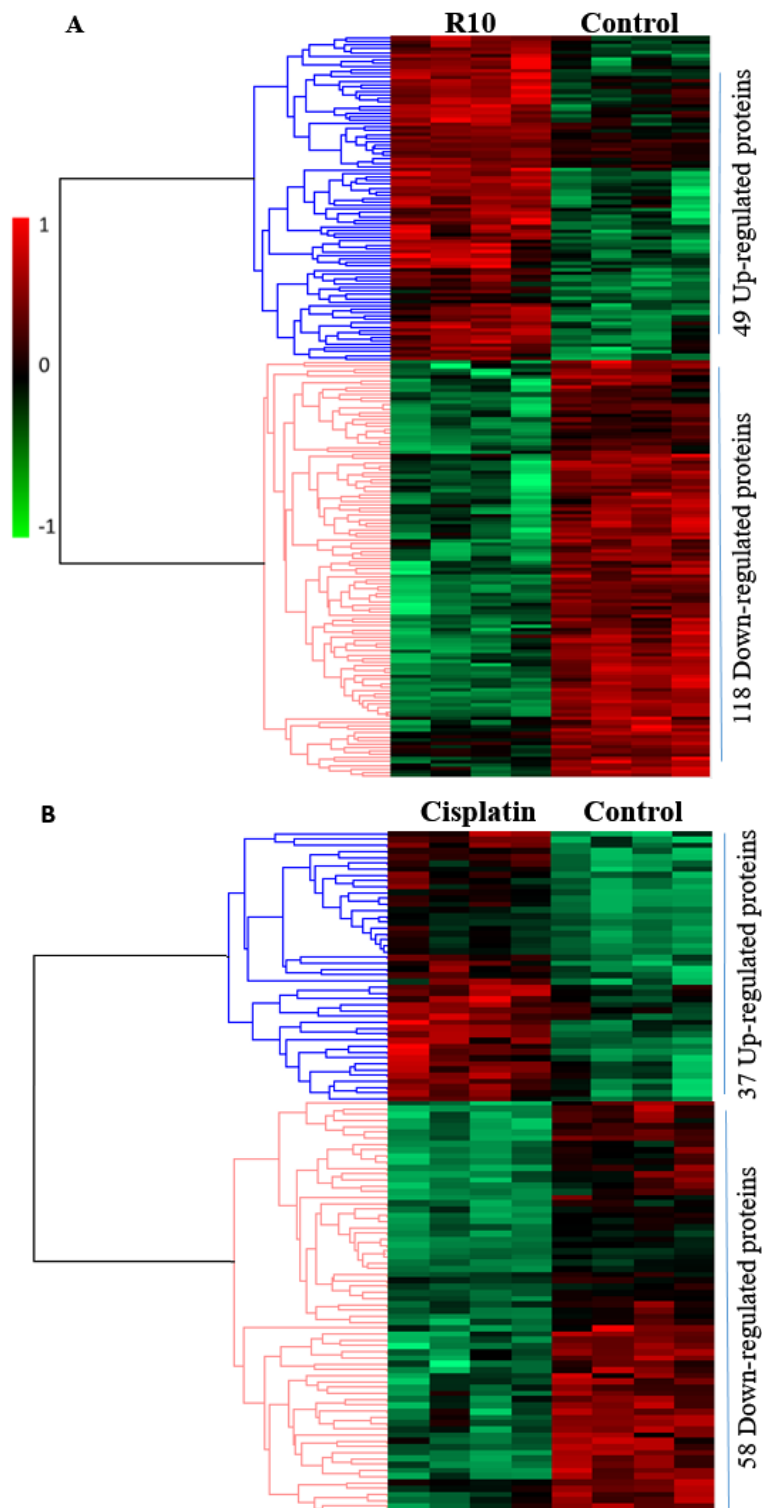


Figure 30. Heat map showing differentially expressed proteins in breast cancer cells. A bidirectional hierarchical clustering heat map constructed using Perseus 1.6.5.0. The expression values are \log_2 fold changes (>1 or <-1 , $FDR < 0.05$) between corresponding MCF-7 treated with R10 (A) and with cisplatin (B) after 24 h and untreated cells. Black represents no change in expression, green represents downregulation, and red represents upregulation.

The results in Volcano plot showed the quantitative difference in the abundance of proteins in cells treated with R10 vs control, R10 vs cisplatin and cisplatin vs control (Figure 31). To find the deregulated genes name and their GO biological process name, see Attachment 1 and 2.

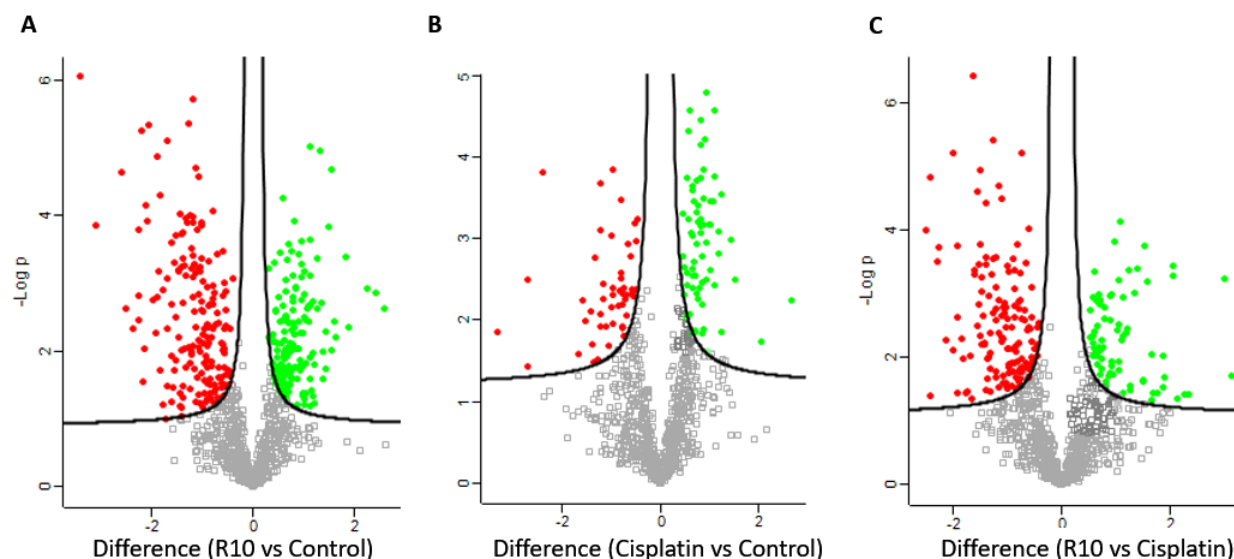
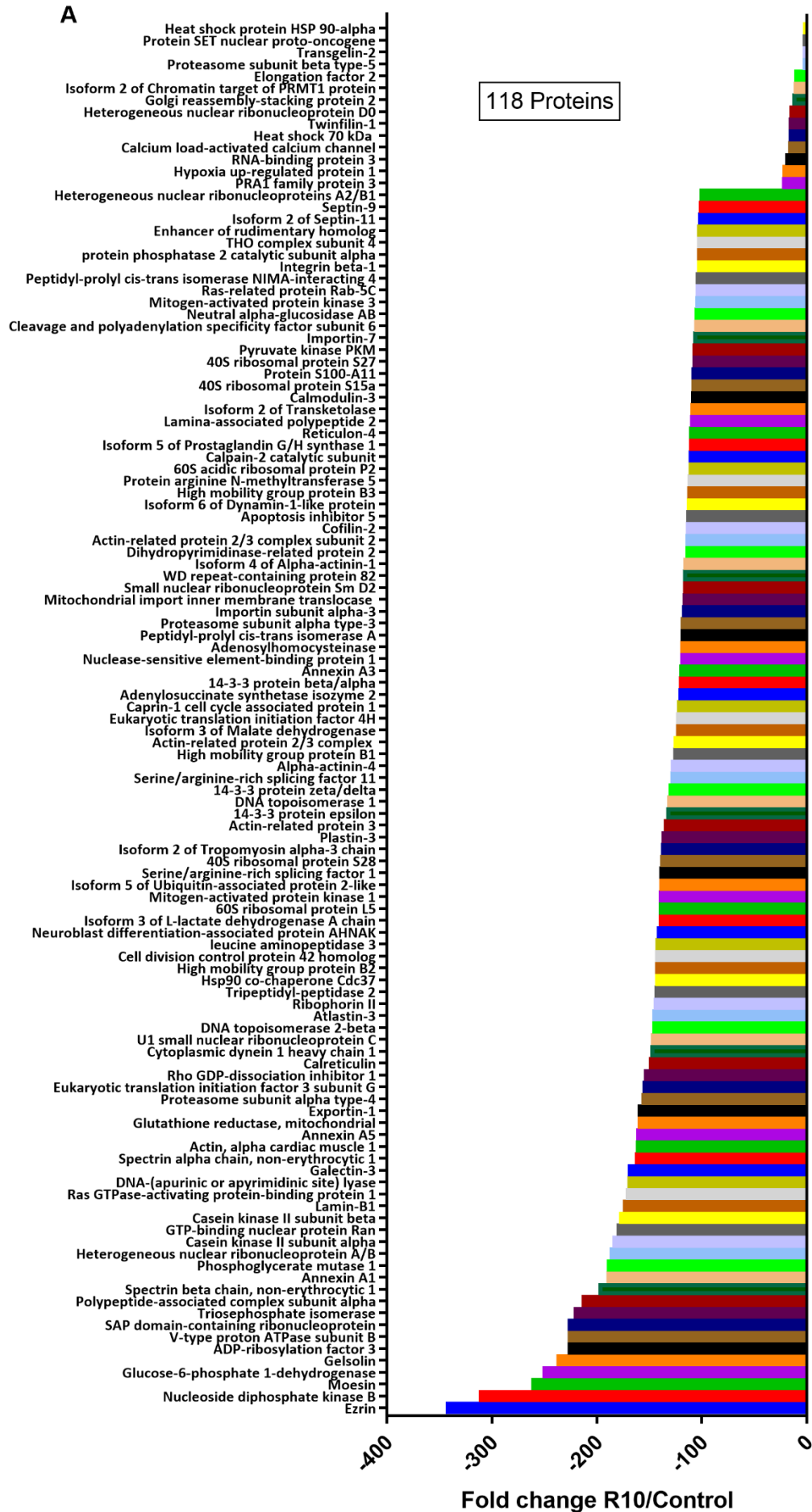
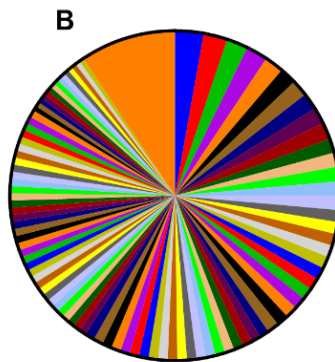


Figure 31. Comparison of proteins altered by R10 and cisplatin treatments in MCF-7 cells. Graphical representation of volcano plot illustrating the $-\log_{10}$ p-values as a function of \log_2 ratios between R10 and control (A), cisplatin and control (B), and R10 and cisplatin (C) treated samples analyzed in biological triplicates. Minus sign represents a decrease (red dots) and plus sign an increase (green dots) in protein expression from MCF-7 cells treated with R10/cisplatin. The gray squares are indicating no abundance change (\log_2 ratio = 0) and the p-value cut off ($p < 0.05$) are indicated.

Statistical analysis data revealed that from 167 proteins identified by R10-treated cells, a total of 194 pathways were altered. From the 167 altered proteins, 118 proteins were significantly downregulated and linked to the 189 downregulated pathways (Figure 32A and B). Moreover, 49 proteins were upregulated that were defined 40 upregulated pathways (Figure 32C and D). On the other hand, from 95 proteins expressed after the treatment with cisplatin, a totally 127 pathways were altered in which 58 proteins were downregulated being responsible for the downregulation of 105 pathways (Figure 33A and B). In addition, 37 proteins were upregulated being associated with the 47 upregulated pathways (Figure 33C and D).





Total=189

- | | |
|--|---|
| Regulation of actin cytoskeleton | NOD-like receptor signaling pathway |
| Viral carcinogenesis | B cell receptor signaling pathway |
| Metabolic pathways | Regulating pluripotency of stem cells |
| PI3K-Akt signaling pathway | cGMP-PKG signaling pathway |
| Tight junction | Fc epsilon RI signaling pathway |
| Fc gamma R-mediated phagocytosis | GnRH secretion |
| Oocyte meiosis | Cell cycle |
| Neurotrophin signaling pathway | B cell receptor signaling pathway |
| Axon guidance | Prolactin signaling pathway |
| Proteoglycans in cancer | Glucagon signaling pathway |
| Adherens junction | Thyroid hormone signaling pathway |
| Apoptosis | FoxO signaling pathway |
| Focal adhesion | mRNA surveillance pathway |
| Pathways in cancer | Gap junction |
| Rap1 signaling pathway | Proteasome |
| Leukocyte transendothelial migration | cAMP signaling pathway |
| Ribosome | TGF-beta signaling pathway |
| RNA transport | Mitophagy |
| Adrenergic signaling in cardiomyocytes | Endocrine resistance |
| Ras signaling pathway | Growth hormone synthesis |
| Autophagy | IL-17 signaling pathway |
| Ribosome biogenesis in eukaryotes | Cholinergic synapse |
| Endocytosis | Biosynthesis of amino acids |
| GnRH signaling pathway | Necroptosis |
| Oxytocin signaling pathway | Carbon metabolism |
| PD-L1 and PD-1 checkpoint pathway | HIF-1 signaling pathway |
| Central carbon metabolism in cancer | Choline metabolism in cancer |
| Phagosome | Vascular smooth muscle contraction |
| Sphingolipid signaling pathway | Glucagon signaling pathway |
| Long-term depression | Glycolysis / Gluconeogenesis |
| Protein processing in ER | ErbB signaling pathway |
| Chemokine signaling pathway | EGFR tyrosine kinase inhibitor resistance |
| Hippo signaling pathway | Platinum drug resistance |
| Spliceosome | Phospholipase D signaling pathway |
| Endocytosis | Glutathione metabolism |
| C-type lectin receptor signaling pathway | TNF signaling pathway |
| MAPK signaling pathway | Retrograde endocannabinoid signaling |
| Long-term potentiation | Wnt signaling pathway |
| mTOR signaling pathway | Th17 cell differentiation |
| Ribosome biogenesis in eukaryotes | Glutamatergic synapse |
| MicroRNAs in cancer | Parathyroid hormone synthesis |
| AGE-RAGE signaling pathway in diabetic | Toll-like receptor signaling pathway |
| Apelin signaling pathway | Base excision repair |
| T cell receptor signaling pathway | AMPK signaling pathway |
| VEGF signaling pathway | Epithelial cell signaling |
| Insulin signaling pathway | Th1 and Th2 cell differentiation |
| Estrogen signaling pathway | Purine metabolism |
| Serotonergic synapse | NF-kappa B signaling pathway |
| Platelet activation | Other |

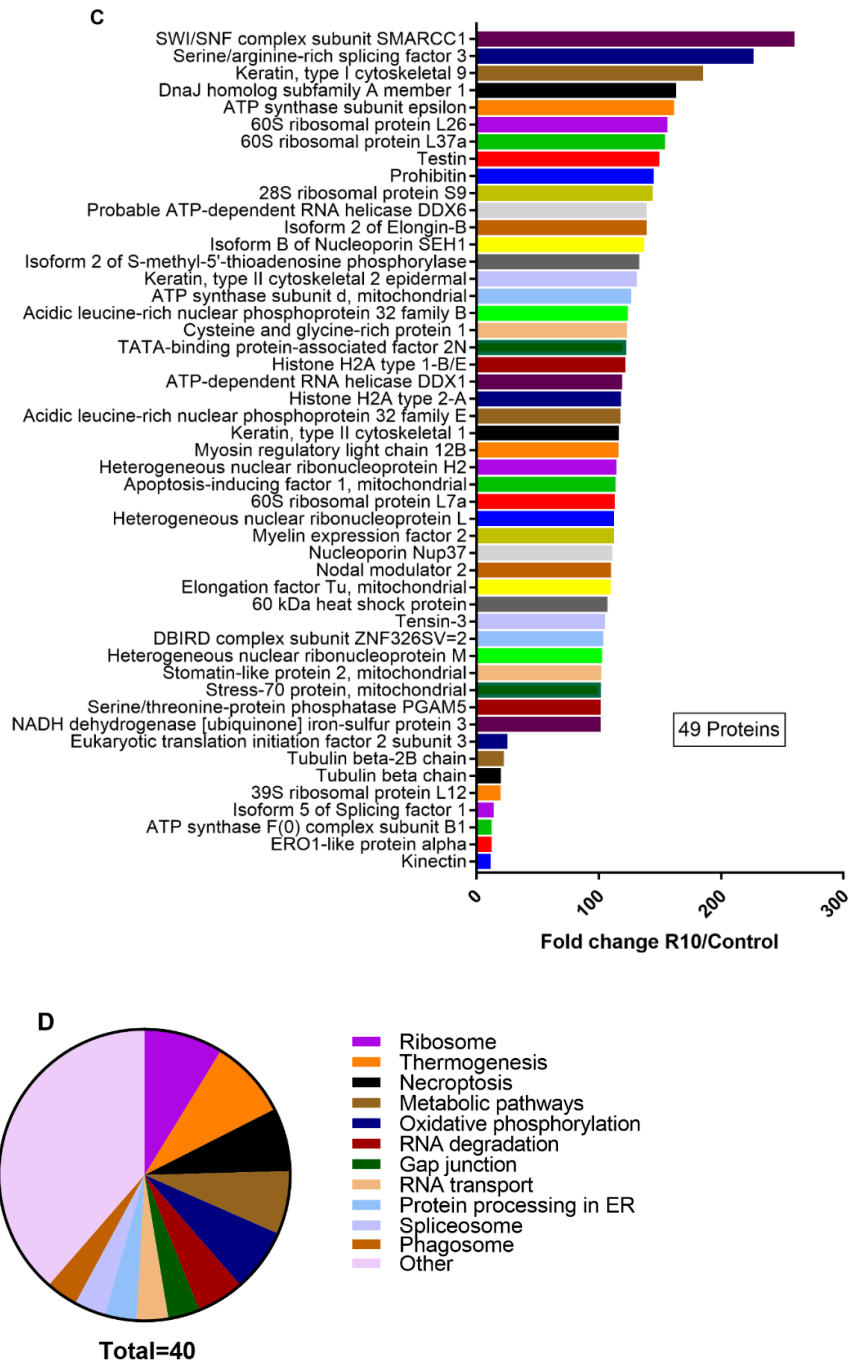
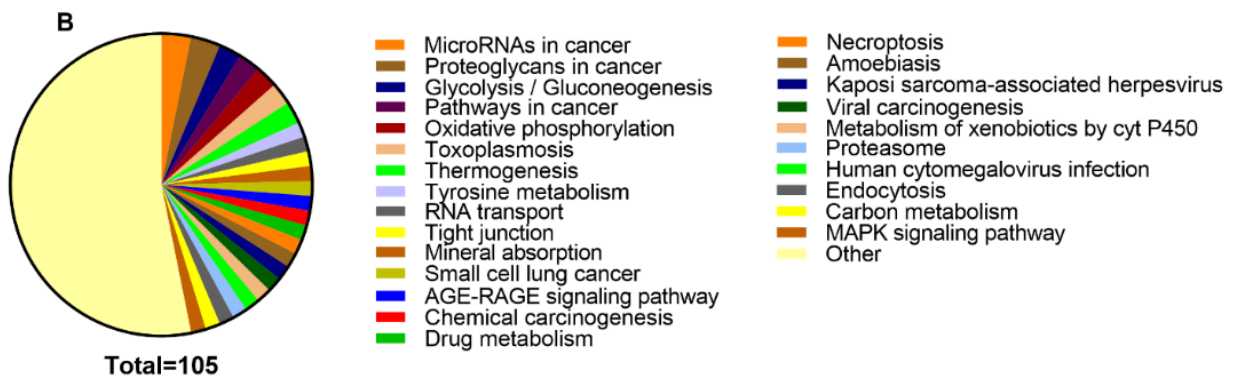
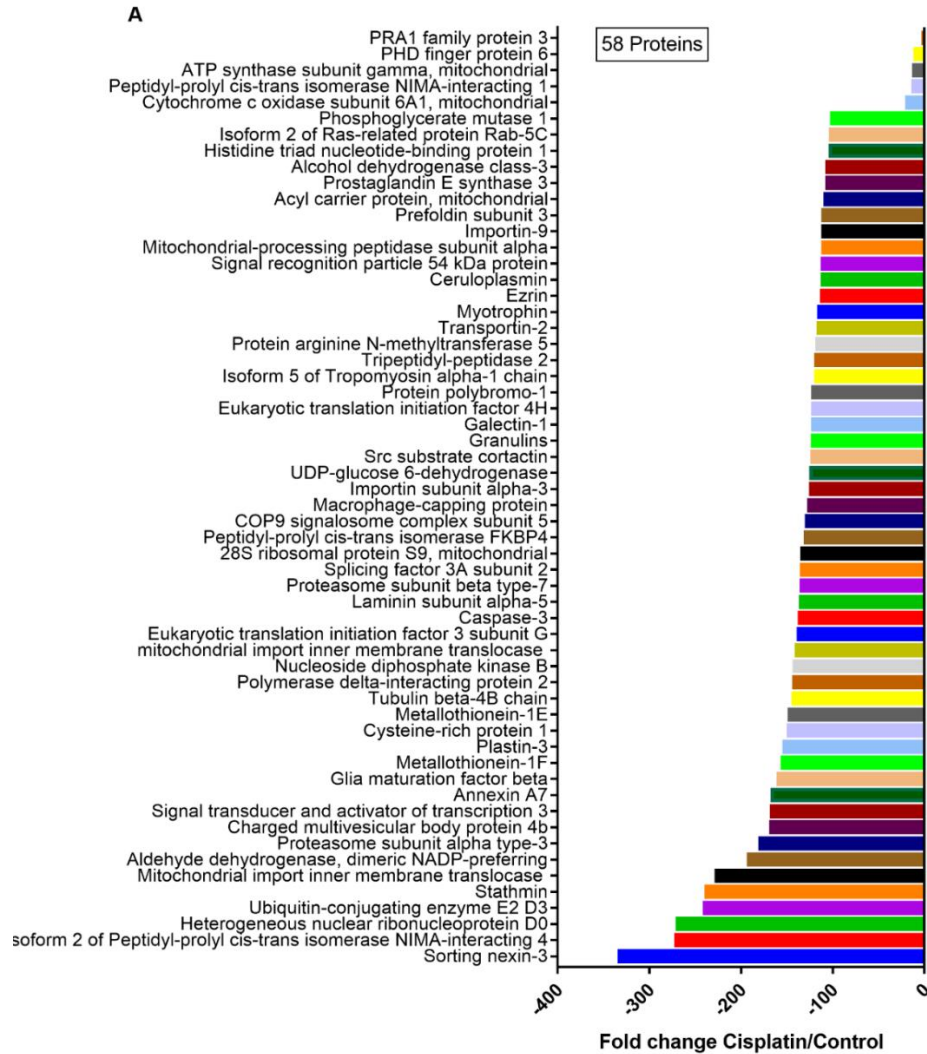


Figure 32. Analysis of differentially expressed proteins and their related pathways after R10-treated MCF-7 cells. Significantly downregulated proteins (A) and upregulated proteins (C) were identified with significant variation in their relative abundance by student T-test (p -value < 0.05) via Perseus software. KEGG mapper analysis was conducted on significantly downregulated proteins after R10-treated MCF-7 cells to address the related downregulated pathways (B). KEGG mapper analysis of significantly upregulated proteins to find the related upregulated pathways (D). Results extract from KEGG mapper and performed in GraphPad Prism version 7.0. Other include 1 protein participated in pathways. A protein was considered as differentially expressed when the fold change was strictly higher than 1 with $P < 0.05$.



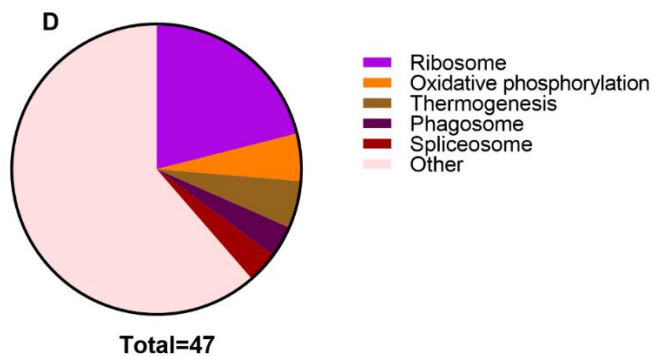
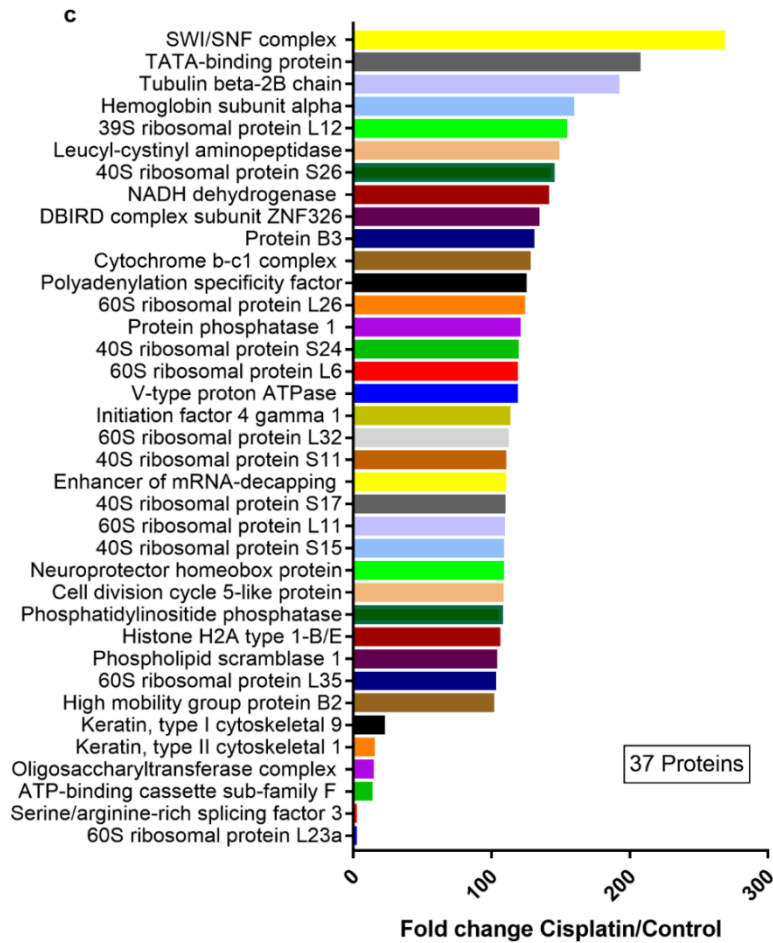


Figure 33. Analysis of differentially expressed proteins and their related pathways after cisplatin-treated MCF-7 cells. Significantly downregulated proteins (A) and upregulated proteins (C) were identified with significant variation in their relative abundance by student T-test (p -value < 0.05) via Perseus software. KEGG mapper analysis was conducted on significantly downregulated proteins after cisplatin-treated MCF-7 cells to address the related downregulated pathways (B). KEGG mapper analysis of significantly upregulated proteins to find the related upregulated pathways (D). Results extract from KEGG mapper and performed in GraphPad Prism version 7.0. Other include 1 protein participated in pathways. A protein was considered as differentially expressed when the fold change was strictly higher than 1 with $P < 0.05$.

Analysis of the results from R10-treated cells, using KEGG mapper for all 167 proteins showed total 189 pathways downregulated. The most downregulated pathways were belong to

the regulation of actin cytoskeleton (12 related proteins), viral carcinogenesis (10 related proteins), metabolic pathways (9 related proteins) and PI3K-Akt signaling pathway (9 related proteins), tight junction (8 related proteins), Fc gamma R-mediated phagocytosis (7 related proteins), oocyte meiosis (7 related proteins), neurotrophin signaling pathway (7 related proteins), axon guidance (7 related proteins) and proteoglycans in cancer (7 related proteins), adherence junction (6 related proteins), apoptosis (6 related proteins), focal adhesion (6 related proteins), pathways in cancer (MAPK signaling pathway, calcium signaling pathway and ECM receptor interaction) (6 related proteins) and Rap1 signaling pathway (6 related proteins) (Figure 32B). The related proteins that participated in each pathway are listed in Table 7. On the other hand, the most upregulated pathways from R10-treated cells was ribosome and thermogenesis (5 related proteins), necroptosis (4 related proteins), metabolic pathways (4 related proteins) and oxidative phosphorylation (4 related proteins) (Figure 32D, Table 7).

Table 7. Proteins differentially expressed in related to the most down/upregulated pathways after R10-treated MCF-7 cells that were analyzed by KEGG mapper.

KEGG ID	Downregulated	Upregulated	No. of proteins	Related proteins to each cell pathways
hsa04810	Regulation of actin cytoskeleton	–	12	ARPC3 (actin related protein 2/3 complex subunit 3), ARPC2;actin related protein 2/3 complex subunit 2, CFL2;cofilin 2,GSN:gelsolin, ITGB1; integrin subunit beta 1, MSN; moesin, NRAS; NRAS proto-oncogene, GTPase,MAPK1;mitogen-activated protein kinase 1, MAPK3;mitogen-activated protein kinase 3, EZR; ezrin, ACTN4; actinin alpha 4, CDC42;cell division cycle 42
hsa05203	Viral carcinogenesis	–	10	GSN; gelsolin, NRAS; NRAS proto-oncogene GTPase, PKM; pyruvate kinase M1/2, MAPK1; mitogen-activated protein kinase 1, MAPK3; mitogen-activated protein kinase 3, YWHAB; tyrosine 3-monooxygenase/tryptophan 5monooxygenase activation protein beta, YWHAE; tyrosine 3-monooxygenase/tryptophan 5-monooxygenase activation protein epsilon, YWHAZ; tyrosine 3-monooxygenase/tryptophan 5-monooxygenase activation protein zeta, ACTN4; actinin alpha 4, CDC42; cell division cycle 42
hsa04151	PI3K-Akt signaling pathway	–	–	CDC37; cell division cycle 37 HSP90 cochaperone, ITGB1; integrin subunit beta 1, NRAS; NRAS proto-oncogene, GTPase, PPP2CA; protein phosphatase 2 catalytic subunit alpha, MAPK1; mitogen-activated protein kinase 1, MAPK3; mitogen-activated protein kinase 3, YWHAB; tyrosine 3monooxygenase/tryptophan 5-monooxygenase activation protein beta, YWHAE; tyrosine 3monooxygenase/tryptophan 5-monooxygenase activation protein epsilon, YWHAZ; tyrosine 3monooxygenase/tryptophan 5-monooxygenase activation protein zeta
hsa01100	Metabolic pathways	–	9	ADSS2; adenylosuccinate synthase 2, AHCY; adenosyl homocysteinase, GSR; glutathionedisulfide reductase, LAP3; leucine aminopeptidase 3, PGAM1; phosphoglycerate mutase 1, ATP6V1B2; ATPase H+ transporting V1 subunit B2, PKM; pyruvate kinase M1/2, RPN2; ribophorin II,
hsa04151	PI3K-Akt signaling pathway	–	9	CDC37; cell division cycle 37 HSP90 cochaperone, ITGB1; integrin subunit beta 1, NRAS; NRAS proto-oncogene,

				GTPase, PPP2CA; protein phosphatase 2 catalytic subunit alpha, MAPK1; mitogen-activated protein kinase 1, MAPK3; mitogen-activated protein kinase 3, YWHAB; tyrosine 3monooxygenase/tryptophan 5-monooxygenase activation protein beta, YWHAE; tyrosine 3monooxygenase/tryptophan 5-monooxygenase activation protein epsilon, YWHAZ; tyrosine 3monooxygenase/tryptophan 5-monooxygenase activation protein zeta
hsa04530	Tight junction	–	8	ACTR3; actin related protein 3, HSPA4; heat shock protein family A (Hsp70) member 4, ITGB1; integrin subunit beta 1, MSN; moesin PPP2CA; protein phosphatase 2 catalytic subunit alpha, EZR; ezrin, ACTN4; actinin alpha4, CDC42; cell division cycle 42
hsa04666	Fc gamma R-mediated phagocytosis	–	7	ARPC3; actin related protein 2/3 complex subunit 3, ARPC2; actin related protein 2/3 complex subunit 2, CFL2; cofilin 2, GSN; gelsolin, MAPK1; mitogen-activated protein kinase 1, MAPK3; mitogen-activated protein kinase 3, CDC42; cell division cycle 42
hsa04114	Oocyte meiosis	–	7	PPP2CA; protein phosphatase 2 catalytic subunit alpha, MAPK1; mitogen-activated protein kinase 1, MAPK3; mitogen-activated protein kinase 3, YWHAB; tyrosine 3monooxygenase/tryptophan 5-monooxygenase activation protein beta, YWHAE; tyrosine 3monooxygenase/tryptophan 5-monooxygenase activation protein epsilon, YWHAZ; tyrosine 3monooxygenase/tryptophan 5-monooxygenase activation protein zeta, CALM3; calmodulin 3
hsa04722	Neurotrophin signaling pathway	–	7	ARHGDI2; Rho GDP dissociation inhibitor alpha, NRAS; NRAS proto-oncogene, GTPase, MAPK1; mitogen-activated protein kinase 1, MAPK3; mitogen-activated protein kinase 3, YWHAE; tyrosine 3-monooxygenase/tryptophan 5-monooxygenase activation protein epsilon, CALM3; calmodulin 3, CDC42; cell division cycle42
hsa04360	Axon guidance	–	7	CFL2; cofilin 2, DPYSL2; dihydropyrimidinase like 2, ITGB1; integrin subunit beta 1, NRAS; NRAS proto-oncogene, GTPase, MAPK1; mitogen-activated protein kinase 1, MAPK3; mitogen-activated protein kinase 3, CDC42; cell division cycle 42
hsa05205	Proteoglycans in cancer	–	7	ITGB1; integrin subunit beta 1, MSN; moesin, NRAS; NRAS proto-oncogene GTPase, MAPK1; mitogen-activated protein kinase 1, MAPK3; mitogen-activated protein kinase 3, EZR; ezrin, CDC42; cell division cycle 42
hsa04520	Adherens junction	–	6	CSNK2A1; casein kinase 2 alpha 1, CSNK2B; casein kinase 2 beta, MAPK1; mitogen-activated protein kinase 1, MAPK3; mitogen-activated protein kinase 3, ACTN4; actinin alpha 4, CDC42; cell division cycle 42
hsa04210	Apoptosis	–	6	LMNB1; lamin B1, NRAS; NRAS protooncogene GTPase, MAPK1; mitogen-activated protein kinase 1, MAPK3; mitogen-activated protein kinase 3, SPTAN1; spectrin alpha, non-erythrocytic 1, CAPN2; calpain 2
hsa04510	Focal adhesion	–	6	ITGB1; integrin subunit beta 1, MAPK1; mitogen activated protein kinase 1, MAPK3; mitogen activated protein kinase 3, ACTN4; actinin alpha4, CAPN2; calpain 2, CDC42; cell division cycle42
hsa05200	Pathways in cancer	–	6	ITGB1; integrin subunit beta 1, NRAS; NRAS proto-oncogene, GTPase, MAPK1; mitogenactivated protein kinase 1, MAPK3; mitogenactivated protein kinase 3, CALM3; calmodulin 3, CDC42; cell division cycle 42
hsa04015	Rap1 signaling pathway	–	6	ITGB1; integrin subunit beta 1, NRAS; NRAS proto-oncogene, GTPase, MAPK1; mitogenactivated protein kinase 1, MAPK3; mitogenactivated protein kinase 3, CALM3; calmodulin 3, CDC42; cell division cycle 42
hsa03010	–	Ribosome	5	RPL7A; ribosomal protein L7a, RPL26; ribosomal protein L26, RPL37A; ribosomal protein L37a, MRPL12; mitochondrial ribosomal protein L12, MRPS9; mitochondrial ribosomal protein S9

hsa04714	_	Thermogenesis	5	ATP5PD; ATP synthase peripheral stalk subunit d, NDUFS3; NADH:ubiquinone oxidoreductase core subunit S3, ATP5F1E; ATP synthase F1 subunit epsilon, ATP5PB; ATP synthase peripheral stalk-membrane subunit b, SMARCC1; SWI/SNF related matrix associated actin dependent regulator of chromatin subfamily c member 1
hsa04217	_	Necroptosis	4	PGAM5; PGAM family member 5, mitochondrial serine/threonine protein phosphatase, H2AC4; H2A clustered histone 4, H2AC18; H2A clustered histone 18, AIFM1; apoptosis inducing factor mitochondria associated 1
hsa01100	_	Metabolic pathways	4	ATP5PD; ATP synthase peripheral stalk subunit d, NDUFS3; NADH:ubiquinone oxidoreductase core subunit S3, ATP synthase F1 subunit epsilon, ATP synthase peripheral stalk-membrane subunit b
hsa00190	_	Oxidative phosphorylation	4	ATP5PD; ATP synthase peripheral stalk subunit d, NDUFS3; NADH:ubiquinone oxidoreductase core subunit S3, ATP5F1E; ATP synthase F1 subunit epsilon, ATP5PB; ATP synthase peripheral stalk-membrane subunit b

The table shows the KEGG ID, the most down/up-regulated pathways, number of proteins and the proteins related to each pathway.

Moreover, the KEGG mapper results of cisplatin-treated cells of all 95 proteins revealed the downregulation of 105 pathways. The most downregulated pathways were related to MicroRNAs and proteoglycans in cancer (4 related proteins identified in each pathway), glycolysis/gluconeogenesis (3 related proteins), pathways in cancer (apoptosis, ECM receptor interaction and cytokine-cytokine receptor interaction) (3 related proteins), oxidative phosphorylation (3 related proteins), and thermogenesis (3 related proteins) (Figure 33B, Table 8). The most upregulated pathways related to the cisplatin-treated cells were ribosome (12 related proteins), metabolic pathways (4 related proteins), oxidative phosphorylation (3 related proteins) and thermogenesis (3 related proteins) (Figure 33D, Table 8).

Table 8. Proteins differentially expressed in related to the most down/upregulated pathways after cisplatin-treated MCF-7 cells that were analyzed by KEGG mapper.

KEGG ID	Downregulated	Upregulated	No. of proteins	Related proteins to each cell pathways
hsa01100	Metabolic pathways	_	8	PTGES3; prostaglandin E synthase 3, ADH5; alcohol dehydrogenase 5 (class III), chi polypeptide, COX6A1; cytochrome c oxidase subunit 6A1, ALDH3A1; aldehyde dehydrogenase 3 family member A1, NDUFAB1; NADH: ubiquinone oxidoreductase subunit AB1, ATP5F1C; ATP synthase F1 subunit gamma, PGAM1; phosphoglycerate mutase 1, UGDH; UDP-glucose 6-dehydrogenase
hsa05206	MicroRNAs in cancer	_	4	STMN1; stathmin 1, STAT3; signal transducer and activator of transcription 3, EZR; ezrin, CASP3; caspase 3
hsa05205	Proteoglycans in cancer	_	4	CTTN; cortactin, STAT3; signal transducer and activator of transcription 3, EZR; ezrin, CASP3; caspase 3
hsa00010	Glycolysis / Gluconeogenesis	_	3	ADH5; alcohol dehydrogenase 5 (class III), chi polypeptide, ALDH3A1; aldehyde dehydrogenase 3 family member A1, PGAM1; phosphoglycerate mutase 1
hsa05200	Pathways in cancer	_	3	LAMA5; laminin subunit alpha 5, STAT3; signal transducer and activator of transcription 3, CASP3; caspase 3

hsa04714	Thermogenesis	–	3	COX6A1; cytochrome c oxidase subunit 6A1, NDUFAB1; NADH: ubiquinone oxidoreductase subunit AB1, ATP5F1C; ATP synthase F1 subunit gamma
hsa00190	Oxidative phosphorylation	–	3	COX6A1; cytochrome c oxidase subunit 6A1, NDUFAB1; NADH: ubiquinone oxidoreductase subunit AB, ATP5F1C; ATP synthase F1 subunit gamma
hsa03010	–	Ribosome	12	RPL35; ribosomal protein L35, RPL6; ribosomal protein L6, RPL11; ribosomal protein L11, RPL23A; ribosomal protein L23a, RPL26; ribosomal protein L26, RPL32; ribosomal protein L32, MRPL12; mitochondrial ribosomal protein L12, RPS11; ribosomal protein S11, RPS15; ribosomal protein S15, RPS17; ribosomal protein S17, RPS24; ribosomal protein S24, RPS26; ribosomal protein S26
hsa01100	–	Metabolic pathways	4	SACM1L; SAC1 like phosphatidylinositide phosphatase, NDUFS3; NADH:ubiquinone oxidoreductase core subunit S3, UQCRC2; ubiquinol-cytochrome c reductase core protein 2, ATP6V0D1; ATPase H ⁺ transporting V0 subunit d1
hsa00190	–	Oxidative phosphorylation	3	NDUFS3; NADH:ubiquinone oxidoreductase core subunit S3, UQCRC2; ubiquinol-cytochrome c reductase core protein 2, ATP6V0D1; ATPase H ⁺ transporting V0 subunit d1
hsa04714	–	Thermogenesis	3	NDUFS3; NADH:ubiquinone oxidoreductase core subunit S3, SMARCC1; SWI/SNF related, matrix associated, actin dependent regulator of chromatin subfamily c member 1, UQCRC2; ubiquinol-cytochrome c reductase core protein 2

The table shows the KEGG ID, the most down/up-regulated pathways, number of proteins and the proteins related to each pathway.

A total of 6 proteins related to the downregulation of apoptosis pathway in R10- treated cell include: lamin B1, NRAS proto-oncogene GTPase, mitogen-activated protein kinase 1, mitogen-activated protein kinase 3, spectrin alpha non-erythrocytic 1 (fodrin) and calpain 2. On the other hand, there is only one protein related to the upregulation of apoptosis, which is named apoptosis inducing factor mitochondria associated 1 (AIFM1) (Figure 34). In cisplatin-treated cell, the caspase 3 was the only protein related to downregulation of apoptosis pathway while there are no reports of protein related to the upregulation of apoptosis pathway in our result (Figure 35). We can observe that treatment with R10 induced different proteins in both up and downregulated apoptotic pathways which are quite different from the proteins expressed in downregulated apoptosis pathway in cisplatin-treated cells.

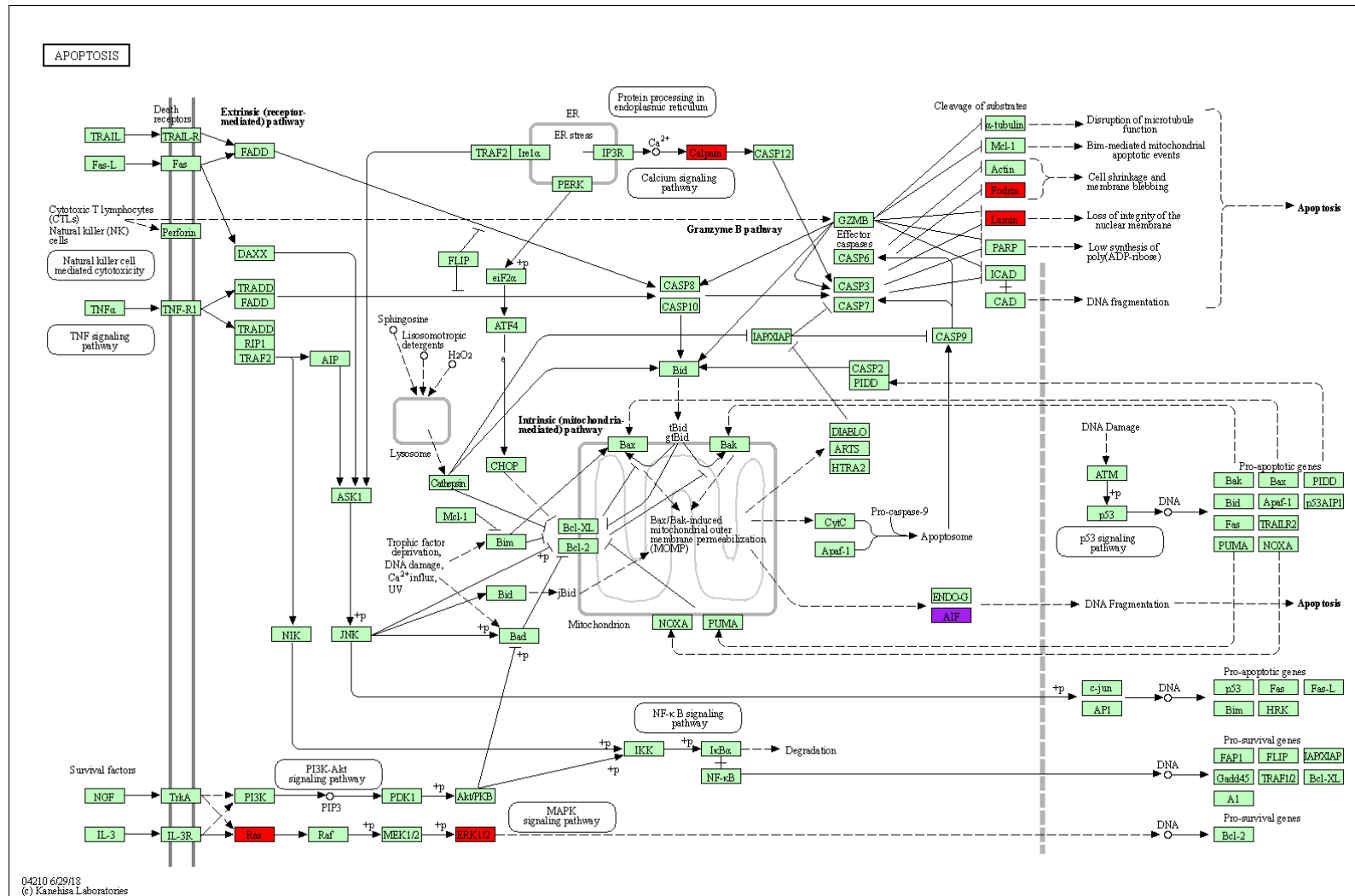


Figure 34. Signaling cascade for inducing apoptosis in R10-treated MCF-7 cells. Down/upregulation of expression of genes in the apoptosis pathway of R10-treated MCF-7 cells. Microarray data was mapped using KEGG Mapper Search & Color pathway. Red colors stand for the downregulated proteins and purple indicates the upregulated protein. The figure was generated using the KEGG Mapper Search & Color pathway program (KEGG mapper https://www.genome.jp/kegg-bin/color_pathway_object).

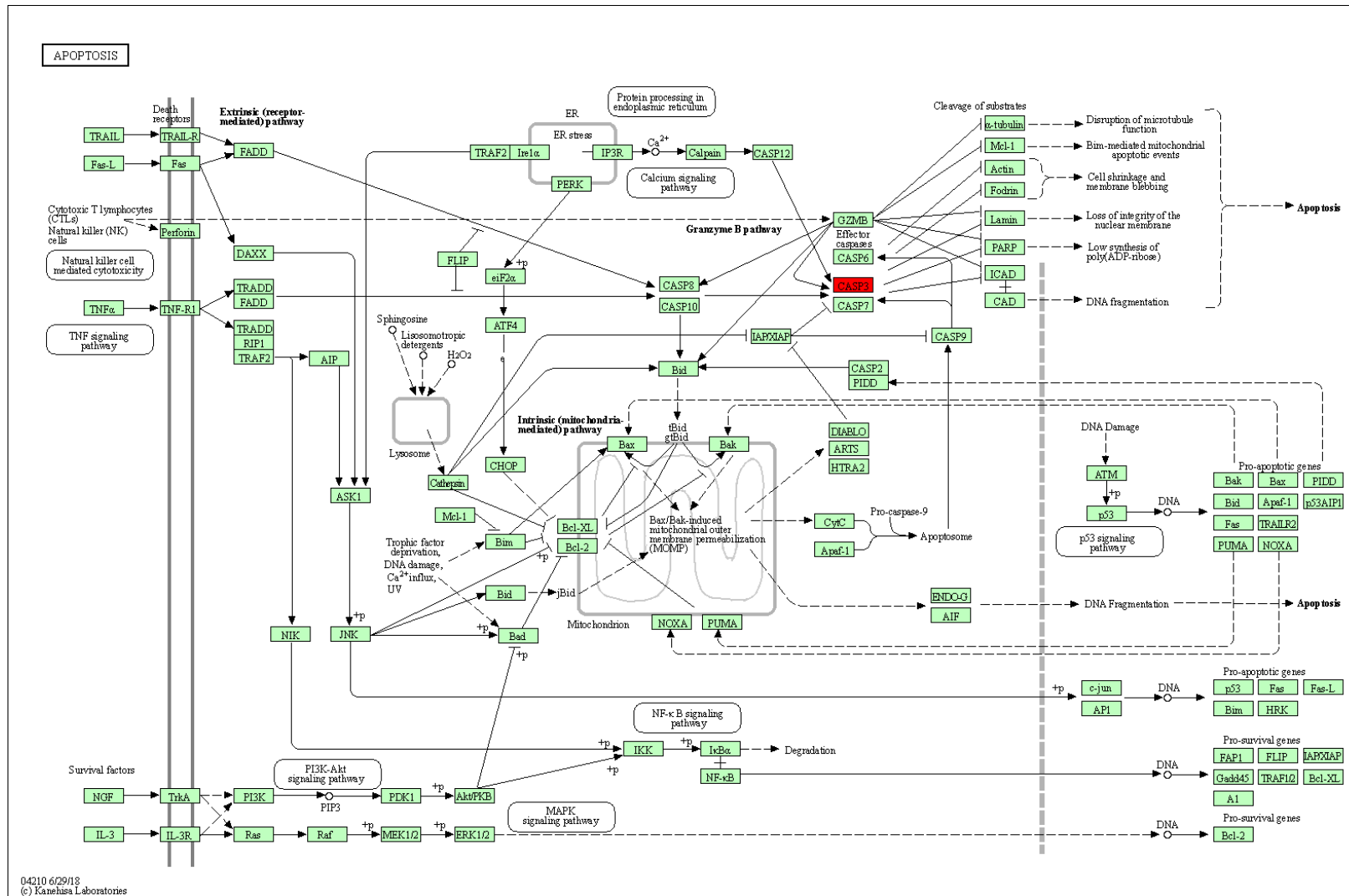


Figure 35. Signaling cascade for inducing apoptosis in cisplatin-treated MCF-7 cells. Microarray data was mapped using KEGG Mapper Search & Color pathway. Red colors indicate the downregulated proteins. The figure was generated using the KEGG Mapper Search & Color pathway program (KEGG mapper https://www.genome.jp/kegg-bin/color_pathway_object).

Venn diagram shows the comparison of up/downregulated proteins expressed in R10- and cisplatin-treated cells (Figure 36A and B). The 118 proteins identified in fraction with R10-treated that is downregulated showed 64%, and 58 proteins in cisplatin-treated represent 26.7%. Moreover, only 15 proteins (9.3%) were commonly expressed in both conditions (Figure 36A). These 15 common proteins are responsible for downregulation of 15 pathways after treatment of MCF-7 cells with both R10 and cisplatin (Figure 37A and B). On the other hand, according to Figure 36B we can see that the 49 proteins expressed in R10-treated cells in upregulated condition indicated 50.7% while 37 proteins expressed in cisplatin-treated cells displayed 34.7%. In addition, they share 14.7% of expressed proteins. 11 common proteins are related to the upregulation of 13 pathways in R0 treated cells and cisplatin-treated cells in MCF-7 cells (Figure 37A and C). These results exhibit the higher and differentiate expressed proteins after R10-treatment in comparison to cisplatin-treated cells. Taken together, we can conclude the possible difference in the mechanism of action of our Cu^{2+} -complex and cisplatin.

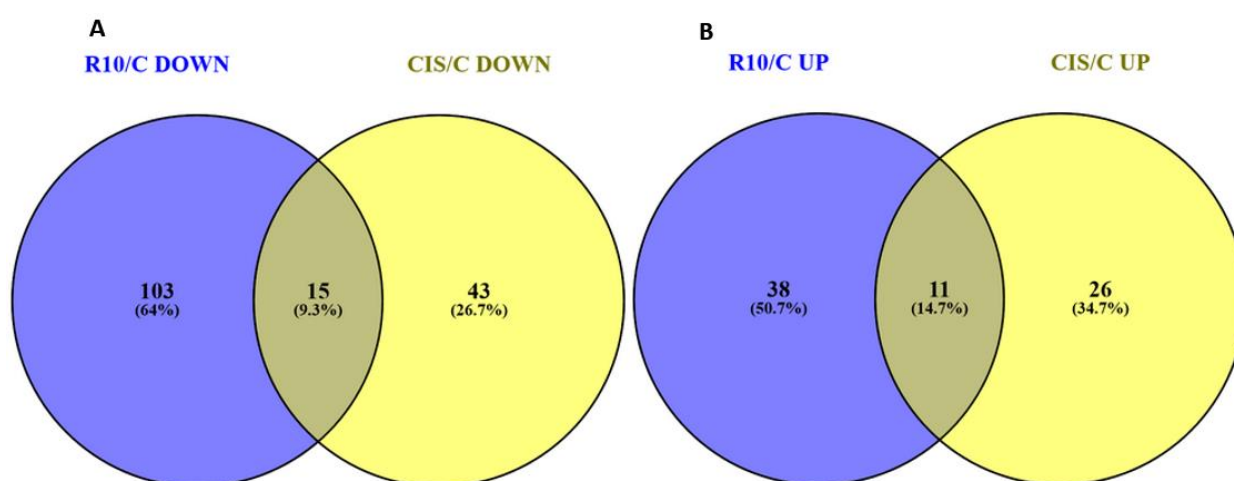


Figure 36. Comparison of the expressed down/upregulated proteins after R10/cisplatin treatment in MCF-7 cells. Venn diagram of overlap of downregulated proteins in R10-treated and cisplatin-treated cells showed in blue and yellow color, respectively (A) and Venn diagram of overlap of upregulated proteins in R10-treated and cisplatin-treated cells showed in blue and yellow color, respectively (B).

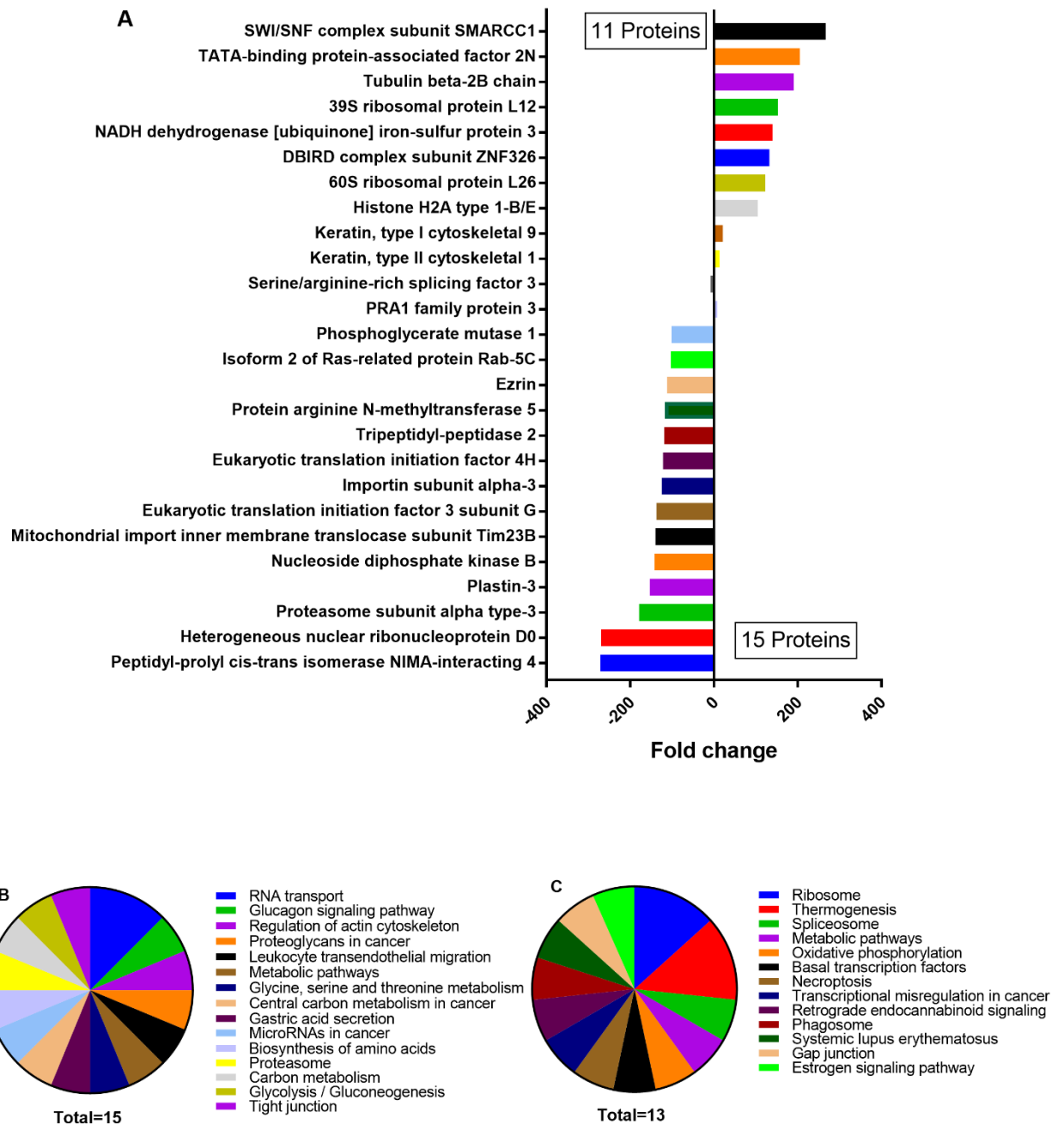


Figure 37. KEGG mapper analysis of common proteins expressed by R10 and cisplatin-treated MCF-7 cells. The common proteins expressed after R10 and cisplatin-treated MCF-7 cells (A). The downregulated pathways related to the common proteins expressed after R10 and cisplatin-treated MCF-7 cells (B). The upregulated pathways related to the common proteins expressed after R10 and cisplatin-treated MCF-7 cells (C). The results extract from KEGG mapper and performed in GraphPad Prism version 7.

In more detailed analysis of R10-treated cells from the KEGG pathway, we highlighted the regulation of actin cytoskeleton, metabolic pathway, apoptosis, RNA transport and ribosome as the principal downregulated biological processes, respectively while, the thermogenesis and apoptosis were chosen as the main upregulated biological process (Figure 38).



Figure 38. The most expressed proteins and their relative pathways in MCF-7 cells treated with R10. KEGG pathway analysis of proteins with statistically significant variation of some of most down and up-regulated expressed proteins and their relative pathways. The results extract from KEGG mapper and performed in GraphPad Prism version 7.

Regarding to the regulation of actin cytoskeleton pathway we can observe that ezrin (-341.86), moesin (-260.30) and gelsolin (-236.34) were the most downregulated expressed proteins after R10 treatment (Figure 38). The second obtained most downregulated pathway; metabolic pathways were associated to V-ATPase subunit B and pyruvate kinase with -225.93- and -106.90-fold change, respectively. PI3K pathway were identified as the third most downregulated pathway associated with, NRAS proto-oncogene GTPase, HSP90, mitogen-activated protein kinase 1, tyrosine 3-monooxygenase/tryptophan 5-monooxygenase activation protein epsilon and tyrosine 3-monooxygenase/tryptophan 5-monooxygenase activation protein zeta 3, tyrosine 3-monooxygenase/tryptophan 5-monooxygenase activation protein beta, mitogen-activated protein kinase3 and, integrin β . The related fold change calculated for these proteins were -173.95

-142.38, -139.09, -131.99, -129.59, -119.63, -104.42 and -102.43. The next most downregulated pathway was adherence junction related to the two main proteins, casein kinase II α (CK α) and casein kinase II β (CK β) with related fold change -183.06 and -176.58, respectively. Apoptosis pathway, downregulated by downregulation of NRAS proto-oncogene GTPase, lamin B1, spectrin alpha chain, mitogen-activated protein kinase 1, calpain-2 catalytic subunit and mitogen-activated protein kinase 3 by -173.95, -172.97, -161.6, -139.09, -104.42-fold change, respectively. GTP-binding nuclear protein Ran by fold change of -178.89 and exportin-1 by -158.72-fold change downregulated the RNA transport that was obtained amongst other downregulated pathways. The last but not the least, was the proteasome function which due to R10 treatment we identify the downregulation of proteasome subunit alpha type-3, proteasome subunit alpha type-4 and proteasome subunit beta type-5 in -117.85, -155.16- and -2.17-fold change, respectively.

Among upregulated pathways, the two most upregulated pathway were identified, thermogenesis and apoptosis. Protein SWI/SNF complex subunit SMARCC1 was related to the upregulation of thermogenesis by 258.64-fold change and the upregulation of apoptosis was related to upregulation of apoptosis-inducing factor 1, mitochondrial by 112-fold change.

6. Discussion

The increase in the incidence of various types of cancer in the world population has made this disease the second largest cause of death in the world. For this reason, great efforts to improve cancer prevention and therapies have been carried out in several countries. Within this context, chemotherapy remains the most common procedure used for several types of cancer. However, the intrinsic or acquired resistance of some tumors to specific drugs or to multiple drugs has been pointed out as the main limitation in cancer chemotherapy (SIDDIK, 2003; THIRUMARAN; PRENDERGAST; GILMAN, 2007). Thus, efforts are continuing to discover new antitumor drugs, increasing treatment options, and consequently therapeutic success. Therefore, based on the therapeutic success of cisplatin, metal-based drugs have been highlighted as a promising alternative for the development of new strategies in chemotherapy treatment (LIU *et al.*, 2013; ZAKI; ARJMAND; TABASSUM, 2016).

Over the last century, the number of metal-based complexes used in medicine has increased significantly (FREZZA *et al.*, 2010; GENG *et al.*, 2016; MEGGER *et al.*, 2017; WU *et al.*, 2016c). Recent developments of metallodrugs composed of different metals such as Pt, Cu, Fe, etc. have shown excellent potential as antitumor agents (FAGHIH *et al.*, 2018; MURTINHO *et al.*, 2015). Platinum-based drugs, such as carboplatin, cisplatin and oxaliplatin are being used in the treatment of approximately 50-70% of cancers (BRUNO *et al.*, 2017). Following the success of platinum-based drugs and considering their high toxicity, other metal compounds have been investigated that aim to be more effective and efficient in terms of: (i) pharmacology; (ii) increased patient survival; (iii) reduction of side effects and; (iv) reduction of clinical treatment costs. In addition, the synthesis of such compounds aims to increase interaction with DNA, overcoming the inherent or acquired resistance to cisplatin. In particular, great focus has been directed towards the development of novel copper compounds, whose anticancer activity has guided many researches with the objective of discovering new agents that are capable of overcome resistance and side effects associated with cisplatin. Therefore, due to the side effects of the drugs used in the current clinic, there is an urgent need in relation to the synthesis and development of new chemotherapeutic drugs. The high toxicity of platinum, causing a range of undesirable side effects, the emergence of tumor cell lines resistant to therapy and economical disadvantages, because platinum being a relatively rare metal, the cost of starting reagents for the synthesis of metallodrugs based on this metal are very expensive, which greatly increases the final price of drugs. Most of these problems are avoided by applying copper to the

synthesis, a cheap metal, much more reactive than platinum (which reduces the synthesis time of metallodrugs) and, even more importantly, a physiological metal that significantly reduces the side effects associated with its prolonged use in chemotherapy cycles.

Suntharalingam et al. (2016) have prepared a series of copper(II)-phenanthroline complexes containing indomethacin ligands as the Cu metallodrugs (BOODRAM et al., 2016). 1,10-Phenanthroline (phen) is a classic ligand in coordination chemistry, with specific properties that can increase versatility in metal ion binding. Indomethacin is nonsteroidal anti-inflammatory drug (NSAID) that is a potent inhibitor of COX isoenzymes, COX-1 and COX-2. Copper(II)-4,7-diphenyl-1,10-phenanthroline complex bearing two indomethacin moieties was tested against two human mammary epithelial cell lines, human bulk breast cancer/CSC-depleted cells (HMLER) and breast CSC-enriched cells (HMLER-shEcad) for 72 h. The compound was found to be the most promising antitumor candidate, with potent toxicity (IC_{50} of $0.31 \pm 0.01 \mu\text{M}$) towards breast CSCs for HMLER-shEcad over HMLER (SHIN; ESKANDARI; SUNTHARA LINGAM, 2019). Mechanistic studies showed that these Cu^{+2} -complexes containing phenanthroline and indomethacin exerts a cytotoxic effect through inhibition of COX-2 activity. In addition, the oxidative mechanism by which these Cu^{+2} -complexes induced DNA cleavage revealed that H_2O_2 was the major ROS intermediate formed during the DNA cleavage process. Cu^{+2} -complexes containing phenanthroline and indomethacin underwent reduction to the corresponding copper(I) form by guanine bases in DNA. The copper(I) formed then reduced molecular oxygen to superoxide, which generated hydrogen peroxide.

Metallodrugs containing Fe showed promising antitumor activity. Ferrocene-containing compounds an iron(II) metal center which is located between two cyclopentadienyl rings, have been extensively studied as antiproliferative agents (OSSOLA *et al.*, 2003; PATRA; GASSER, 2017; SWARTS *et al.*, 2008; ZHANG, PINGYU; SADLER, 2017). The antitumor properties of ferrocifen derivatives (derivatives of tamoxifen) designed to target hormone-independent breast cancers (JAOUEN; VESSIÈRES; TOP, 2015; PATRA; GASSER, 2017). Pigeon et al. (2017) recently reported that ferrociphenol compounds with cyclic imides have shown strong antiproliferative effects. Heterocyclic ferrociphenols bearing a succinimidyl compound were tested against three ovarian epithelial cancer cell lines, one of which is resistant to cisplatin, and exhibited high activity against SK-OV-3, A2780 and A2780-cisplatin resistant cell lines with IC_{50} (μM) of 0.30 ± 0.02 , 0.035 ± 0.005 and 0.49 ± 0.003 , respectively (PIGEON et al., 2017).

In this work, the cytotoxicity of two new dinuclear Cu^{+2} -complexes, $[\text{Cu}_2(\mu\text{-CH}_3\text{COO})(\text{OH}_2)(\text{L}_2)] \cdot 1\frac{1}{2}\text{H}_2\text{O}$ (R9) and $[\text{Cu}_2(\mu\text{-OH})(\text{OH}_2)(\text{HL}_2)]\text{ClO}_4 \cdot 2\text{H}_2\text{O}$ (R10), were tested against MCF-

7, A549 and PC3 and compared to cisplatin, a well-known standard metal-based chemotherapeutic agent, which was used as a control. The metal complexes in this work were synthesized by the group of Professor Nicolás A. Rey from the Pontifícia Universidade Católica do Rio de Janeiro (PUC-RJ) (RAFAELA DOS SANTOS MORAES; NICOLÁS ÁDRIAN REY, 2016). A common characteristic of both metal complexes used in this work is the presence of the H₃L1 ligand. The structure of the Cu⁺²-complexes generated from H₃L1, with exogenous hydroxide bridge (-OH) attached to the R9 and exogenous acetate bridge (-CH₃COO) attached to the R10. The copper (II) dinuclear complexes generated from H₃L1, both with an exogenous hydroxide bridge R9 and with exogenous acetate bridge R10 (prodrugs that would generate the biologically active form by hydrolysis reaction in the organism), have copper (II) centers unsaturated or containing labile ligands, such as the water molecule, which allows their interaction with biological macromolecules such as DNA, RNA and/or proteins.

Copper is an endogenous biologically relevant metal, necessary in many biological pathways and in enzymatic catalytic processes (NDAGI; MHLONGO; SOLIMAN, 2017; ZHANG; SADLER, 2017b). Redox chemistry of free copper ions can lead to the formation of ROS. Hence, copper concentration in the body should be highly regulated (GINOTRA et al., 2016). Copper can be effectively trapped and transported across cell membranes because copper can easily bound by many amino acid residues, such as methionine, histidine and cysteine (ÖHRVIK; THIELE, 2014). The importance of copper in the healthy functioning of cells, and the potential altered metabolism in cancer cells have encouraged researchers to investigate the use of copper complexes as an anticancer agent (NDAGI; MHLONGO; SOLIMAN, 2017; ZHANG; SADLER, 2017a). Many of copper complexes have been found to target DNA by intercalation, groove binding, inhibiting topoisomerase or proteasome enzymes (SANTINI *et al.*, 2014).

There are studies and developments that seek the transition between platinum and copper, but have not yet achieved the desired result. For example, the Brazilian patent, BR112-0190241353, with priority date 05/18/2017, entitled “combination therapies for the treatment of cancer”, reports a method for treating cancer by means of combination therapy involving an inhibitor agent of poly [ADPribose] polymerase (PARP) signaling and a second agent that regulates activity within the tumor microenvironment, being an inhibitor of regulatory T cells (Treg), a macrophage inhibiting agent, an antigen specific immune response enhancing agent or even a combination of them. More specifically, the pharmaceutical composition described in this document deals with a group of macrophages inhibiting agents, among which a copper chelate stands out. The study deals with a therapy against cancer (breast, lung and/or prostate) through the adjuvant use of copper chelates, but does not propose the use of metallodrugs based

on the metal itself. In addition, the intrinsic mechanism behind the anti-tumor action is proposed to be the improvement of the immune response or the increase in the activity of an immune cell in cancer patient (KAIMING SUN, JING WANG, 2017).

Another even closer example would be the document EP145711, with priority date 06/10/1983, which is entitled “copper complex for cancer treatment” and presents copper (II) complexes exhibiting activities analogous to the enzyme superoxide dismutase (SOD) in mammalian cells. This property is used for the treatment of cancer, since it replaces the lost or significantly reduced SOD activity in cancer cells. The treatment proposed in document EP145711 has advantages when compared to other methods, demonstrating that copper has the potential to reduce tumor growth, increase the survival of the host organism, decrease tumor metastases or even effects on differentiation morphology of cancer cells. However, the proposed mechanism of action targets only one of the characteristics of tumor cells, that is the recompositing of SOD activity lost in cancer cells, thus creating a condition to interrupt cell division and, consequently, tumor growth. As the mode of action of these complexes does not involve the cell death process, and therefore it is impossible to associate it to the concept of cytotoxicity (IC_{50}), it is difficult to compare their effectiveness with other cytotoxic compounds. Thus, it is clear that the rational development of new complexes that exhibiting alternative, and preferably multiple mechanisms of action can greatly improve the effectiveness of the new antitumor agents (OBERLEY LARRY; SORENSON JOHN R J, 1983).

An important class of copper complexes proposed in the context of cancer chemotherapy is described in American documents US5107005 and US5576326, dated 4/21/1992 and 11/19/1996, respectively. Under the titles “Process to obtain new mixed copper aminoacidate complexes from phenylate phenanthrolines to be used as anticancerigenic agents” and “copper amino acidate diimine nitrate compounds and their methyl derivatives and a process for preparing them”, these inventions refer to the synthesis of a series of new ternary copper (II) mononuclear complexes containing amino acids and aromatic phenanthrolines as ligands. The compounds have been proposed as antitumor agents with preferential therapeutic use for the treatment of solid and blood tumors (e.g. leukemia). The cytotoxicity results showed that the copper mononuclear complex tested, namely $[Cu(4,7\text{-dimethyl-}1,10\text{-phenanthroline})(\text{glycinate})]NO_3$ has activity subtly superior to cisplatin, but inferior to mitomycin, reference drugs used in cancer therapy. *In vivo* study with experimental animals (rats of the B6D2F1 strain) showed that only at higher doses of the compound, it was possible to verify increased survival of animals affected by the inoculation of lymphoid leukemia cells. However, its lower activity in relation to the reference drug (mitomycin), the lack of an improved statistical test to compare the results

obtained with cisplatin, the lack of comparison of animal tests with the reference drugs, the lack of definition regarding the mechanism of death (e.g. apoptosis or necrosis) and the fact that the invention refers only to copper mononuclear complexes leave an open field for the improvement of these metallodrugs (AZUARA, 1992; AZUARA, 1996).

The development of new drugs requires a series of laboratory tests to find out the basics of biological activity. An essential characteristic of a compound that is thought to be a potential antineoplastic drug is cytotoxicity in tumor cells. Cytotoxicity effect of Cu^{2+} -complexes on lung, breast and prostate cancer cells was performed using the MTT method (ALBRECHT et al., 2003). It is important to note that cisplatin was used as a positive control because it was the most successful antineoplastic coordination compound used in cancer therapeutics, though it is not the first line of chemotherapy treatment for breast cancer.

The cytotoxic results obtained for the Cu^{2+} -complexes used in this work were extremely promising. The complexes showed a very high cytotoxic effect close to $1 \mu\text{M}$, against the cancer cell lines MCF-7, A549 and PC3. In comparison to the standard drug, cisplatin, the obtained IC_{50} values for each Cu^{2+} -complexes (R9 or R10) was around 13 to 30 times lower than that of obtained for cisplatin in those three cancer cell lines (MCF-7, A549 and PC3). Despite the high cytotoxic effect of Cu^{2+} -complexes on different types of cancer (breast, lung and prostate), the toxicity is reduced in healthy human mammary epithelial cell line MCF10A. Moreover, the cytotoxicity of R9 and R10 on MCF-10A cells was almost 7 and 8 times lower than that of observed in the MCF-7 cell line, respectively. The numerous copper-based complexes as an antineoplastic have been demonstrating high cytotoxicity effect with low IC_{50} in different tumor types (CHAVEZ-GONZALEZ et al., 2017; RUIZ-AZUARA; E. BRAVO-GOMEZ, 2010; SANTINI et al., 2014). In this context, regarding to Cu^{2+} -complexes, the series of mononuclear Cu^{2+} -complexes named casiopeinas (set of coordination complexes with a central copper atom bound to organic ligands designed to be used as antineoplastic) are the most successful copper-based complexes with antitumor potential (CARVALLO-CHAIGNEAU *et al.*, 2008; CHAVEZ-GONZALEZ *et al.*, 2017; RUIZ-AZUARA; E. BRAVO-GOMEZ, 2010). Casiopeina III-ia [aqua, 4,4-dimethyl-2,2-bipyridine, acetylacetonate copper(II) nitrate] has completed preclinical trials and entered clinical phase I in Mexico (GALINDO-MURILLO et al., 2015; MEJÍA; ORTEGA-ROSALES; RUIZ-AZUARA, 2018). The casiopeina $[\text{Cu}(\text{L})(\text{acetylacetonate-})]\text{NO}_3$, with L= (4,4'-dimethyl-2, 2'-bipyridine), named casiopeina III, has been one of the most investigated prototypes of a wide series of similar complexes (BRAVO-GOMEZ et al, 2010). Casiopeina III showed promising *in vivo* activity against xenografts of HCT-15 colorectal cancer cells (CARVALLO-CHAIGNEAU et al, 2008). The *in vitro* effects of casiopeina III-Ea, on cells from

patients with chronic myeloid leukemia (CML) revealed an IC_{50} of 0.5 μM for K562 cells (human myelogenous leukemia cell line), 0.63 μM for MEG01 cells (human mega karyoblastic leukemia *cell line*), 0.38 μM for CML $CD34^+lin^-$ cells [primary $CD34^+$ Lineage-negative (Lin^-) cells selected from CML bone marrow) and 1 μM for normal $CD34^+lin^-$ cells (CHAVEZ-GONZALEZ et al., 2017). The IC_{50} calculated in cancer cell lines (K562, MEG01 and CML $CD34^+lin^-$) was 2, 1.5 and 2.6 times lower in cultures of CML cells as compared to their normal counterparts, respectively. Given that, the histological analysis of casiopeina III revealed a chronic irritative effect for peritoneal necrosis. Comparing the effect of casiopeina III-Ea on normal cells counterparts (normal $CD34^+lin^-$ cells) with our result showed that R9 and R10 are less harmful to the non-cancer cells.

The mechanisms of cytotoxicity of metal-based drugs in general are quite diverse. Subtle changes in the structure of the metal complexes can cause large changes in the physico-chemical properties of them and consequently change their biological activity (LIN et al., 2013). The activity of these classes of drugs depends not only on the metal itself but also on the oxidation state and the structure of the ligand. In this context, many metal-based complexes require redox modifications before reaching their goal to become active (CHEN et al., 2009; GILL; VALLIS, 2019). The active complexes may cause several cellular challenges, including DNA breaks, topoisomerase inhibition, ROS generation, endoplasmic reticulum stress and inhibition of proteasome (GILL; VALLIS, 2019). These cellular effects may cease the cell cycle or cause the induction of apoptosis. After detection of promising activity of the Cu^{2+} -complexes R9 and R10 in breast, lung and prostate cancer cell lines, the mechanism of action of the compounds was investigated.

Apoptotic cells can be identified by morphological changes such as shrinkage of the cell, condensation of chromatin (pyknosis), nucleus fragmentation (karyorrhexis) and disintegration of the cell to apoptotic body (SARASTE; PULKKI, 2000). As an early event in apoptosis, cells change to round shape and undergo the reduction of the cell size, loss of contact with their neighbors and shrinkage (PISTRITTO et al., 2016; SARASTE; PULKKI, 2000). The cell rounding followed by chromatin condensation, organelle compaction, membrane blebbing and the formation of intact apoptotic bodies is the characteristic of apoptotic cells (HÄCKER, 2000; KERR; WYLLIE; CURRIE, 1972).

We started exploring the mechanism of action of Cu^{2+} -complexes by observation of the pictures of cells obtained by light microscope to evaluate the extension of morphological changes occurred after 24 h treatment of MCF-7 and A549 cells with IC_{50} concentration of R9 and R10. The results revealed some relevant morphological changes when compared to untreated cells.

The most significant alterations were rounding in shape with swollen of cell body after treatment with both Cu^{2+} -complexes. Foo et al. (2019) reported the change in morphology of MCF-7 cells by the copper complex (*S*-benzyl dithiocarbamate and 3-acetylcoumarin) $[\text{Cu}(\text{SBCM})_2]$. The $\text{Cu}(\text{SBCM})_2$ -treated MCF-7 cells at IC_{50} (30 μM) concentration demonstrated characteristics of apoptosis such as shrinkage at 48 hours. Nevertheless, other features of apoptosis such as chromatin condensation and formation of apoptotic bodies were not observed. While in our study, MCF-7 and A549 treated with R9 and R10 at IC_{50} (1 μM), both showed the shrinkage and detachment of cells after 24 h that may relate to the higher activity of R9 and R10 against cancer cells in comparison to the $[\text{Cu}(\text{SBCM})_2]$ (FOO et al., 2019).

The morphologic alterations study of casiopeina III-ia [(4,4-dimethyl-2,2-bipyridine) (acetylacetonate) copper(II) nitrate] on colon adenocarcinoma HCT-15 cell line revealed that Cas III-ia induces morphological changes (CARVALLO-CHAIGNEAU et al., 2008). Treatment of cells with 5 μM Cas III-ia after 24 h showed swollen organelles and rupture of plasmatic membrane that didn't occur on lower concentration (2.5 μM). Comparing to our results, the concentration of Cas III-ia used was higher than that of used in our experiment with R9 and R10. This indicates that R9 and R10 seem to be more effective than Cas III-ia to induce cell morphology changes.

Perusing this result, we design our experiment to find the other plausible changes in the cancer cells after treatment with Cu^{2+} -complexes. Thus, as cell death pathways, such as apoptosis, may also be associated with alterations in cellular granularity, we explore the effect of Cu^{2+} -complexes on granularity of cancer cells (DIVE et al., 1992). The result suggests that change in morphology may also affect intracellular granularity, which in turn may be associated with cell death. Accordingly, our results showed an increase of intracellular granularity in both MCF-7 and A549 cell lines after R9 and R10 exposure at IC_{50} (1 μM) concentration for 24 h. Increases in intracellular granularity have been observed during several physiological processes that include senescence, apoptosis and autophagy, making this phenotypic change a useful marker for identifying chemotherapeutic drug that induce cellular growth arrest or death (GAO et al., 2019; PUSPITA; BEDFORD, 2017). For example, treatment of DU145 prostate cancer cells with boric acid results in increased intracellular granularity and decreased proliferation which indicates the growth arrest associated with increased intracellular granularity (BARRANCO; ECKHERT, 2006; HAYNES et al., 2009). As we know, one of the targets for cancer therapeutics is the cell death through autophagy and an important aspect of autophagy is the production of autophagic vacuoles (MARINKOVIĆ et al., 2018). The presence of numerous vacuole-like structures in autophagy reminiscent that autophagic cells progressively detached

from the others and acquired a rounded shape and increase granularity (GOSSELIN et al., 2009). The chemotherapy drugs such as tamoxifen (anti-estrogens) cause extensive accumulations of autophagic vacuoles in MCF-7 cells, metformin promotes autophagy and apoptosis in esophageal squamous cell carcinoma and docetaxel has been demonstrated to induce senescence in murine TC-1 cells that correlate with cell death (BURSCH et al., 1996; SAPEGA et al., 2018). Thus, chemotherapeutic exposure may be associated with increased intracellular granularity in cell lines derived from human cancers. Haynes et al. (2009) have developed a phenotypic assay regarding androgen-induced increases in intracellular granularity in the LNCaP prostate cancer cell line. This study revealed that intracellular granularity in cancer cell lines may provide a simple and rapid screening tool for agents that exhibit favorable qualities as cancer therapeutic agents. Herein, the increase intracellular granularity of both cancer cells after treatment with R9 and R10 can be an indicative of cellular injury similar to the process of apoptosis.

Following the change in morphology and granularity of breast and lung cancer cells caused by Cu^{2+} -complexes, we next determined whether Cu^{2+} -complexes induce apoptosis in both cancer cells. According to the literature, the great majority of antineoplastic drugs show the induction of cell death by apoptosis as their mechanism of action. Hence, the experiments of Sub-G1 and TUNEL were chosen to measure the number of cells with DNA degradation. Treatment with R9 and R10 showed an increase of cell population in Sub-G1 and concomitant decrease in G1, S and G2/M phase in both tested cell lines. Comparing the results of DNA fragmentation in untreated cells (control), the induction of 277.4 and 165.2 times higher in DNA fragmentation (Sub-G1) was observed in R9- and R10-treated MCF-7. This amount was slight lower in A549 treated cells reaching to 136.5 and 96-times higher than control. In our experimental conditions, the levels of cells with DNA fragmentation and consequently possible apoptosis reached more than 50% in both tested cell lines by the effect of R9 and R10, that is significantly higher than the percentage of DNA fragmented cells induced by cisplatin. The comparison with cisplatin demonstrated the percentage of DNA in Sub-G1 phase showed 1.6 and 1.5 times higher in MCF-7 treated by R9 and R10, respectively and 3.2 and 2.2 times higher in A549 treated by R9 and R10, respectively. Therefore, in the IC_{50} (μM) concentration tested both Cu^{2+} -complexes demonstrated a significant greater capacity than cisplatin to induce DNA fragmentation.

In recently synthesized copper complex (*S*-benzyl dithiocarbamate and 3-acetylcoumarin) $[\text{Cu}(\text{SBCM})_2]$ it was found that $\text{Cu}(\text{SBCM})_2$ induced G₂/M cell cycle arrest and apoptosis in MCF-7 cells (FOO et al., 2019). MCF-7 cells treated with IC_{50} concentration (30 μM) of $\text{Cu}(\text{SBCM})_2$ resulted in increments in G₂/M phase in comparison to the untreated cells in which

the percentage was increased from 15.21 % in untreated control to 24.92% in treated cells at 24 h (1.6 times higher than the control). Whereas, in our results, treatment with R9 and R10 caused DNA fragmentation at concentration of IC_{50} (1 μ M) after 24 h with percentage of DNA in Sub-G1 phase about 277.4 and 165.2 times higher than control. There is great difference between the results of Cu^{+2} -complexes study here and the $[Cu(SBCM)_2]$ indicating that R9 and R10 may be a promising anticancer compounds.

In other study, ternary complex $[Cu(Z)-2-((1-(3-chlorophenyl)-3-methyl-5-oxo-4,5-dihydro-1H-pyrazol-4-yl)(p-tolyl)methylene) hydrazine carbothioamide, 1,10-phenanthroline]$ $[Cu(TMCPMP-TS)(Phen)]$ was synthesized by Vyas et al. (2013). The cell cycle analysis of an untreated control group showed 3.33% of cells in the Sub-G1 phase whereas, the $[Cu(TMCPMP-TS)(Phen)]$ effect on A549 at IC_{50} concentration (0.24 μ M) after 24 h, recorded 83.3% of cells in the Sub-G1 phase (25.2 times more than that of control) (Vyas et al 2013). The result of R9 and R10 at IC_{50} (1 μ M), 24 h in the A549 cell was 136.5 and 96 times higher than control, respectively. Compared to $[Cu(TMCPMP-TS)(Phen)]$, the R9 and R10 have more ability to induce apoptotic cells in A549 cell line.

Cu^{+2} -complex with tridentate N_2O ligand di(2-pyridil) ketone-1-adamantoyl hydrazine (Addpy) of the formula $[Cu^{II}_2 Cu^I_2(Addpy)_2 Br_2(\mu -Br_4)]$ synthesized by Rodić et al. (2016), showed IC_{50} of 1.24 ± 0.30 against HeLa cells. Treatment of HeLa cells with an IC_{50} concentrations of the compound does not lead to any significant changes in the cell cycle distribution while, the $2 \times IC_{50}$ concentrations (2.5 μ M) of this Cu^{+2} -complex caused a slight increase of cells in the Sub-G1 phase (RODIĆ et al., 2016). Of note, our result clearly shows that R9 and R10 have the ability to increase the percentage of cells in the Sub-G1 phase at the IC_{50} concentration.

Since we have observed the increase in percentage of cells in the Sub-G1 phase in MCF-7 and A549 after Cu^{+2} -complexes treatment, an additional experiment was necessary to confirm the occurrence of DNA fragmentation. The TUNEL analysis, as it is more sensitive and specific than the technique performed by detection of DNA fragmentation by Sub-G1, reduces the possibility of quantifying cells in other mechanisms of cell death such as necrosis or autophagy. The results from TUNEL assay, displayed the number of cells with DNA degradation that might be related to the apoptotic cells. The percentage of cells with DNA degradation induced by R9 and R10 in MCF-7 were 3.5 and 3.6 times higher than the control, respectively. On the other hand, the R9 and R10 induced the percentage of cells with DNA degradation to 2.1 times higher than control in A549. The result corroborates with the one observed in the analysis performed with the cells in Sub-G1 except for the cisplatin that induced the same percentage of apoptotic cells as R9 and R10 in both cell lines. The fact that cytotoxicity occurs

by induction of apoptosis is particularly important since this type of cell death, as it is contained in apoptotic bodies, avoid triggering an inflammatory process and damaging to neighboring tissues (SALGANIK, 2001). For example, copper-based complexes with variations of the ligand thiosemicarbazone (TSC) such as $[\text{Cu}^+(\text{TSC})(\text{H}_2\text{O})_2]\text{Cl}_2 \cdot 2\text{H}_2\text{O}$ promote DNA fragmentation and induction of apoptosis in tumor cells (TISATO et al., 2010).

Two Cu^{+2} -complexes of the type $[\text{Cu}(\text{bimda})(\text{diimine})]$, where bimda is *N*-benzylimino diacetic acid, diimine is 1,10-phenanthroline (phen) and dipyrido[3,2-*d*: 2',3'-*f*]quinoxaline (dpq) were reported to assess their cytotoxicity against human breast cancer cell lines (MCF-7) after 24 h of treatment that exhibited IC_{50} (μM) of 13.4 ± 1.8 and 9.2 ± 0.7 , respectively (SANTINI et al., 2014). Moreover, they induced a remarkable DNA fragmentation in MCF-7 cells at IC_{50} concentration after 24 h about 70% and 76.5%. In Comparison to our result, R9 and R10 induced 60.2% and 61.2% of the DNA degraded cells in MCF-7 at the IC_{50} concentration (1 μM). Though in both studies, the MCF-7 cells treated with Cu^{+2} -complexes resulted in more than 50% of DNA fragmented cells, but our compounds, R9 and R10 induced DNA fragmentation at 1 μM concentration whereas, $[\text{Cu}(\text{N-benzyliminodiacetic acid})(1,10\text{-phenanthroline})]$ and $[\text{Cu}(\text{N-benzyliminodiacetic acid})(\text{dipyrido}[3,2\text{-}d: 2',3'\text{-}f]\text{quinoxaline})]$ induced DNA damaged at the concentration of 13.4 μM and 9.2 μM , respectively. The concentrations of R9 and R10 used in our experiment is around 13 and 10 times lower than complexes synthesized by Santini et al. 2014, respectively. Hence, R9 and R10 may have higher potential to act as effective anticancer drugs than $[\text{Cu}(\text{N-benzyliminodiacetic acid})(1,10\text{-phenanthroline})]$ and $[\text{Cu}(\text{N-benzyliminodiacetic acid})(\text{di-pyrido}[3,2\text{-}d: 2',3'\text{-}f]\text{quinoxaline})]$.

The casiopeinas were explicitly designed to interact with genetic material, producing oxidation and DNA fragmentation, through the generation of ROS after copper reduction (SERMENT-GUERRERO et al., 2011). Serment-Guerreo et al. (2011), studied the genotoxicity of four complexes. (a) casiopeina III-Ea $[\text{Cu}(4,7\text{-dimethyl-}1,10\text{-phenanthroline})\text{acac}]\text{NO}_3$, (b) casiopeina III-Ia $[\text{Cu}(4,4'\text{-dimethyl-}2,2'\text{-bipyridine})\text{acac}]\text{NO}_3$, (c) casiopeina III-Ha $[\text{Cu}(4,7\text{-diphenyl-}1,10\text{-phenanthroline})\text{acac}]\text{NO}_3$, and (d) casiopeina II-gly $[\text{Cu}(4,7\text{-dimethyl-}1,10\text{-phenanthroline})(\text{glycinato})]\text{NO}_3$. DNA degradation was assessed in Hela cells by SCGE (single cell gel electrophoresis). It can be seen that all casiopeinas exposed to almost $40 \times \text{IC}_{50}$ concentration (40 μM) at 30 min, produced DNA fragmentation with cell percentage of 37%, 19%, 85% and 9% in casiopeina III-Ea, casiopeina III-Ia, casiopeina III-Ha and casiopeina II-g, respectively. Comparing to our results, the treatment time induction in this study was 30 minutes that is 12 times lower than the treatment time in our study (24 h). Moreover, the concentration of casio-

peinas induced in HeLa cells were 40 μM which is 40 times higher than the R9 and R10 concentration induced in MCF-7 and A549. Overall, these four casiopeinas, R9 and R10 are capable of damaging in DNA.

Several reports show that cell apoptosis can be indicated *via* the mitochondrial pathway, which may be dependent on ROS generation (CUI et al., 2018; LI et al., 2014; SINHA et al., 2013). Mitochondrial-derived ROS have increasingly been reported to function as signaling molecules that might change cellular physiology. The excessive generation of ROS is one of the factors that lead to intracellular damage which may cause the activation of the intrinsic pathway of apoptosis signaling. Oxidative stress occurs in cells when the phase generation of ROS overwhelms the cellular antioxidant system. Oxidative imbalance due to metabolic properties has been observed in various types of cancer. One of the consequences of increased ROS is that cancer cells become more susceptible to agents that cause oxidative damage. Hence, the development of drugs that cause an oxidative imbalance has been shown to be an efficient alternative for the elimination of neoplastic cells (SULLIVAN; CHANDEL, 2014).

Our results showed the induction of ROS in both MCF-7 and A549 cell lines after 24 h of treatment with R9 and R10 in all concentration tested $\frac{1}{2} \text{IC}_{50}$, IC_{50} and $2 \times \text{IC}_{50}$. The increase of ROS occurred in a dose dependent way. In recently synthesized Cu^{+2} -complex (*S*-benzyl dithiocarbazate and 3-acetylcoumarin) $[\text{Cu}(\text{SBCM})_2]$, the induction of intracellular ROS was not detected in MCF-7 cells (FOO et al., 2019). On the other hand, The Cu^{+2} -complex 1-methyl-2-(2-pyridinyl) benzimidazole $\text{Cu}(\text{pbzMe})$ synthesized by Prosser et al. (2017), showed the intracellular ROS generation in the A549 cell line after 1.5 h at $2 \times \text{IC}_{50}$ (10 μM), showed the induction of ROS that was 6 times higher than that of in control (PROSSER et al., 2017). In our result, A549 cell line treated with both Cu^{+2} -complexes at the concentrations of $2 \times \text{IC}_{50}$ after 24 h revealed the %ROS generated 3.5 times higher than the control. Given the difference in time incubation of cells with $\text{Cu}(\text{pbzMe})$, R9 and R10, we can conclude that ROS can significantly generate in all complexes of both study in A549 cells.

Borges et al (2013) reported the effect of [bis-(2-oxindol-3-yl-imino)-2-(2-aminoethyl)pyridine-N, N] copper(II) perchlorate $[\text{Cu}(\text{isaepy})]$, on melanoma TM1MNG3 and TM1G3 cells (melanoma cell line that lost galectin-3 expression). Exposing cells to 60 μM $[\text{Cu}(\text{isaepy})]$ for 24 h led to increases of 1.6 and 1.8 times higher in mean fluorescence intensity (MFI) intracellular oxidation in melanoma TM1MNG3 and TM1G3 cells, respectively compared with the control (BORGES et al., 2013). However, in our results, mean fluorescence intensity in MCF-7 by the effect of R9 and R10 at the highest concentrations $2 \times \text{IC}_{50}$ (2 μM) were about 3.4 and 3.7 times higher than that of in control, respectively. Furthermore, in R9 and R10-treated A549

cells, MFI calculated at the highest concentration $2 \times IC_{50}$ (2 μ M) was 4.2 and 4.6 times higher than control, respectively. The ROS induction calculated in both MCF-7 and A549 treated with R9 and R10 at 2 μ M concentrations was much higher than that of induced in TM1MNG3 and TM1G3 cells at 60 μ M by [Cu(isaepy)].

The copper(II) complex derived from N,N'-dimethyl ethylene diamine and 2-hydroxyacetophenone Schiff base ligand, Cu(BrHAP)₂ demonstrated increase in ROS formation at $2 \times IC_{50}$ concentration (6 μ M) after 24 h in colon carcinoma HT-29 cells (HAJREZAIE et al., 2012). The ROS produced by Cu(BrHAP)₂ at the IC_{50} (2.87 μ M) concentration was non-significant while at $2 \times IC_{50}$, ROS production increased 2 times more than untreated cells (HAJREZAIE et al., 2012). In our results, the amount of ROS produced by the effect of R9 and R10 at $2 \times IC_{50}$ (2 μ M) were about 3.4 and 3.7 times higher than the control in MCF-7 and 4.2 and 4.6 times higher than the control in A549 cells, respectively. We can clearly see that the induction of ROS in HT-29 cells by Cu(-BrHAP)₂ at 6 μ M concentration was lower than that of induced by R9 and R10 at 2 μ M in MCF-7 and A549 cells. Study the mechanism of Cu(4,7-dimethyl-phenanthroline)(glycinate)]NO₃(Casiopéina IIgly) on A549 by Kachadourian et al. (2010) showed that A549 cells treated with Cas IIgly at IC_{50} concentration (5 μ M) after 24 h, showed increased levels of ROS around 2 times higher than untreated control (KACHADOURIAN et al., 2010). R9 and R10 showed the production of ROS after 24 h at IC_{50} concentration (1 μ M) in A549 about 3.7 and 4.1, respectively that is higher than the ROS amount produced by Cas IIgly.

Increased intracellular oxidation in both MCF-7 and A549 cells might have effect on mitochondrial membrane potential dissipation. The mitochondrial membrane potential ($\Delta\Psi_m$) is an essential component in the process of energy production generated by complexes I, III and IV (proton pumps) during oxidative phosphorylation. The movement of electrons along the respiratory chain pumps protons across the inner mitochondrial membrane during aerobic respiration building an electrochemical proton motive force, embracing of a hyperpolarized transmembrane voltage (Ψ_{IM} , negative inside) (GLAGOLEV; SKULACHEV, 1978). Via an electrochemical gradient, protons move down through ATP synthase to generate ATP. Dissipation of hyperpolarization across inner mitochondrial membranes, lead to open the voltage-sensitive permeability transition pore (PTP) and may release pro-apoptotic agents (e.g. cytochrome c) into the cytoplasm and drive apoptotic cell death (ZAMZAMI et al., 1995). Many researchers indicate that in some apoptosis there is a change in mitochondrial structure and ($\Delta\Psi_m$). Marzo et al (2001) showed that loss of $\Delta\Psi_m$ may occur in two stages. Initially, $\Delta\Psi_m$ dissipation occurs before the caspase is activated, so that the loss of an initial partial $\Delta\Psi_m$ may be due to a non-caspase agent that

is still sufficient to signal an obligation for the cell to undergo apoptosis. Subsequently, the release of cytochrome c (Cyt c) and/or AIF with the activation of caspase-9 leads to caspase activation and increased $\Delta\Psi_m$ dissipation. Therefore, the activation of the caspase may provide a reinforcing feedback loop that result in the destruction of $\Delta\Psi_m$. Finally, complete loss of $\Delta\Psi_m$ and induction of apoptosis may occur due to an unknown caspase (MARZO et al., 2001). Our results indicated a marked reduction in mitochondrial membrane potential of MCF-7 and A549 with both Cu^{2+} -complexes at the concentration of $\frac{1}{2}\text{IC}_{50}$, IC_{50} and $2\times\text{IC}_{50}$ and a nearly complete depolarization of the mitochondrial membrane potential at concentrations of $2\times\text{IC}_{50}$ like the inhibitor of the mitochondrial function FCCP. The copper-imidazo[1,2-a]pyridines complex has been reported by Harmse et al. (2019) represented high cytotoxicity effect against HT-29 cells with an IC_{50} value lower than 1 μM . Treatment of HT-29 cells with the copper-imidazo[1,2-a]pyridines complex at $10\times\text{IC}_{50}$ after 12 h resulted in a loss of mitochondrial membrane potential. In our study, we performed the assay with $\frac{1}{2}\text{IC}_{50}$, IC_{50} and $2\times\text{IC}_{50}$ concentrations at 24 h which we observed the loss of mitochondrial membrane potential in all concentrations (HARMSE et al., 2019). Given that, Harmse et al. and colleagues performed lower treatment time (12 h) compare to our study, but to induction of mitochondrial dissipation, they used the 10 times higher concentration ($10\times\text{IC}_{50}$) of compound because at the lower concentration they didn't see mitochondrial depolarization. It might be concluded that R9 and R10 may have higher impact on mitochondrial depolarization at lower concentration than copper-imidazo[1,2-a]pyridines complex.

$\text{Cu}(4,7\text{-dimethyl-phenanthroline})(\text{glycinate})\text{NO}_3$ (Casiopeína IIgly) investigated by Remy Kachadourian et al.(2010) on A549 caused a depolarization of the mitochondrial membrane of A549 cells at IC_{50} concentration (5 μM) after 16 h. R9 and R10 lead to mitochondrial membrane loss of A549 at $\frac{1}{2}\text{IC}_{50}$, IC_{50} and $2\times\text{IC}_{50}$ concentrations which is lower than the concentration of Casiopeína IIgly used by Kachadourian et al. (2010) (KACHADOURIAN et al., 2010).

Maciel et al.(2020) reported the synthesis of copper complex $[\text{Cu}(\text{L}1)\text{Cl}]\text{Cl}\cdot 2\text{H}_2\text{O}$, where $\text{L}1= 1\text{-}[2\text{-hydroxybenzyl}(2\text{-pyridylmethyl})\text{amino}]\text{-3-(1-naphthylloxy)-2-propanol}$ with IC_{50} of $26.5 \mu\text{M} \pm 1.1$ on lung carcinoma cell NCI-H460. After 24 h treatment with $2\times\text{IC}_{50}$, cells showed high loss of mitochondrial membrane potential. Dissipation of mitochondrial membrane occurred by R9 and R10 in A549 and MCF-7 at $\frac{1}{2}\text{IC}_{50}$, IC_{50} and $2\times\text{IC}_{50}$ concentrations that is very lower than the concentration of $[\text{Cu}(\text{L}1)\text{Cl}]\text{Cl}\cdot 2\text{H}_2\text{O}$ used by Maciel et al (MACIEL et al., 2020).

Cytotoxic compounds can induce apoptosis by different signaling pathways (e.g. extrinsic and/or intrinsic signal). In the intrinsic pathway, internally damages caused by cytotoxic drugs provokes changes in mitochondrial functioning and thus, altering the mitochondrial membrane potential, which permits the release of cytochrome c. Consequently, the release of Cyt c from mitochondria promotes the activation of Apaf-1 protein, which leads to the activation of caspase 9 (ELMORE, 2007; WU et al., 2016a). Caspase 9 is an initiator caspase, belongs to a family of caspases, cysteine-aspartic proteases involved in apoptosis and cytokine signaling and is a key player in the intrinsic or mitochondrial pathway which is involved in various stimuli, like chemotherapies, stress agents and radiation (LI et al., 2017; MCILWAIN; BERGER; MAK, 2013). Thus, in order to ascertain by which signaling, extrinsic or intrinsic, the Cu^{2+} -complexes induced the process of apoptosis, we evaluated whether caspase 8 and/or caspase 9 enzymes are activated. Since our results point to the activation of caspase 9, but not the caspase 8, in breast and lung cancer cells treated with Cu^{2+} -complexes, we conclude that the mechanism of action of both Cu^{2+} -complexes is related to the induction of intrinsic apoptotic signaling pathway.

Study of copper-imidazo[1,2-a]pyridines complex at $10 \times \text{IC}_{50}$ on HT-29 cells at 12 h resulted in increased caspase-9 activity. The absence of caspase-8 activity indicated activation of the intrinsic apoptotic pathway (HARMSE et al., 2019). In our study, results showed in both MCF-7 and A549 cell lines, R9 and R10 induced caspase 9 activity with IC_{50} concentrations at 24 h. Hence, copper-imidazo[1,2-a]pyridines and our Cu^{2+} -complexes induced intrinsic apoptotic pathway by activation of caspase 9 activity in different cancer cell lines.

The activity of casiopeina II [$\text{Cu}(1,4\text{-dimethyl-1,10-phenanthroline})(\text{glycine})\text{NO}_3$], was tested in CH1 human ovarian carcinoma by De Vizcaya-Ruiz et al. (2000). Cell line treated by casiopeina II at $2 \times \text{IC}_{50}$ concentration (3 μM) at 24 h showed the increase of caspase activity by 3 times when compared with that of the untreated cells. Caspase activation (measured by Z-Asp-Glu-Val-Asp-7-amino-4-trifluoromethylcoumarin; Z-DEVD-AFC) confirm that casiopeina II can induced apoptotic cell death (DE VIZCAYA-RUIZ et al., 2000). In our study, R9 and R10-treated MCF-7 cells with 1 μM at 24 h showed the 2.2 and 1.9 times higher relative caspase 9 activity than that of control, respectively. In addition, in A549 treated cells with R9 and R10, the relative caspase 9 activity was 2.8 and 2.5 times above the control, respectively. Comparing to the casiopeina II, in our study, the induction of caspases activity in cancer cells with R9 and R10 was performed at almost 3 times less concentration. This might help us to explain the lower amount of caspase 9 induced by R9 and R10 comparing to the casiopeina II.

Copper ions are involved in regular activities such as cellular respiration hence; the interaction of copper ions with DNA has received special attention (GOVINDARAJU et al., 2013). Copper can generate large number of DNA attacking ROS *via* a Fenton reaction lead to lipids, proteins and DNA damage (HARTTER; BARNEA, 1988). Copper can also directly bind to protein and DNA leading to structural and functional modifications and is involved in chromatin condensation. The presence of metal-binding sites in DNA structure makes it a good target for metallodrugs such as cisplatin (ROSENBERG et al., 1969). There are many reports in the literature describing the interaction of Cu^{+2} -complexes with DNA (DIMIZA et al., 2011; ERXLEBEN, 2018; PAGES et al., 2015). In order to investigate whether the Cu^{+2} -complexes tested in this study present the ability to bind DNA, we set the simple experiment based on the DNA binding competition between the Cu^{+2} -compounds with PI. Interestingly, our results confirmed that Cu^{+2} -complexes couldn't bind to DNA as an intercalating agent; however, since we did not analyze any other form of DNA binding, we cannot reject any other possible interaction with DNA.

The binding ability of Schiff-base metal complex including Cu(II) to DNA has been reported by Dehkhodaei M et al, 2018. The experimental DNA-binding results (spectroscopic and viscosity measurements) as well as computational docking and ONIOM data suggest that the Cu^{+2} (2-tert-butyliminomethyl-phenol)₂ interact with DNA, presumably by the groove-binding mechanism (DEHKHODAEI et al., 2018). In another study, mononuclear and dinuclear Cu^{+2} -complexes with thiophene carboxylic acid, $[\text{Cu}(3\text{-TCA})_2(2,2'\text{-bpy})]$, and $[\text{Cu}_2(2,5\text{-TDCA})(\text{DMF})_2(\text{H}_2\text{O})_2(2,2'\text{-bpy})_2](\text{ClO}_4)_2$ (where 3-TCA=3-thiophene carboxylic acid; 2,5-TDCA=thiophene-2,5-dicarboxylic acid; 2,2'-bpy=2,2'-bipyridyl; DMF=*N,N*-dimethylformamide), were synthesized and by computational analysis the authors suggest that these compounds can bind to the minor groove DNA (GURUDEVARU *et al.*, 2018). These studies and many other in literature may support the possible hypothesis about binding of R9 and R10 on DNA maybe occurred through minor or major groove but undoubtedly, they would not act as an intercalating agent.

Despite the wide variety of available antineoplastic drugs, they are generally unable to fight tumor tissue without affecting the patient's healthy cells and tissues (SARASTE; PULKKI, 2000). Thus, it is extremely important that the side effects of new drugs be minimized (CAMPI-LLOS *et al.*, 2008). Therefore, it is necessary to know the toxicity of the compounds so that the treatment dose used is as less harmful as possible. Larvae of *G. mellonella* have been widely used as *in vivo* screening model to assess the therapeutic potential of different novel drugs (CUTULI et al., 2019; ENTWISTLE; COOTE, 2018; HORNSEY; WAREHAM, 2011). The innate defenses of insects *G. mellonella*, consist of structural and passive barriers as well as humoral and

cellular responses within the hemolymph that is analogous to the blood of mammals (DUNPHY; THURSTON, 2018). The larvae of the greater wax moth have been shown to be an excellent model organism, convenient and inexpensive that replaces the use of small mammals for *in vivo* toxicity experiments (KAVANAGH; REEVES, 2004; RENWICK; KAVANAGH, 2007). *In vivo* study by *G. mellonella*, revealed the lower toxicity of R9 in comparison to cisplatin at the same concentration (50 mg/kg) on *G. mellonella* that agrees with the LD₅₀ calculated in mice treated with R9 and cisplatin. This result is in a line with the results of toxicity evaluation of R9 and cisplatin by *G. mellonella* via injecting 50 mg/kg. *G. mellonella* showed lower tolerance to cisplatin, and high toxicity of cisplatin (70% kill) being observed at 50 mg/kg compare to R9 (30% kill). This value for cisplatin correlates well with the known LD₅₀ value for this drug (6.6 mg/kg body weight) and LD₅₀ value of R9 (71.6 mg /kg) in the mouse model. These differences may occur in mammals due to the dose-limiting toxicity of cisplatin toward renal tubular damage (DEO et al., 2018; JOHNSTONE; SUNTHARALINGAM; LIPPARD, 2016). The result obtained in mice is promising since the value of 71.6 mg/kg is much higher than the LD₅₀ of cisplatin, 6.6 mg/kg (ASTON et al., 2017). In addition, the results of LD₅₀ is well correlated with the data obtained during the treatment with the MCF10A cells showing that the R9 complex has a low toxicity to its relative non-cancerous cells. This result from MTT assay showed the toxicity of our compound R9 is 10.85 times lower than the cisplatin and it has a great potential of chemotherapeutic drug. The *in vivo* drug tolerance of dinuclear Cu²⁺ bis-phenanthroline octanedioate compound [Cu₂(μ₂-oda)(phen)₄](ClO₄)₂ synthesized by Kellet et al. (2011) represented 50% kill at 67 mg/kg after 3 days in *G. mellonella*. In addition, cisplatin was the least tolerated of the test compounds, with high toxicity (100% kill) being observed at 67 mg/kg (KELLETT et al., 2011). In our study cisplatin was the least tolerated in *G. mellonella*, with high toxicity (20% kill) being observed at 50 mg/kg of *G. mellonella* compare to R9 (0% kill) after day 3. The comparison clearly illustrated that R9 is less toxic than the [Cu₂(μ₂-oda)(phen)₄](ClO₄)₂ to *G. mellonella*. On the other hand, the difference in our results of both study regarding cisplatin is controversial and may be related to experimental condition. According to Hall et al. 2014, DMSO has the ability to react with the complexes, interfering in their cytotoxicity (HALL et al., 2014). We presume that the high toxicity observed in Kellet et al. groups might be related to the DMSO not the cisplatin per se. In our study while cisplatin was dissolve in DMEM instead of DMSO.

Since we observed a similar profile of R9 and R10 in both MCF-7 and A549 cell lines, we decided to choose R10 to investigate the differential expression of proteins in MCF-7 cells. Until now, our study revealed that R9 and R10 is cytotoxic for breast and lung cancer cells

showing changes in granularity, dissipation of mitochondrial membrane potential, induction of ROS, DNA fragmentation and activate the intrinsic apoptosis pathway. By using label free proteomics, we searched for the most relevant proteins expressed with significant fold change (control vs treatment) higher than 1.2 to correlate and improve our previous results. The Label-free-based quantitative proteomics were employed to identify differentially expressed proteins after R10 and cisplatin treatment.

Statistical analysis data revealed that from 167 proteins identified by R10-treated cells, a total of 194 pathways were altered. Moreover, from these 167 altered proteins, 118 proteins were significantly downregulated and linked to the 189 downregulated pathways, and 49 proteins were upregulated indicating that 40 pathways being upregulated. On the other hand, from 95 proteins expressed after the treatment with cisplatin, a totally of 127 pathways were altered in which 58 proteins were downregulated being responsible for the downregulation of 105 pathways. In addition, 37 proteins were upregulated being associated with the upregulation of 47 pathways.

The most downregulated pathways after R10 treatment, belong to the regulation of actin cytoskeleton (12 related proteins), viral carcinogenesis (10 related proteins), metabolic pathways (9 related proteins) and PI3K-Akt signaling pathway (9 related proteins), tight junction (8 related proteins), Fc gamma R-mediated phagocytosis (7 related proteins), oocyte meiosis (7 related proteins), neurotrophin signaling pathway (7 related proteins), axon guidance (7 related proteins), and proteoglycans in cancer (7 related proteins), adherence junction (6 related proteins), apoptosis (6 related proteins), focal adhesion (6 related proteins), pathways in cancer (MAPK signaling pathway, calcium signaling pathway and ECM receptor interaction) (6 related proteins) and Rap1 signaling pathway (6 related proteins). On the other hand, the most upregulated pathways from R10-treated cells were ribosome (5 related proteins), thermogenesis (5 related proteins), necroptosis (4 related proteins), metabolic pathways (4 related proteins) and oxidative phosphorylation (4 related proteins).

The most downregulated pathways after cisplatin treatment, were related to Micro-RNAs and proteoglycans in cancer (4 related proteins identified in each pathway), glycolysis/gluconeogenesis (3 related proteins), pathways in cancer (apoptosis, ECM receptor interaction and cytokine-cytokine receptor interaction) (3 related proteins), oxidative phosphorylation (3 related proteins), and thermogenesis (3 related proteins). The most upregulated pathways related to the cisplatin-treated cells were ribosome (12 related proteins), metabolic pathways (4 related proteins), oxidative phosphorylation (3 related proteins) and thermogenesis (3 related proteins).

Of note, 6 proteins related to the downregulation of apoptosis pathway in R10-treated cell include: Lamin B1, NRAS proto-oncogene, mitogen activated protein kinase 1, mitogen activated protein kinase 3, spectrin alpha and calpain 2. Whereas, there is one protein participated in upregulation of apoptosis named apoptosis inducing factor mitochondria associated 1 (AIFM1). Moreover, in cisplatin-treated cells there is only 1 protein associated to the downregulation of apoptosis pathway, named caspase 3 while there is no report regarding the upregulation of apoptosis pathway in cisplatin-treated cells in our result.

Hence, treatment with R10 induced different proteins in apoptotic pathway in both up and downregulated ways that is completely different from proteins expressed in apoptosis pathway downregulated in cisplatin-treated cells. The results from Venn diagram confirmed the difference of up/downregulated proteins expressed in R10 and cisplatin-treated cells. It showed the only 9.3% of expressed proteins were common amongst the downregulated proteins in R10/cisplatin-treated cells whereas, 14.7% of expressed proteins were the same in upregulated proteins in R10/cisplatin-treated cells. Based on the results, we might suggest the possible different mechanism of action of our Cu^{2+} -complex R9 and cisplatin.

In more detailed analysis of R10-treated cells, we highlighted the regulation of actin cytoskeleton, metabolic pathway, apoptosis, RNA transport and ribosome as the principal downregulated biological processes, respectively. While, the thermogenesis and apoptosis were identified as the main upregulated biological process.

Focus on highlighted pathways and their associate proteins revealed that the most downregulated expressed protein was ezrin that together with other downregulated proteins like moesin and gelsolin, have an important role in the regulation of actin cytoskeleton. Ezrin is an important member of the ERM (ezrin-radixin-moesin) cytoskeleton-associated proteins family, which is a transit protein between membrane proteins and actin filaments (BRETSCHER; RECKEK; BERRYMAN, 1997). Ezrin was found to be upregulated in breast cancer tissues (LI et al., 2019a). Studies have revealed that ezrin is an important signaling molecule that plays a vital role in tumorigenesis, development, invasion and metastasis in a variety of human malignancies as well as breast cancer via association with many cellular processes, including cell proliferation, cell adhesion, cell motility and signal transduction (DENG et al., 2007; FRÖSE et al., 2018; LI et al., 2019a; ZHANG et al., 2019). The proteins in biological pathways associated with ezrin include protein kinase C, Rho-kinase, NF- κ B, PI3 kinase/Akt (LONG; WANG, 2016; QUAN et al., 2019). Sperka et al. (2011), suggests that ezrin not only acts as a scaffold assembling RAS and SOS (son of sevenless) but also participates in SOS activity control (SPERKA et al., 2011). Our experiments on cell shape and morphology confirmed the impact of the R10 on

actin cytoskeleton. The actin cytoskeleton is key to cell shape and motility, that are important in the metastasis phenomenon. In this regard, a finding that may be of interest in anticancer strategies. Proteomic study of 8-hydroxyquinoline-copper complex on leukemic cells RAW 264.7 cell line after 24 h of treatment time by Dalzon et al. (2019) also showed the modulation of actin cytoskeleton pathway, but they didn't correlate the changes in cytoskeleton with the changes of relevant target proteins involved in the cytoskeleton organization (DALZON et al., 2019).

The downregulation of ezrin may affect the activation of RAS, which was downregulated in our study and reduce RAS/MAPK signaling (MAPK1 and MAPK3 mitogen activated protein kinase). This might happen through downregulation of multiprotein complex at the plasma membrane in response to low ezrin that comprises RAS, SOS, filamentous actin, and co-receptors such as β 1-integrin. Co-receptors, in this case β 1-integrin, which is downregulated, responsible to focus these complexes to relevant sites of receptor tyrosine kinase (RTK) activity at the plasma membrane/F-actin interface.

The MAPK pathway contains several key signaling components and phosphorylation events that play an important role in tumorigenesis. Anomalies in the RAS-MAPK complex have been implicated in several human cancers, suggesting that this complex would be an attractive therapeutic target (NEUZILLET et al., 2013; PRATILAS; SOLIT, 2010; YANG; LIU, 2017; GHASEMISHAHRESTANI et al., 2020). Activation of receptor tyrosine kinase RTK, generates binding sites for adaptor proteins like growth factor receptor-bound protein 2 (GRB2), that recruit the (guanine nucleotide exchange factor GEF) SOS at the plasma membrane and in turn activates the membrane-bound RAS by converting GDP to GTP (RAMOS, 2008). Upon activation of RAS, RAF acts as a MAP kinase kinase kinase (MAPKKK) to activate MEK1 and MEK2, which in turn, catalyze the activation of the effector ERK1 and ERK2 kinases, and their translocation into the nucleus. Once activated, ERK1/ERK2 broadly phosphorylate several nuclear and cytoplasmic effector proteins such as FOXO involved in diverse cellular responses such as cell proliferation, survival, differentiation and motility in this regard, downregulation of RAS can downregulate the RAF-MEK-ERK cascade (CHAMBARD *et al.*, 2007; VAIDYAN ATHAN *et al.*, 2007).

The 3-tyrosine monooxygenase, 5 tryptophan monooxygenase (14-3-3 protein) epsilon ϵ , beta β , and zeta ζ were also downregulated in our result. The 14-3-3 ϵ protein appears to function in multiple RTK pathways, indicating that it is a component of the RAS1 signaling cascade. 14-3-3 β has oncogenic potential, through enhancing Raf-1 activation result in amplification of MAPK signaling cascade (TAKIHARA, 2000). 14-3-3 ζ has been shown to be involved in the

onset and progression of cancer and its overexpression in all types of cancer is reported in the literature. In contrast, 14-3-3 sigma σ can act as a tumor suppressor and its expression is lost in many breast cancers which is interestingly we did not observe any changes in 14-3-3 sigma σ in our results (FERGUSON et al., 2000). It is known that 14-3-3 proteins can form homodimers or heterodimers with other isoforms (VERDOODT et al., 2006). In the cancer field, overexpression of 14-3-3 ζ may impair the balance of different dimer compositions in the cell that lead to substrate bias for 14-3-3 ζ dimers, which may explain why the increase in 14-3-3 ζ , even in the presence of other 14-3-3 proteins, leads to an increase in alteration of apoptosis. Neal CL et al. (2009), reported 14-3-3 ζ binding to phosphorylated FOXO3a transcription factor leads to translocation of it to the cytoplasm and sequestration of FOXO3a that can mediate apoptosis resistance (BRUNET et al., 1999; NEAL et al., 2009). The FOXO is a subfamily of forkhead transcription factor family that plays an important role in tumor suppression in a wide range of cancers. Given this, downregulating 14-3-3 ζ may sensitize cells to apoptosis by increased activity of FOXO via ERK and serve as effective anticancer strategies in patients with breast cancer with overexpressed 14-3-3 ζ . ERK mediated FOXO3 phosphorylation through ERK leads to interaction with MDM2 (Mouse double minute 2 also known as E3-ubiquitin ligase) (YANG et al., 2008). MDM2 polyubiquitinates FOXO3 rendering it a substrate for proteasomes and proteolysis.

Exportins are transport receptor proteins for nuclear export better studied as potential targets in tumorigenesis (DAS et al., 2015). The most important and best studied exportin is CRM1 (chromosomal maintenance 1) also called exportin 1 (XPO1) (LI et al., 2019b). In our results, the downregulation of RAN GTPase-RAS-related nuclear protein and CRM1/XPO1 may be related to reduce the FOXO (Members of the class O of forkhead box transcription factors) translocation to the cytoplasm and help in the apoptotic process. PFOXO3a in turn acts as an inhibitor of nuclear factor-kappa B (NF-kB). It has been reported that CRM1/XPO1 is responsible for the transport of many tumor suppressor proteins and oncoproteins such as FOXOs and NF-kB which are significant targets in oncogenesis (SENAPEDIS; LANDESMAN, 2014).

Our results revealed that downregulation of casein kinase α and β and subsequently downregulation of calpain, may results in downregulation of NF-kB. Casein kinase (CK2) is a tetrameric holoenzyme, with two catalytic (CK α) and two regulatory (CK β) subunits (ALLENDE; ALLENDE, 1995). CK2 activity and/or expression are significantly increased in many human cancers such as breast cancer (FILHOL et al., 2015). In addition, the ubiquitous calpains were notably shown to regulate the cell cycle with two key cyclins, cyclin D1 and cyclin E (JÁNOS SY et al., 2004). Downregulation of calpain is in agreement with our biochemical assay results

which showed the cell cycle arrest of breast cancer cell line after R10 treatment (Section 5.5). CK2 can regulate signal transduction cascades such as NF- κ B-regulated pathway, and may promote tumorigenesis through stabilization of the proto-oncogene Myc and activation of NF- κ B (anti-apoptotic factor) in breast cancer (CHANNAVAJHALA; SELDIN, 2002; DOMINGUEZ; SONENSHEIN; SELDIN, 2009; ROMIEU-MOUREZ *et al.*, 2002). Therefore, downregulation of CK2 through calpain dependent, may cause the reduction of NF- κ B activity especially when the proteasome activity halted as proteasome is responsible for degradation of I κ B (inhibitor of NF- κ B) and subsequent translocation of active NF- κ B to the nucleus. In our study, it seems the downregulation of casein kinase α , β and subsequently downregulation of calpain may results in downregulation of NF- κ B. On the other side, we showed through the downregulation of RAS/ERK pathway, we would have probably increased the activity of FOXO that act as an inhibitor of NF- κ B. NF- κ B and its target genes have been implicated as mediators in all of the hallmarks of cancer (HANAHAN; WEINBERG, 2011; PAHL, 1999). Constitutive activation of NF- κ B has been demonstrated in breast cancer cell line (CHUA *et al.*, 2007). In response to factors such as stress like effect of R10, I κ B α , an inhibitor of NF- κ B, can be targeted for ubiquitination and proteasomal degradation.

The ubiquitin proteasome pathway (UPP) selectively mediates cellular protein degradation which regulates cell cycle progression, signal transduction, differentiation, proliferation and apoptosis (NALEPA; ROLFE; HARPER, 2006). The labeled proteins are degraded by the 26S proteasome, which consists of one 20S core particle and two 19S regulatory particles (Peters JM, 1993). The results of downregulated catalytic subunit β 5 as well as the regulatory subunits α 3 and α 4 may related to induce cancer cell death in breast cancer cells. Verani *et al.* (2012) demonstrated the association of the inhibition of proteasomal CT-like (chymotrypsin-like) activity with tumor cell apoptosis revealing the selective inhibition of proteasome in cancer cells could be a potential anticancer strategy (VERANI, 2012). In this regard, Zhang *et al.* (2015), studied the effect of three ternary copper complexes with 3-indole carboxylic and 1,10-phenanthroline in human breast cancer cells that inhibit the CT-like activity of the proteasome and induce cancer cell death in human cancer cells via binding with catalytic site of subunit β 5 (ZHANG *et al.*, 2017). The downregulation of catalytically active β 5 together with α 3 and α 4 regulatory subunit in our result, may be related to induce cancer cell death in breast cancer cells. Numerous proteins identified in the proteasome/ubiquitin pathway, known to be a target of the copper complexes (CHEN *et al.*, 2009; DALZON *et al.*, 2019; DANIEL *et al.*, 2004; OLIVERI *et al.*, 2017). Dalzon *et al.* (2019) reported the effect of 8-hydroxyquinoline-copper complex on leukemic cells RAW 264.7 cell line after 24 h of treatment, lead to decrease all

modulated proteasome subunits detected in the proteomic screen, suggesting a destabilization of the proteasome (DALZON et al., 2019).

Apoptosis-inducing factor (AIF) is a mitochondrial oxidoreductase that aids cell death programs and participates in the assembly of the respiratory chain. During apoptosis and upon dissipation of the mitochondrial membrane potential, AIF is released from the mitochondria and translocate to the nucleus in a caspase-independent manner (SUSIN et al., 1996, 1999). Based on our proteomic results, upregulation of AIF might have related to non-caspase apoptosis. The upregulation of AIF can be explained by the fact that during apoptosis, AIF nuclear translocation occurs downstream of mitochondrial permeabilization via the increase in the levels of ROS and dissipation of mitochondrial membrane potential that is in agreement with our previous biochemical study results (Section 5.3 and 5.4). In the cytosol, truncated AIF physically interacts with multiple proteins, including heat shock 70-kDa protein (HSP70). Hence, downregulation of HSP70 that promotes AIF retention in the cytoplasm may related in free AIF, which is released from the mitochondria and translocate to the nucleus in a caspase-independent manner (RAVAGNAN et al., 2001). Ferrando-May et al. (2001) reported the existence of caspase-independent pathways that show the initiation of death program through the signal to the nucleus (FERRANDO-MAY et al., 2001). In this regard, it might be reasonable to assume that AIF translocation does not require active transport, but may be facilitated by the increased permeability of the nuclear pore complex during cell death (BANO et al., 2010; FERRANDO-MAY et al., 2001). Lamins contribute to the structural integrity of the nucleus and are important for the spacing of nuclear pores (ALHABOUBI *et al.*, 2011; GOLDBERG *et al.*, 1995; OSOUDA *et al.*, 2005; SMYTHE; JENKINS; HUTCHISON, 2000). In this context, the downregulation of lamin in our result, might favor the entrance of AIF.

The Vacuolar ATPase (V-ATPase) is a complex multisubunit enzyme that translocate protons from the cytoplasm into intracellular compartments and across the plasma membrane. It helps in maintaining an alkaline intracellular environment favorable for growth and an acidic extracellular environment favorable for invasion (SENNOUNE; MARTINEZ-ZAGUILAN, 2007). A hallmark of cancer is the Warburg effect where cells shift from oxidative phosphorylation to aerobic glycolysis. Alkalization of cytosol activates glycolysis while suppressing oxidative phosphorylation (ALFAROUC et al., 2014). Therefore, downregulation of V-ATPase may help to reverse this process from suppressing the glycolysis to reactivate the oxidative phosphorylation. Our previous biochemical results revealed the ROS production after effect of R10 on MCF-7 that might be correlated with the reverse of cancer metabolism from glycolysis to oxidative phosphorylation (section 5.4). In tumors, V-ATPase expression has been shown to be higher

and lead the proliferating of many cancer cells like breast, prostate, lung cancers (COTTER et al., 2015). The high expression of V-ATPase is a well-designed compensatory mechanism which evolves survival and growth advantages of cancer cells (FORGAC, 2007). In our result, the downregulation of V-ATPase may help in suppressing the growth and survival of tumor.

Pyruvate kinase (PKM2), which converts phosphoenolpyruvate (PEP) to pyruvate, regulates the glycolytic flux and lactate production in cancer cells. In the majority of cancer cells, the expression of PKM2 is increased, which suggests that downregulation of PKM2 may be an attractive target for cancer therapy (DONG et al., 2016; GHASEMISHAHRESTANI et al., 2020). The increased of PKM2 activity is well correlated with metastasis and advanced tumor stage and size (LU et al., 2016). In this regard, together with downregulated V-ATPase the downregulation of pyruvate kinase muscle isozyme M2 (PKM2) in result, might have a great impact in tumor growth and survival suppression.

SWI/SNF chromatin remodeler was the most abundant expressed protein found in this study. The proper functioning of the SWI/SNF chromatin-remodeling complex is vital to appropriate cell cycle control and tumor suppression. The SWI/SNF complex control cell proliferation and act as tumor suppressor via its association with cell cycle checkpoint genes, such as BRCA1, cyclin E, p21, p53 and p16 (BETZ et al., 2002; DEL BOVE et al., 2011). Highly expression of SWI/SNF complex may be related to the tumor suppressor activity of the complex on MCF-7 via cell cycle control that could be related to our previous results regarding the DNA fragmentation in MCF-7 cells at concentration of IC_{50} in about 77% (Session 5.5).

In summary, R10 treatment may cause MCF-7 cell death mainly through intrinsic apoptosis pathway or by direct activation of apoptosis through AIF by downregulation of RAS-ERK pathway. The downregulation of protein casein kinases, calpain as well as catalytic and regulatory subunits of proteosome may also activate pathways for DNA degradation. Moreover, downregulation of a rate-limiting glycolytic enzyme pyruvate kinase may have great impact in downregulation of glycolysis and force the cells through oxidative phosphorylation (Figure 39).

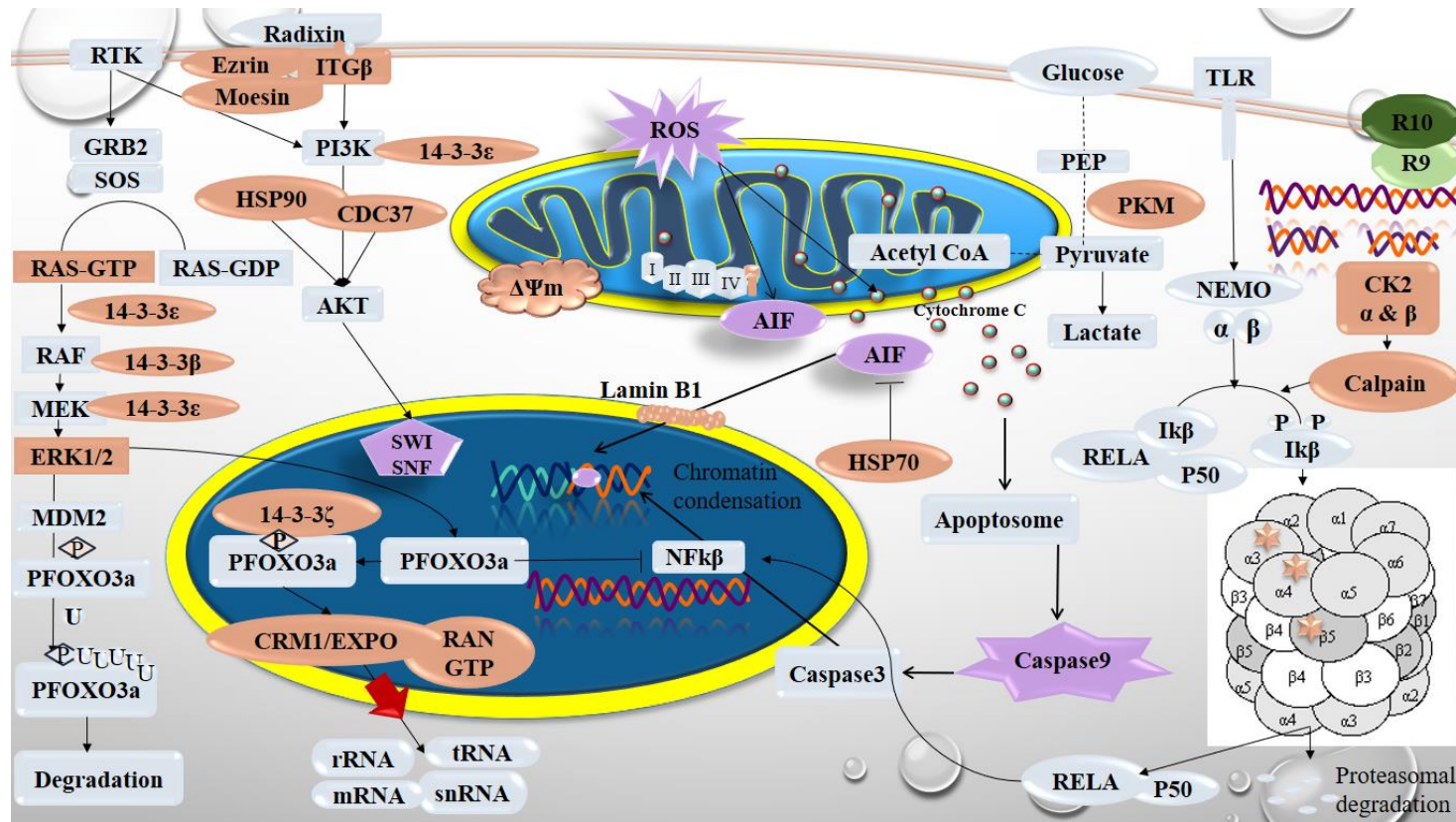


Figure 39. The effect of Cu^{2+} -complexes in breast cancer cell signaling pathways. The cytotoxicity, significant reduction in $\Delta\Psi_m$, induction of high amount of ROS, and together by activation of caspase 9 and DNA break at Sub-G1 showed that R9 and R10 treatment may cause cell death mainly through intrinsic apoptosis pathway or by direct activation of apoptosis through AIF by downregulation of RAS-ERK pathway. The downregulation of protein casein kinases, calpain as well as catalytic and regulatory subunits of proteasome may also activate pathways for DNA degradation. Moreover, downregulation of a rate-limiting glycolytic enzyme pyruvate kinase may have great impact in downregulation of glycolysis and force the cells through oxidative phosphorylation. The pink color represents the downregulated proteins and the purple color shows the upregulated protein.

7. Conclusion

- ❖ MCF-7, A549 and PC3, all presented high cytotoxicity effect against R9 and R10 with IC_{50} around $1\mu M$ that is very low as compare to cisplatin.
- ❖ Despite the high cytotoxic effect of Cu^{2+} -complexes on breast, lung and prostate cancer, the toxicity is reduced in healthy human mammary epithelial cell line MCF10A cells almost 7 and 8 times lower than observed for the MCF-7 cell line
- ❖ There is significant cell morphology change and increase granularity through effect of R9 & R10 in both cell lines MCF-7 and A549.
- ❖ Both compounds exhibited mitochondrial membrane potential disruption, show similar effects to cisplatin in MCF-7 and have a greater effect than cisplatin in the A549.
- ❖ Percentage of ROS and the amount of ROS produced by R9 and R10 was high when compared to control.
- ❖ Activation of caspase 9, improves that the treatment may causing cell death through intrinsic apoptosis pathway.
- ❖ MCF-7 and A549 showed the DNA damage (fragmentation) after treatment with R9 & R10.
- ❖ R9 and R10 didn't bind to DNA as an intercalator.
- ❖ *In vivo* assay by *G. mellonella* revealed the low toxicity of R9 in comparison to cisplatin.
- ❖ The LD_{50} values from BALB/c nude mice represent 10.85 times less toxicity of R9 compare to the therapeutic drug cisplatin.
- ❖ Treatment with R10 induces different proteins in apoptotic pathway in both up and downregulated ways that is completely different from proteins expressed in apoptosis pathway down/upregulated in cisplatin-treated cells.
- ❖ Regarding to the regulation of actin cytoskeleton pathway we observed that ezrin, moesin and gelsolin were the most downregulated expressed proteins after R10 treatment.
- ❖ The second obtained most downregulated pathway; metabolic pathways were associated to V-ATPase subunit B and pyruvate kinase.
- ❖ PI3K pathway were identified as the third most downregulated pathway associated with, NRAS proto-oncogene GTPase, HSP90, MAPK 1, MAPK 3, 14-3-3 protein β , 14-3-3 protein ϵ and 14-3-3 protein ζ and, integrin β .

- ❖ The next most downregulated pathway was adherence junction related to the two main proteins, casein kinase II α (CK α) and casein kinase II β (CK β).
- ❖ Apoptosis pathway, downregulated by downregulation of NRAS proto-oncogene GTPase, lamin B1, spectrin alpha chain, MAPK 1, calpain-2 catalytic subunit and MAPK 3.
- ❖ GTP-binding nuclear protein Ran and exportin-1 downregulated the RNA transport.
- ❖ Proteosomal function downregulated via downregulation of proteasome subunit alpha type-3, alpha type-4 and proteasome subunit beta type-5.
- ❖ Among upregulated pathways, the two most upregulated pathway were identified, thermogenesis and apoptosis. Protein SWI/SNF complex subunit SMARCC1 was related to the upregulation of thermogenesis and the upregulation of apoptosis was related to upregulation of apoptosis-inducing factor 1.
- ❖ The results may consider R9 and R10 a potential therapeutic agent for breast, lung and prostate cancer that is highly competitive with cisplatin chemotherapy drug.

The main mechanism of action of the Cu²⁺-complexes seems to occur by dissipation of mitochondrial membrane potential and generation of ROS that appears to play an important role in the cytotoxicity of these compounds and in the induction of apoptosis signaling. Due to the cytotoxicity and induction of high amount of ROS, significant reduction in $\Delta\Psi_m$ and together by activation of caspase 9 and DNA break at Sub-G1 we conclude that R9 and R10 treatment induce cell death mainly through intrinsic apoptosis pathway or by direct activation of apoptosis through AIF by downregulation of RAS-ERK pathway. The downregulation of protein casein kinases, calpain as well as catalytic and regulatory subunits of proteasome may also activate pathways for DNA degradation. Moreover, downregulation of a rate-limiting glycolytic enzyme pyruvate kinase may have great impact in downregulation of glycolysis and force the cells through oxidative phosphorylation. Moreover, the *in vivo* assay by *G. mellonella* revealed the low toxicity of R9 in comparison to cisplatin and this result was confirmed with the LD₅₀ values from BALB/c nude mice that represent 10.85 times less toxicity of R9 compare to the therapeutic drug cisplatin. Overall, the results may consider R9 and R10 a promising therapeutic agent for breast, lung and prostate cancer.

8. Perspective of the project

In our biochemical assays, we observed the very close result of induction of intrinsic apoptosis pathway via induction of high amount of ROS, significant reduction in $\Delta\Psi_m$, activation of caspase 9 and DNA break at Sub-G1 in R9 and R10 Cu^{2+} -complexes compare to cisplatin. However, there are some questions remained unclear.

- Do Cu^{2+} -complexes bind to DNA directly or indirectly?
- How will be the metal homeostasis in the cell?
- Which organelle is the most affected by treatment with the Cu^{2+} -complexes?
- What is the cell's capacity to produce energy when exposed to Cu^{2+} -complexes?
- Do the compounds remain intact or dissociate?
- How animal models (xenograft model) would respond to cancer treatment with these Cu^{2+} -complexes?
- Will the use of these compounds in combination with cisplatin or other drugs be beneficial or not?

Regarding the last question, our proteomic results revealed the very high probability of different proteins expressed after R10 and cisplatin treatment. This clearly show the possibility of different mechanism of action in R10 and cisplatin. Clarification of some of the mechanisms of action of the Cu^{2+} -complexes, after its proven effectiveness in combating tumor cells, and the possible different mechanism of action of our Cu^{2+} -complex with cisplatin provides important information for finding the synergism tests between these compounds and cisplatin or other currently available antitumor drugs.

9. References

- ABID, M.; SHAMSI, F.; AZAM, A. Ruthenium Complexes: An Emerging Ground to the Development of Metallopharmaceuticals for Cancer Therapy. **Mini-Reviews in Medicinal Chemistry**, 2015.
- AL-HABOUBI, T. et al. Distinct association of the nuclear pore protein Nup153 with A- and B-type lamins. **Nucleus**, 2011.
- ALBRECHT, H. et al. Cellular Assays in Drug Discovery. In: [s.l: s.n.].
- ALEXANDROV, L. B. et al. Mutational signatures associated with tobacco smoking in human cancer. **Science**, 2016.
- ALFAROUC, K. O. et al. Glycolysis, tumor metabolism, cancer growth and dissemination. A new pH-based etiopathogenic perspective and therapeutic approach to an old cancer question. **Oncoscience**, 2014.
- ALFIERI, C.; ZHANG, S.; BARFORD, D. **Visualizing the complex functions and mechanisms of the anaphase promoting complex/cyclosome (APC/C)** *Open Biology*, 2017.
- ALLENDE, J. E.; ALLENDE, C. C. Protein kinase CK2: an enzyme with multiple substrates and a puzzling regulation. **The FASEB Journal**, 1995.
- ANTHONY J. TREVOR, BERTRAM G. KATZUNG, MARIEKE M. KRUIDERING-HALL, S. B. M. Chapter 54. Cancer Chemotherapy. In: **Cancer Chemotherapy**. 10. ed. [s.l: s.n.].
- APARICIO, T.; BAER, R.; GAUTIER, J. DNA double-strand break repair pathway choice and cancer. **DNA Repair**, 2014.
- ARJMAND, F. et al. Molecular drug design, synthesis and crystal structure determination of Cu II-Sn IV heterobimetallic core: DNA binding and cleavage studies. **European Journal of Medicinal Chemistry**, 2012.
- ASLAM, M. S. et al. Side Effects of Chemotherapy in Cancer Patients and Evaluation of Patients Opinion about Starvation Based Differential Chemotherapy. **Journal of Cancer Therapy**, 2014.
- ASTON, W. J. et al. A systematic investigation of the maximum tolerated dose of cytotoxic chemotherapy with and without supportive care in mice. **BMC Cancer**, 2017.
- AYKIN-BURNS, N. et al. Increased levels of superoxide and H₂O₂ mediate the differential susceptibility of cancer cells versus normal cells to glucose deprivation. **Biochemical Journal**, 2009.
- AZUARA, L. R. **Process to obtain new mixed copper aminoactidate complexes from phenylate phenathrolines to be used as anticancerigenic agents**, [s.d.].
- AZUARA, L. R. **copper amino acidate diimine nitrate compounds and their methyl derivatives and a process for preparing them**, [s.d.].

BADVE, S. Tumor heterogeneity in breast cancer. In: **Molecular Pathology of Breast Cancer**. [s.l: s.n.].

BAE, Y. S. et al. Epidermal growth factor (EGF)-induced generation of hydrogen peroxide. Role in EGF receptor-mediated tyrosine phosphorylation. **Journal of Biological Chemistry**, 1997.

BAE, Y. S. et al. Platelet-derived growth factor-induced H₂O₂ production requires the activation of phosphatidylinositol 3-kinase. **Journal of Biological Chemistry**, 2000.

BANO, D. et al. Alteration of the nuclear pore complex in Ca²⁺-mediated cell death. **Cell Death and Differentiation**, 2010.

BARRANCO, W. T.; ECKHERT, C. D. Cellular changes in boric acid-treated DU-145 prostate cancer cells. **British Journal of Cancer**, 2006.

BARTON, J. K. Metals and DNA: Molecular left-handed complements. **Science**, 1986.

BERGAMO, A.; DYSON, P. J.; SAVA, G. **The mechanism of tumour cell death by metal-based anticancer drugs is not only a matter of DNA interactions** **Coordination Chemistry Reviews**, 2018.

BETZ, B. L. et al. Re-expression of hSNF5/INI1/BAF47 in pediatric tumor cells leads to G1 arrest associated with induction of p16^{ink4a} and activation of RB. **Oncogene**, 2002.

BIENERT, G. P. et al. Specific aquaporins facilitate the diffusion of hydrogen peroxide across membranes. **Journal of Biological Chemistry**, 2007.

BLAIR, B. G. et al. Copper transporter 2 regulates endocytosis and controls tumor growth and sensitivity to cisplatin in vivo. **Molecular Pharmacology**, 2011.

BOODRAM, J. N. et al. Breast Cancer Stem Cell Potent Copper(II)-Non-Steroidal Anti-Inflammatory Drug Complexes. **Angewandte Chemie - International Edition**, 2016.

BORGES, B. E. et al. De novo galectin-3 expression influences the response of melanoma cells to isatin-Schiff base copper (II) complex-induced oxidative stimulus. **Chemico-Biological Interactions**, 2013.

BOTTONE, M. et al. Morphological Features of Organelles during Apoptosis: An Overview. **Cells**, 2013.

BOYLAND, E. **Tumour initiators, promoters, and complete carcinogens** **British Journal of Industrial Medicine**, 1985.

BRAVO-GÓMEZ, M. E. et al. Antiproliferative activity and QSAR study of copper(II) mixed chelate [Cu(N-N)(acetylacetonato)]NO₃ and [Cu(N-N)(glycinato)]NO₃ complexes, (Casiopeínas®). **Journal of Inorganic Biochemistry**, 2009.

BRAY, F. et al. Global cancer statistics 2018: GLOBOCAN estimates of incidence and mortality worldwide for 36 cancers in 185 countries. **CA: A Cancer Journal for Clinicians**, 2018.

BRETSCHER, A.; RECZEK, D.; BERRYMAN, M. **Ezrin: A protein requiring conformational activation to link microfilaments to the plasma membrane in the assembly of cell surface structures** *Journal of Cell Science*, 1997.

BRINTON, L. A.; GAUDET, M. M.; GIERACH, G. L. Breast cancer. In: **Schottenfeld and Fraumeni Cancer Epidemiology and Prevention, Fourth Edition**. [s.l: s.n.].

BRUIJNINCX, P. C.; SADLER, P. J. **New trends for metal complexes with anticancer activity** *Current Opinion in Chemical Biology*, 2008.

BRUNET, A. et al. Akt promotes cell survival by phosphorylating and inhibiting a forkhead transcription factor. *Cell*, 1999.

BRUNO, P. M. et al. A subset of platinum-containing chemotherapeutic agents kills cells by inducing ribosome biogenesis stress. *Nature Medicine*, 2017.

BURRELL, R. A. et al. **The causes and consequences of genetic heterogeneity in cancer evolution** *Nature*, 2013.

BURSCH, W. et al. Active cell death induced by the anti-estrogens tamoxifen and ICI 164 384 in human mammary carcinoma cells (MCF-7) in culture: The role of autophagy. *Carcinogenesis*, 1996.

BURTON, D. G. A.; KRIZHANOVSKY, V. **Physiological and pathological consequences of cellular senescence** *Cellular and Molecular Life Sciences*, 2014.

CAMPILLOS, M. et al. Drug target identification using side-effect similarity. *Science*, 2008.

CAO, Q. et al. **G-quadruplex DNA targeted metal complexes acting as potential anticancer drugs** *Inorganic Chemistry Frontiers*, 2017.

CARVALLO-CHAIGNEAU, F. et al. Casiopeina III-ia induces apoptosis in HCT-15 cells in vitro through caspase-dependent mechanisms and has antitumor effect in vivo. *BioMetals*, 2008.

CASSIDY, J. W.; BRUNA, A. Tumor heterogeneity. In: **Patient Derived Tumor Xenograft Models: Promise, Potential and Practice**. [s.l: s.n.].

CERNANEC, J. M. et al. Influence of oxygen tension on interleukin 1-induced peroxynitrite formation and matrix turnover in articular cartilage. *Journal of Rheumatology*, 2007.

CHAMBARD, J. C. et al. **ERK implication in cell cycle regulation** *Biochimica et Biophysica Acta - Molecular Cell Research*, 2007.

CHANG, C. H.; MEARES, C. F. Light-Induced Nicking of Deoxyribonucleic Acid by Cobalt(III) Bleomycins. *Biochemistry*, 1982.

CHANNAVAJHALA, P.; SELDIN, D. C. Functional interaction of protein kinase CK2 and c-Myc in lymphomagenesis. *Oncogene*, 2002.

CHAVEZ-GONZALEZ, A. et al. Casiopeina III-Ea, a copper-containing small molecule, inhibits the in vitro growth of primitive hematopoietic cells from chronic myeloid leukemia.

Leukemia Research, 2017.

CHAVIARA, A. T. et al. Copper(II) Schiff base coordination compounds of dien with heterocyclic aldehydes and 2-amino-5-methyl-thiazole: Synthesis, characterization, antiproliferative and antibacterial studies. Crystal structure of CudienOOC12. **Journal of Inorganic Biochemistry**, 2004.

CHEN, D. et al. Metal Complexes, their Cellular Targets and Potential for Cancer Therapy. **Current Pharmaceutical Design**, 2009.

CHENG, C. F. et al. Pravastatin attenuates carboplatin-induced cardiotoxicity via inhibition of oxidative stress associated apoptosis. **Apoptosis**, 2008.

CHIVERS, T. Metal Complexes. In: **A Guide to Chalcogen-Nitrogen Chemistry**. [s.l: s.n.].

CHOVANEK, M. et al. **Long-term toxicity of cisplatin in germ-cell tumor survivors***Annals of Oncology*, 2017.

CHUA, H. L. et al. NF- κ B represses E-cadherin expression and enhances epithelial to mesenchymal transition of mammary epithelial cells: Potential involvement of ZEB-1 and ZEB-2. **Oncogene**, 2007.

CIARIMBOLI, G. et al. Cisplatin nephrotoxicity is critically mediated via the human organic cation transporter 2. **American Journal of Pathology**, 2005.

CINI, M.; BRADSHAW, T. D.; WOODWARD, S. **Using titanium complexes to defeat cancer: The view from the shoulders of titans***Chemical Society Reviews*, 2017.

CLARKE, D. J. **Cell surface damage activates a cell cycle checkpoint (comment on DOI: 10.1002/bies.201600210)***BioEssays*, 2017.

COGHLIN, C.; MURRAY, G. I. **Current and emerging concepts in tumour metastasis***Journal of Pathology*, 2010.

COHEN, G. M. **Caspases: The executioners of apoptosis***Biochemical Journal*, 1997.

COLLIN, F. **Chemical basis of reactive oxygen species reactivity and involvement in neurodegenerative diseases***International Journal of Molecular Sciences*, 2019.

CONKLIN, K. A. **Chemotherapy-associated oxidative stress: Impact on chemotherapeutic effectiveness***Integrative Cancer Therapies*, 2004.

COOPER, G. M.; HAUSMAN, R. E. The Development and Causes of Cancer. **The Cell: A Molecular Approach**, 2007.

CORREIA, I. et al. Vanadium(IV) and copper(II) complexes of salicylaldimines and aromatic heterocycles: Cytotoxicity, DNA binding and DNA cleavage properties. **Journal of Inorganic Biochemistry**, 2015.

COTTER, K. et al. **Recent Insights into the Structure, Regulation, and Function of the V-ATPases***Trends in Biochemical Sciences*, 2015.

- COWAN, J. A. **Chemical nucleases***Current Opinion in Chemical Biology*, 2001.
- CRANS, D. C. et al. Health benefits of vanadium and its potential as an anticancer agent. In: **Metallo-Drugs: Development and Action of Anticancer Agents**. [s.l: s.n.].
- CROMPTON, M. **The mitochondrial permeability transition pore and its role in cell death***Biochemical Journal*, 1999.
- CUI, L. et al. Apoptosis induction by alantolactone in breast cancer MDA-MB-231 cells through reactive oxygen species-mediated mitochondrion-dependent pathway. **Archives of Pharmacal Research**, 2018.
- CUTULI, M. A. et al. **Galleria mellonella as a consolidated in vivo model hosts: New developments in antibacterial strategies and novel drug testing***Virulence*, 2019.
- DALZON, B. et al. A proteomic view of cellular responses to anticancer quinoline-copper complexes. **Proteomes**, 2019.
- DAM, J. et al. Synthesis of copper and zinc 2-(pyridin-2-yl)imidazo[1,2-a]pyridine complexes and their potential anticancer activity. **European Journal of Medicinal Chemistry**, 2017.
- DANIEL, K. G. et al. Organic copper complexes as a new class of proteasome inhibitors and apoptosis inducers in human cancer cells. **Biochemical Pharmacology**, 2004.
- DAS, A. et al. **Selective inhibitors of nuclear export (SINE) in hematological malignancies***Experimental Hematology and Oncology*, 2015.
- DASARI, S.; BERNARD TCHOUNWOU, P. **Cisplatin in cancer therapy: Molecular mechanisms of action***European Journal of Pharmacology*, 2014.
- DE FALCO, M.; DE LUCA, A. Cell Cycle as a Target of Antineoplastic Drugs. **Current Pharmaceutical Design**, 2010.
- DE VIZCAYA-RUIZ, A. et al. Induction of apoptosis by a novel copper-based anticancer compound, casiopeina II, in L1210 murine leukaemia and CH1 human ovarian carcinoma cells. **Toxicology in Vitro**, 2000.
- DEEGAN, C. et al. In vitro cancer chemotherapeutic activity of 1,10-phenanthroline (phen), [Ag₂(phen)₃(mal)] · 2H₂O, [Cu(phen)₂(mal)] · 2H₂O and [Mn(phen)₂(mal)] · 2H₂O (malH₂ = malonic acid) using human cancer cells. **Cancer Letters**, 2007.
- DEHKHODAEI, M. et al. DNA and HSA interaction of Vanadium (IV), Copper (II), and Zinc (II) complexes derived from an asymmetric bidentate Schiff-base ligand: multi spectroscopic, viscosity measurements, molecular docking, and ONIOM studies. **Journal of Biological Inorganic Chemistry**, 2018.
- DEL BOVE, J. et al. Identification of a core member of the SWI/SNF complex, BAF155/SMARCC1, as a human tumor suppressor gene. **Epigenetics**, 2011.
- DEL RÍO, L. A. et al. **Metabolism of oxygen radicals in peroxisomes and cellular implications***Free Radical Biology and Medicine*, 1992.

DEL RÍO, L. A.; LÓPEZ-HUERTAS, E. **ROS generation in peroxisomes and its role in cell signaling***Plant and Cell Physiology*, 2016.

DENG, X. et al. Parathyroid hormone-related protein and ezrin are up-regulated in human lung cancer bone metastases. **Clinical and Experimental Metastasis**, 2007.

DENIZOT, F.; LANG, R. Rapid colorimetric assay for cell growth and survival. Modifications to the tetrazolium dye procedure giving improved sensitivity and reliability. **Journal of Immunological Methods**, 1986.

DENOYER, D.; CLATWORTHY, S. A. S.; CATER, M. A. Copper complexes in cancer therapy. In: **Metallo-Drugs: Development and Action of Anticancer Agents**. [s.l: s.n.].

DEO, K. M. et al. **Platinum coordination compounds with potent anticancer activity***Coordination Chemistry Reviews*, 2018.

DEVEREUX, M. et al. Synthesis, superoxide dismutase mimetic and anticancer activities of metal complexes of 2,2-dimethylpentanedioic acid(2dmepdaH₂) and 3,3-dimethylpentanedioic acid(3dmepdaH₂): X-ray crystal structures of [Cu(3dmepda)(bipy)]₂·6H₂O and [Cu(2dmepda)(bipy)] (Et. **Bioinorganic Chemistry and Applications**, 2006.

DILRUBA, S.; KALAYDA, G. V. **Platinum-based drugs: past, present and future***Cancer Chemotherapy and Pharmacology*, 2016.

DIMIZA, F. et al. Interaction of copper(II) with the non-steroidal anti-inflammatory drugs naproxen and diclofenac: Synthesis, structure, DNA- and albumin-binding. **Journal of Inorganic Biochemistry**, 2011.

DIVE, C. et al. Analysis and discrimination of necrosis and apoptosis (programmed cell death) by multiparameter flow cytometry. **BBA - Molecular Cell Research**, 1992.

DOGAN, N. Global Patterns of Incidence and Mortality in Lung Cancer. **Eurasian Journal of Medicine and Oncology**, 2019.

DOMINGUEZ, I.; SONENSHEIN, G. E.; SELDIN, D. C. Protein kinase CK2 in health and disease: CK2 and its role in Wnt and NF-kappaB signaling: linking development and cancer. **Cellular and molecular life sciences : CMLS**, 2009.

DONG, G. et al. **PKM2 and cancer: The function of PKM2 beyond glycolysis (Review)***Oncology Letters*, 2016.

DOU, X. et al. **Evidence for immortality and autonomy in animal cancer models is often not provided, which causes confusion on key issues of cancer biology***Journal of Cancer*, 2020.

DRABLØS, F. et al. **Alkylation damage in DNA and RNA - Repair mechanisms and medical significance***DNA Repair*, 2004.

DRAKSHARAPU, A. et al. Characterisation of the interactions between substrate, copper(ii) complex and DNA and their role in rate acceleration in DNA-based asymmetric catalysis. **Dalton Transactions**, 2015.

DRÖGE, W. **Free radicals in the physiological control of cell function** *Physiological Reviews*, 2002.

DUNPHY, G. B.; THURSTON, G. S. Insect immunity. In: **Entomopathogenic Nematodes in Biological Control**. [s.l: s.n.].

DYAKOVA, L. et al. 3d metal complexes with meloxicam as therapeutic agents in the fight against human glioblastoma multiforme and cervical carcinoma. **Biotechnology and Biotechnological Equipment**, 2015.

ELJACK, N. D. et al. Mechanisms of cell uptake and toxicity of the anticancer drug cisplatin. **Metalomics**, 2014.

ELMORE, S. **Apoptosis: A Review of Programmed Cell Death** *Toxicologic Pathology*, 2007.

ENGELAND, K. **Cell cycle arrest through indirect transcriptional repression by p53: I have a DREAM** *Cell Death and Differentiation*, 2018.

ENTWISTLE, F. M.; COOTE, P. J. Evaluation of greater wax moth larvae, *Galleria mellonella*, as a novel in vivo model for non-tuberculosis mycobacteria infections and antibiotic treatments. **Journal of Medical Microbiology**, 2018.

ERXLEBEN, A. **Interactions of copper complexes with nucleic acids** *Coordination Chemistry Reviews*, 2018.

FAGHIH, Z. et al. Palladium (II) complexes based on Schiff base ligands derived from orthovanillin; synthesis, characterization and cytotoxic studies. **Inorganica Chimica Acta**, 2018.

FAVALORO, B. et al. **Role of apoptosis in disease** *Aging*, 2012.

FEINBERG, A. P.; KOLDOBSKIY, M. A.; GÖNDÖR, A. **Epigenetic modulators, modifiers and mediators in cancer aetiology and progression** *Nature Reviews Genetics*, 2016.

FERGUSON, A. T. et al. High frequency of hypermethylation at the 14-3-3 σ locus leads to gene silencing in breast cancer. **Proceedings of the National Academy of Sciences of the United States of America**, 2000.

FERRANDO-MAY, E. et al. Caspases mediate nucleoporin cleavage, but not early redistribution of nuclear transport factors and modulation of nuclear permeability in apoptosis. **Cell Death and Differentiation**, 2001.

FILHOL, O. et al. **Protein kinase CK2 in breast cancer: The CK2 β regulatory subunit takes center stage in epithelial plasticity** *Cellular and Molecular Life Sciences*, 2015.

FOO, J. B. et al. Induction of cell cycle arrest and apoptosis by copper complex Cu(SBCM)₂ towards oestrogen-receptor positive MCF-7 breast cancer cells. **RSC Advances**, 2019.

FORGAC, M. **Vacuolar ATPases: Rotary proton pumps in physiology and pathophysiology** *Nature Reviews Molecular Cell Biology*, 2007.

FOUAD, Y. A.; AANEI, C. **Revisiting the hallmarks of cancer** *American Journal of Cancer*

Research, 2017.

FRANKLIN, M. **A549 - A Model for Non-Small Cell Lung Cancer**.

FREZZA, M. et al. Novel Metals and Metal Complexes as Platforms for Cancer Therapy. **Current Pharmaceutical Design**, 2010.

FRIK, M. et al. In vitro and in vivo evaluation of water-soluble iminophosphorane ruthenium(II) compounds. A potential chemotherapeutic agent for triple negative breast cancer. **Journal of Medicinal Chemistry**, 2014.

FRÖSE, J. et al. Epithelial-Mesenchymal Transition Induces Podocalyxin to Promote Extravasation via Ezrin Signaling. **Cell Reports**, 2018.

FUHRMANN, A. et al. Metastatic State of Cancer Cells May Be Indicated by Adhesion Strength. **Biophysical Journal**, 2017.

GALARIS, D.; EVANGELOU, A. **The role of oxidative stress in mechanisms of metal-induced carcinogenesis***Critical Reviews in Oncology/Hematology*, 2002.

GALINDO-MURILLO, R. et al. Intercalation processes of copper complexes in DNA. **Nucleic Acids Research**, 2015.

GAMA, S. et al. Copper(II) complexes with tridentate pyrazole-based ligands: Synthesis, characterization, DNA cleavage activity and cytotoxicity. **Journal of Inorganic Biochemistry**, 2011.

GANESHPANDIAN, M. et al. New ruthenium(II) arene complexes of anthracenyl-appended diazacycloalkanes: Effect of ligand intercalation and hydrophobicity on DNA and protein binding and cleavage and cytotoxicity. **Dalton Transactions**, 2014.

GAO, Y. et al. Cisplatin-resistant A549 non-small cell lung cancer cells can be identified by increased mitochondrial mass and are sensitive to pemetrexed treatment. **Cancer Cell International**, 2019.

GARCÍA-RAMOS, J. C. et al. **Erratum: Potential cytotoxic and amoebicide activity of first row transition metal compounds with 2,9-bis-(2',5'-diazahexanyl)-1,1-phenanthroline (L1) (Dalton Transactions (2012) 41 (10164-10174) DOI: 10.1039/C2DT30224A)***Dalton Transactions*, 2012.

GARCÍA-TOJAL, J. et al. Revisiting the thiosemicarbazonecopper(II) reaction with glutathione. Activity against colorectal carcinoma cell lines. **Journal of Inorganic Biochemistry**, 2018.

GATENBY, R. A.; GILLIES, R. J. **Why do cancers have high aerobic glycolysis?***Nature Reviews Cancer*, 2004.

GAVRIELI, Y.; SHERMAN, Y.; BEN-SASSON, S. A. Identification of programmed cell death in situ via specific labeling of nuclear DNA fragmentation. **Journal of Cell Biology**, 1992.

GENG, J. et al. A novel manganese complex selectively induces malignant glioma cell death

by targeting mitochondria. **Molecular Medicine Reports**, 2016.

GERSTEN, O.; WILMOTH, J. R. **The cancer transition in Japan since 1951** **Demographic Research**, 2002.

GEWIRTZ, D. A. A critical evaluation of the mechanisms of action proposed for the antitumor effects of the anthracycline antibiotics adriamycin and daunorubicin. **Biochemical Pharmacology**, 1999.

GILL, M. R.; VALLIS, K. A. **Transition metal compounds as cancer radiosensitizers** **Chemical Society Reviews**, 2019.

GINOTRA, Y. P. et al. Histidine availability is decisive in ROS-mediated cytotoxicity of copper complexes of A β 1-16 peptide. **Free Radical Research**, 2016.

GLAGOLEV, A. N.; SKULACHEV, V. P. The proton pump is a molecular engine of motile bacteria. **Nature**, 1978.

GOKDUMAN, K. Strategies Targeting DNA Topoisomerase I in Cancer Chemotherapy: Camptothecins, Nanocarriers for Camptothecins, Organic Non-Camptothecin Compounds and Metal Complexes. **Current Drug Targets**, 2016.

GOLDBERG, M. et al. Xenopus lamin B3 has a direct role in the assembly of a replication competent nucleus: Evidence from cell-free egg extracts. **Journal of Cell Science**, 1995.

GONG, J. P.; TRAGANOS, F.; DARZYNKIEWICZ, Z. A selective procedure for DNA extraction from apoptotic cells applicable for gel electrophoresis and flow cytometry. **Analytical Biochemistry**, 1994.

GORRINI, C.; HARRIS, I. S.; MAK, T. W. **Modulation of oxidative stress as an anticancer strategy** **Nature Reviews Drug Discovery**, 2013.

GOSSELIN, K. et al. Senescent keratinocytes die by autophagic programmed cell death. **American Journal of Pathology**, 2009.

GOVINDARAJU, M. et al. Copper interactions with DNA of chromatin and its role in neurodegenerative disorders. **Journal of Pharmaceutical Analysis**, 2013.

GREAVES, M.; MALEY, C. C. **Clonal evolution in cancer** **Nature**, 2012.

GRISCHKE, E. M.; BRUCKER, S. Y. **Cervical cancer** **Medizinische Monatsschrift fur Pharmazeuten**, 2019.

GRIVENNIKOV, S. I.; GRETEN, F. R.; KARIN, M. **Immunity, Inflammation, and Cancer** **Cell**, 2010.

GUPTA, G. P. et al. Mediators of vascular remodelling co-opted for sequential steps in lung metastasis. **Nature**, 2007.

GURUDEVARU, C. et al. Synthesis and structural and DNA binding studies of mono- and dinuclear copper(II) complexes constructed with —O and —N donor ligands: Potential anti-skin cancer drugs. **Applied Organometallic Chemistry**, 2018.

HAAS, K. L.; FRANZ, K. J. ChemInform Abstract: Application of Metal Coordination Chemistry to Explore and Manipulate Cell Biology. **ChemInform**, 2010.

HÄCKER, G. **The morphology of apoptosis** *Cell and Tissue Research*, 2000.

HADJILIADIS, N.; SLETTEN, E. **Metal Complex-DNA Interactions**. [s.l: s.n.].

HAJREZAIE, M. et al. Acute Toxicity and Gastroprotection Studies of a New Schiff Base Derived Copper (II) Complex against Ethanol-Induced Acute Gastric Lesions in Rats. **PLoS ONE**, 2012.

HALL, M. D. et al. Say no to DMSO: Dimethylsulfoxide inactivates cisplatin, carboplatin, and other platinum complexes. **Cancer Research**, 2014.

HAN, D.; WILLIAMS, E.; CADENAS, E. Mitochondrial respiratory chain-dependent generation of superoxide anion and its release into the intermembrane space. **Biochemical Journal**, 2001.

HANAHAN, D.; WEINBERG, R. A. **The hallmarks of cancer** *Cell*, 2000.

HANAHAN, D.; WEINBERG, R. A. **Hallmarks of cancer: The next generation** *Cell*, 2011.

HANAUSKE, U. et al. Biphasic Effect of Vanadium Salts on In Vitro Tumor Colony Growth. **The International Journal of Cell Cloning**, 1987.

HARMSE, L. et al. c. **Apoptosis**, 2019.

HARTTER, D. E.; BARNEA, A. Brain tissue accumulates ⁶⁷copper by two ligand-dependent saturable processes. A high affinity, low capacity and a low affinity, high capacity process. **Journal of Biological Chemistry**, 1988.

HAYES, S. C. **Acceptance and commitment therapy, relational frame theory, and the third wave of behavioral and cognitive therapies**. Behavior Therapy. **Anais...**2004

HAYNES, M. K. et al. Detection of intracellular granularity induction in prostate cancer cell lines by small molecules using the HyperCyt® high-throughput flow cytometry system. **Journal of Biomolecular Screening**, 2009.

HEDLEY, D. W. et al. Effect of Gallium on DNA Synthesis by Human T-Cell Lymphoblasts. **Cancer Research**, 1988.

HELLEDAY, T. et al. **DNA repair pathways as targets for cancer therapy** *Nature Reviews Cancer*, 2008.

HOLZER, A. K. et al. The copper influx transporter human copper transport protein 1 regulates the uptake of cisplatin in human ovarian carcinoma cells. **Molecular Pharmacology**, 2004.

HORNSEY, M.; WAREHAM, D. W. In vivo efficacy of glycopeptide-colistin combination therapies in a *Galleria mellonella* model of *Acinetobacter baumannii* infection. **Antimicrobial Agents and Chemotherapy**, 2011.

HOWARD, R. A.; BEAR, J. L.; KIMBALL, A. P. Mechanism of Action of Tetra- μ -

Carboxylatodirhodium(II) in L1210 Tumor Suspension Culture. **Cancer Research**, 1979.

HU, W. et al. P53 Signalling Controls Cell Cycle Arrest And Caspase-Independent Apoptosis In Macrophages Infected With Pathogenic Leptospira Species. **Cellular Microbiology**, 2013.

HURLEY, L. H. **DNA and its associated processes as targets for cancer therapy** *Nature Reviews Cancer*, 2002.

IGHODARO, O. M.; AKINLOYE, O. A. First line defence antioxidants-superoxide dismutase (SOD), catalase (CAT) and glutathione peroxidase (GPX): Their fundamental role in the entire antioxidant defence grid. **Alexandria Journal of Medicine**, 2018.

ITO, M.; HOUKIN, K. Cell culture. In: **Cell Therapy against Cerebral Stroke: Comprehensive Reviews for Translational Researches and Clinical Trials**. [s.l.: s.n.].

JACKSON, S. P.; BARTEK, J. **The DNA-damage response in human biology and disease** *Nature*, 2009.

JAIVIDHYA, P. et al. Efficient DNA cleavage mediated by mononuclear mixed ligand copper(II) phenolate complexes: The role of co-ligand planarity on DNA binding and cleavage and anticancer activity. **Journal of Inorganic Biochemistry**, 2012.

JÁNOSSY, J. et al. Calpain as a multi-site regulator of cell cycle. **Biochemical Pharmacology**, 2004.

JAOUEN, G.; VESSIÈRES, A.; TOP, S. **Ferrocifen type anti cancer drugs** *Chemical Society Reviews*, 2015.

JAYASEELAN, P. et al. Synthesis, characterization, anti-microbial, DNA binding and cleavage studies of Schiff base metal complexes. **Arabian Journal of Chemistry**, 2016.

JOHNSTONE, T. C.; SUNTHARALINGAM, K.; LIPPARD, S. J. **The Next Generation of Platinum Drugs: Targeted Pt(II) Agents, Nanoparticle Delivery, and Pt(IV) Prodrugs** *Chemical Reviews*, 2016.

JONES, Z. W. et al. A drift-diffusion checkpoint model predicts a highly variable and growth-factor-sensitive portion of the cell cycle G1 phase. **PLoS ONE**, 2018.

JUNGWIRTH, U. et al. **Anticancer activity of metal complexes: Involvement of redox processes** *Antioxidants and Redox Signaling*, 2011.

KACHADOURIAN, R. et al. Casiopeína II gly-induced oxidative stress and mitochondrial dysfunction in human lung cancer A549 and H157 cells. **Toxicology**, 2010.

KAIMING SUN, JING WANG, Z. W. **TERAPIAS DE COMBINAÇÃO PARA O TRATAMENTO DE CÂNCER**, [s.d.].

KALYANARAMAN, B. et al. **A review of the basics of mitochondrial bioenergetics, metabolism, and related signaling pathways in cancer cells: Therapeutic targeting of tumor mitochondria with lipophilic cationic compounds** *Redox Biology*, 2018.

KAR, S. **Unraveling Cell-Cycle Dynamics in Cancer** *Cell Systems*, 2016.

- KASTAN, M. B.; BARTEK, J. **Cell-cycle checkpoints and cancer***Nature*, 2004.
- KAUFMANN, S. H.; EARNSHAW, W. C. Induction of apoptosis by cancer chemotherapy. **Experimental Cell Research**, 2000.
- KAVANAGH, K.; REEVES, E. P. **Exploiting the potential of insects for in vivo pathogenicity testing of microbial pathogens***FEMS Microbiology Reviews*, 2004.
- KEENE, F. R.; SMITH, J. A.; COLLINS, J. G. **Metal complexes as structure-selective binding agents for nucleic acids***Coordination Chemistry Reviews*, 2009.
- KELLETT, A. et al. Water-soluble bis(1,10-phenanthroline) octanedioate Cu²⁺ and Mn²⁺ complexes with unprecedented nano and picomolar in vitro cytotoxicity: Promising leads for chemotherapeutic drug development. **MedChemComm**, 2011.
- KERR, J. F. R.; WYLLIE, A. H.; CURRIE, A. R. Apoptosis: A basic biological phenomenon with wide-ranging implications in tissue kinetics. **British Journal of Cancer**, 1972.
- KIELKOPF, C. L. et al. Structure of a photoactive rhodium complex intercalated into DNA. **Nature Structural Biology**, 2000.
- KLAUNIG, J. E. Epigenetic mechanisms of chemical carcinogenesis. **Human and Experimental Toxicology**, 2000.
- KONDO, N. et al. **DNA damage induced by alkylating agents and repair pathways***Journal of Nucleic Acids*, 2010.
- KOTAMRAJU, S. et al. Transferrin receptor-dependent iron uptake is responsible for doxorubicin-mediated apoptosis in endothelial cells. Role of oxidant-induced iron signaling in apoptosis. **Journal of Biological Chemistry**, 2002.
- KUMARI, S. et al. **Reactive Oxygen Species: A Key Constituent in Cancer Survival***Biomarker Insights*, 2018.
- L., K. The resurgence of platinum-based cancer chemotherapy. **Nature Reviews Cancer**, 2007.
- LARSON, C. A. et al. The role of the mammalian copper transporter 1 in the cellular accumulation of platinum-based drugs. **Molecular Pharmacology**, 2009.
- LERMAN, L. S. Structural considerations in the interaction of DNA and acridines. **Journal of Molecular Biology**, 1961.
- LI, N. et al. Ezrin promotes breast cancer progression by modulating AKT signals. **British Journal of Cancer**, 2019a.
- LI, P. et al. Isofraxidin, a potent reactive oxygen species (ROS) scavenger, protects human leukemia cells from radiation-induced apoptosis via ROS/mitochondria pathway in p53-independent manner. **Apoptosis**, 2014.
- LI, P. et al. **Caspase-9: Structure, mechanisms and clinical application***Oncotarget*, 2017.

LI, Y. et al. Distinct RanBP1 nuclear export and cargo dissociation mechanisms between fungi and animals. **eLife**, 2019b.

LIANG, J. X. et al. **Recent development of transition metal complexes with in vivo antitumor activity** *Journal of Inorganic Biochemistry*, 2017.

LIGUORI, I. et al. **Oxidative stress, aging, and diseases** *Clinical Interventions in Aging*, 2018.

LIN, C. C. et al. Lysophosphatidic acid induces reactive oxygen species generation by activating protein kinase C in PC-3 human prostate cancer cells. **Biochemical and Biophysical Research Communications**, 2013.

LIPFERT, J. et al. Understanding Nucleic Acid–Ion Interactions. **Annual Review of Biochemistry**, 2014.

LIU, H.; BALIGA, R. Endoplasmic reticulum stress-associated caspase 12 mediates cisplatin-induced LLC-PK1 cell apoptosis. **Journal of the American Society of Nephrology**, 2005.

LIU, Y. R. et al. Transplatin enhances effect of cisplatin on both single DNA molecules and live tumor cells. **Archives of Biochemistry and Biophysics**, 2013.

LONDON, W. T.; PETRICK, J. L.; MCGLYNN, K. A. Liver cancer. In: **Schottenfeld and Fraumeni Cancer Epidemiology and Prevention, Fourth Edition**. [s.l: s.n.].

LONG, Z. Y.; WANG, T. H. **Advances of the Role of Ezrin in Migration and Invasion of Breast Cancer Cells** *Sheng li ke xue jin zhan [Progress in physiology]*, 2016.

LOU, X. et al. Phorbol esters modulate spontaneous and Ca²⁺-evoked transmitter release via acting on both Munc13 and protein kinase C. **Journal of Neuroscience**, 2008.

LU, W. et al. Up-regulation of PKM2 promote malignancy and related to adverse prognostic risk factor in human gallbladder cancer. **Scientific Reports**, 2016.

MA, D. L. et al. **Iridium(III) Complexes Targeting Apoptotic Cell Death in Cancer Cells** *Molecules (Basel, Switzerland)*, 2019.

MACIEL, L. L. F. et al. In vitro and in vivo anti-proliferative activity and ultrastructure investigations of a copper(II) complex toward human lung cancer cell NCI-H460. **Journal of Inorganic Biochemistry**, 2020.

MAHESWARI, P. U. et al. The square-planar cytotoxic [CuII(pyrimol)Cl] complex acts as an efficient DNA cleaver without reductant. **Journal of the American Chemical Society**, 2006.

MALVEZZI, H. et al. Sperm quality after density gradient centrifugation with three commercially available media: A controlled trial. **Reproductive Biology and Endocrinology**, 2014.

MAŁYSZKO, J. et al. **Nephrotoxicity of anticancer treatment** *Nephrology Dialysis Transplantation*, 2017.

MANIKANDAMATHAVAN, V. M. et al. Cytotoxic copper(II) complex of

tripyrrodoquinoxaline with DNA hydrolase activity. **Polyhedron**, 2011.

MAQSOOD, M. I. et al. **Immortality of cell lines: Challenges and advantages of establishment** *Cell Biology International*, 2013.

MARINKOVIĆ, M. et al. **Autophagy modulation in cancer: Current knowledge on action and therapy** *Oxidative Medicine and Cellular Longevity*, 2018.

MARKY, L. A. et al. Thermodynamics of drug-dna interactions. **Journal of Biomolecular Structure and Dynamics**, 1983.

MARZO, I. et al. Cladribine induces apoptosis in human leukaemia cells by caspase-dependent and -independent pathways acting on mitochondria. **Biochemical Journal**, 2001.

MASOOD, I. et al. **Major contributions towards finding a cure for cancer through chemotherapy: A historical review** *Tumori*, 2016.

MASSIMILIANO DAIUTO, G. P. Organo-Metallic Compounds: Novel Molecules in Cancer Therapy. **Biochemistry & Pharmacology: Open Access**, 2014.

MATÉS, J. M.; SÁNCHEZ-JIMÉNEZ, F. M. Role of reactive oxygen species in apoptosis: Implications for cancer therapy. **International Journal of Biochemistry and Cell Biology**, 2000.

MCGIVERN, T. J. P.; AFSHARPOUR, S.; MARMION, C. J. **Copper complexes as artificial DNA metallonucleases: From Sigman's reagent to next generation anti-cancer agent?** *Inorganica Chimica Acta*, 2018.

MCILWAIN, D. R.; BERGER, T.; MAK, T. W. Caspase functions in cell death and disease. **Cold Spring Harbor Perspectives in Biology**, 2013.

MEGGER, D. A. et al. Structurally related hydrazone-based metal complexes with different antitumor activities variably induce apoptotic cell death. **Dalton Transactions**, 2017.

MILLER, A. B. Cancer Prevention. In: **International Encyclopedia of Public Health**. [s.l: s.n.].

MINAMOTO, T.; OUGOLKOV, A. V.; MAI, M. **Detection of oncogenes in the diagnosis of cancers with active oncogenic signaling** *Expert Review of Molecular Diagnostics*, 2002.

MIROŃCZUK-CHODAKOWSKA, I.; WITKOWSKA, A. M.; ZUJKO, M. E. **Endogenous non-enzymatic antioxidants in the human body** *Advances in Medical Sciences*, 2018.

MITTAL, V. et al. The microenvironment of lung cancer and therapeutic implications. In: **Advances in Experimental Medicine and Biology**. [s.l: s.n.].

MOHAMMADIZADEH, F. et al. The cytotoxicity effects of a novel Cu complex on MCF-7 human breast cancerous cells. **BioMetals**, 2018.

MORALES-SÁNCHEZ, A.; FUENTES-PANANÁ, E. M. **Human viruses and cancer** *Viruses*, 2014.

MORO-OKA, Y. Activation of dioxygen molecules on dinuclear metal centers. **Proceedings of the Indian Academy of Sciences: Chemical Sciences**, 1999.

MOUDI, M. et al. **Vinca alkaloids** *International Journal of Preventive Medicine*, 2013.

MUHAMMAD, N.; GUO, Z. **Metal-based anticancer chemotherapeutic agents** *Current Opinion in Chemical Biology*, 2014.

MURATORI, M. et al. Functional and ultrastructural features of DNA-fragmented human sperm. **Journal of Andrology**, 2000.

MURTINHO, D. et al. Synthesis, characterization and assessment of the cytotoxic activity of Cu(II), Fe(III) and Mn(III) complexes of camphoric acid-derived salen ligands. **Applied Organometallic Chemistry**, 2015.

NAKAHATA, D. H. et al. Sulfonamide-containing copper(II) metallonucleases: Correlations with in vitro antimycobacterial and antiproliferative activities. **Journal of Inorganic Biochemistry**, 2018.

NALEPA, G.; ROLFE, M.; HARPER, J. W. Drug discovery in the ubiquitin - Proteasome system. **Nature Reviews Drug Discovery**, 2006.

NDAGI, U.; MHLONGO, N.; SOLIMAN, M. E. **Metal complexes in cancer therapy – An update from drug design perspective** *Drug Design, Development and Therapy*, 2017.

NEAL, C. L. et al. 14-3-3 ζ overexpression defines high risk for breast cancer recurrence and promotes cancer cell survival. **Cancer Research**, 2009.

NEUZILLET, C. et al. **Targeting the Ras-ERK pathway in pancreatic adenocarcinoma** *Cancer and Metastasis Reviews*, 2013.

NICOLETTI, I. et al. A rapid and simple method for measuring thymocyte apoptosis by propidium iodide staining and flow cytometry. **Journal of Immunological Methods**, 1991.

NISHIHARA, R. et al. **Molecular pathological epidemiology gives clues to paradoxical findings** *European Journal of Epidemiology*, 2015.

NITISS, J. L. **Targeting DNA topoisomerase II in cancer chemotherapy** *Nature Reviews Cancer*, 2009.

NUNES, C. J. et al. Reactivity of dinuclear copper(II) complexes towards melanoma cells: Correlation with its stability, tyrosinase mimicking and nuclease activity. **Journal of Inorganic Biochemistry**, 2015.

NUNEZ, R. DNA measurement and cell cycle analysis by flow cytometry. **Current Issues in Molecular Biology**, 2001.

O'CONNOR, M. et al. Copper(II) complexes of salicylic acid combining superoxide dismutase mimetic properties with DNA binding and cleaving capabilities display promising chemotherapeutic potential with fast acting in vitro cytotoxicity against cisplatin sensitive and resistant. **Journal of Medicinal Chemistry**, 2012.

OBERLEY LARRY; SORENSON JOHN R J. **COPPER COMPLEX FOR TREATING CANCER.**, [s.d.].

OGATA, H. et al. **KEGG: Kyoto encyclopedia of genes and genomes***Nucleic Acids Research*, 1999.

OGINO, S. et al. **Review article: The role of molecular pathological epidemiology in the study of neoplastic and non-neoplastic diseases in the era of precision medicine***Epidemiology*, 2016.

ÖHRVIK, H.; THIELE, D. J. How copper traverses cellular membranes through the mammalian copper transporter 1, Ctr1. *Annals of the New York Academy of Sciences*, 2014.

OLIVEIRA, P. A. et al. Chemical carcinogenesis. *Anais da Academia Brasileira de Ciencias*, 2007.

OLIVERI, V. et al. Amino- and chloro-8-hydroxyquinolines and their copper complexes as proteasome inhibitors and antiproliferative agents. *Metallomics*, 2017.

OMRAN, A. R. The epidemiologic transition. A theory of the epidemiology of population change. *The Milbank Memorial Fund quarterly*, 1971.

ONYANGO, A. N. **The Contribution of Singlet Oxygen to Insulin Resistance***Oxidative Medicine and Cellular Longevity*, 2017.

OSOUDA, S. et al. Null mutants of Drosophila B-type lamin Dm0 show aberrant tissue differentiation rather than obvious nuclear shape distortion or specific defects during cell proliferation. *Developmental Biology*, 2005.

OSSOLA, F. et al. Synthesis, structure and properties of new ferrocene-containing compounds. *Inorganica Chimica Acta*, 2003.

OTSUKA, M. et al. A human transporter protein that mediates the final excretion step for toxic organic cations. *Proceedings of the National Academy of Sciences of the United States of America*, 2005.

OZAWA, S. et al. Kinetic Analysis of Cell Killing Effect Induced by Cytosine Arabinoside and Cisplatin in Relation to Cell Cycle Phase Specificity in Human Colon Cancer and Chinese Hamster Cells. *Cancer Research*, 1989.

PAGES, B. J. et al. **Metal complex interactions with DNA***Dalton Transactions*, 2015.

PAHL, H. L. **Activators and target genes of Rel/NF- κ B transcription factors***Oncogene*, 1999.

PAHONȚU, E. et al. Synthesis and characterization of novel Cu(II), Pd(II) and Pt(II) complexes with 8-ethyl-2-hydroxytricyclo(7.3.1.0^{2,7})tridecan-13-one-thiosemicarbazone: Antimicrobial and in Vitro antiproliferative activity. *Molecules*, 2016.

PANIERI, E.; SANTORO, M. M. **Ros homeostasis and metabolism: A dangerous liason in cancer cells***Cell Death and Disease*, 2016.

PATRA, M.; GASSER, G. The medicinal chemistry of ferrocene and its derivatives. **Nature Reviews Chemistry**, 2017.

PATTAN, S. R. et al. **The scope of metal complexes in drug design - A review** **Indian Drugs**, 2012.

PERERA, D. et al. Differential DNA repair underlies mutation hotspots at active promoters in cancer genomes. **Nature**, 2016.

PIGEON, P. et al. A New Series of Succinimido-ferrociphenols and Related Heterocyclic Species Induce Strong Antiproliferative Effects, Especially against Ovarian Cancer Cells Resistant to Cisplatin. **Journal of Medicinal Chemistry**, 2017.

PISTRITTO, G. et al. **Apoptosis as anticancer mechanism: Function and dysfunction of its modulators and targeted therapeutic strategies** **Aging**, 2016.

POBEZINSKAYA, Y. L.; LIU, Z. **The role of TRADD in death receptor signaling** **Cell Cycle**, 2012.

POIRIER, M. C.; SANTELLA, R. M.; WESTON, A. **Carcinogen macromolecular adducts and their measurement** **Carcinogenesis**, 2000.

POMMIER, Y. **Topoisomerase I inhibitors: Camptothecins and beyond**. **Nature Reviews Cancer**. **Anais...**2006

PONTIKI, E.; HADJIPAVLOU-LITINA, D.; CHAVIARA, A. T. Evaluation of anti-inflammatory and antioxidant activities of Copper (II) Schiff mono-base and Copper(II) Schiff base coordination compounds of dien with heterocyclic aldehydes and 2-amino-5-methylthiazole. **Journal of Enzyme Inhibition and Medicinal Chemistry**, 2008.

PRASETYANTI, P. R.; MEDEMA, J. P. **Intra-tumor heterogeneity from a cancer stem cell perspective** **Molecular Cancer**, 2017.

PRATILAS, C. A.; SOLIT, D. B. **Targeting the mitogen-activated protein kinase pathway: Physiological feedback and drug response** **Clinical Cancer Research**, 2010.

PROSSER, K. E. et al. Anticancer copper pyridine benzimidazole complexes: ROS generation, biomolecule interactions, and cytotoxicity. **Journal of Inorganic Biochemistry**, 2017.

PUSPITA, N. A.; BEDFORD, A. Morphological Changes of Cisplatin-resistant Human Breast Cancer MCF-7 Cell Line. **International Journal of Integrated Health Sciences**, 2017.

QUAN, C. et al. Ezrin promotes pancreatic cancer cell proliferation and invasion through activating the Akt/mTOR pathway and inducing YAP translocation. **Cancer Management and Research**, 2019.

R.-M., L.; K.A., G. P. Oxidative stress and glutathione in TGF- β -mediated fibrogenesis. **Free Radical Biology and Medicine**, 2010.

RABIK, C. A.; DOLAN, M. E. **Molecular mechanisms of resistance and toxicity associated with platinating agents** **Cancer Treatment Reviews**, 2007.

RAFAELA DOS SANTOS MORAES; NICOLÁS ÁDRIAN REY. Homo and heterodinuclear complexes containing isoniazid-derived ligands as potential antitumor agents. 2016.

RAICA, M.; CIMPEAN, A. M.; RIBATTI, D. **Angiogenesis in pre-malignant conditions***European Journal of Cancer*, 2009.

RAJSKI, S. R.; WILLIAMS, R. M. DNA cross-linking agents as antitumor drugs. **Chemical Reviews**, 1998.

RAMAN, N.; SOBHA, S. Exploring the DNA binding mode of transition metal based biologically active compounds. **Spectrochimica Acta - Part A: Molecular and Biomolecular Spectroscopy**, 2012.

RAMAWAT, K. G.; MERILLON, J. M. (EDS.). **Bioactive Molecules and Medicinal Plants**. Berlin, Heidelberg: Springer Berlin Heidelberg, 2008.

RAMOS, J. W. **The regulation of extracellular signal-regulated kinase (ERK) in mammalian cells***International Journal of Biochemistry and Cell Biology*, 2008.

RAVAGNAN, L. et al. Heat-shock protein 70 antagonizes apoptosis-inducing factor. **Nature Cell Biology**, 2001.

RAZAK, N. A. et al. Cytotoxicity of eupatorin in MCF-7 and MDA-MB-231 human breast cancer cells via cell cycle arrest, anti-angiogenesis and induction of apoptosis. **Scientific Reports**, 2019.

READ, S. A.; DOUGLAS, M. W. **Virus induced inflammation and cancer development***Cancer Letters*, 2014.

REBBECK, T. R. **Prostate Cancer Genetics: Variation by Race, Ethnicity, and Geography***Seminars in Radiation Oncology*, 2017.

RENU, K. et al. **Molecular mechanism of doxorubicin-induced cardiomyopathy – An update***European Journal of Pharmacology*, 2018.

RENWICK, J.; KAVANAGH, K. Insects as models for studying the virulence of fungal pathogens of humans. In: **New Insights in Medical Mycology**. [s.l: s.n.].

RIBEIRO, R. C. B. et al. A new strategy for the synthesis of nonsymmetrical 3,3'-(aryl/alkyl-methylene) bis-2-hydroxy-1,4-naphthoquinones and their cytotoxic effects in PC3 prostate cancer cells. **Journal of the Brazilian Chemical Society**, 2020.

RITTIÉ, L.; PERBAL, B. **Enzymes used in molecular biology: A useful guide***Journal of Cell Communication and Signaling*, 2008.

ROCHA, C. R. R. et al. **DNA repair pathways and cisplatin resistance: An intimate relationship***Clinics*, 2018.

RODIĆ, M. V. et al. Synthesis, characterization, cytotoxicity and antiangiogenic activity of copper(II) complexes with 1-adamantoyl hydrazone bearing pyridine rings. **European Journal of Medicinal Chemistry**, 2016.

ROMIEU-MOUREZ, R. et al. Protein kinase CK2 promotes aberrant activation of nuclear factor- κ B, transformed phenotype, and survival of breast cancer cells. **Cancer Research**, 2002.

ROSENBERG, B. et al. **Platinum compounds: A new class of potent antitumour agents** [24]**Nature**, 1969.

ROUX, P. P. et al. Tumor-promoting phorbol esters and activated Ras inactivate the tuberous sclerosis tumor suppressor complex via p90 ribosomal S6 kinase. **Proceedings of the National Academy of Sciences of the United States of America**, 2004.

RUIZ-AZUARA, L.; E. BRAVO-GOMEZ, M. Copper Compounds in Cancer Chemotherapy. **Current Medicinal Chemistry**, 2010.

RYBAK, L. P.; WHITWORTH, C.; SOMANI, S. Application of antioxidants and other agents to prevent cisplatin ototoxicity. **Laryngoscope**, 1999.

SAFAEI, R. et al. The CXXC motifs in the metal binding domains are required for ATP7B to mediate resistance to cisplatin. **Journal of Inorganic Biochemistry**, 2012.

SAHAI, E. **Mechanisms of cancer cell invasion****Current Opinion in Genetics and Development**, 2005.

SAKAMURU, S.; ATTENE-RAMOS, M. S.; XIA, M. Mitochondrial membrane potential assay. **Methods in Molecular Biology**, 2016.

SALGA, M. S. et al. Acute oral toxicity evaluations of some Zinc(II) complexes derived from 1-(2-Salicylaldiminoethyl)piperazine schiff bases in rats. **International Journal of Molecular Sciences**, 2012.

SALGANIK, R. I. The Benefits and Hazards of Antioxidants: Controlling Apoptosis and Other Protective Mechanisms in Cancer Patients and the Human Population. **Journal of the American College of Nutrition**, 2001.

SANDOVAL, J.; ESTELLER, M. **Cancer epigenomics: Beyond genomics****Current Opinion in Genetics and Development**, 2012.

SANTINI, C. et al. **Advances in copper complexes as anticancer agents****Chemical Reviews**, 2014.

SAPEGA, O. et al. Distinct phenotypes and “bystander” effects of senescent tumour cells induced by docetaxel or immunomodulatory cytokines. **International Journal of Oncology**, 2018.

SARASTE, A.; PULKKI, K. **Morphologic and biochemical hallmarks of apoptosis****Cardiovascular Research**, 2000.

SARIN, N. et al. Cisplatin resistance in non-small cell lung cancer cells is associated with an abrogation of cisplatin-induced G2/M cell cycle arrest. **PLoS ONE**, 2017.

SCHIEBER, M.; CHANDEL, N. S. **ROS function in redox signaling and oxidative stress****Current Biology**, 2014.

SENNOUNE, S. R.; MARTINEZ-ZAGUILAN, R. **Plasmalemmal vacuolar H⁺-ATPases in angiogenesis, diabetes and cancer** *Journal of Bioenergetics and Biomembranes*, 2007.

SERMENT-GUERRERO, J. et al. Genotoxicity of the copper antineoplastic coordination complexes casiopeinas®. **Toxicology in Vitro**, 2011.

SHAMBERGER, R. J. Chemoprevention of cancer. In: **Diet, Nutrition and Cancer: A Critical Evaluation: Volume II: Micronutrients, Nonnutritive Dietary Factors, and Cancer**. [s.l: s.n.].

SHERR, C. J.; BARTEK, J. Cell Cycle-Targeted Cancer Therapies. **Annual Review of Cancer Biology**, 2017.

SHIN, J.; ESKANDARI, A.; SUNTHARALINGAM, K. Modulating the chemical and biological properties of cancer stem cell-potent copper(II)-Nonsteroidal anti-inflammatory drug complexes. **Molecules**, 2019.

SIDDIK, Z. H. **Cisplatin: Mode of cytotoxic action and molecular basis of resistance** *Oncogene*, 2003.

SIDDIQUI, I. A. et al. Resveratrol nanoformulation for cancer prevention and therapy. **Annals of the New York Academy of Sciences**, 2015.

SIES, H.; JONES, D. Oxidative Stress. In: **Encyclopedia of Stress**. [s.l: s.n.].

SIGMAN, D. S. et al. Oxygen-dependent cleavage of DNA by the 1,10-phenanthroline.cuprous complex. Inhibition of Escherichia coli DNA polymerase I. **Journal of Biological Chemistry**, 1979.

SINGH, N. et al. Inflammation and cancer. **Annals of African Medicine**, 2019.

SINGH, R. K. et al. **Therapeutic journey of nitrogen mustard as alkylating anticancer agents: Historic to future perspectives** *European Journal of Medicinal Chemistry*, 2018.

SINHA, K. et al. **Oxidative stress: The mitochondria-dependent and mitochondria-independent pathways of apoptosis** *Archives of Toxicology*, 2013.

SMILEY, S. T. et al. Intracellular heterogeneity in mitochondrial membrane potentials revealed by a J-aggregate-forming lipophilic cation JC-1. **Proceedings of the National Academy of Sciences of the United States of America**, 1991.

SMYTHE, C.; JENKINS, H. E.; HUTCHISON, C. J. Incorporation of the nuclear pore basket protein Nup153 into nuclear pore structures is dependent upon lamina assembly: Evidence from cell-free extracts of *Xenopus* eggs. **EMBO Journal**, 2000.

SOLL, J. M.; SOBOL, R. W.; MOSAMMAPARAST, N. **Regulation of DNA Alkylation Damage Repair: Lessons and Therapeutic Opportunities** *Trends in Biochemical Sciences*, 2017.

SONG, H.; KAISER, J. T.; BARTON, J. K. Crystal structure of Δ -[Ru(bpy)₂dppz]²⁺ bound to mismatched DNA reveals side-by-side metalloinsertion and intercalation. **Nature Chemistry**, 2012.

SOUTHAM, H. M. et al. The Microbiology of Ruthenium Complexes. In: **Advances in Microbial Physiology**. [s.l: s.n.].

SPERKA, T. et al. Activation of ras requires the ERM-dependent link of actin to the plasma membrane. **PLoS ONE**, 2011.

STEINBACH, G. et al. Antibiotic treatment of gastric lymphoma of mucosa-associated lymphoid tissue: An uncontrolled trial. **Annals of Internal Medicine**, 1999.

SULLIVAN, L. B.; CHANDEL, N. S. **Mitochondrial reactive oxygen species and cancer****Cancer and Metabolism**, 2014.

SUNDARESAN, M. et al. Requirement for generation of H₂O₂ for platelet-derived growth factor signal transduction. **Science**, 1995.

SUSIN, S. A. et al. Bcl-2 inhibits the mitochondrial release of an apoptogenic protease. **Journal of Experimental Medicine**, 1996.

SUSIN, S. A. et al. Molecular characterization of mitochondrial apoptosis-inducing factor. **Nature**, 1999.

SWARTS, J. C. et al. Cytotoxicity of a series of ferrocene-containing β -diketones. **Anticancer Research**, 2008.

SWIFT, L. H.; GOLSTEYN, R. M. **Genotoxic anti-cancer agents and their relationship to DNA damage, mitosis, and checkpoint adaptation in proliferating cancer cells****International Journal of Molecular Sciences**, 2014.

SZATROWSKI, T. P.; NATHAN, C. F. Production of Large Amounts of Hydrogen Peroxide by Human Tumor Cells. **Cancer Research**, 1991.

SZNARKOWSKA, A. et al. **Inhibition of cancer antioxidant defense by natural compounds****Oncotarget**, 2017.

TAKEMURA, G.; FUJIWARA, H. Doxorubicin-Induced Cardiomyopathy. From the Cardiotoxic Mechanisms to Management. **Progress in Cardiovascular Diseases**, 2007.

TAKIHARA, Y. Role of the beta isoform of 14-3-3 proteins in cellular proliferation and oncogenic transformation. **Carcinogenesis**, 2000.

TAKIMOTO, C. H. et al. High inter- and inpatient variation in 5-fluorouracil plasma concentrations during a prolonged drug infusion. **Clinical Cancer Research**, 1999.

TAN, S. J. et al. Copper, gold and silver compounds as potential new anti-tumor metallodrugs. **Future Medicinal Chemistry**, v. 2, n. 10, p. 1591–1608, out. 2010.

TASHIRO, H.; BRENNER, M. K. **Immunotherapy against cancer-related viruses****Cell Research**, 2017.

THIRUMARAN, R.; PRENDERGAST, G. C.; GILMAN, P. B. Cytotoxic Chemotherapy in Clinical Treatment of Cancer. In: **Cancer Immunotherapy**. [s.l: s.n.].

THU, K. L. et al. **Targeting the cell cycle in breast cancer: towards the next phase** *Cell Cycle*, 2018.

TIEKINK, E. R. T. **Anti-cancer potential of gold complexes** *Inflammopharmacology*, 2008.

TIKU, M. L.; LIESCH, J. B.; ROBERTSON, F. M. Production of hydrogen peroxide by rabbit articular chondrocytes. Enhancement by cytokines. *Journal of Immunology*, 1990.

TINHOFER, I. et al. **Cancer stem cell characteristics of circulating tumor cells** *International Journal of Radiation Biology*, 2014.

TISATO, F. et al. **Copper in diseases and treatments, and copper-based anticancer strategies** *Medicinal Research Reviews*, 2010.

TOLCHER, A. W. Preliminary phase I results of G3139 (bcl-2 antisense oligonucleotide) therapy in combination with docetaxel in hormone-refractory prostate cancer. *Seminars in Oncology*, 2001.

TURAJLIC, S. et al. **Resolving genetic heterogeneity in cancer** *Nature Reviews Genetics*, 2019.

TYANOVA, S. et al. **The Perseus computational platform for comprehensive analysis of (prote)omics data** *Nature Methods*, 2016.

USMAN, M. et al. Coumarin centered copper(II) complex with appended-imidazole as cancer chemotherapeutic agents against lung cancer: Molecular insight: Via DFT-based vibrational analysis. *RSC Advances*, 2017.

VAIDYANATHAN, H. et al. ERK MAP kinase is targeted to RSK2 by the phosphoprotein PEA-15. *Proceedings of the National Academy of Sciences of the United States of America*, 2007.

VALKO, M. et al. **Free radicals, metals and antioxidants in oxidative stress-induced cancer** *Chemico-Biological Interactions*, 2006.

VAN RIJT, S. H.; SADLER, P. J. **Current applications and future potential for bioinorganic chemistry in the development of anticancer drugs** *Drug Discovery Today*, 2009.

VERANI, C. N. **Metal complexes as inhibitors of the 26S proteasome in tumor cells** *Journal of Inorganic Biochemistry*, 2012.

VERDOODT, B. et al. Characterization of 14-3-3sigma dimerization determinants: Requirement of homodimerization for inhibition of cell proliferation. *Cell Cycle*, 2006.

VIALARD, C.; LARRIVÉE, B. **Tumor angiogenesis and vascular normalization: alternative therapeutic targets** *Angiogenesis*, 2017.

W.T., S.; E., B.; Y., L. Clinical translation of nuclear export inhibitors in cancer. *Seminars in Cancer Biology*, 2014.

WANG, J.; YI, J. **Cancer cell killing via ROS: To increase or decrease, that is a**

questionCancer Biology and Therapy, 2008.

WANG, T. et al. Copper ion attenuated the antiproliferative activity of di-2-pyridylhydrazone dithiocarbamate derivative; however, there was a lack of correlation between ROS generation and antiproliferative activity. **Molecules**, 2016.

WEINFELD, M. et al. **Tidying up loose ends: The role of polynucleotide kinase/phosphatase in DNA strand break repair***Trends in Biochemical Sciences*, 2011.

WEST, J. D.; MARNETT, L. J. **Endogenous reactive intermediates as modulators of cell signaling and cell death***Chemical Research in Toxicology*, 2006.

WILLCOX, J. K.; ASH, S. L.; CATIGNANI, G. L. Antioxidants and prevention of chronic disease. **Critical Reviews in Food Science and Nutrition**, 2004.

WILSON, J. T. et al. Examination of the Impact of Copper(II) α -(N)-Heterocyclic Thiosemicarbazone Complexes on DNA Topoisomerase II α . **Chemical Research in Toxicology**, 2016.

WOLKENBERG, S. E.; BOGER, D. L. Total synthesis of anhydrolicorinone utilizing sequential intramolecular Diels-Alder reactions of a 1,3,4-oxadiazole. **Journal of Organic Chemistry**, 2002.

WOODS, D.; TURCHI, J. J. **Chemotherapy induced DNA damage response Convergence of drugs and pathways***Cancer Biology and Therapy*, 2013.

WU, C. C. et al. The Apaf-1 apoptosome induces formation of caspase-9 homo- and heterodimers with distinct activities. **Nature Communications**, 2016a.

WU, S. et al. Substantial contribution of extrinsic risk factors to cancer development. **Nature**, 2016b.

WU, S. C. et al. Water-soluble dinitrosyl iron complex (DNIC): A nitric oxide vehicle triggering cancer cell death via apoptosis. **Inorganic Chemistry**, 2016c.

XIA, Y. et al. A new Schiff base coordinated copper(II) compound induces apoptosis and inhibits tumor growth in gastric cancer. **Cancer Cell International**, 2019.

XING, Z. et al. The use of Gene Ontology terms and KEGG pathways for analysis and prediction of oncogenes. **Biochimica et Biophysica Acta - General Subjects**, 2016.

YANG, C. et al. Anticancer osmium complex inhibitors of the HIF-1 α and p300 protein-protein interaction. **Scientific Reports**, 2017.

YANG, J. Y. et al. ERK promotes tumorigenesis by inhibiting FOXO3a via MDM2-mediated degradation. **Nature Cell Biology**, 2008.

YANG, S.; LIU, G. **Targeting the RAS/RAF/MEK/ERK pathway in hepatocellular carcinoma***Oncology Letters*, 2017.

YONEZAWA, A. et al. Cisplatin and oxaliplatin, but not carboplatin and nedaplatin, are substrates for human organic cation transporters (SLC22A1-3 and multidrug and toxin

extrusion family). **Journal of Pharmacology and Experimental Therapeutics**, 2006.

YU, Z.; COWAN, J. A. **Metal complexes promoting catalytic cleavage of nucleic acids — biochemical tools and therapeutics** *Current Opinion in Chemical Biology*, 2018.

ZAKI, M.; ARJMAND, F.; TABASSUM, S. **Current and future potential of metallo drugs: Revisiting DNA-binding of metal containing molecules and their diverse mechanism of action** *Inorganica Chimica Acta*, 2016.

ZAMBLE, D. B.; LIPPARD, S. J. **Cisplatin and DNA repair in cancer chemotherapy** *Trends in Biochemical Sciences*, 1995.

ZAMZAMI, N. et al. Sequential reduction of mitochondrial transmembrane potential and generation of reactive oxygen species in early programmed cell death. **Journal of Experimental Medicine**, 1995.

ZBYTEK, B. et al. Corticotropin-releasing hormone triggers differentiation in HaCaT keratinocytes. **British Journal of Dermatology**, 2005.

ZHANG, P.; SADLER, P. J. **Redox-Active Metal Complexes for Anticancer Therapy** *European Journal of Inorganic Chemistry*, 2017a.

ZHANG, P.; SADLER, P. J. Advances in the design of organometallic anticancer complexes. **Journal of Organometallic Chemistry**, 2017b.

ZHANG, R. et al. High expression of EZR (ezrin) gene is correlated with the poor overall survival of breast cancer patients. **Thoracic Cancer**, 2019.

ZHANG, X. F. et al. Trichostatin a enhances the apoptotic potential of palladium nanoparticles in human cervical cancer cells. **International Journal of Molecular Sciences**, 2016.

ZHANG, Z. et al. Novel copper complexes as potential proteasome inhibitors for cancer treatment (Review). **Molecular Medicine Reports**, 2017.

ZOU, Z. et al. **Induction of reactive oxygen species: an emerging approach for cancer therapy** *Apoptosis*, 2017.

10. Attachments

Attachment 1. List of differential Proteins expressed by R10 on MCF-7. Accession number, gene name, fold change, q-value, up/downregulated proteins and their GO biological process name.

Accession number	Gene name	fold change	q-value	Regulation	GOBP name
P15311	EZR	-341.86	0.000831841	Down	Actin cytoskeleton organization; Proteoglycans in cancer, Tight junction
P22392-2	NME2	-310.10	0.00473651	Down	Biological adhesion; biological regulation; biosynthetic process
P26038	MSN	-260.30	0.0018044	Down	Anatomical structure development; biological adhesion
P11413-2	P11413-2	-249.72	0.0197693	Down	Alcohol biosynthetic process; alcohol catabolic process
P06396	GSN	-236.34	0.0296707	Down	Actin cytoskeleton organization; Proteoglycans in cancer, Tight junction
P61204	ARF3	-225.94	0.0260694	Down	Biological regulation; biosynthetic process
P21281	ATP6V1B2	-225.93	0.0158571	Down	Metabolic pathways, Oxidative phosphorylation, mTOR signaling pathway
P82979	SARNP	-225.80	0.00502156	Down	Biological regulation; biosynthetic process
P60174	TPI1	-220.21	0.0153248	Down	Metabolic pathways, Carbon metabolism, Inositol phosphate metabolism
E9PAV3	NACA	-212.62	0.0042344	Down	Biological regulation; biosynthetic process
Q01082	SPTBN1	-196.26	0.0173689	Down	Actin filament capping; axon guidance; biological regulation
P04083	ANXA1	-188.88	0.0163012	Down	Alpha-beta T cell differentiation
P18669	PGAM1	-188.28	0.00874454	Down	Glycolysis / Gluconeogenesis, metabolic pathway
Q99729-2	HNRNPAB	-185.36	0.00968497	Down	Anatomical structure morphogenesis; biological regulation
P68400	CSNK2A1	-183.06	0.0065269	Down	Adherens junction; cell death; cell division
P62826	RAN	-178.89	0.0141059	Down	RNA transport
P67870	CSNK2B	-176.58	0.0188121	Down	Adherens junction
P01111	NRAS	-173.95	0.0361131	Down	PI3K-Akt signaling pathway, apoptosis
P20700	LMNB	-172.97	0.00653491	Down	Apoptosis
Q13283	G3BP1	-170.63	0.0135105	Down	Biological regulation; cellular macromolecule metabolic process
P27695	APEX1	-168.62	0.0288133	Down	Regulation of apoptotic process
P17931	LGALS3	-168.34	0.0110758	Down	Anatomical structure development; biological regulation
Q13813	SPTAN1	-161.60	0.00643425	Down	Actin filament capping; apoptosis

P68032	ACTC1	-160.51	0.0312561	Down	Actin filament-based movement
P08758	ANXA5	-160.39	0.0186809	Down	Biological regulation
P00390	GSR	-158.78	0.0412565	Down	Metabolic pathway
O14980	XPO1	-158.72	0.0397152	Down	RNA transport
P25789	PSMA4	-155.16	0.0294159	Down	Proteasomal protein catabolic process
O75821	EIF3G	-154.47	0.00897153	Down	RNA transport
P52565	ARHGDI1A	-153.11	0.0237821	Down	Biological regulation; cell surface receptor linked signaling pathway
P27797	CALR	-148.14	0.00960142	Down	Actin cytoskeleton organization
Q14204	DYNC1H1	-146.72	0.00968497	Down	Antigen processing and presentation
P09234	SNRPC	-146.45	0.0361131	Down	Cellular component assembly
Q02880	TOP2B	-145.33	0.00140085	Down	DNA topological change
Q6DD88	ATL3	-145.23	0.0294159	Down	Endoplasmic reticulum organization
P04844	RPN2	-143.84	0.0537831	Down	Metabolic pathway
P29144	TPP2	-142.73	0.0361581	Down	Proteolysis
Q16543	CDC37	-142.38	0.00925193	Down	PI3K-Akt signaling pathway
P26583	HMGB2	-142.27	0.00545579	Down	Anatomical structure development; apoptosis
P60953	CDC42	-142.26	0.0460909	Down	Regulation of actin cytoskeleton; regulation metabolic process
P28838	LAP3	-141.91	0.0560915	Down	Proteolysis
Q09666	AHNAK	-140.86	0.00948588	Down	Biological regulation; cellular component assembly
P00338-3	LDHA	-139.11	0.0296707	Down	Glycolytic process, response to hypoxia
P46777	RPL5	-139.09	0.00948588	Down	Ribosome, biosynthetic process; catabolic process
P28482	MAPK1	-139.09	0.0192685	Down	PI3K signaling pathway
Q14157-5	UBAP2L	-138.58	0.0178295	Down	Cell recognition; cell-cell recognition
Q07955	SRSF1	-138.42	0.00844671	Down	Biological regulation; biosynthetic process
P62857	RPS28	-137.53	0.00520552	Down	Biosynthetic process; catabolic process
P06753-2	TPM3	-136.63	0.00915199	Down	Actin filament-based movement; actin filament-based process
P13797	PLS3	-136.43	0.0460288	Down	Anatomical structure development; bone development
P61158	ACTR3	-134.19	0.0554742	Down	Actin polymerization-dependent cell motility
P62258	YWHAE	-131.99	0.00461913	Down	PI3K signaling pathway; apoptosis; cell cycle; cell cycle process

P11387	TOP1	-130.75	0.0294159	Down	DNA replication
P63104	YWHAZ	-129.59	0.00461913	Down	PI3K signaling pathway, amine transport; apoptosis, cell cycle
Q05519	SRSF11	-127.72	0.0454764	Down	Biosynthetic process; cellular biosynthetic process
O43707	ACTN4	-127.38	0.00106039	Down	Actin cytoskeleton organization
P09429	HMGB1	-125.23	0.00461913	Down	Apoptosis; base-excision repair, DNA ligation
O15145	ARPC3	-124.68	0.0416197	Down	Regulation of actin cytoskeleton
P40925-3	MDH1	-122.43	0.00948588	Down	Acetyl-CoA catabolic process; acetyl-CoA metabolic process
Q15056	EIF4H	-122.36	0.0984128	Down	Cadherin binding, translation factor activity, RNA binding
Q14444	CAPRIN1	-121.47	0.00739486	Down	Negative regulation of biological process
P30520	ADSS2	-120.29	0.0484145	Down	Metabolic pathways
P31946	YWHAZ	-119.63	0.00818932	Down	PI3K signaling pathway; apoptosis; cell cycle
P12429	ANXA3	-119.33	0.010545	Down	Biological regulation; cell activation
P67809	YBX1	-118.34	0.000892855	Down	Biological regulation; biosynthetic process; cellular biosynthetic process
P23526	AHCY	-118.29	0.00461913	Down	Metabolic pathways
P62937	PPIA	-118.01	0.00461913	Down	Biological regulation; biosynthetic process
P25788	PSMA3	-117.85	0.0162398	Down	Activation of immune response
O00629	KPNA4	-116.78	0.0427357	Down	Nuclear import signal receptor activity
Q5SRD1	TIMM23B	-116.29	0.0285846	Down	Protein import into mitochondrial matrix
P62316	SNRPD2	-115.98	0.00915199	Down	Cellular component assembly
Q6UXN9	WDR82	-115.69	0.0488734	Down	Histone H3-K4 trimethylation
P12814-4	ACTN1	-115.51	0.0203601	Down	Actin crosslink formation; actin cytoskeleton organization
Q16555	DPYSL2	-113.64	0.0018044	Down	Anatomical structure development, biological regulation
O15144	ARPC2	-113.44	0.00668988	Down	Regulation of actin cytoskeleton
Q9Y281	CFL2	-113.32	0.0100448	Down	Actin cytoskeleton organization
Q9BZZ5	API5	-112.59	0.0294159	Down	Apoptosis; biological regulation; cell death
O00429-6	DNM1L	-112.43	0.0184193	Down	Apoptotic mitochondrial changes
O15347	HMGB3	-111.87	0.0432298	Down	DNA recombination
O14744	PRMT5	-111.34	0.0294159	Down	RNA transport
P05387	RPL5	-110.31	0.00502156	Down	Ribosome, biosynthetic process; catabolic process

P17655	CAPN2	-110.26	0.0412691	Down	Focal adhesion; apoptosis
P23219-5	PTGS1	-110.18	0.0460909	Down	Inflammatory response, regulation of cell population proliferation
Q9NQC3	RTN4	-110.15	0.0296707	Down	Apoptotic process
P42167	TMPO	-109.11	0.0336521	Down	Lamin binding
P29401-2	TKT	-108.88	0.0154888	Down	Alcohol biosynthetic process; alcohol catabolic process
P0DP25	CALM3	-108.40	0.00192719	Down	Rap1 signaling pathway
P62244	RPS15A	-107.79	0.0118932	Down	Biosynthetic process; catabolic process
P31949	S100A11	-107.76	0.0387137	Down	Biological regulation; cellular process
P42677	RPS27	-106.95	0.00948588	Down	Biological adhesion; biosynthetic process; catabolic process
P14618	PKM	-106.90	0.0472681	Down	Glycolysis/Gluconeogenesis, metabolic pathway
O95373	IPO7	-106.18	0.0294159	Down	Protein import into nucleus
Q16630-2	CPSF6	-105.26	0.00948588	Down	Cellular component assembly; cellular component organization
Q14697-2	GANAB	-104.57	0.0474527	Down	Carbohydrate metabolic process
P27361	MAPK3	-104.42	0.0467589	Down	PI3Ksignaling pathway
P51148-2	RAB5C	-103.82	0.00461913	Down	GDP binding, GTPase activity
Q9Y237-2	PIN4	-103.67	0.0280516	Down	DNA and RNA binding
P05556	ITGB1	-102.43	0.0202324	Down	Actin cytoskeleton organization;PI3Ksignaling pathway
P67775	PPP2CA	-102.43	0.00844671	Down	PI3Ksignaling pathway; apoptosis
Q86V81	ALYREF	-102.34	0.00473651	Down	RNA transport; biosynthetic process; cell differentiation
P84090	ERH	-102.27	0.0177163	Down	Biological regulation; biosynthetic process; cell cycle; cell differentiation
Q9NVA2-2	SEPTIN11	-101.57	0.00461913	Down	Cell cycle; cell division; cellular component assembly
Q9UHD8	SEPTIN9	-100.59	0.0410607	Down	Cell cycle; cell division; cellular component assembly
P22626	HNRNPA2B1	-100.13	0.0118932	Down	Biological regulation; cellular macromolecule metabolic process
O75915	ARL6IP5	-21.36	0.0460909	Down	Acidic amino acid transport
Q9Y4L1	HYOU1	-20.94	0.00461913	Down	Protein processing in endoplasmic reticulum
P98179	RBM3	-18.25	0.00345038	Down	Biological regulation; biosynthetic process
Q9UM00	TMCO1	-15.97	0.0610605	Down	Endoplasmic reticulum calcium ion homeostasis
P34932	HSPA4	-15.38	0.0110758	Down	Tight junction
Q12792-3	TWF1	-15.31	0.00561608	Down	Biological regulation; cellular component organization

Q14103	HNRNPD	-14.50	0.00461913	Down	Biological regulation; biosynthetic process
Q9H8Y8-3	GORASP2	-11.89	0.0439162	Down	Cell cycle; cellular component organization
Q9Y3Y2-3	CHTOP	-10.41	0.00968497	Down	Biological regulation; biosynthetic process
P13639	EEF2	-10.11	0.0612693	Down	AMPK signaling pathway
P28074	PSMB5	-2.17	0.0260694	Down	Activation of immune response; activation of innate immune response
P37802-2	TAGLN2	-2.07	0.00106039	Down	Cell differentiation; cellular developmental process
Q01105	SET	-1.92	0.0324279	Down	Biological regulation; biosynthetic process; cell cycle
P07900-2	HSP90AA1	-1.68	0.00123674	Down	Apoptosis; axon guidance; biological regulation
Q86UP2	KTN1	10.20	0.0412691	UP	Biological regulation; cellular component movement
Q96HE7	ERO1A	10.98	0.0260694	UP	Metabolic process; transport
P24539	ATP5PB	11.07	0.0512197	UP	ATP synthesis coupled proton transport
Q15637-5	SF1	12.61	0.0260694	UP	Biological regulation; biosynthetic process; cell differentiation
P52815	MRPL12	18.22	0.00844671	UP	Biological regulation;
P07437	TUBB	18.78	0.010545	UP	Biological regulation; cell cycle; induction of apoptosis
Q9BVA1	TUBB2B	20.98	0.0488734	UP	Mitotic cell cycle, microtubule cytoskeleton organization
P41091	EIF2S3	24.16	0.0202324	UP	Biosynthetic process; transport
O75489	NDUFS3	100.03	0.0189917	UP	Oxidative phosphorylation, metabolic pathway
Q96HS1	PGAM5	100.13	0.0280356	UP	Necroptotic process
P38646	HSPA9	100.23	0.010545	UP	RNA degradation; cellular metabolic process, transport
Q9UJZ1	STOML2	100.53	0.0237821	UP	Signaling pathway; ATP metabolic process; transmembrane transport
P52272	HNRNPM	101.47	0.00461913	UP	Cellular metabolic process
Q5BKZ1	ZNF326	102.47	0.0360792	UP	Regulation of DNA-templated transcription, elongation
Q68CZ2	TNS3	103.63	0.0460909	UP	Anatomical structure development; biological regulation; cell migration
P10809	HSPD1	105.56	0.0197693	UP	RNA degradation, activation of caspase activity; signaling pathway
P49411	TUFM	108.19	0.00915199	UP	Biosynthetic process
Q5JPE7	NOMO2	108.61	0.0189917	UP	Biological regulation, metabolic process
Q8NFH4	NUP37	109.76	0.0178295	UP	RNA transport; cell cycle; signaling pathway
Q9P2K5	MYEF2	111.00	0.0260694	UP	Cell differentiation, metabolic process
P14866	HNRNPL	111.12	0.0203601	UP	Cellular metabolic process

P62424	RPL7A	111.53	0.0361131	UP	Biosynthetic process; catabolic process
O95831	AIFM	112.44	0.0460909	UP	Activation of caspase activity; apoptosis
P55795	HNRNP2	113.00	0.0189917	UP	Cellular metabolic process;
O14950	MYL12B	114.82	0.0136898	UP	Transmembrane receptor protein tyrosine kinase signaling pathway
P04264	KRT1	115.08	0.0410607	UP	Complement activation, lectin pathway
Q9BTT0	ANP32E	116.34	0.0860691	UP	Inhibits activity of protein phosphatase 2A (PP2A)
Q6FI13	H2AC4	116.68	0.0141047	UP	Chromatin organization
Q92499	DDX1	117.60	0.0249827	UP	Biological regulation
P04908	H2AC18	120.28	0.00795725	UP	Keratinocyte activation
Q92804	TAF15	120.99	0.0464077	UP	Basal transcription factors
P21291	CSRP1	121.61	0.0104337	UP	Cellular process
Q92688	ANP32B	122.37	0.00897153	UP	Negative regulation of cell differentiation
O75947	ATP5PD	124.99	0.0684144	UP	Oxidative phosphorylation, metabolic pathway
P35908	KRT2	129.50	0.0186809	UP	keratinization
Q13126-2	MTAP	131.73	0.0388999	UP	Metabolic process
Q96EE3-1	SEH1L	135.50	0.00795725	UP	Attachment of spindle microtubules to chromosome
Q15370-2	ELOB	137.65	0.0410336	UP	Biological regulation
P26196	DDX6	137.74	0.00461913	UP	RNA degradation
P82933	MRPS9	142.70	0.0484145	UP	Biosynthetic process
P35232	PHB	143.17	0.0460909	UP	Biological regulation, steroid hormone receptor signaling pathway
Q9UGI8	TES	148.09	0.00473651	UP	Negative regulation of cell proliferation
P61513	RPL37A	152.56	0.00844671	UP	Cellular catabolic process
P61254	RPL26	154.80	0.0186809	UP	Biosynthetic process; catabolic process
P56381	ATP5F1E	160.14	0.0193612	UP	Thermogenesis, metabolic pathway, oxidative phosphorylation
P31689	DNAJA1	161.78	0.0173689	UP	Protein processing in endoplasmic reticulum
P35527	KRT9	183.81	0.0412691	UP	Intermediate filament organization
P84103	SRSF3	225.18	0.0460288	UP	Spliceosome
Q92922	SMARCC1	258.64	0.0197693	UP	Thermogenesis, anatomical structure development

Attachment 2. List of differential Proteins expressed by cisplatin on MCF-7. Accession number, gene name, fold change, q-value, up/downregulated proteins and their GO biological process name.

Accession number	Gene name	fold change	q-value	Regulation	GOBP name
O60493	SNX3	-332.66	0.103807411	Down	Endocytic recycling, regulation of intracellular protein transport
Q9Y237-2	PIN4	-270.58	0.048057182	Down	rRNA processing
Q14103	HNRNPD	-269.36	0.164431289	Down	Regulation of RNA metabolic process
P61077-3	UBE2D3	-239.58	0.013162483	Down	Ubiquitin-dependent protein catabolic process
P16949	STMN1	-237.91	0.257636154	Down	Mitotic cytokinesis, regulation of cytoskeleton organization
Q3ZCQ8-2	TIMM50	-226.64	0.241708149	Down	Protein import into mitochondrial matrix
P30838	ALDH3A1	-191.41	0.319114133	Down	Cellular aldehyde metabolic process
P25788	PSMA3	-178.97	0.355549923	Down	Proteasomal protein catabolic process
Q9H444	CHMP4B	-167.11	0.138569601	Down	Autophagy
P40763	STAT3	-166.48	0.19012899	Down	Cytokine-mediated signaling pathway
P20073	ANXA7	-165.68	0.33537125	Down	Autophagy, epithelial cell differentiation
P60983	GMFB	-159.28	0.061430831	Down	Actin filament debranching
P04733	MT1F	-154.58	0.317503005	Down	Cellular response to copper ion
P13797	PLS3	-152.97	0.087473714	Down	Actin filament bundle assembly
P50238	CRIP1	-148.03	0.334168232	Down	Cellular response to antibiotic, immune response
P04732	MT1E	-146.93	0.342561477	Down	Detoxification of copper ion
P68371	TUBB4B	-143.11	0.617686766	Down	Microtubule-based process
Q9Y2S7	POLDIP2	-142.24	0.365400766	Down	Error-free translation synthesis
P22392-2	NME2	-141.65	0.075132753	Down	Regulation of apoptotic process
Q5SRD1	TIMM23B	-139.40	0.120169279	Down	Protein import into mitochondrial matrix
O75821	EIF3G	-137.22	0.271243168	Down	Translational initiation
P42574	CASP3	-136.14	0.154260839	Down	Keratinocyte differentiation, neuron differentiation
O15230	LAMA5	-134.54	0.031898359	Down	Morphogenesis of a polarized epithelium, tissue development
Q99436	PSMB7	-134.22	0.360948072	Down	Proteasomal protein catabolic process
Q15428	SF3A2	-133.86	0.374272932	Down	Spliceosomal complex assembly

P82933	MRPS9	-133.24	0.37011471	Down	DNA damage response, detection of DNA damage
Q02790	FKBP4	-129.77	0.250261504	Down	Protein peptidyl-prolyl isomerization
Q92905	COPS5	-128.47	0.147612662	Down	Negative regulation of apoptotic process
P40121	CAPG	-125.71	0.286092654	Down	Protein-containing complex assembly
O00629	KPNA4	-124.16	0.279675689	Down	NLS-bearing protein import into nucleus
O60701	UGDH	-123.35	0.021179047	Down	Glycosaminoglycan biosynthetic process
Q14247	CTTN	-122.05	0.245396433	Down	Positive regulation of actin filament polymerization
P28799	GRN	-121.90	0.234449764	Down	Regulation of inflammatory response
P09382	LGALS1	-121.43	0.013457713	Down	Regulation of apoptotic process
Q15056	EIF4H	-121.30	0.098349678	Down	Regulation of translational initiation
Q86U86	PBRM1	-121.13	0.078997212	Down	ATP-dependent chromatin remodeling
P09493-5	TPM1	-118.43	0.619240763	Down	Actin filament organization
P29144	TPP2	-118.37	0.38827112	Down	Proteolysis
O14744	PRMT5	-117.10	0.052276137	Down	Histone arginine methylation
O14787-2	TNPO2	-115.58	0.442885913	Down	Protein import into nucleus
P58546	MTPN	-115.24	0.060050142	Down	Positive regulation of cell growth
P15311	EZR	-111.88	0.097505058	Down	Actin cytoskeleton reorganization
P00450	CP	-111.32	0.19012899	Down	Iron ion homeostasis
P61011	SRP54	-110.99	0.632344629	Down	Protein targeting to ER, response to drug
Q10713	PMPCA	-110.72	0.473455877	Down	Protein processing involved in protein targeting to mitochondrion
Q96P70	IPO9	-110.70	0.589208467	Down	Protein import into nucleus
P61758	VBP1	-110.54	0.429441048	Down	Microtubule-based process
O14561	NDUFAB1	-108.11	0.39001549	Down	Mitochondrial respiratory chain complex I assembly
Q15185	PTGES3	-106.30	0.122299138	Down	Protein folding
P11766	ADH5	-106.23	0.35392907	Down	Formaldehyde catabolic process
P49773	HINT1	-102.71	0.636239029	Down	Intrinsic apoptotic signaling pathway by p53 class mediator
P51148-2	RAB5C	-102.37	0.312268869	Down	Intracellular protein transport, Rab protein signal transduction
P18669	PGAM1	-100.72	0.021819468	Down	Glycolytic process
P12074	COX6A1	-18.82	0.499183294	Down	Mitochondrial electron transport, cytochrome c to oxygen

Q13526	PIN1	-12.44	0.19012899	Down	Negative regulation of amyloid-beta formation
P36542	ATP5F1C	-11.40	0.556655322	Down	ATP biosynthetic process
Q8IWS0	PHF6	-10.17	0.488364874	Down	RNA binding, tubulin binding, histone deacetylase binding
O75915	ARL6IP5	-1.19	0.355549923	Down	Intrinsic apoptotic signaling pathway in response to oxidative stress
P62750	RPL23A	1.18	0.030955303	Up	Ribosomal large subunit assembly
P84103	SRSF3	1.27	0.205252324	Up	Regulation of alternative mRNA splicing, via spliceosome
Q9UG63-2	ABCF2	12.65	0.147612662	Up	ATP binding
Q9NRP0-2	OSTC	13.61	0.234449764	Up	Protein N-linked glycosylation via asparagine
P04264	KRT1	14.31	0.474443644	Up	Complement activation, lectin pathway
P35527	KRT9	21.60	0.442659363	Up	Intermediate filament organization
P26583	HMGB2	100.64	0.018775575	Up	Chromatin remodeling
P42766	RPL35	102.14	0.014461538	Up	Maturation of LSU-rRNA from tricistronic rRNA transcript
O15162	PLSCR1	102.75	0.042987455	Up	Apoptotic process
P04908	H2AC4	104.89	0.138569601	Up	Chromatin organization
Q9NTJ5	SACM1L	107.08	0.334851581	Up	Phosphatidylinositol dephosphorylation
Q99459	CDC5L	107.43	0.014461538	Up	Signal transduction involved in DNA damage checkpoint
Q9H2P0	ADNP	107.64	0.174208931	Up	Cellular response to extracellular stimulus
P62841	RPS15	107.73	0.335371256	Up	Ribosomal small subunit assembly
P62913	RPL11	108.24	0.258971065	Up	Cytoplasmic translation
P08708	RPS17	108.79	0.013162483	Up	Erythrocyte homeostasis
Q6P2E9	EDC4	109.38	0.053322399	Up	Deadenylation-independent decapping of nuclear-transcribed mRNA
P62280	RPS11	109.46	0.261597506	Up	Translation
P62910	RPL32	111.13	0.008415824	Up	Cytoplasmic translation
Q04637-9	EIF4G1	112.22	0.567356359	Up	Regulation of translational initiation
P61421	ATP6V0D1	117.66	0.319114133	Up	Vacuolar acidification
Q02878	RPL6	117.80	0.021179047	Up	Ribosomal large subunit assembly
P62847	RPS24	118.38	0.226834511	Up	Erythrocyte homeostasis
O14974	PPP1R12A	119.56	0.190293055	Up	Centrosome cycle
P61254	RPL26	122.94	0.014461538	Up	Cytoplasmic translation

O43809	NUDT21	124.13	0.103807411	Up	Messenger ribonucleoprotein complex assembly
P22695	UQCRC2	126.92	0.165209447	Up	Protein processing involved in protein targeting to mitochondrion
O15347	HMGB3	129.52	0.189988235	Up	Chromatin remodeling
Q5BKZ1	ZNF326	133.25	0.149729965	Up	Regulation of DNA-templated transcription, elongation
O75489	NDUFS3	140.32	0.24795612	Up	Negative regulation of intrinsic apoptotic signaling pathway
P62854	RPS26	144.36	0.02390207	Up	Cytoplasmic translation
Q9UIQ6	LNPEP	147.74	0.29950131	Up	Metalloaminopeptidase activity
P52815	MRPL12	153.39	0.04805718	Up	Mitochondrial translational elongation
P69905	HBA1	158.42	0.48215501	Up	Positive regulation of cell death
Q9BVA1	TUBB2B	191.09	0.50486869	Up	Microtubule cytoskeleton organization
Q92804	TAF15	206.22	0.1169057	Up	Positive regulation of transcription, DNA-templated
Q92922	SMARCC1	267.46	0.0611784	Up	ATP-dependent chromatin remodeling

Publications (2016-2020)

1. Ghasemishahrestani Z, Francisco RSM ; Arias JPR ; Santos ALS ; Rey NA ; Pereira MD. Effect of novel copper complexes on tumorigenesis and their mechanism of action on breast, lung and prostate cancer. *PATENT Process number: BR 10 2020 0132407. Petition number: 870200080165. Date: 26.06.2020.*
2. Bortolot CS, Forezi LSM, Marra RKF, Reis, MLP, Sá BVF, Ricardo Filho I, Ghasemishahrestani Z, Sola-Penna M, Zancan P, , Ferreira VF, Da Silva F C. Design, Synthesis and Biological Evaluation of 1H-1,2,3-Triazole-Linked- 1H-Dibenzo[b,h] xanthenes as Inductors of ROS-Mediated Apoptosis in the Breast Cancer Cell Line MCF-7. *Medicinal Chemistry* 2019; 15: 119-129. DOI: 10.2174/1573406414666180524071409 (IF 6,205).
3. Ghasemishahrestani Z, Mattos LMM, Santos ALS, Tilli TM, Pereira MD. Pieces of the complex puzzle of cancer cell energy metabolism: an overview of energy metabolism and alternatives for targeted cancer therapy. *Current Medicinal Chemistry*. BMS-CMC-2020-211. DOI: 10.2174/0929867327999200819123357 (IF 3.250).
4. França BM, Ghasemishahrestani Z, Souza GFM, daSilva RN, Queiroz DD, Pierre BMR, Pereira MD, Bello S, Corrêa RJ. *In vitro* studies of antitumor effect, toxicity/cytotoxicity and skin permeation/retention of a green fluorescence pyrene-based dye for PDT application. *Journal of Photochemistry & Photobiology, B: Biology* Manuscript number: JPHOTOBIOL_2019_1201. (IF 4.17).



**Pedido nacional de Invenção, Modelo de Utilidade, Certificado de
Adição de Invenção e entrada na fase nacional do PCT**

Número do Processo: BR 10 2020 013240 7

Dados do Depositante (71)

Depositante 1 de 2

Nome ou Razão Social: FACULDADES CATOLICAS

Tipo de Pessoa: Pessoa Jurídica

CPF/CNPJ: 33555921000170

Nacionalidade: Brasileira

Qualificação Jurídica: Instituição de Ensino e Pesquisa

Endereço: Rua Marquês de São Vicente, 225, Gávea

Cidade: Rio de Janeiro

Estado: RJ

CEP: 22451-900

País: Brasil

Telefone: (21) 3114-1303/4/5

Fax: (21) 3114-1309

Email: shirley@dctc.puc-rio.br

Depositante 2 de 2

Nome ou Razão Social: UNIVERSIDADE FEDERAL DO RIO DE JANEIRO - UFRJ

Tipo de Pessoa: Pessoa Jurídica

CPF/CNPJ: 33663683000116

Nacionalidade: Brasileira

Qualificação Jurídica: Instituição de Ensino e Pesquisa

Endereço: Avenida Pedro Calmon, nº 550, Prédio da Reitoria, 2º Andar, Cidade Universitária

Cidade: Rio de Janeiro

Estado: RJ

CEP: 21941-901

País: BRASIL

Telefone:

Fax:

Email:

Dados do Pedido

Natureza Patente: 10 - Patente de Invenção (PI)

Título da Invenção ou Modelo de Utilidade (54): LIGANTES BINUCLEANTES FENÓLICOS, COMPOSTOS METÁLICOS BINUCLEARES, COMPOSIÇÃO MÉDICO-VETERINÁRIA, PROCESSOS DE SÍNTESE DE LIGANTES BINUCLEANTES, PROCESSO DE SÍNTESE DE COMPOSTOS BINUCLEARES, MÉTODO DE TRATAMENTO DE NEOPLASIAS E DOENÇAS FÚNGICAS E USO

Resumo: A presente invenção trata de novas metalodrogas contendo um centro de coordenação binuclear de cobre(II) e os ligantes binucleantes não-simétricos 2-hidroxi-3-[(2-hidroxibenzil)(2-piridilmetil)amino]-metil]-5-metilbenzaldeído isonicotinoil hidrazona (H3L1) ou 2-hidroxi-3-{bis[(2-piridilmetil)amino]-metil]-5-metilbenzaldeído isonicotinoil hidrazona (H2L2) adequadas para o tratamento de neoplasias envolvendo tumores sólidos e/ou leucemias, bem como doenças de natureza oportunista, tais como as doenças causadas por fungos patogênicos.

Figura a publicar: 1

Dados do Procurador

Procurador:

Nome ou Razão Social: Francisco Carlos Rodrigues Silva

Numero OAB:

Numero API: 507

CPF/CNPJ: 51318601720

Endereço: Avenida Rio Branco, 01, Sala 2011, Centro

Cidade: Rio de Janeiro

Estado: RJ

CEP: 20090-003

Telefone: (21) 32128200

Fax:

Email: silva@atemesa.com.br

Dados do Inventor (72)

Inventor 1 de 6

Nome: NICOLÁS ADRIÁN REY

CPF: 01287999603

Nacionalidade: Argentina

Qualificação Física: Físico, químico, meteorologista, geólogo, oceanógrafo e afins

Endereço: Rua Alceu Amoroso Lima, 105/1308, Barra da Tijuca

Cidade: Rio de Janeiro

Estado: RJ

CEP: 22631-010

País: BRASIL

Telefone:

Fax:

Email:

Inventor 2 de 6

Nome: MARCOS DIAS PEREIRA

CPF: 07032553710

Nacionalidade: Brasileira

Qualificação Física: Professor do ensino superior

Endereço: Rua Joaquim Pinheiro, 290 apt 407, Freguesia

Cidade: Rio de Janeiro

Estado: RJ

CEP: 07032-553

País: BRASIL

Telefone:

Fax:

Email:

Inventor 3 de 6

Nome: JESICA PAOLA RADA ARIAS

CPF: 06242166755

Nacionalidade: Colombiana

Qualificação Física: Físico, químico, meteorologista, geólogo, oceanógrafo e afins

Endereço: Rua Pacheco Leão, 1818, Jardim Botânico

Cidade: Rio de Janeiro

Estado: RJ

CEP: 22460-036

País: BRASIL

Telefone:

Fax:

Email:

Inventor 4 de 6

Nome: RAFAELA DOS SANTOS MORAES FRANCISCO

CPF: 10722463766

Nacionalidade: Brasileira

Qualificação Física: Físico, químico, meteorologista, geólogo, oceanógrafo e afins

Endereço: Servidão Procópio Pereira, 34, Floresta

Cidade: Joinville

Estado: SP

CEP: 89211-325

País: BRASIL

Telefone:

Fax:

Email:

Inventor 5 de 6

Nome: ZEINAB GHASEMISHAHRESTANI

CPF: 06381075716

Nacionalidade: Iraniana

Qualificação Física: Doutorando

Endereço: Rua Felipe de Oliveira 4 apt 811, Copacabana

Cidade: Rio de Janeiro

Estado: RJ

CEP: 22011-030

País: BRASIL

Telefone:

Fax:

Email:

Inventor 6 de 6

Nome: ANDRÉ LUIS SOUZA DOS SANTOS

CPF: 02600664785

Nacionalidade: Brasileira

Qualificação Física: Professor do ensino superior

Endereço: Rua Comandante Rubens Silva 76/apto 202, Freguesia

Cidade: Rio de Janeiro

Estado: RJ

CEP: 22745-282

País: BRASIL

Telefone:

Fax:

Email:

Documentos anexados

Tipo Anexo	Nome
Procuração	01-PUC-Rio-Procuracao.pdf
Procuração	02-Procuração A&S.pdf
Delegação	03-Portaria 9095_19 Delegação Flávia.pdf
GRU	04-0088-0002-PAT-Complexos Binucleares-Guia depósito de PI.pdf
Comprovante de pagamento de GRU 200	05-0088-0002-PAT-Complexos Binucleares-ComprovPagto.pdf
Relatório Descritivo	06-Patente_PUC_RJ_0088_0002_vf_NAR - Relatório Descritivo.pdf
Reivindicação	07-Patente_PUC_RJ_0088_0002_vf_NAR - Reivindicação.pdf
Desenho	08-Figuras_Patente_PUC_RJ_0088_0002_Cobre_FINAL.pdf
Resumo	09-Patente_PUC_RJ_0088_0002_vf_NAR - Resumo.pdf

Acesso ao Patrimônio Genético

- Declaração Negativa de Acesso - Declaro que o objeto do presente pedido de patente de invenção não foi obtido em decorrência de acesso à amostra de componente do Patrimônio Genético Brasileiro, o acesso foi realizado antes de 30 de junho de 2000, ou não se aplica.

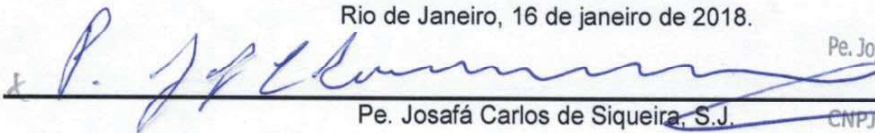
Declaração de veracidade

- Declaro, sob as penas da lei, que todas as informações acima prestadas são completas e verdadeiras.

PROCURAÇÃO

FACULDADES CATÓLICAS, Associação sem fins lucrativos, Mantenedora da **PONTIFÍCIA UNIVERSIDADE CATÓLICA DO RIO DE JANEIRO – PUC-Rio**, declarada de utilidade pública pelo Decreto Federal nº 43.454/58 e reconhecida como de fins filantrópicos pelo Conselho Nacional de Assistência Social, registrada sob o nº 20081202-1626028, em 9 de janeiro de 2009, no Registro Civil de Pessoas Jurídicas, inscrita no CNPJ-MF sob o nº 33.555.921/0001-70, inscrição municipal nº 00.819.271, qualificada pela Portaria 679, de 12 de novembro de 2014, da Secretaria de Regulação e Supervisão da Educação Superior, como Instituição Comunitária de Ensino Educação Superior (ICES), com sede na Rua Marquês de São Vicente, 225, doravante denominada PUC-Rio, neste ato representada pelo seu Reitor Pe. Josafá Carlos de Siqueira, S.J., portador da identidade nº 28.659.444-5, expedida por DETRAN-RJ, e CIC sob o nº 056.010.531-20, residente e domiciliado à Rua Marquês de São Vicente, 389, Gávea, Rio de Janeiro, RJ, CEP 22451-041, pela presente, outorga aos Srs. **FRANCISCO CARLOS RODRIGUES SILVA** – CPF No. 513.186.017-20 – API No. 0507, **BERNARDO ATEM FRANCISCHETTI** - CPF nº 005.924.917-06 - OAB/RJ 81.517 – API No. 1907, **DOMICIANO NORONHA DE SÁ** - CPF nº 085.741.367-86 - OAB/RJ 123.116 – API No. 1910, **ANTENOR BARBOSA DOS SANTOS JÚNIOR** – CPF nº 701.703.637-91 – OAB/RJ 54.283, **LUIZ AUGUSTO DE SOUZA E MARQUES** – CPF No. 042. 962. 787-46 – API No. 1674, **FRÉDÉRIC ROGER JOUÉ** – CPF No. 748.558.911-34 – API No. 2166, todos brasileiros, residentes e domiciliados em território brasileiro, com escritório na Praça Floriano, 19, 28º andar, na Cidade do Rio de Janeiro, CEP: 20031-050, RJ, República Federativa do Brasil, amplos poderes, incluindo administrativos, para, conjunta ou separadamente e independentemente da ordem de nomeação, representar a(o) Outorgante perante a União, os Estados, os Territórios, o Distrito Federal e seus órgãos de administração direta ou indireta, em especial o Instituto Nacional da Propriedade Industrial, o Banco Central do Brasil, o Departamento Nacional de Registro de Comércio, as Juntas Comerciais dos Estados, o Ministério do Desenvolvimento, Indústria e Comércio Exterior, o Núcleo de Informação e Coordenação do Ponto BR – NIC BR, o Comitê Gestor Internet do Brasil, o Conselho Nacional de Auto-Regulamentação Publicitária (“CONAR”), para o fim de obter a proteção de direitos relativos à propriedade industrial e intelectual e agir na defesa ativa e passiva dos interesses da(o) Outorgante, podendo, para tais efeitos, requerer e obter a proteção/extensão de: nome empresarial; registros de marcas de produto e/ou serviço; marcas coletivas, de certificação, tridimensionais e outras; indicações geográficas; desenhos industriais; programas de computador e nomes de domínio; requerer e obter patente de invenção e de modelos de utilidade, bem como certificados de adição de invenção; requerer divisão e/ou exame acelerado de pedidos; promover a prova de uso de marcas, de patentes e de nomes de domínio; pagar retribuições e anuidades; requerer prorrogações ou renovações; apresentar protestos, oposições, recursos e petições, réplicas e defesas, escritas ou orais; instaurar procedimentos administrativos de nulidade; cumprir exigências; requerer anotações de cessão e/ou transferência de titular, alterações de nome e/ou de sede; desistir de e/ou retirar pedidos; requerer a averbação e registro de contratos de licença para exploração relacionados a quaisquer dos direitos acima mencionados, contratos de prestação de serviços técnicos e de fornecimento de tecnologia, de participação em custo de pesquisa e desenvolvimento, contratos de franquia e outros atos ou contratos correlatos; pedir vistas de processos, enviar notificações extrajudiciais e contra-notificar as recebidas de terceiros; desistir e renunciar, dar e receber quitação, substabelecer e revogar, no todo ou em parte, os poderes aqui conferidos, incluindo-se nos presentes poderes os da cláusula “ad judicia”, bem como os de receber citações judiciais em ações relativas a direitos de propriedade intelectual, desde a data de depósito dos pedidos feitos ou processados com base na presente procuração, tanto em relação aos quais a presente procuração for apresentada, como durante a vigência dos respectivos pedidos/patentes ou registros. Por fim, são, pela presente, ratificados todos os atos já praticados pelos Outorgados em conformidade com a presente procuração.

Rio de Janeiro, 16 de janeiro de 2018.



Pe. Josafá Carlos de Siqueira, S.J.

Pe. Josafá Carlos de Siqueira, S.J.
Reitor
PUC RIO
CNPJ: 33.555.921/0001-70


* NÃO NECESSITA RECONHECIMENTO DE FIRMA



Esclarecimento sobre alteração de sede

Informamos que a **AeS Assessoria e Consultoria em Propriedade Intelectual S/S Ltda.**, inscrita no CNPJ sob o número 18.444.355/0001-35, alterou o endereço de sua sede da Praça Floriano, 19, 28º andar, Centro, Rio de Janeiro, RJ, CEP 20031-050 para a **Avenida Rio Branco, número 1, sala 2011, parte, Centro, Rio de Janeiro, RJ, CEP 20090-003**, conforme a Ficha de Informações Cadastrais da Prefeitura Municipal do Rio de Janeiro, que segue em anexo.

Atenciosamente,

A handwritten signature in blue ink, appearing to read 'Francisco Carlos Rodrigues Silva', with a long horizontal stroke extending to the left.

Francisco Carlos Rodrigues Silva
API No. 0507



Prefeitura da Cidade do Rio de Janeiro
Secretaria Municipal de Fazenda

FICHA DE INFORMAÇÕES CADASTRAIS (SUBSTITUI O CARTÃO DE INSCRIÇÃO MUNICIPAL)

INSCRIÇÃO MUNICIPAL	GRLF	DIV ISS	CPF/CNPJ	INÍCIO DE ATIVIDADE ECONÔMICA	DATA DE EMISSÃO	TIPO DE ESTABELECIMENTO
0583153-9	1	03	18444355000135	15/07/2013	02/03/2020	Principal

NOME / FIRMA / RAZÃO SOCIAL

A E S ASSESSORIA E CONSULTORIA EM PROPRIEDADE INTELECTUAL S/S LTDA

ENDEREÇO

AVN RIO BRANCO, 1, SALA 2011 C DEP NO 21 AND, CENTRO

CATEGORIA DO CONTRIBUINTE

SOC. P/ QUOTAS DE RESPONSABILIDADE LTDA

CÓDIGO E DESCRIÇÃO DE ATIVIDADES ECONÔMICAS (CAE)

2.10.10.2 AGENCIAMENTO DE PROPRIEDADE INDUSTRIAL

CADASTRO DE SÓCIOS - 10 MAIORES PARTICIPAÇÕES

NOME: FRANCISCO CARLOS RODRIGUES SILVA PARTICIPAÇÃO: 44.50%
IDENTIDADE: 00023154006 CPF/CNPJ: 51318601720
QUALIFICAÇÃO: Sócio/Diretor
ENDEREÇO: FREIJO 173 JACAREPAGUA RIO DE JANEIRO 22753-802 RJ BRASIL

NOME: BERNARDO ATEM FRANCISCHETTI PARTICIPAÇÃO: 44.50%
IDENTIDADE: 81517 CPF/CNPJ: 00592491706
QUALIFICAÇÃO: Sócio/Diretor
ENDEREÇO: JOAQUIM NABUCO 198 APTO 301 COPACABANA RIO DE JANEIRO 22080-030 RJ BRASIL

NOME: LUIZ AUGUSTO DE SOUZA E MARQUES PARTICIPAÇÃO: 5.50%
IDENTIDADE: 161939 CPF/CNPJ: 04296278746
QUALIFICAÇÃO: Sócio/Diretor
ENDEREÇO: ASSUNÇÃO 2 BL. 2 APTO. 102 BOTAFOGO RIO DE JANEIRO 22251-030 RJ BRASIL

<p>NOME: RODRIGO GUERRA MOURA E SILVA</p> <p>IDENTIDADE: 29359</p> <p>QUALIFICAÇÃO: Sócio/Diretor</p> <p>ENDEREÇO: ROSA D APARECIDA T MESCHIAT 326 CONDOMINIO PAINEIRAS BETEL PAULINIA 13148-913 SP BRASIL</p>	<p>PARTICIPAÇÃO: 1.00%</p> <p>CPF/CNPJ: 01674248741</p>
<p>NOME: ANDRE LUIZ SOUZA ALVAREZ</p> <p>IDENTIDADE: 1998104320</p> <p>QUALIFICAÇÃO: Sócio/Diretor</p> <p>ENDEREÇO: DO BANANAL 699 BL 2 APTO 606 FREGUESIA RIO DE JANEIRO 22750-013 RJ BRASIL</p>	<p>PARTICIPAÇÃO: 1.00%</p> <p>CPF/CNPJ: 03246382727</p>
<p>NOME: MARCOS ALEXANDRE SOARES SPIRITO</p> <p>IDENTIDADE: 343285409</p> <p>QUALIFICAÇÃO: Sócio/Diretor</p> <p>ENDEREÇO: TIRADENTES 108 INGA NITEROI 24210-510 RJ BRASIL</p>	<p>PARTICIPAÇÃO: 1.00%</p> <p>CPF/CNPJ: 04161801599</p>
<p>NOME: BRUNA SANTOS DE FRANCA</p> <p>IDENTIDADE: 212868046</p> <p>QUALIFICAÇÃO: Sócio/Diretor</p> <p>ENDEREÇO: BARBOSA ARAUJO 28 QUADRA 02 PARQUE FELICIDADE DUQUE DE CAXIAS 25080-570 RJ BRASIL</p>	<p>PARTICIPAÇÃO: 0.50%</p> <p>CPF/CNPJ: 11651436746</p>
<p>NOME: AIDA GOMES DE ALMEIDA YAMAZAKI ROSA</p> <p>IDENTIDADE: 108056029</p> <p>QUALIFICAÇÃO: Sócio/Diretor</p> <p>ENDEREÇO: CARDOSO JUNIOR 280 402 LARANJEIRAS RIO DE JANEIRO 22245-000 RJ BRASIL</p>	<p>PARTICIPAÇÃO: 1.00%</p> <p>CPF/CNPJ: 07962926716</p>
<p>NOME: FELIPE BONFIM TAVARES DA SILVA</p> <p>IDENTIDADE: 2018108599</p> <p>QUALIFICAÇÃO: Sócio/Diretor</p> <p>ENDEREÇO: PAU MARFIM 51 ANIL RIO DE JANEIRO 22753-803 RJ BRASIL</p>	<p>PARTICIPAÇÃO: 1.00%</p> <p>CPF/CNPJ: 09938518788</p>
<p>NOME:</p> <p>IDENTIDADE:</p> <p>QUALIFICAÇÃO:</p> <p>ENDEREÇO:</p>	<p>PARTICIPAÇÃO:</p> <p>CPF/CNPJ:</p>



PROCURAÇÃO

UNIVERSIDADE FEDERAL DO RIO DE JANEIRO - UFRJ, doravante denominada OUTORGANTE, CNPJ nº 33.663.683/0001-16, pessoa jurídica de Direito Público, nos termos do Decreto-Lei nº 8.393/45, organizada na forma de autarquia especial, segundo seu estatuto baixado com o Decreto nº 66536/70, com sede na Avenida Pedro Calmon, nº 550, Prédio da Reitoria, 2º Andar, Cidade Universitária, Rio de Janeiro/RJ, CEP 21941-901, neste ato representada pela Coordenadora da Agência UFRJ de Inovação, Profa. Flavia Lima do Carmo, brasileira, professora, portadora da carteira de identidade nº 124384520, emitida pelo DETRAN-RJ, inscrito no Cadastro de Pessoa Física sob nº 090.798.457-60; com poderes atribuídos pela Portaria nº 9095 de 30 de Agosto de 2019 da UFRJ, pela presente, outorga aos Srs. **FRANCISCO CARLOS RODRIGUES SILVA** – CPF No. 513.186.017-20 – API No. 0507, **BERNARDO ATEM FRANCISCHETTI** - CPF nº 005.924.917-06 - OAB/RJ 81.517 – API No. 1907, **LUIZ AUGUSTO DE SOUZA E MARQUES** – CPF No. 042. 962. 787-46 – API No. 1674, todos brasileiros, residentes e domiciliados em território brasileiro, integrantes do escritório **A&S ASSESSORIA E CONSULTORIA EM PROPRIEDADE INTELECTUAL S/S LTDA**, CNPJ/MF 18.444.355/0001-35, situado na Avenida Rio Branco, número 1, sala 2011, parte, Centro, na Cidade do Rio de Janeiro, CEP: 20090-003, RJ, República Federativa do Brasil, poderes para, conjunta ou separadamente e independentemente da ordem de nomeação, representar a Outorgante perante a União, os Estados, os Territórios, o Distrito Federal e seus órgãos de administração direta ou indireta, em especial o Instituto Nacional da Propriedade Industrial, para o fim de obter a proteção de direitos relativos à propriedade industrial e intelectual e agir na defesa ativa e passiva dos interesses da Outorgante, em relação ao pedido de patente intitulado **“LIGANTES BINUCLEANTES FENÓLICOS, COMPOSTOS METÁLICOS BINUCLEARES, COMPOSIÇÃO MÉDICO-VETERINÁRIA, PROCESSOS DE SÍNTESE DE LIGANTES BINUCLEANTES, PROCESSO DE SÍNTESE DE COMPOSTOS BINUCLEARES, MÉTODO DE TRATAMENTO DE NEOPLASIAS E DOENÇAS FÚNGICAS E USO”** podendo, para tais efeitos, requerer e obter a patente de invenção; promover a prova de uso de patentes, pagar as retribuições e anuidades devidas, requerer as prorrogações ou renovações cabíveis, apresentar protestos, oposições, petições, recursos, réplicas e defesas, escritas ou orais, caducidade e instauração de processos administrativos ou de nulidade, anotações de transferências, bem como, alterações de nome ou sede .

Rio de Janeiro 18 de Junho de 2020.

FLAVIA LIMA DO
CARMO:09079845760

Assinado de forma digital por
FLAVIA LIMA DO
CARMO:09079845760
Dados: 2020.06.18 15:17:13 -03'00'

FLÁVIA LIMA DO CARMO
COORDENADORA
AGÊNCIA UFRJ DE INOVAÇÃO

* NÃO NECESSITA RECONHECIMENTO DE FIRMA



PORTARIA N.º 9095, de 30 de agosto de 2019

A REITORA DA UNIVERSIDADE FEDERAL DO RIO DE JANEIRO, no uso das atribuições conferidas pelo Decreto de 31 de maio de 2019, publicado no Diário Oficial nº 105 de 03/06/2019, seção 2, página 1,

Delega competência à Coordenadora da Agência UFRJ de Inovação e dá outras providências,

A Reitora, no uso de suas atribuições estatutárias e regimentais, e considerando a obrigação de resguardar a propriedade intelectual e o sigilo das criações desenvolvidas na UFRJ; a necessidade de agilizar os atos praticados pela UFRJ atinentes à proteção da propriedade intelectual, assinatura de termos de sigilo e transferência de materiais biológicos; o princípio da eficiência da Administração Pública, preconizado no art.37 da Constituição da República, modificado pela Emenda Constitucional nº19, de 04 de junho de 1998; que a Agência UFRJ de Inovação é responsável por acompanhar o processamento dos pedidos de patentes e pela manutenção dos títulos de propriedade intelectual da UFRJ, em conformidade com a Lei nº10.973, de 2 de dezembro de 2004 e com o parágrafo terceiro da Portaria 2754, de 16 de outubro de 2007, de criação da Agência UFRJ de Inovação; a atuação da Agência UFRJ de Inovação na observação da política institucional de estímulo à proteção das criações da UFRJ conforme Resolução CEPG nº1/2011, resolve:

Art.1º Delegar competência à Coordenadora da Agência UFRJ de Inovação Flávia Lima do Carmo, matrícula Siape nº 2104770, para, a partir desta data, sem prejuízo das atribuições regimentalmente atinentes ao citado cargo, praticar os atos administrativos a seguir enumerados:

I Solicitar, em nome da UFRJ, junto aos órgãos competentes do País e do exterior a proteção dos direitos relativos à propriedade intelectual sobre as criações, assim definidas da Lei nº10.973, de 2 de dezembro de 2004, podendo praticar os seguintes atos:

- a) Requerer depósito de pedido de patente e concessão de patentes (patentes de invenção, modelos de utilidade e certificado de adição);
- b) Requerer registro de marcas, desenhos industriais, programas de computador (software), indicações geográficas e proteção de cultivares;
- c) Requerer registro de direito autoral;
- d) Requerer buscas e certidões;
- e) Requerer exames técnicos de patentes, cumprir exigências formais e técnicas, efetuar pagamentos de anuidades;
- f) Apresentar oposições, impugnações, pedidos de reconsideração, recursos e réplicas;



PORTARIA N.º 7095, de 30 de agosto de 2019

- g) Requerer a anotação de alteração de nome, transferência de titularidade e a averbação de transferências ou cessões, averbação de contratos de licença de uso de tecnologias e assistência técnica em benefício da UFRJ;
- h) Assinar procurações conferindo poderes a instituições parceiras ou escritórios de propriedade intelectual para representar a UFRJ junto aos órgãos competentes no Brasil e no exterior, na adoção de providências que visem à proteção e manutenção dos direitos de propriedade intelectual da UFRJ;
- i) Providenciar todos os demais atos que tenham por objetivo solicitar a proteção e a manutenção dos direitos de propriedade intelectual da UFRJ no Brasil e no exterior.

II Firmar compromissos, acordos e instrumentos congêneres, em nome da UFRJ, com a finalidade exclusiva de resguardar o sigilo e os direitos de propriedade intelectual da UFRJ, tais como:

- a) Acordos de Confidencialidade, definidos como sendo acordos que têm por objetivo proteger o sigilo das criações, informações confidenciais, conhecimentos (know-how) e segredos de negócios desenvolvidos pelos pesquisadores da UFRJ e instituições parceiras;
- b) Acordos de Transferência de Material Biológico, definidos como sendo acordos que visam assegurar os direitos das partes sobre os materiais biológicos de sua propriedade, na transferência, para fins de pesquisa, para uma instituição parceira.

III Firmar compromissos, acordos e instrumentos congêneres, em nome da UFRJ, relacionados à propriedade intelectual, inovação e empreendedorismo que não envolvam recursos financeiros ou despesas para as partes.

Art. 2º Este ato entra em vigor na data de sua publicação e revogam-se as disposições em contrário, em especial a Portaria nº 1.191 de 18 de fevereiro de 2016.


Denise Pires de Carvalho
Reitora da UFRJ
Siape 6366005

UFRJ - Seção de Publicações
Publicado no BUFRJ n.º 36
Data: 05 / 09 / 2019

0088/0002-PAT-Complexos Binucleares-Guia depósito de PI-Pagamento 26/06/2020-AtemeSá-AFR

INSTRUÇÕES:

A data de vencimento não prevalece sobre o prazo legal. O pagamento deve ser efetuado antes do protocolo. Órgãos públicos que utilizam o sistema SIAFI devem utilizar o número da GRU no campo Número de Referência na emissão do pagamento. Serviço: 200-Pedido nacional de Invenção, Modelo de Utilidade, Certificado de Adição de Invenção e entrada na fase nacional do PCT

Clique aqui e pague este boleto através do Auto Atendimento Pessoa Física.

Clique aqui e pague este boleto através do Auto Atendimento Pessoa Jurídica.

Recibo do Pagador



001-9

00190.00009 02940.916196 20598.064176 6 83270000007000

Nome do Pagador/CPF/CNPJ/Endereço

FACULDADES CATOLICAS CPF/CNPJ: 33555921000170

RUA MARQUES DE SAO VICENTE 225 GAVEA, RIO DE JANEIRO -RJ CEP:22451900

Sacador/Avalista

Nosso-Número	Nr. Documento	Data de Vencimento	Valor do Documento	(=) Valor Pago
29409161920598064	29409161920598064	25/07/2020	70,00	

Nome do Beneficiário/CPF/CNPJ/Endereço

INSTITUTO NACIONAL DA PROPRIEDADE INDUST CPF/CNPJ: 42.521.088/0001-37

RUA MAYRINK VEIGA 9 24 ANDAR ED WHITE MARTINS , RIO DE JANEIRO - RJ CEP: 20090910

Agência/Código do Beneficiário
2234-9 / 333028-1

Autenticação Mecânica



001-9

00190.00009 02940.916196 20598.064176 6 83270000007000

Local de Pagamento

PAGÁVEL EM QUALQUER BANCO ATÉ O VENCIMENTO

Data de Vencimento

25/07/2020

Nome do Beneficiário/CPF/CNPJ

INSTITUTO NACIONAL DA PROPRIEDADE INDUST CPF/CNPJ: 42.521.088/0001-37

Agência/Código do Beneficiário

2234-9 / 333028-1

Data do Documento	Nr. Documento	Espécie DOC	Aceite	Data do Processamento	Nosso-Número
26/06/2020	29409161920598064	DS	N	26/06/2020	29409161920598064
Uso do Banco	Carteira	Espécie	Quantidade	xValor	(=) Valor do Documento
29409161920598064	17	R\$			70,00

Informações de Responsabilidade do Beneficiário

A data de vencimento não prevalece sobre o prazo legal.

O pagamento deve ser efetuado antes do protocolo.

Órgãos públicos que utilizam o sistema SIAFI devem utilizar o número da GRU no campo Número de Referência na emissão do pagamento.

Serviço: 200-Pedido nacional de Invenção, Modelo de Utilidade, Certificado de Adição de Invenção e entrada na fase nacional do PCT

(-) Desconto/Abatimento

(+) Juros/Multa

(-) Valor Cobrado

Nome do Pagador/CPF/CNPJ/Endereço

FACULDADES CATOLICAS CPF/CNPJ: 33555921000170

RUA MARQUES DE SAO VICENTE 225 GAVEA,

RIO DE JANEIRO-RJ CEP:22451900

Código de Baixa

Sacador/Avalista

Autenticação Mecânica

Ficha de Compensação




Comprovante de pagamento de boleto

Dados da conta debitada / Pagador Final

Agência/conta: 0540/27415-6 CPF/CNPJ: 07.456.675/0001-99 Empresa: ATEM SA ADVOGADOS ASSOCIADOS

Dados do pagamento

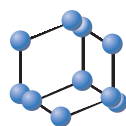
Identificação no meu comprovante: 0088 0002 GUIA DEPOSITO DE PI

		00190 00009 02940 916196 20598 064176 6 83270000007000
Beneficiário:	INSTITUTO NACIONAL DA PROPRIED	CPF/CNPJ do beneficiário:
Razão Social:	INSTITUTO NACIONAL DA PROPRI	42.521.088/0001-37
		Data de vencimento:
		25/07/2020
		Valor do boleto (R\$):
		70,00
		(-) Desconto (R\$):
		0,00
		(+)Mora/Multa (R\$):
		0,00
Pagador:	FACULDADES CATOLICAS	CPF/CNPJ do pagador:
		33.555.921/0001-70
		(=) Valor do pagamento (R\$):
		70,00
		Data de pagamento:
		26/06/2020
Autenticação mecânica		Pagamento realizado em espécie:
A8A5FA9D882D251F95CE4D5E51A0E630915CFAE6		Não

Operação efetuada em 26/06/2020 às 12:48:56 via Sispag, CTRL 768625411000017.

RESEARCH ARTICLE

Design, Synthesis and Biological Evaluation of 1*H*-1,2,3-Triazole-Linked-1*H*-Dibenzo[*b,h*]xanthenes as Inductors of ROS-Mediated Apoptosis in the Breast Cancer Cell Line MCF-7



**BENTHAM
SCIENCE**



Carolina S. Bortolot^a, Luana da S.M. Forezi^a, Roberta K.F. Marra^a, Marcelo I.P. Reis^a, Bárbara V.F. e Sá^a, Ricardo I. Filho^b, Zeinab Ghasemishahrestani^b, Mauro Sola-Penna^c, Patricia Zancan^b, Vitor F. Ferreira^{d,*} and Fernando de C. da Silva^{a,*}

^aUniversidade Federal Fluminense, Departamento de Química Orgânica, Instituto de Química, Campus do Valonguinho, CEP 24020-150, Niterói-RJ, Brazil; ^bUniversidade Federal do Rio de Janeiro, Laboratório de Oncobiologia Molecular (LabOMol), Departamento de Biotecnologia Farmacêutica, Faculdade de Farmácia, CEP 21941-902, Rio de Janeiro-RJ, Brazil; ^cUniversidade Federal do Rio de Janeiro, Laboratório de Enzimologia e Controle do Metabolismo (LabECoM) Departamento de Biotecnologia Farmacêutica, Faculdade de Farmácia, CEP 21941-902, Rio de Janeiro-RJ, Brazil; ^dUniversidade Federal Fluminense, Departamento de Tecnologia Farmacêutica, Faculdade de Farmácia, R. Dr. Mario Vianna, 523, Santa Rosa, CEP 24241-002, Niterói-RJ, Brazil

Abstract: Background: Low molecular weight 1,2,3-triazoles and naphthoquinones are endowed with various types of biological activity, such as against cancer, HIV and bacteria. However, in some cases, the conjugation of these two nuclei considerably increases their biological activities.

Objective: In this work, we decided to study the synthesis and screening of bis-naphthoquinones and xanthenes tethered to 1,2,3-triazoles against cancer cell lines, specifically the human breast cancer cell line MCF-7.

Results: Starting from lawsone and aryl-1*H*-1,2,3-triazole-4-carbaldehydes (**10a-h**) several new 7-(1-aryl-1*H*-1,2,3-triazol-4-yl)-6*H*-dibenzo[*b,h*]xanthene-5,6,8,13(7*H*)-tetraones (**12a-h**) and 3,3'-((1-aryl-1*H*-1,2,3-triazol-4-yl)methylene)bis(2-hydroxynaphthalene-1,4-diones) **11a-h** were synthesized and evaluated for their cytotoxic activities using the human breast cancer cell line MCF-7 and the non-tumor cell line MCF10A as control. We performed test of cell viability, cell proliferation, intracellular ATP content and cell cytometry to determine reactive oxygen species (ROS) formation.

Conclusions: Based on these results, we found that compound **12a** promotes ROS production, interfering with energy metabolism, cell viability and proliferation, and thus promoting whole cell damage.

Keywords: Cell viability, naphthoquinones, lawsone, MTT assay, ATP, CyQuant assay.

1. INTRODUCTION

There are several synthetic and natural naphthoquinones of low molecular weight with many applications in various scientific and technological fields. These naphthoquinones also have potential clinical utility in the treatment of several diseases. Naphthoquinones bearing pyran ring [1] have been reported to have bioactivity against several microorganisms

and cancer cell lines due to their ability to accept one or two electrons in the so-called redox cycle. This allows them to form deleterious species *in situ* such as free radicals, anion radicals and hydrogen peroxide, which are known as a reactive oxygen species (ROS) [2, 3]. Through this mechanism, quinones are cytotoxic and lead cells to a programmed death pathway (apoptosis) [4, 5]. Among the pyranonaphthoquinones, β -lapachone (**1**) has received great attention because of its pronounced cytotoxic activity. Indeed, it has been in clinical trials for the treatment of pancreatic cancer as ARQ501 [6] (ArQule Inc.) combined with Taxol or Gemcitabine [7, 8]. As further advances new clinical trials were started with ARQ 761 (Code C99146), a water-soluble pro-drug clinical trials [9]. It is also worth noting that pyranonaphthoquinones **2** and **3** can inhibit dengue virus replication (Fig. 1) [10].

*Address correspondence to these authors at the Universidade Federal Fluminense, Departamento de Tecnologia Farmacêutica, Faculdade de Farmácia, R. Dr. Mario Vianna, 523, Santa Rosa, CEP 24241-002, Niterói-RJ, Brazil; E-mail: cegvito@vm.uff.br, and Universidade Federal Fluminense, Departamento de Química Orgânica, Instituto de Química, Campus do Valonguinho, CEP 24020-150, Niterói-RJ, Brazil; E-mail: gqofermando@vm.uff.br

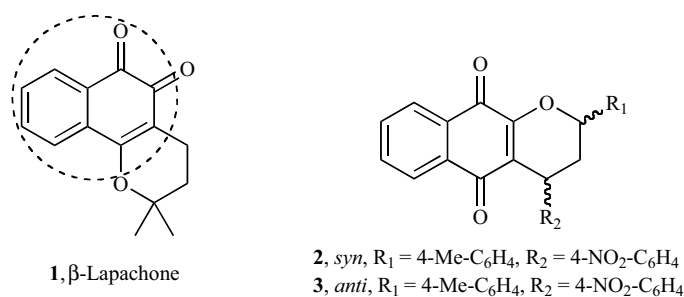
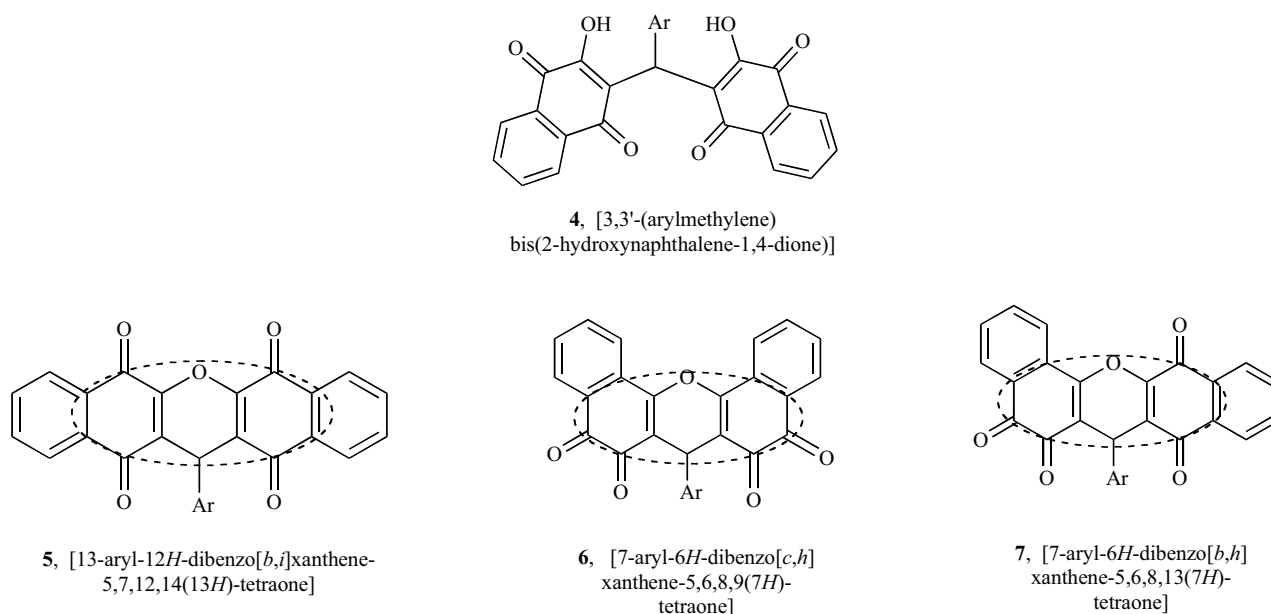


Fig. (1). Important pyranonaphthoquinones.

Fig. (2). Possible structural isomer formed in the reaction of **9** with aldehydes.

Xanthenes are a general class of natural and synthetic heterocyclic compounds [11-13] that exhibit a broad spectrum of activities, including antiviral [14], antibacterial [15, 16], antiplasmodial [17, 18], anti-malarial [19], anti-fungal [20], anti-inflammatory [21], anticancer [22-25] and anti-hypertensive properties [26].

2-Hydroxy-1,4-naphthoquinone (lawsone, **9**) can react with 1*H*-1,2,3-triazole-4-carbaldehydes to generate bis-pyranonaphthoquinones **11a-h**, which are fused to the pyran ring on two sides. In this case, there is the possibility for the formation of open adduct **4** and three structural isomers **5**, **6** and **7** (Fig. 2). According to the literature, the formation of symmetrical isomer **5** starts with the addition of lawsone (**9**) to the appropriate aldehyde under acidic conditions, leading to an o-quinone methide intermediate. That intermediate reacts with a second molecule of lawsone, which upon cyclization affords the bis-pyranonaphthoquinones. A wide variety of aryl and heteroaryl aldehydes possessing different functional groups have been used in these reactions, which can be carried out in several solvents or solvent-free conditions using diverse catalysts [27-37]. Despite the methods described in the literature for preparing compounds with general structures **4** (3,3'-(arylmethylene) bis(2-hydroxynaphthalene-1,4-dione) and **5** (dibenzo[*b,i*]xanthene), the corresponding synthesis of dibenzoxanthenes of **6** (dibenzo[*b,h*]xanthene) has not yet been reported and recently our re-

search group reported the preparation of **7** (6*H*-Dibenzo[*b,h*]xanthenes) [38].

It is well established that structural modifications in the naphthoquinone unit can greatly increase their bioactivity [1, 39]. In fact, our research group has previously shown that 1,2-furanonaphthoquinones linked to 1,2,3-*1H*-triazoles, such as compound **8** (Fig. 3), were highly selective against lymphoblastic leukemia yet have low activity against normal hematopoietic cells [40].

Continuing our interests in the chemistry of pyranonaphthoquinones, in this work, we decided to study this cycloaddition reaction with the expectation of preparing the triazole-linked-isomer type of **7** from the open bis-adduct, and screening that family of compounds against cancer cell lines, specifically the human breast cancer cell line MCF-7.

2. MATERIALS AND METHODS

2.1. Chemistry

The reagents were purchased from Sigma-Aldrich Brazil and were used without further purification. Column chromatography was performed with silica gel 60 (Merck 70-230 mesh). Analytical thin layer chromatography was performed with silica gel plates (Merck, TLC silica gel 60 F254), and the plates were visualized using UV light or aqueous solu-

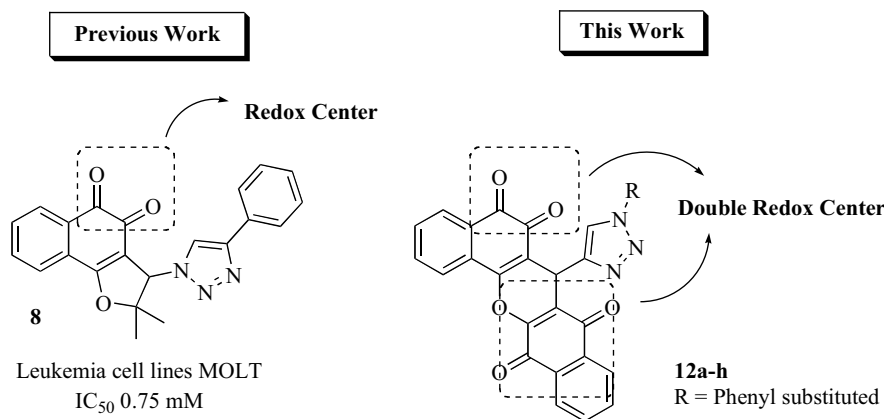


Fig. (3). Rationalization naphthoquinones linked to 1,2,3-1*H*-triazoles.

tions of ammonium sulfate. The indicated yields refer to chromatographically and spectroscopically homo-geneous materials. Melting points were obtained on a Fischer-Johns apparatus and were uncorrected. Infrared spectra were collected using KBr pellets on a Perkin-Elmer model 1420 FT-IR spectrophotometer, and the spectra were calibrated relative to the 1601.8 cm^{-1} absorbance of polystyrene. NMR spectra were recorded on a Varian Unity Plus VXR (500 MHz) instrument in DMSO- d_6 or CDCl_3 solution. The chemical shift data were reported in units of δ (ppm) downfield from solvent, and solvent was used as an internal standard; coupling constants (J) are reported in hertz and refer to apparent peak multiplicities. High-resolution mass spectra (HRMS) were recorded on a MICROMASS Q-TOF mass spectrometer (Waters).

2.1.1. General Procedure for the Preparation of 11a-h

In a 50 mL round-bottom flask containing a solution of **9** (1 mmol) and triazole aldehyde **10** (1 mmol) in 30 mL of ethanol/ H_2O 1:1 was heated to reflux for 4-6 h. A yellow precipitate formed in the reaction flask, and it was isolated by filtration under reduced pressure.

3,3'-((1-(1-phenyl-1*H*-1,2,3-triazol-4-yl)methylene)bis(2-hydroxynaphthalene-1,4-dione) (11a). Yellow solid, 52 % yield; m.p. 224-225 °C; IR (KBr, cm^{-1}): ν 3332, 3291, 3145, 1673, 1650, 1591, 1500, 1460, 1366, 1341, 1280, 1253, 1230, 1178, 1048, 1028, 979, 760, 742, 726, 688, 657; ^1H NMR (DMSO- d_6 , 500.00 MHz): 8.29 (1H, s), 7.98 (2H, dd, J 0, 7 and 7.5 Hz), 7.97 (2H, dd, J 0,7 and 7.5 Hz), 7.83 (2H, td, J 1.4 and 7.4 Hz), 7.78 (2H, td, J 1.4 and 7.4 Hz), 7.76 (2H, d, J 8.7 Hz), 7.71 (1H, d, J 2.5 Hz), 7.66 (1H, dd, J 2.5 and 8.7 Hz), 6.20 (1H, s); ^{13}C NMR (DMSO- d_6 , 125.0 MHz APT): 29.4, 121.4, 125.2, 125.7, 127.0, 127.3, 129.5, 130.6, 131.6, 131.9, 132.0, 132.7, 134.3, 135.3, 146.2, 156.3, 180.9, 182.9; HR-ESIMS [M+H] m/z calcd. for $\text{C}_{29}\text{H}_{18}\text{N}_3\text{O}_6$: 504.1196. Found: m/z 504.1175. $\Delta = 4.2$ ppm.

3,3'-((1-(3,4-dichlorophenyl)-1*H*-1,2,3-triazol-4-yl)methylene)bis(2-hydroxynaphthalene-1,4-dione) (11b). Yellow solid, 72 % yield; m.p. 212-213 °C; IR (KBr, cm^{-1}): ν 3323, 3136, 3095, 2973, 2594, 1680, 1643, 1593, 1578, 1487, 1460, 1439, 1362, 1338, 1305, 1276, 1246, 1219, 1073, 1011, 1003, 837, 819, 742, 735, 729; ^1H NMR (DMSO- d_6 , 500.00 MHz): 8.64 (1H, s), 8.17 (1H, d, J 2.6 Hz), 8.01 (2H, dd, J 1.0 and 7.5 Hz), 7.96 (2H, dd, J 1.0 and 7.5 Hz), 7.94

(1H, d, J 2.6 Hz), 7.84 (2H, td, J 1.4 and 7.5 Hz), 7.82 (1H, d, 8.9 Hz), 7.79 (2H, td, J 1.4 and 7.5 Hz), 6.13 (1H, s); ^{13}C NMR (DMSO- d_6 , 125.0 MHz APT): 29.9, 119.3, 120.8, 121.5, 125.7, 126.1, 129.9, 130.4, 131.8, 132.3, 132.4, 133.2, 134.8, 136.4, 148.3, 156.6, 181.2, 183.2; HR-ESIMS [M+H] m/z calcd. for $\text{C}_{29}\text{H}_{16}\text{Cl}_2\text{N}_3\text{O}_6$: 572.0416. Found: m/z 572.0392. $\Delta = 4.2$ ppm.

3,3'-((1-(3,5-dichlorophenyl)-1*H*-1,2,3-triazol-4-yl)methylene)bis(2-hydroxynaphthalene-1,4-dione) (11c). Yellow solid, 82 % yield; m.p. 209-210°C; IR (KBr, cm^{-1}): ν 3393, 3351, 3144, 3090, 2974, 1672, 1645, 1593, 1582, 1479, 1459, 1439, 1368, 1334, 1306, 1276, 1232, 1217, 1045, 725; ^1H NMR (DMSO- d_6 , 500.00 MHz): 8.65 (1H, s), 8.01 (2H, dd, J 0.9 and 7.5 Hz); 7.99 (2H, d, J 1.8 Hz), 7.96 (2H, d, J 7.5 Hz), 7.84 (2H, td, J 1.3 and 7.5 Hz), 7.79 (2H, td, J 1.2 and 7.5 Hz), 7.68 (1H, t, J 1.8 Hz), 6.15 (1H, s); ^{13}C NMR (DMSO- d_6 , 125.0 MHz APT): 30.1, 118.2, 121.5, 121.8, 126.1, 126.5, 127.9, 130.4, 132.7, 133.5, 135.1, 135.8, 138.8, 148.8, 157.3, 181.7, 183.5; HR-ESIMS [M+H] m/z calcd. for $\text{C}_{29}\text{H}_{16}\text{Cl}_2\text{N}_3\text{O}_6$: 572.0416. Found: m/z 572.0433. $\Delta = 3.0$ ppm.

3,3'-((1-(2,5-dichlorophenyl)-1*H*-1,2,3-triazol-4-yl)methylene)bis(2-hydroxynaphthalene-1,4-dione) (11d). Yellow solid, 74 % yield; m.p. 221-222°C; IR (KBr, cm^{-1}): ν 3257, 2345, 1668, 1637, 1350, 1279, 1046, 727; ^1H NMR (DMSO- d_6 , 500.00 MHz): 8.30 (1H, s), 7.99 (2H, dd, J 1.0 and 7.6 Hz), 7.97 (2H, dd, J 1.0 and 7.7 Hz), 7.83 (2H, td, J 1.4 and 7.6 Hz), 7.78 (2H, td, J 1.4 and 7.5 Hz), 7.76 (1H, d, J 8.7Hz), 7.72 (1H, d, J 2.5 Hz), 7.67 (1H, dd, J 2.5 and 8.7 Hz), 6.18 (1H, s); ^{13}C NMR (DMSO- d_6 , 125.0 MHz APT): 29.8, 121.8, 125.6, 126.1, 127.4, 127.8, 129.9, 131.0, 132.1, 132.2, 132.4, 133.2, 134.7, 135.8, 146.7, 156.6, 181.3, 183.3; HR-ESIMS [M+H] m/z calcd. for $\text{C}_{29}\text{H}_{16}\text{Cl}_2\text{N}_3\text{O}_6$: 572.0416. Found: m/z 572.0411. $\Delta = 0.8$ ppm.

3,3'-((1-(4-chlorophenyl)-1*H*-1,2,3-triazol-4-yl)methylene)bis(2-hydroxynaphthalene-1,4-dione) (11e). Yellow solid, 39 % yield; m.p. 168-169°C; IR (KBr, cm^{-1}): ν 3400, 2974, 1671, 1647, 1593, 1501, 1454, 1364, 1303, 1277, 1217, 1093, 1048, 984, 834, 729; ^1H NMR (DMSO- d_6 , 500.00 MHz): 8.59 (1H, s), 8.01 (2H, dd, J 1.3 and 7.4 Hz), 7.96 (2H, dd, J 1.6 and 7.6 Hz), 7.91 (2H, d, J 8.8 Hz), 7.84 (2H, td, J 1.8 and 7.6 Hz), 7.79 (2H, td, J 1.8 and 7.6 Hz), 7.62 (2H, d, J 8.8Hz), 6.12 (1H, s); ^{13}C NMR (DMSO- d_6 , 125.0 MHz APT): 29.8, 120.9, 121.0, 121.6, 125.6, 126.1, 129.7,

129.9, 132.3, 132.4, 133.1, 134.6, 135.6, 147.9, 156.6, 181.2, 183.2; HR-ESIMS [M+H] m/z calcd. for $C_{29}H_{17}ClN_3O_6$: 538.0806. Found: m/z 538,0807. $\Delta = 0.2$ ppm.

3,3'-((1-(*m*-tolyl)-1*H*-1,2,3-triazol-4-yl)methylene)bis(2-hydroxynaphthalene-1,4-dione) (**11f**). Yellow solid, 51 % yield; m.p. 257-258 °C; IR (KBr, cm^{-1}): ν 3330, 3147, 2973, 1673, 1651, 1613, 1592, 1494, 1460, 1366, 1341, 1300, 1279, 1232, 1049, 786, 742, 735, 726; 1H NMR (DMSO- d_6 , 500.00 MHz): 8.44 (1H, s), 7.94 (2H, dd, J 1.0 and 7.5 Hz), 7.89 (2H, dd, J 1.0 and 7.6 Hz), 7.77 (2H, td, J 1.3 and 7.5 Hz), 7.72 (2H, td, J 1.3 and 7.5 Hz), 7.61-7.58 (2H, m), 7.34 (1H, t, J 7.6 Hz), 7.17 (1H, d, J 7.6 Hz), 6.07 (1H, s), 2.31 (3H, s); ^{13}C NMR (DMSO- d_6 , 125.0 MHz APT): 21.0, 29.9, 116.5, 119.7, 120.9, 121.7, 125.6, 126.1, 128.7, 130.0, 132.8, 133.1, 134.7, 136.9, 139.5, 147.6, 156.6, 181.3, 183.3; HR-ESIMS [M+H] m/z calcd. for $C_{29}H_{17}N_4O_8$: 518.1352. Found: m/z 518.1327. $\Delta = 4.8$ ppm.

3,3'-((1-(4-nitrophenyl)-1*H*-1,2,3-triazol-4-yl)methylene)bis(2-hydroxynaphthalene-1,4-dione) (**11g**). Yellow solid, 72 % yield; m.p. 225-226 °C; IR (KBr, cm^{-1}): ν 3352, 3132, 1683, 1645, 1597, 1578, 1524, 1346, 1305, 1230, 1073, 960, 857, 737, 722; 1H NMR (DMSO- d_6 , 500.00 MHz): 8.89 (1H, s), 8.53 (2H, d, J 9.2 Hz), 8.30 (2H, d, J 9.3 Hz), 8.14 (2H, dd, J 1.0 and 7.5 Hz), 8.08 (2H, dd, J 1.0 and 7.5 Hz), 7.96 (2H, td, J 1.5 and 7.5 Hz), 7.91 (2H, td, J 1.4 and 7.5 Hz), 6.26 (1H, s); ^{13}C NMR (DMSO- d_6 , 125.0 MHz APT): 29.9, 119.8, 121.3, 121.4, 125.6, 125.7, 126.1, 129.9, 132.3, 133.1, 134.8, 141.1, 146.4, 148.7, 156.6, 181.2, 183.2. HR-ESIMS [M+H] m/z calcd. for $C_{29}H_{18}N_3O_6$: 549.1046. Found: m/z 549.1043. $\Delta = 0.5$ ppm.

3,3'-((1-(4-methoxyphenyl)-1*H*-1,2,3-triazol-4-yl)methylene)bis(2-hydroxynaphthalene-1,4-dione) (**11h**). Yellow solid, 55 % yield; m.p. 191-192 °C; IR (KBr, cm^{-1}): ν 3314, 3149, 1681, 1639, 1604, 1519, 1460, 1334, 1276, 1233, 1078, 1025, 964, 877, 835, 808, 770, 742; 1H NMR (DMSO- d_6 , 500.00 MHz): 8.44 (1H, s), 8.03 (2H, dd, J 1.0 and 7.6 Hz), 7.96 (2H, dd, J 1.0 and 7.0 Hz), 7.83 (2H, td, J 1.5 and 7.5 Hz), 7.80-7.78 (2H, m), 7.76 (2H, d, J 9.1 Hz), 7.08 (2H, d, J 9.0 Hz), 6.15 (1H, s), 3.80 (3H, s); ^{13}C NMR (DMSO- d_6 , 125.0 MHz APT): 29.9, 55.6, 114.8, 121.0, 121.8, 125.6, 126.1, 130.0, 130.4, 132.3, 133.1, 134.7, 147.4, 156.5, 158.9, 181.3, 183.3. HR-ESIMS [M+H] m/z calcd. for $C_{30}H_{20}N_3O_7$: 534.1301. Found: m/z 534.1281. $\Delta = 3.7$ ppm.

2.1.2. General Procedure for Preparing 12a-h

Bis-naphthoquinones (1 mmol) and 10 mL of sulfuric acid were combined in a 50 mL round bottomed flask. The reaction was carried out at room temperature and was monitored by TLC. When finished, the reaction mixture was poured into ice water. The mixture was then extracted with chloroform (2 x 50 mL). The combined organic phases were washed with distilled water (1 x 50 mL) and dried with anhydrous sodium sulfate. Evaporation of the solvent gave **12a-h** as yellow solids.

7-(1-phenyl-1*H*-1,2,3-triazol-4-yl)-5*H*-dibenzo[*b,h*]xanthene-5,6,8,13(7*H*)-tetraone (**12a**). Orange solid, 54 % yield; m.p. 259-260 °C; IR (KBr, cm^{-1}): ν 3434, 1662, 1611, 1591, 1502, 1363, 1286, 1227, 1194, 1042, 944, 776, 719; 1H NMR (DMSO- d_6 , 500.00 MHz): 8.78 (s, 1H), 8.17-8.15 (1H, m), 8.11 (1H, d, J 7.3 Hz), 8.06-8.02 (2H, m), 7.97 (1H, td, J

1.0 and 7.8 Hz), 7.95-7.90 (2H, m), 7.83 (2H, d, J 7.8 Hz), 7.76 (1H, td, J 1.0 and 7.8 Hz), 7.54 (2H, t, J 7.8 Hz), 7.44 (1H, t, J 7.6 Hz), 5.44 (1H, s); ^{13}C NMR (DMSO- d_6 and CF_3CO_2D , 125.0 MHz APT): 184.2, 181.8, 180.1, 174.4, 169.4, 167.6, 162.2, 156.7, 147.9, 135.3, 133.7, 132.9, 131.3, 130.5, 130.4, 130.3, 126.7, 126.2, 124.5, 122.2, 122.0, 121.3, 121.3, 120.9, 120.7, 120.4, 30.6; HR-ESIMS [M+H] m/z calcd. for $C_{29}H_{16}N_3O_5$: 486.1090. Found: m/z 486.1085. $\Delta = 1.0$ ppm.

7-(1-(3,4-dichlorophenyl)-1*H*-1,2,3-triazol-4-yl)-5*H*-dibenzo[*b,h*]xanthene-5,6,8,13(7*H*)-tetraone (**12b**). Orange solid, 63 % yield; m.p. 255-257 °C; IR (KBr, cm^{-1}): ν 3067, 1661, 1559, 1487, 1363, 1284, 1226, 1188, 1096, 1041, 941, 880, 824, 770, 715, 611; 1H NMR (DMSO- d_6 , 500.00 MHz): 8.89 (1H, s), 8.17-8.15 (2H, m), 8.12 (1H, d, J 7.7 Hz), 8.07 (1H, d, J 7.1 Hz), 8.07-8.02 (1H, m), 7.98 (1H, t, J 7.7 Hz), 7.92-7.91 (2H, m), 7.89 (1H, dd, J 2.2 and 11.0 Hz), 7.80 (1H, d, J 8.8 Hz), 7.76 (1H, t, J 7.7 Hz), 5.45 (1H, s); ^{13}C NMR (DMSO- d_6 and CF_3CO_2D , 125.0 MHz APT): 183.5, 182.6, 177.8, 177.2, 156.2, 149.5, 147.9, 135.5, 135.0, 134.6, 133.0, 132.6, 132.1, 131.8, 131.4, 131.3, 130.8, 130.7, 130.3, 129.6, 129.0, 128.5, 122.3, 122.1, 121.8, 120.1, 113.8, 25.0; HR-ESIMS [M+Na] m/z calcd. for $C_{29}H_{13}Cl_2N_3NaO_5$: 576.0130. Found: m/z 576.0111. $\Delta = 3.3$ ppm.

7-(1-(3,5-dichlorophenyl)-1*H*-1,2,3-triazol-4-yl)-5*H*-dibenzo[*b,h*]xanthene-5,6,8,13(7*H*)-tetraone (**12c**). Orange solid, 63 % yield; m.p. 246-247 °C; IR (KBr, cm^{-1}): ν 3144, 3066, 2919, 2850, 1660, 1613, 1508, 1359, 1265, 1226, 1191, 1094, 1040, 1009, 973, 944, 853, 802, 767, 719, 666; 1H NMR (DMSO- d_6 , 500.00 MHz): 8.92 (1H, s), 8.17-8.15 (1H, m), 8.12 (1H, dd, J 1.1 and 7.7 Hz), 8.07 (1H, dd, J 1.1 and 7.7 Hz), 8.05-8.03 (1H, m), 7.98 (1H, dd, J 1.1 and 8.9 Hz), 7.97 (2H, d, J 1.6 Hz), 7.93-7.91 (m, 2H), 7.76 (1H, td, J 1.1 and 8.2 Hz), 7.68 (1H, s), 5.45 (1H, s); ^{13}C NMR (DMSO- d_6 and CF_3CO_2D , 125.0 MHz APT): 183.8, 182.8, 181.4, 178.1, 177.5, 177.2, 156.6, 156.4, 149.6, 148.4, 148.2, 135.7, 135.7, 134.9, 134.6, 132.7, 130.9, 130.5, 130.2, 129.8, 129.2, 126.4, 125.9, 124.7, 122.5, 121.8, 119.6, 118.3, 25.2; HR-ESIMS [M+Na] m/z calcd. for $C_{29}H_{13}Cl_2N_3NaO_5$: 576.0130. Found: m/z 576.0103. $\Delta = 4.6$ ppm.

7-(1-(2,5-dichlorophenyl)-1*H*-1,2,3-triazol-4-yl)-5*H*-dibenzo[*b,h*]xanthene-5,6,8,13(7*H*)-tetraone (**12d**). Orange solid, 93 % yield; m.p. 239-240 °C; IR (KBr, cm^{-1}): ν 3609, 3098, 2920, 2851, 1663, 1614, 1592, 1436, 1354, 1269, 1227, 1195, 1147, 1097, 1037, 1007, 945, 878, 804, 769, 714; 1H NMR (DMSO- d_6 , 500.00 MHz): 8.55 (1H, s), 8.17-8.15 (1H, m), 8.12 (1H, d, J 7.7 Hz), 8.08-8.05 (2H, m), 7.98 (1H, td, J 1.1 and 7.7 Hz), 7.94-7.92 (2H, m), 7.78 (1H, td, J 1.1 and 7.7 Hz), 7.77-7.74 (2H, m), 7.67 (1H, dd, J 2.2 and 11.0 Hz), 5.47 (1H, s); ^{13}C NMR (DMSO- d_6 and CF_3CO_2D , 125.0 MHz APT): 185.0, 182.7, 181.5, 180.6, 172.8, 166.8, 156.4, 155.8, 145.0, 135.0, 134.9, 133.6, 132.5, 132.2, 132.1, 130.5, 130.1, 126.3, 125.9, 117.7, 117.0, 115.5, 20.8; HR-ESIMS [M+H] m/z calcd. for $C_{29}H_{14}Cl_2N_3O_5$: 554.0311. Found: m/z 554.0309. $\Delta = 0.4$ ppm.

7-(1-(4-chlorophenyl)-1*H*-1,2,3-triazol-4-yl)-5*H*-dibenzo[*b,h*]xanthene-5,6,8,13(7*H*)-tetraone (**12e**). Orange solid, 98 % yield; m.p. 237-239 °C; IR (KBr, cm^{-1}): ν 3444, 1663, 1614, 1593, 1502, 1361, 1287, 1229, 1195, 1095, 1041, 989, 945, 773; 1H NMR (DMSO- d_6 , 500.00 MHz): 8.80 (1H, s),

8.17-8.15 (1H, m), 8.12 (1H, dd, J 1.1 and 7.7 Hz), 8.06 (1H, dd, J 1.1 and 8.2 Hz), 8.04-8.02 (1H, m), 7.97 (1H, td, 1.6 and 7.7 Hz), 7.93-7.92 (2H, m), 7.86 (2H, d, J 9.3 Hz), 7.76 (1H, td, J 1.1 and 7.7 Hz), 7.60 (2H, d, J 9.3 Hz), 5.45 (1H, s); ^{13}C NMR (DMSO- d_6 and $\text{CF}_3\text{CO}_2\text{D}$, 125.0 MHz APT): 183.0, 182.7, 177.9, 177.3, 177.1, 168.8, 149.5, 147.7, 135.1, 134.6, 133.3, 131.4, 130.7, 130.1, 129.9, 129.6, 129.1, 128.5, 126.5, 126.3, 124.5, 122.6, 122.2, 122.0, 121.9, 113.9, 25.0; HR-ESIMS $[\text{M}+\text{Na}]$ m/z calcd. for $\text{C}_{29}\text{H}_{14}\text{ClN}_3\text{NaO}_5$: 542.0520. Found: m/z 542.0507. $\Delta = 2.4$ ppm.

7-(1-(*m*-tolyl)-1H-1,2,3-triazol-4-yl)-5H-dibenzo[b,h]xanthene-5,6,8,13(7H)-tetraone (**12f**). Orange solid, 85 % yield; m.p. 251-252°C; IR (KBr, cm^{-1}): ν 3132, 2923, 1659, 1611, 1591, 1360, 1283, 1225, 1192, 1093, 1043, 1008, 973, 944, 849, 771, 715, 659, 645; ^1H NMR (DMSO- d_6 , 500.00 MHz): 8.73 (1H, s), 8.17-8.15 (1H, m), 8.12 (1H, dd, J 1.0 and 7.8 Hz), 8.06 (1H, dd, J 1.1 and 7.3 Hz), 8.05-8.03 (1H, m), 7.97 (1H, td, J 1.4 and 7.8 Hz), 7.95-7.93 (1H, m), 7.76 (1H, td, J 1.1 and 7.3 Hz), 7.65 (1H, s), 7.61 (1H, dd, J 1.5 and 7.8 Hz), 7.41 (1H, t, J 7.8 Hz), 7.26 (1H, dd, J 1.1 and 7.3 Hz), 5.45 (1H, s), 2.38 (3H, s); ^{13}C NMR (DMSO- d_6 and $\text{CF}_3\text{CO}_2\text{D}$, 125.0 MHz APT): 183.7, 182.7, 181.3, 178.0, 177.3, 177.1, 168.2, 156.2, 149.6, 147.5, 140.8, 139.9, 137.3, 133.2, 132.4, 130.2, 129.7, 128.2, 126.4, 124.6, 122.0, 120.7, 117.4, 93.6, 25.1, 20.9; HR-ESIMS $[\text{M}+\text{H}]$ m/z calcd. for $\text{C}_{30}\text{H}_{18}\text{N}_3\text{O}_5$: 500.1246. Found: m/z 500.1225. $\Delta = 4.2$ ppm.

7-(1-(4-nitrophenyl)-1H-1,2,3-triazol-4-yl)-5H-dibenzo[b,h]xanthene-5,6,8,13(7H)-tetraone (**12g**). Orange solid, 51 % yield; m.p. 239-240°C; IR (KBr, cm^{-1}): ν 3435, 1661, 1615, 1596, 1520, 1506, 1345, 1266, 1228, 1195, 1114, 1039, 946, 775; ^1H NMR (DMSO- d_6 , 500.00 MHz): 9.00 (1H, s), 8.38 (2H, d, J 9.3 Hz), 8.17-8.14 (1H, m), 8.15 (2H, d, J 9.3 Hz), 8.13 (1H, d, J 7.8 Hz), 8.07 (1H, dd, J 1.0 and 7.8 Hz), 8.05-8.03 (1H, m), 7.98 (1H, td, J 1.0 and 7.8 Hz), 7.93-7.91 (2H, m), 7.76 (1H, td, J 1.0 and 7.8 Hz), 5.48 (1H, s); ^{13}C NMR (DMSO- d_6 and $\text{CF}_3\text{CO}_2\text{D}$, 125.0 MHz APT): 183.9, 183.9, 181.8, 181.5, 161.7, 160.0, 156.5, 148.5, 147.7, 147.0, 141.5, 141.3, 140.7, 135.1, 133.5, 132.5, 131.1, 130.1, 128.7, 127.6, 126.5, 126.0, 125.7, 125.6, 121.7, 120.5, 111.4, 20.9; HR-ESIMS $[\text{M}+\text{Na}]$ m/z calcd. for $\text{C}_{29}\text{H}_{14}\text{N}_4\text{NaO}_7$: 553.0760. Found: m/z 553.0742. $\Delta = 3.2$ ppm.

7-(1-(4-methoxyphenyl)-1H-1,2,3-triazol-4-yl)-5H-dibenzo[b,h]xanthene-5,6,8,13(7H)-tetraone (**12h**). Orange solid, 91 % yield; m.p. 247-249°C; IR (KBr, cm^{-1}): ν 3393, 2917, 2848, 1658, 1613, 1591, 1518, 1360, 1254, 1225, 1193, 1041, 1010, 945, 833, 769, 714; ^1H NMR (DMSO- d_6 , 500.00 MHz): 8.65 (1H, s), 8.16-8.14 (1H, m), 8.11 (1H, dd, J 1.1 and 7.7 Hz), 8.06 (1H, dd, J 1.1 and 7.7 Hz), 8.05-8.02 (1H, m), 7.97 (1H, td, J 1.3 and 7.7 Hz), 7.93-7.91 (2H, m), 7.75 (1H, td, J 1.1 and 7.7 Hz), 7.72 (2H, d, J 8.8 Hz), 7.07 (2H, d, J 8.8 Hz), 5.43 (1H, s), 3.80 (3H, s); ^{13}C NMR (DMSO- d_6 and $\text{CF}_3\text{CO}_2\text{D}$, 125.0 MHz APT): 183.9, 183.0, 181.7, 181.6, 162.0, 156.5, 147.4, 135.1, 133.6, 133.5, 132.6, 130.2, 128.7, 127.4, 126.5, 126.0, 122.8, 122.8, 122.1, 121.8, 121.7, 115.4, 115.4, 115.3, 115.3, 111.4, 55.9, 30.4; HR-ESIMS $[\text{M}+\text{H}]$ m/z calcd. for $\text{C}_{30}\text{H}_{18}\text{N}_3\text{O}_6$: 516.1196. Found: m/z 516.1172. $\Delta = 4.6$ ppm.

2.2. Biological Assays

2.2.1. Cells

MCF-7 cell line was obtained from the Rio de Janeiro Cell Bank (BCRJ; www.bcrj.org.br) and the human non-tumor cell line MCF10A was a kind gift from Dr. Mítzi Brentani (USP, São Paulo, Brazil). The former was grown in Dulbecco's modified Eagle's medium (DMEM, Invitrogen, São Paulo, SP, Brazil) supplemented with 10% (v/v) fetal bovine serum (FBS; Invitrogen, São Paulo, SP, Brazil) and 5 mM L-glutamine (Sigma-Aldrich Chemical Co, St Louis, MO USA) and the later was kept in DMEM/F12 medium (Invitrogen, São Paulo, SP, Brazil) supplemented with 5% fetal horse serum (FHS; Invitrogen, São Paulo, SP, Brazil) containing 0.02 $\mu\text{g}/\text{ml}$ epidermal growth factor (EGF), 5 $\mu\text{g}/\text{ml}$ insulin, 1.25 $\mu\text{g}/\text{ml}$ hydrocortisone and 0.1 $\mu\text{g}/\text{ml}$ cholera toxin (Sigma-Aldrich Chemical Co, St Louis, MO, USA). The cells were grown at 37°C at a 5% CO_2 atmosphere [41].

2.2.2. MTT Assay

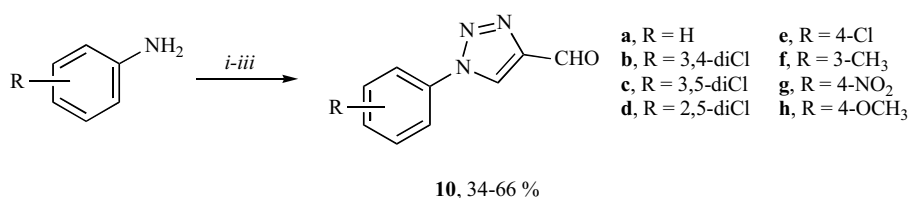
The cells metabolic activity was assayed using the MTT assay as described previously [42]. Cells were seeded in 96-well plates (5×10^4 cells/well) and grown to confluence. Then, the medium was removed, fresh medium was added, and the cells were returned to the incubator in the presence of different drugs used. After 24 h, the cells were incubated with 5 mg/mL MTT reagent (3,4,5-dimethylthiazol-2,5-diphenyltetrazolium bromide, Sigma-Aldrich Co., St. Louis, MO, USA) for 3 h. Thereafter, the formazan crystals were dissolved in DMSO, and the absorbance at 560 nm was evaluated using a VICTOR3 multilabel microplate reader (PerkinElmer, Waltham, MA, USA) with subtraction of the background absorbance at 670 nm.

2.2.3. Intracellular ATP Quantification

ATP quantification. Cells were seeded in 96-well plates (5×10^4 cells/well) and grown to confluence. Then, the medium was removed, fresh medium was added, and the cells were treated with different drugs for 24 h. After this incubation, the medium was removed, and the ATP Lite kit reagents (Luminescence ATP Detection Assay System - PerkinElmer, Waltham, MA, USA) were added. This system is based on the production of light by luciferase because it consumes ATP and D-luciferin. The luminescence is proportional to the concentration of cellular ATP and was analyzed using a VICTOR3 multilabel microplate reader (PerkinElmer, Waltham, MA, USA) [43].

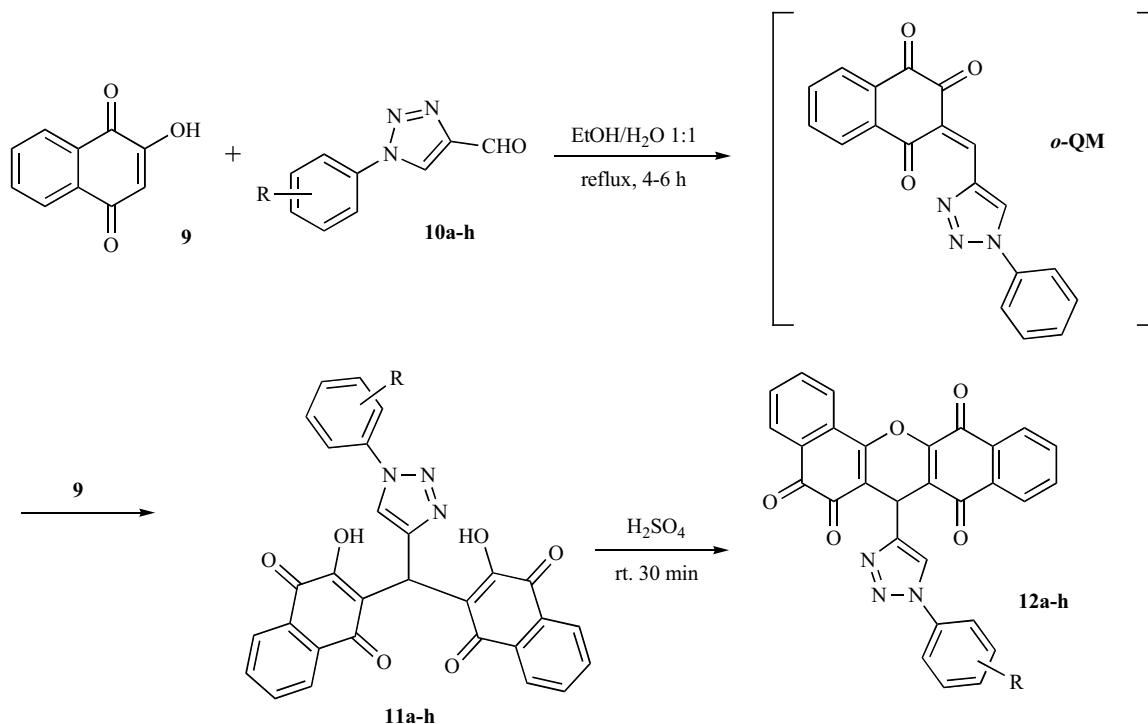
2.2.4. Cell Proliferation Assay

MCF-7 cells proliferation was assessed by the CyQuant method (Thermo Fisher Scientific, Waltham, MA, USA). Cells were seeded in 96-well plates (5×10^4 cells/well) and grown to confluence. Then, the medium was removed, fresh medium was added, and the cells were treated with different drugs for 24 h. After this incubation, the medium was removed, and the instructions of the manufacturer were strictly followed.



i) NaNO₂, HCl, 0-5 °C, 30 min. then NaN₃ (aq), 1h.
 ii) Propargylic alcohol, CuSO₄, sodium ascorbate, *t*BuOH:H₂O, 24h, rt.
 iii) IBX, DMSO/H₂O.

Scheme 1. Synthesis of 1*H*-1,2,3-triazole-4-carbaldehydes (**10a-h**).



Scheme 2. Synthesis of bis-naphthoquinones **11a-h** and dibenzoxanthenes **12a-h**.

2.2.5. Cell Viability and ROS Production

Cells were seeded in 24-well plates (1 x 10⁵ cells/well) and grown in DMEN supplemented with 10% FBS for 24 hours. After this period, 10 μM DCFDA was added and cells were incubated for 30 minutes. Then, the medium was removed and a fresh medium containing the different treatments were added and cells were incubated for additional 24 hours. Then, the medium was removed, the cells were hashed, and suspended in phosphate buffer solution containing 1% bovine serum albumin and 1 μM 7-AAD. The staining was evaluated on a Muse[®] Cell Analyzer (Merck Millipore, Billerica, MA, USA).

3. RESULTS AND DISCUSSION

Initially, the triazole aldehydes **10a-h** were prepared according to the reported methodology [44, 45] from the protocol based on a Huisgen 10,3-dipolar cycloaddition. In this reaction, the reaction between an aryl azide and a propargylic alcohol was catalyzed by Cu(I), providing only the 1,4-disubstituted regioisomer, followed by partial oxidation of the alcohol to generate the 4-carboxaldehyde-1*H*-1,2,3-

triazoles (**10a-h**) with overall yields ranging from 34-66 % (Scheme 1).

Recently, our research group demonstrated that the cycloaddition of lawsone (**9**) to substituted benzaldehydes in the presence of a ground mixture of solid *p*-toluenesulfonic acid and silica gel at 80°C in a pre-heated oven over 6-7 h produced **7** (6*H*-dibenzo[*b,h*]xanthenes) in high yields, rather than the isomer **5**, as has been reported in some studies [29-34]. However, the reaction temperature of these reactions must be strictly controlled. We found that increasing the temperature to 100°C causes the yield of products to decrease dramatically with the use of 1*H*-1,2,3-triazole-4-carbaldehydes (**10a-h**). If the temperature exceeds 120°C, there is complete degradation of both the starting material and the product.

Thus, to obtain triazole-linked-xanthenes **12a-h** a two-step route from bis-adduct of lawsone **9** with several 1*H*-1,2,3-triazole-4-carbaldehydes (**10a-h**) was proposed. Cyclization of compounds of type **4** would lead to compounds 6*H*-dibenzo[*b,h*]xanthenes of type **7c** (Scheme 2).

Table 1. Chemical yields and melting points of the 11a-h and 12a-h.

Compounds	R	Yields	m.p
11a	H	52 %	224-225 °C
11b	3,4-diCl	72 %	212-213 °C
11c	3,5-diCl	82 %	209-210 °C
11d	2,5-diCl	74 %	221-222 °C
11e	4-Cl	39 %	168-169 °C
11f	3-CH ₃	51 %	257-258 °C
11g	4-NO ₂	72 %	225-226 °C
11h	4-OCH ₃	55 %	191-192 °C
12a	H	54 %	259-260 °C
12b	3,4-diCl	63 %	255-257 °C
12c	3,5-diCl	63 %	246-247 °C
12d	2,5-diCl	93 %	239-240 °C
12e	4-Cl	98 %	237-239 °C
12f	3-CH ₃	85 %	251-252 °C
12g	4-NO ₂	51 %	239-240 °C
12h	4-OCH ₃	91 %	247-249 °C

The first step involved the *in situ* generation of *o*-QM via Knoevenagel condensation between lawsone (**9**) and 1H-1,2,3-triazole-4-carbaldehydes (**10a-h**), followed by addition of another equivalent of **9** generated **11a-h** as synthetic intermediates in good yields (Table 1). Then, the treatment of **11** with concentrated sulfuric acid led the formation of 6H-dibenzo[*b,h*]xanthenes (**12a-h**) in good yields (Table 1) as a yellow solid which was filtered under reduced pressure (Scheme 2).

The structures of the products were elucidated by spectroscopic techniques (see SI). For example, for compound **11a** hydroxyl and carbonyl bands were present in the IR spectrum at 3332 cm⁻¹ and 1673 and 1650 cm⁻¹, respectively, and the ¹H NMR signals from methine protons were observed at δ 6.20 ppm and δ 8.29 ppm (triazolic ring), which together confirm the open structure of the compound. In contrast, the ¹H NMR spectrum for **12a** showed unsymmetrical signals indicative of the isomer coupling pattern, with methine signals at δ 5.44 ppm and δ 8.79 ppm (triazolic ring), and the HRMS ([M+H]⁺ m/z 486.1085) showed the loss of a water molecule, which also confirmed the cyclization.

The products **11a-h** and **12a-h** were screened for their cytotoxic activities using the human breast cancer cell line MCF-7. The initial screening was performed by an MTT assay after incubating the cells for 24 hours in the presence of 25 or 50 μM solutions of each product. This assay is indicative of the cell metabolizing activity and has been widely used for initial assessments of the cytotoxic properties of potential drugs [46-48]. The anticancer drug, doxorubicin, was used as positive control. According to the results, all the products from the **11** series were ineffective to MCF-7 cells

metabolizing activity after 24 hours of incubation (Fig. 4A). These results were not different when the cells were incubated for longer periods (48, 72 and 96 hours) in the presence of these products (data not shown). On the other hand, among the products from **12** series, only the products **12b** and **12c** did not interfere with the MTT assay of MCF-7 cells after 24 hours of incubation (Fig. 4B). This picture does not significantly change by incubating MCF-7 cells with these products for 48, 72 or 96 hours (Fig. 4C). Therefore, we set the concentration of 50 μM and the incubation time of 24 hours as our standard conditions for the further experiments. The specificity of the products from series **12** was evaluated as a result of their effects on the non-tumor human breast cancer cell line, MCF10A. Fig. 4D summarizes these results where it can be seen that none of the products of series **12**, used at the concentration of 50 μM, were able to interfere with the MTT assay of MCF10A cells after 24 hours of incubation. Additionally, we also tested the products **12a**, **12e** and **12f** at 100 μM in the assay medium without any additional effect as compared to the results presented in Fig. 4D (data not shown). This is a strong indicative that these compounds have selective effects on cancer cells and are promising anti-proliferative agents. Indeed, most of the products from series **12** were able to decrease MCF-7 cells metabolizing activity in more than 50% without interfering with the non-tumor cell line, MCF10A. With regard to their effects on the cancer cells, products **12a** and **12f** were the most effective, decreasing the MTT assay in 55 and 62%, respectively, at 25 μM and after 24 hours of incubation. The products **12e**, **12g** and **12h** presented intermediate inhibitory properties and **12d** decreased the MTT assay in 47% under these same conditions. Therefore, we decided to continue the

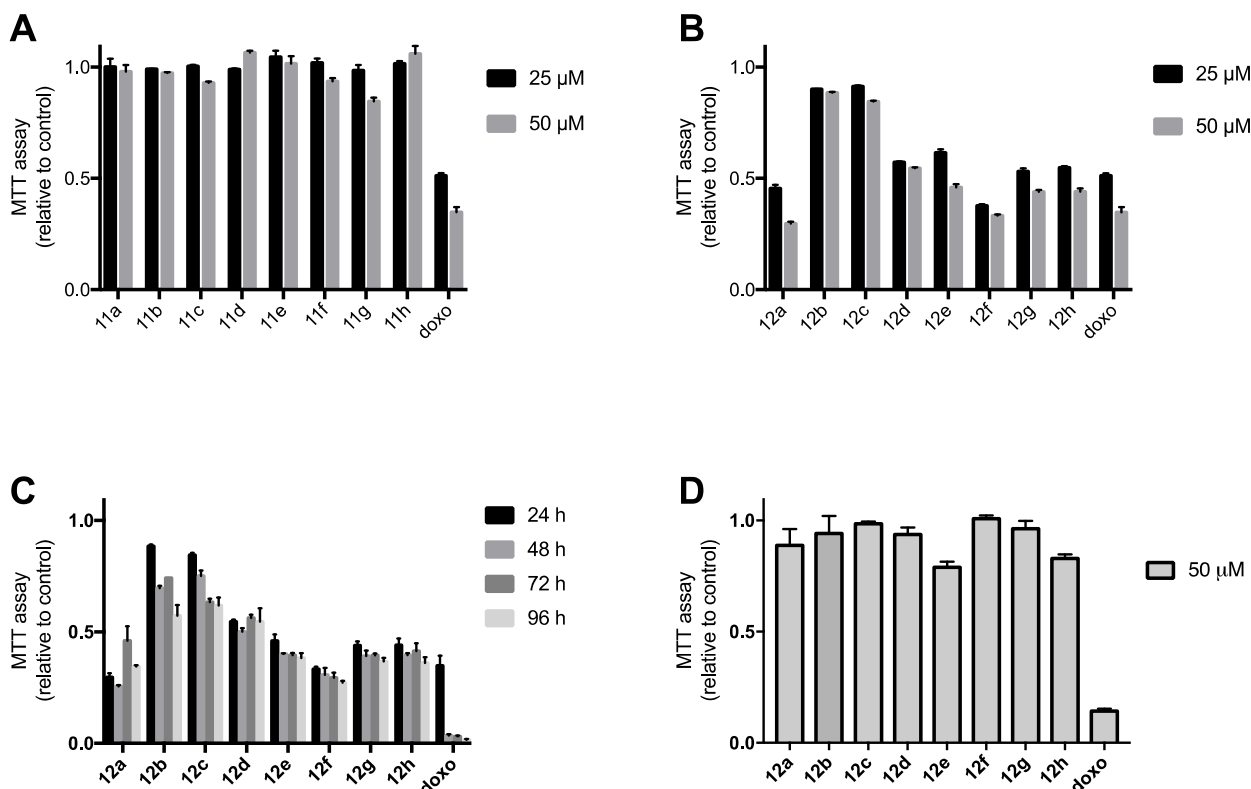


Fig. (4). Human breast cancer cells metabolizing activity (MTT assay). MTT assay of MCF-7 cells treated for 24 hours in the presence of the products **11a-h** (panel A) or **12a-h** (panel B), treated with 50 μM of the products for different time periods (panel C), and MTT assay of MCF10A cells treated for 24 hours in the presence of the products **12a-h** (panel D). Doxorubicin is presented as positive control for the three panels. Experiments were performed as described in Materials and Methods. Data are represented as mean \pm S.E.M of 3 independent experiments ($n=3$).

screening with products **12a**, **12d**, **12e**, **12f**, **12g** and **12h**, discarding only the products **12b** and **12c**. It is important to notice that, as compared to the effects of the positive control, the effects of the products of the chosen products from series **12** were not different from the effects of the anticancer drug doxorubicin. Moreover, these products of series **12** presented selective effects on the cancer cell line, not interfering with the non-tumor cell line metabolic activity, whereas the widely used drug, doxorubicin, promoted similar effects on both cell lines. All the following experiments were carried on only with the tumor cell line MCF-7.

Following the screening, MCF-7 cells were incubated in the presence of the selected products for 24h and their intracellular ATP content was assessed as a major product of cell metabolism and crucial for cell survival. Among the products tested, only **12d** did not interfere with the intracellular ATP content (Fig. 5). Product **12a** was the most effective and, together with **12f**, **12g** and **12h**, were even more effective than doxorubicin, used as positive control. Product **12e** was as effective as doxorubicin in decreasing the intracellular ATP content. Although known for its effects on cell metabolism and ATP production, doxorubicin is also known to present consistent but moderate effects on the intracellular ATP content [49-51]. This is easily observed in the present results were the incubation of MCF-7 cells with 50 μM doxorubicin for 24 hours decreased the intracellular ATP content in $32 \pm 1\%$, as compared to the control. Even though, doxorubicin is very lethal to the cells, and this moderate effect is related to the disruption of cell metabolism. Thus, the

fact that the products **12a**, **12f**, **12g** and **12h** presented higher levels of effects on the intracellular ATP content can not be, so far, directly interpreted as a higher effectiveness of these products as anti-tumor drugs.

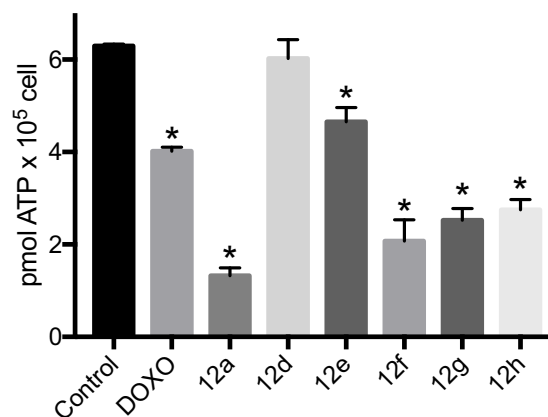


Fig. (5). Intracellular ATP content of MCF-7 cells. Cells were plated in 96-well plates and treated for 24 hours in the presence of 50 μM of each compound or DMSO (0.2% v/v), used as control. Intracellular ATP content was assessed as described in Materials and Methods. Bars represent mean \pm S.E.M of 3 independent experiments ($n=3$).

In order to evaluate the effects of the products on MCF-7 cells proliferation, we performed a CyQuant assay, which evaluate the DNA content, directly proportional to the num-

ber of the cells [52]. The results are presented in Fig. (6) and show that, at different levels, all the products tested decreased MCF-7 cells proliferation, as compared to the control. Indeed, although statistically significant, the effects of **12d** are very modest and might have insignificant or none biological relevance. All the other products tested were very effective, decreasing the proliferation of the cells in more than 50%, after 24 hours of treatment. However, for this assay, none of the drugs were as effective as antimycin A (AMA), used as a positive control for antiproliferative drug. Indeed, AMA is extremely effective decreasing cell proliferation [53, 54], which is due to its highly toxic effects. Thus, instead of being an excellent positive control for cell proliferation inhibitor, AMA is not an anticancer drug due to its highly toxic effects, which seems not to be the case of the products of the 12 series tested here. These products, except **12d**, presented moderate but significant attenuation of cell proliferation, suggesting a lower toxic effect when compared to AMA.

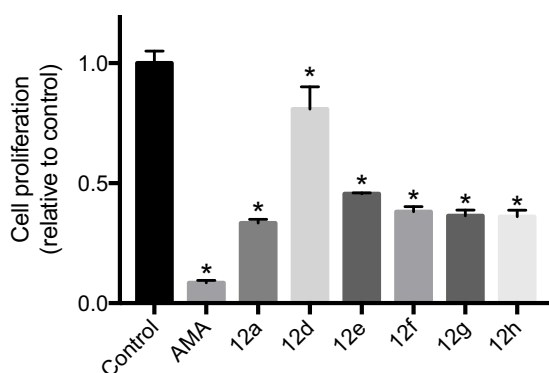


Fig. (6). Cell proliferation assay of MCF-7 cells. Cells were plated in 96-well plates and treated for 24 hours in the presence of 50 μ M of each compound or DMSO (0.2% v/v), used as control. Cell proliferation was assessed by the CyQuant method as described in Materials and Methods. Bars represent mean \pm S.E.M of 3 independent experiments (n=3).

The mechanism by which these products are promoting their anti-tumor effects was evaluated assessing the oxidative stress on MCF-7 cells treated for 24 hours in the presence of 50 μ M of each compound. To assess the oxidative stress, treated cells were incubated with 7-AAD (7-aminoactinomycin D) and DCFDA (2',7'-dichlorodihydrofluorescein diacetate). The former, when enters the cells due to a leak on plasma membrane, intercalates with DNA and emits fluorescence at 650 nm. The latter freely enters the cells and reacts with reactive oxygen species (ROS) forming 2',7'-dichlorofluorescein, which emits fluorescence at 520 nm. Thus, treated cells can be evaluated for cell viability (when stained by 7-AAD) and oxidative stress (when stained by DCFDA) in a flow cytometer dual detection (650 and 520 nm). The results for these experiments are shown in the Fig. (7). Panels A-H show representative plots for each tested conditions. Control and positive control for cell leakage and ROS production (doxorubicin) are shown in panels A and B, respectively. It is clearly seen that upon doxorubicin treatment, the cell population change its pattern from a no stained to a double stained population (compare panel A and panel B for control and doxorubicin-treated cells, respectively). The product **12a** produced a pattern similar to

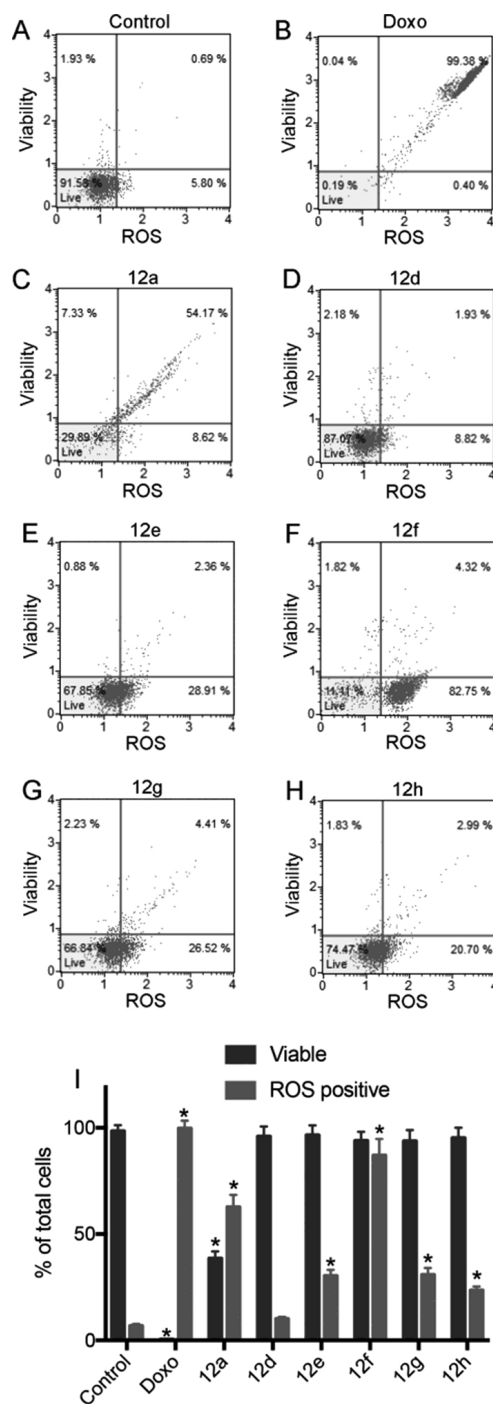


Fig. (7). Cell viability and ROS production by MCF-7 cells treated with the products. Cells were plated in 24-well plates and treated for 24 hours in the presence of 50 μ M of each compound or DMSO (0.2% v/v), used as control. Results were obtained by flow cytometer as described in Materials and Methods. Panels A-H are representative results of a series of three independent experiments. In Panel I, bars represent mean \pm S.E.M of 3 independent experiments (n=3).

doxorubicin, decreasing cell viability and increasing ROS production simultaneously (Fig. 7C). While the product **12d** presented no effects on both, cell viability and ROS production, the products **12e**, **12f**, **12g** and **12h** promoted an increase in ROS production but no change in the cells viability. The panel I summarizes the results obtained by flow cy-

tometry including the results of three independent analyses. A remarkable effect can be attributed to the product **12f**, since almost the totality of the cells was positive to ROS (similar to doxorubicin-treated cells) but no leakage on cell membrane was detected by this technique. This is quite intriguing since this drug decreased the metabolic activity, the ATP content and the cells proliferation, discarding that the anti-oxidative pathways of the cells would be fully-active upon the treatment with product **12f**. It might be that the increase in ROS production in this case, such as for the products **12e**, **12g** and **12h**, is enough to be detected and to interfere with cell metabolism and proliferation, but not as high as to disrupt the cell membrane. Indeed, among the products tested, only **12a** promoted both, ROS production and cell membrane damage.

CONCLUSION

Evaluating series of new 3,3'-((1-aryl-1*H*-1,2,3-triazol-4-yl)methylene)bis(2-hydroxynaphthalene-1,4-diones) **11a-h** and 7-(1-aryl-1*H*-1,2,3-triazol-4-yl)-5*H*-dibenzo[*b,h*]xanthene-5,6,8,13(7*H*)-tetraones **12a-h**, we concluded that compound **12a** is an important candidate for an anti-cancer drug due to its properties on promoting both ROS production and cell membrane damage. However, *in vivo* tests are required previous to any advanced conclusion in this direction.

ETHICS APPROVAL AND CONSENT TO PARTICIPATE

Not applicable.

HUMAN AND ANIMAL RIGHTS

No Animals/Humans were used for studies that are the basis of this research.

CONSENT FOR PUBLICATION

Not applicable.

CONFLICT OF INTEREST

The authors declare no conflict of interest, financial or otherwise.

ACKNOWLEDGEMENTS

The authors would like to acknowledge the agencies that fund our research: CNPq (National Council of Research of Brazil), CAPES, FAPERJ and FIOCRUZ (for the HRMS). Fellowships granted by CNPq, CAPES and FAPERJ are gratefully acknowledged.

SUPPLEMENTARY MATERIAL

Supplementary material is available on the publisher's website along with the published article.

REFERENCES

- da Silva, F.C.; Ferreira, V.F. Natural naphthoquinones with great importance in medicinal chemistry. *Curr. Org. Synth.*, **2016**, *13*, 334-371.
- Salmon-Chemin, L.; Buisine, E.; Yardley, V.; Kohler, S.; Debreu, M.A.; Landry, V.; Sergheraert, C.; Croft, S.L.; Krauth-Siegel, R.L.; Davioud-Charvet, E. 2- and 3-substituted 1,4-naphthoquinone derivatives as subversive substrates of trypanothione reductase and lipamide dehydrogenase from *Trypanosoma cruzi*: synthesis and correlation between redox cycling activities and *in vitro* cytotoxicity. *J. Med. Chem.*, **2001**, *44*, 548-565.
- Müller, T.; Johann, L.; Jannack, B.; Brückner, M.; Lanfranchi, D.A.; Bauer, H.; Sanchez, C.; Yardley, V.; Deregnaucourt, C.; Schrével, J.; Lanzer, M.; Schirmer, R.H.; Davioud-Charvet, E. Glutathione reductase-catalyzed cascade of redox reactions to bioactivate potent antimalarial 1,4-naphthoquinones—a new strategy to combat malarial parasites. *J. Am. Chem. Soc.*, **2011**, *133*, 11557-11571.
- Benites, J.; Valderrama, J.A.; Rivera, F.; Rojo, L.; Campos, N.; Pedro, M.; José Nascimento, M.S. Studies on quinones. Part 42: Synthesis of furylquinone and hydroquinones with antiproliferative activity against human tumor cell lines. *Bioorg. Med. Chem.*, **2008**, *16*, 862-868.
- Silva, M.N.; de Souza, M.C.B.V.; Ferreira, V.F.; Pinto, A.V.; Pinto, M.C.R.F.; Wardell, S.M.S.V.; Wardell, J.L. Synthesis of new aldehyde derivatives from β -lapachone and nor- β -lapachone. *Arquivoc*, **2003**, 156-168.
- Yang, R.Y.; Kizer, D.; Wu, H.; Volkova, E.; Miao, X.S.; Ali, S.M.; Tandon, M.; Savage, R.E.; Chan, T.C.; Ashwell, M.A. Synthetic methods for the preparation of ARQ 501 (beta-Lapachone) human blood metabolites. *Bioorg. Med. Chem.*, **2008**, *16*, 5635-5643.
- Khong, H.T.; Dreisbach, L.; Kindler, H.L.; Trent, D.F.; Jezierski, K.G.; Bonderenko, I.; Popiela, T.; Yagovane, D.M.; Dombal, G. A phase 2 study of ARQ 501 in combination with gemcitabine in adult patients with treatment naïve, unresectable pancreatic adenocarcinoma. *J. Clin. Oncol.*, **2007**, *25*, 15017.
- ArQule, Inc. ArQule presents preliminary interim phase 1 data for ARQ 501 and announces combination study with taxotere. PR Newswire. Available at: <http://www.prnewswire.com/news-releases/arqule-presents-preliminary-interim-phase-1-data-for-arq-501-and-announces-combination-study-with-taxotere-73972182.html>, 2004 (Accessed 27.07.17).
- Cragg, G.M.; Grothaus, P.G.; Newman, D.J. New horizons for old drugs and drug leads. *J. Nat. Prod.*, **2014**, *77*, 703-723.
- da Costa, E.C.B.; Amorim, R.; da Silva, F.C.; Papa M.P.; de Aruda, L.B.; Mohana-Borges, R.; Ferreira, V.F.; Tanuri, A.; da Costa, L.J.; Ferreira, S.B. Synthetic 1,4-pyran naphthoquinones are potent inhibitors of dengue virus replication. *Plos One*, **2013**, *8*, e82504.
- Moosophon, P.; Kanokmedhakul, S.; Kanokmedhakul, K.; Soy-tong, K. Prenylxanthenes and a bicyclo[3.3.1]nona-2,6-diene derivative from the fungus *Emericella rugulosa*. *J. Nat. Prod.*, **2009**, *72*, 1442-1446.
- Hay, A.E.; Aumond, M.C.; Mallet, S.; Dumontet, V.; Litaudon, M.; Rondeau, D.; Richomme, P. Antioxidant xanthenes from *Garcinia vieillardii*. *J. Nat. Prod.*, **2004**, *67*, 707-709.
- Hashim, N.; Rahmani, M.; Sukari, M.A.; Ali, A.M.; Alitheen, N.B.; Go, R.; Ismail, H.B. Two new xanthenes from *Artocarpus obtusus*. *J. Asian Nat. Prod. Res.*, **2010**, *12*, 106-112.
- Jamison, J.M.; Krabill, K.; Hatwalkar, A.; Jamison, E.; Tsai, C.C. Potentiation of the antiviral activity of poly r(A-U) by xanthene dyes. *Cell Biol. Int. Rep.*, **1990**, *14*, 1075-1084.
- Evangelinou, O.; Hatzidimitriou, A.G.; Velali, E.; Pantazaki, A.A.; Voulgarakis, N.; Aslanidis, P. Mixed-ligand copper(I) halide complexes bearing 4,5-bis(diphenylphosphano)-9,9-dimethyl-xanthene and N-methylbenzothiazole-2-thione: Synthesis, structures, luminescence and antibacterial activity mediated by DNA and membrane damage. *Polyhedron*, **2014**, *72*, 122-129.
- Yunnikova, L.P.; Gorokhov, V.Y.; Makhova, T.V.; Aleksandrova, G.A. Synthesis and Antimicrobial Activity of Amines with Azaxanthene Fragments. *Pharm. Chem. J.*, **2013**, *47*, 139-141.
- Azebaze, A.G.; Meyer, M.; Valentin, A.; Nguemfo, E.L.; Fomum, Z.T.; Nkengfack, A.E. Prenylated xanthone derivatives with antiplasmodial activity from *Allanblackia monticola* STANER L.C. *Chem. Pharm. Bull.*, **2006**, *54*, 111-113.
- Zelefack, F.; Guilet, D.; Fabre, N.; Bayet, C.; Chevalley, S.; Ngouela, S.; Lenta, B.N.; Valentin, A.; Tsamo, E.; Dijoux-Franca, M.G. Cytotoxic and antiplasmodial xanthenes from *Pentadesma butyracea*. *J. Nat. Prod.* **2009**, *72*, 954-957.

- [19] Laphookhieo, S.; Syers, J.K.; Kiattansakul, R.; Chantrapromma, K. Cytotoxic and antimarial prenylated xanthenes from *Cratogeomys cochinchinense*. *Chem. Pharm. Bull.*, **2006**, *54*, 745-747.
- [20] Djoufack, G.L.; Valant-Vetschera, K.M.; Schinnerl, J.; Brecker, L.; Lorbeer, E.; Robien, W. Xanthenes, biflavanones and triterpenes from *Pentadesma grandifolia* (Clusiaceae): structural determination and bioactivity. *Nat. Prod. Commun.*, **2010**, *5*, 1055-1060.
- [21] Poupelin, J.P.; Saint-Ruf, G.; Foussard-Blanpin, O.; Narcisse, G.; Uchida-Ermouf, G.; Lacroix, R. Synthesis and antiinflammatory properties of bis (2-hydroxy-1-naphthyl)methane derivatives I. *Eur. J. Med. Chem.*, **1978**, *13*, 67-71.
- [22] Rewcastle, G.W.; Atwell, G.J.; Li, Z.A.; Baguley, B.C.; Denny, W.A. Potential antitumor agents. 61. Structure-activity relationships for in vivo colon 38 activity among disubstituted 9-oxo-9H-xanthene-4-acetic acids. *J. Med. Chem.*, **1991**, *34*, 217-222.
- [23] Niu, S.L.; Li, Z.L.; Ji, F.; Liu, G.Y.; Zhao, N.; Liu, X.Q.; Jing, Y.K.; Hua, H.M. Xanthenes from the stem bark of *Garcinia bracteata* with growth inhibitory effects against HL-60 cells. *Phytochemistry*, **2012**, *77*, 280-286.
- [24] Lee, K.H.; Chai, H.B.; Tamez, P.A.; Pezzuto, J.M.; Cordell, G.A.; Win, K.K.; Tin-Wa, M. Biologically active alkylated coumarins from *Kayea assamica*. *Phytochemistry*, **2003**, *64*, 535-541.
- [25] Tao, S.J.; Guan, S.H.; Wang, W.; Lu, Z.Q.; Chen, G.T.; Sha, N.; Yue, Q.X.; Liu, X.; Guo, D.A. Cytotoxic polyprenylated xanthenes from the resin of *Garcinia hanburyi*. *J. Nat. Prod.*, **2009**, *72*, 117-124.
- [26] Diniz, T.F.; Pereira, A.C.; Capettini, L.S.A.; Santos, M.H.; Nagem, T.J.; Lemos, V.S.; Cortes, S.F. Mechanism of the vasodilator effect of mono-oxygenated xanthenes: a structure-activity relationship study. *Planta Med.*, **2013**, *79*, 1495-1500.
- [27] Rao, T.V.P.; Venkateswarlu, V. Chemical examination of *embelia ribes-VI*: Synthesis of some new methylene-bisbenzoquinones. *Tetrahedron*, **1964**, *20*, 2967-2970.
- [28] Tisseh, Z.N.; Azimi, S.C.; Mirzaei, P.; Bazgir, A. The efficient synthesis of aryl-5H-dibenzo[b,i]xanthene-5,7,12,14(13H)-tetraone leuco-dye derivatives. *Dyes Pigments*, **2008**, *79*, 273-275.
- [29] Tavakoli, H.R.; Moosavi, S.M.; Bazgir, A. $ZrOCl_2 \cdot 8H_2O$ as an efficient catalyst for the synthesis of dibenzo [b,i]xanthene-tetraones and fluorescent hydroxyl naphthalene-1,4-diones. *Res. Chem. Intermed.*, **2015**, *41*, 3041-3046.
- [30] Chen, Y.; Wu, S.; Tu, S.; Li, C.; Shi, F. A simple procedure for the synthesis of benzoxanthene derivatives under microwave irradiation conditions. *J. Heterocycl. Chem.*, **2008**, *45*, 931-934.
- [31] Shaterian, H.R.; Azizi, K.; Fahimi, N. Phosphoric acid supported on alumina (H_3PO_4/Al_2O_3) as an efficient and reusable catalyst for the one-pot synthesis of benzoxanthene pigments. *Res. Chem. Intermed.*, **2014**, *40*, 1403-1414.
- [32] Shaterian, H.R.; Rigi, F. An efficient synthesis of quinazoline and xanthene derivatives using starch sulfate as a biodegradable solid acid catalyst. *Res. Chem. Intermed.*, **2015**, *41*, 721-738.
- [33] Amini, M.M.; Fazaeli, Y.; Yassaei, Z.; Shahzad, F.; Ayoob, B. Polytungstozincate Acid: A new and efficient catalyst for the synthesis of xanthenes under solvent-free conditions. *Open Catal. J.*, **2009**, *2*, 40-44.
- [34] Khaligh, N.G. Poly(4-vinylpyridinium) hydrogen sulfate: an efficient catalyst for the synthesis of xanthene derivatives under solvent-free conditions. *Catal. Sci. Technol.*, **2012**, *2*, 2211-2215.
- [35] Liu, D.; Gao, J.; Li, L.; Zhou, S.; Xu, D. Silica-supported sodium hydrogen sulfate catalyzed synthesis of 13-aryl-12h-dibenzo[b,i]xanthene-5,7,12,14(13h)-tetraones. *Chem Heterocycl. Compd.*, **2013**, *49*, 1370-1373.
- [36] Shaterian, H.R.; Sedghipour, M.; Mollashahi, E. Brønsted acidic ionic liquids catalyzed the preparation of 13-aryl-5H-dibenzo[b,i]xanthene-5,7,12,14(13H)-tetraones and 3,4-dihydro-1H-benzo[b]xanthene-1,6,11(2H,12H)-triones. *Res. Chem. Intermed.*, **2014**, *40*, 1345-1355.
- [37] Bazgir, A.; Tisseh, Z.N.; Mirzaei, P. An efficient synthesis of spiro[dibenzo[b,i]xanthene-13,3'-indoline]-pentaones and 5H-dibenzo[b,i]xanthene-tetraones. *Tetrahedron Lett.*, **2008**, *49*, 5165-5168.
- [38] Carneiro, P.F.; Pinto, M.C.F.R.; Marra, R.K.F.; Campos, V.R.; Resende, J.A.; Delarmelina, M.; Carneiro, J.W.; Lima, E.S.; da Silva, F. C.; Ferreira, V.F. Insight into and Computational Studies of the Selective Synthesis of 6H-Dibenzo[b,h]xanthenes. *J. Org. Chem.*, **2016**, *81*, 5525-5537.
- [39] Ferreira, V.F.; Nicoletti, C.D.; Ferreira, P.G.; Futuro, D.O.; da Silva, F.C. Strategies for increasing the solubility and bioavailability of anticancer compounds: β -Lapachone and other naphthoquinones. *Curr. Pharm. Des.*, **2016**, *22*, 5899-5914.
- [40] Cardoso, M.F.C.; Rodrigues, P.C.; Oliveira, M.E.I.M.; Gama I.L.; da Silva, I.M.; Santos, I.O.; Rocha, D.R.; Pinho, R.T. Ferreira, V.F.; de Souza M.C.; da Silva, F. C.; Silva-Jr, F.P. Synthesis and evaluation of the cytotoxic activity of 1,2-furanonaphthoquinones tethered to 1,2,3-1H-triazoles in myeloid and lymphoid leukemia cell lines. *Eur. J. Med Chem.*, **2014**, *84*, 708-717.
- [41] Zancan, P.; Sola-Penna, M.; Furtado, C.M.; da Silva, D. Differential expression of phosphofructokinase-1 isoforms correlates with the glycolytic efficiency of breast cancer cells. *Mol. Genet. Metab.*, **2010**, *100*, 372-378.
- [42] Spitz, G.A.; Furtado, C.M.; Sola-Penna, M.; Zancan, P. Acetylsalicylic acid and salicylic acid decrease tumor cell viability and glucose metabolism modulating 6-phosphofructo-1-kinase structure and activity. *Biochem. Pharmacol.*, **2009**, *77*, 46-53.
- [43] Furtado, C.M.; Marcondes, M.C.; Sola-Penna, M.; de Souza, M.L.; Zancan, P. Clotrimazole Preferentially Inhibits Human Breast Cancer Cell Proliferation, Viability and Glycolysis. *Plos One*, **2012**, *7*, e30462.
- [44] Boechat, N.; Ferreira, V.F.; Ferreira, S.B.; M.L.G., Ferreira; F.C.; da Silva; Bastos, M.M.; Costa, M.S.; Lourenço, M.C.; Pinto, A.C.; Krettli, A.U.; Aguiar, A.C.; Teixeira, B.M.; da Silva, N.V.; Martins, P.R.; Bezerra, F.A.; Camilo, A.L.; da Silva, G.P.; Costa, C.C. Novel 1,2,3-Triazole Derivatives for Use against *Mycobacterium tuberculosis* H37Rv (ATCC 27294) Strain. *J. Med. Chem.*, **2011**, *54*, 5988-5999.
- [45] da Silva, I.F.; Martins, P.R.C.; da Silva, E.G.; Ferreira, S.B.; Ferreira, V.F.; da Costa, K.R.; de Vasconcelos, M.C.; Lima, E.S.; da Silva, F.C. Synthesis of 1H-1,2,3-triazoles and Study of their Antifungal and Cytotoxicity Activities. *Med. Chem.*, **2013**, *9*, 1085-1090.
- [46] Gao, S.Y.; Gong, Y.F.; Sun, Q.J.; Bai, J.; Wang, L.; Fan, Z.Q.; Sun, Y.; Su, Y.J.; Gang, J.; Ji, Y.B. Screening antitumor bioactive fraction from *Sauromatum giganteum* (Engl.) Cusimano & Hett and identification by UPLC-TOF-MS. *Molecules*, **2015**, *20*, 4290-4306.
- [47] Zhang, N.; Guo, H.; Zheng, W.; Wang, T.; Ma, X. Design and screening of a chimeric survivin-specific nanobody and its anticancer activities in vitro. *Anticancer Drugs*, **2016**, *27*, 839-847.
- [48] Musumeci, D.; Amato, J.; Zizza, P.; Platella, C.; Cosconati, S.; Cingolani, C.; Biroccio A.; Novellino, E.; Randazzo, A.; Giancola, C.; Pagano, B.; Montesarchio, D. Tandem application of ligand-based virtual screening and G4-OAS assay to identify novel G-quadruplex-targeting chemotypes. *Biochim. Biophys. Acta*, **2017**, *1861*, 1341-1352.
- [49] Tam, K.F.; Ng, T.Y.; Tsang, P.C.; Li, C.F.; Ngan, H.Y. Potential use of the adenosine triphosphate cell viability assay in endometrial cancer. *J. Soc. Gynecol. Investig.*, **2006**, *13*, 518-522.
- [50] Pointon, A.V.; Walker, T.M.; Phillips, K.M.; Luo, J.; Riley, J.; Zhang, S.D.; Parry, J.D.; Lyon, J.J.; Marcylo, E.L.; Gant, T.W. Doxorubicin in vivo rapidly alters expression and translation of myocardial electron transport chain genes, leads to ATP loss and caspase 3 activation. *Plos One*, **2010**, *5*, e12733.
- [51] Bean, J.F.; Qiu, Y.Y.; Yu, S.; Clark, S.; Chu, F.; Madonna, M.B. Glycolysis inhibition and its effect in doxorubicin resistance in neuroblastoma. *J. Pediatr. Surg.*, **2014**, *49*, 981-984.
- [52] Jones, L.J.; Gray, M.; Yue, S.T.; Haugland, R.P.; Singer, V.L. Sensitive determination of cell number using the CyQUANT cell proliferation assay. *J. Immunol. Methods*, **2001**, *254*, 85-98.
- [53] Lee, Y.; Oh, S.B.; Park, H.R.; Kim, H.S.; Kim, M.S.; Lee, J. Selective impairment on the proliferation of neural progenitor cells by oxidative phosphorylation disruption. *Neurosci. Lett.*, **2013**, *535*, 134-139.
- [54] Park, W.H.; You, B.R. Antimycin A induces death of the human pulmonary fibroblast cells via ROS increase and GSH depletion. *Int. J. Oncol.*, **2016**, *48*, 813-820.

REVIEW ARTICLE

Pieces of the Complex Puzzle of Cancer Cell Energy Metabolism: An Overview of Energy Metabolism and Alternatives for Targeted Cancer Therapy

Zeinab Ghasemishahrestani^{1,*}, Larissa Maura Melo Mattos¹, Tatiana Martins Tilli², André Luis Souza dos Santos³ and Marcos Dias Pereira^{1,*}

¹Departamento de Bioquímica, Instituto de Química, Universidade Federal do Rio de Janeiro, Rio de Janeiro, RJ, Brazil; ²Centro de Desenvolvimento Tecnológico em Saúde, Fundação Oswaldo Cruz, Rio de Janeiro, RJ, Brazil; ³Departamento de Microbiologia Geral, Instituto de Microbiologia Paulo de Góes, Universidade Federal do Rio de Janeiro, Rio de Janeiro, RJ, Brazil.

Abstract: Over the past decades, several advances in cancer cell biology have led to relevant details about a phenomenon called the ‘Warburg effect’. Currently, it has been accepted that the Warburg effect is not compatible with all cancer cells, and thus the process of aerobic glycolysis is now challenged by the knowledge of a large number of cells presenting mitochondrial function. The energy metabolism of cancer cells is focused on the bioenergetic and biosynthetic pathways in order to meet the requirements of rapid proliferation. Changes in the metabolism of carbohydrates, amino acids and lipids have already been reported for cancer cells and this might play an important role in cancer progression. To the best of our knowledge, these changes are mainly attributed to genetic reprogramming which leads to the transformation of a healthy into a cancerous cell. Indeed, several enzymes that are highly relevant for cellular energy are targets of oncogenes (*e.g.*, PI3K, HIF1, and Myc) and tumor suppressor proteins (*e.g.*, p53). As a consequence of extensive studies on cancer cell metabolism, some new therapeutic strategies have appeared that aim to interrupt the aberrant metabolism, in addition to influencing genetic reprogramming in cancer cells. In this review, we present an overview of cancer cell metabolism (carbohydrate, amino acid, and lipid), and also describe oncogenes and tumor suppressors that directly affect the metabolism. We also discuss some of the potential therapeutic candidates which have been designed to target and disrupt the main driving forces associated with cancer cell metabolism and proliferation.

ARTICLE HISTORY

Received: May 09, 2020
Revised: July 17, 2020
Accepted: July 22, 2020

DOI:
[10.2174/0929867327999200819123357](https://doi.org/10.2174/0929867327999200819123357)

Keywords: Carbohydrate metabolism, lipid metabolism, amino acid metabolism, oncogenes and tumor suppressors, targeted therapy.

1. INTRODUCTION

Cancer is the name given to a set of more than 100 diseases that have, in common, uncontrolled cell growth. In some instances, the malignant cells may spread from one region of the body to other areas by

invading healthy tissues/organs (metastasis). Thus, in order to supply the required demands for abnormal proliferation, cancer cells exert extensive changes in energy metabolism. In contrast to normal cells, which mostly use mitochondrial oxidative phosphorylation to generate energy for cellular processes, cancer cells almost exclusively depend on aerobic glycolysis, which increases glucose uptake/consumption and impairs oxidative phosphorylation, in a phenomenon called the ‘Warburg effect’ [1, 2]. Thus, it is somewhat of a paradox that despite having a sufficient supply of oxygen, cancer cells frequently produce high lactate concentra-

*Address correspondence to these authors Departamento de Bioquímica, Instituto de Química, Universidade Federal do Rio de Janeiro, Rio de Janeiro, RJ, Brazil. Actual address: Avenida Athos da Silveira Ramos, 149, Bloco A, 5º andar, Lab. 549-C, CEP: 21.941-909, Cidade Universitária, Rio de Janeiro, RJ, Brasil; Tel: +55 21 3938-7359; E-mails: marcosdp@iq.ufjf.br; farzaneh.ghasemi.sha@gmail.com

tions [2]. The etiology of alterations that affect different types of cancers and generate the metabolic heterogeneity, and the dynamic processes that cause modifications from normal to cancer cells, are key questions that should be addressed in order to overcome one of the major concerns about cancer therapy, the metabolic plasticity [3]. Herein, we will briefly discuss the changes in energy metabolism as well as the genetic effect on cancer cell metabolism. Moreover, potential antitumor therapies directed against specific targets of energy metabolism will also be presented.

2. CANCER CELL METABOLISM: AN OVERVIEW

2.1. Carbohydrate Metabolism

Regardless of functional mitochondria, some cancer cells have the ability to reversibly switch between glycolytic and oxidative metabolism. Based on Crabtree's observation, the presence of glucose causes slightly increased or no effect on respiration in normal cells [4]. However, in cancer cells, it is common to find severe changes in metabolic programming, which stimulates aerobic glycolysis and lactate production with the reduction of both oxygen uptake and consumption [4-7]. Among the several changes reported, it has been stated that the Warburg effect induces competition for ADP + Pi between oxidative phosphorylation and glycolysis, which has been attributed to respiratory abnormalities [8-10]. Several authors also reported that the Warburg effect may cause the observed increase in mitochondrial calcium levels, which seems to be associated with $F_{0(oh)}$, F_1 -ATP synthase inhibition and abrogation of respiration [5, 11, 12].

During normal cellular metabolism, glucose is firstly degraded in a process called glycolysis, which after a series of enzyme-catalyzed reactions generates two molecules of ATP, NADH and pyruvate. The fate of pyruvate is mostly related to either aerobic or anaerobic conditions encountered by cells. In non-cancer cells, pyruvate is converted into acetyl-CoA and directed to the tricarboxylic acid (TCA) cycle. Then, the reducing power generated after oxidation of acetate in the TCA cycle is processed by the electron transport chain and oxidative phosphorylation resulting in the generation of 30-32 ATP molecules *per* metabolized glucose molecule (Fig. 1) [13]. Unlike normal cells, cancer cells adapt to use aerobic glycolysis to procure significant amounts of their energy and to produce other metabolic end products to support their rapid growth and proliferation under conditions of low oxygen tension [2, 14]. To the best of our knowledge, the

increased glycolytic flux is the most noticeable and well-known energy metabolism change of cancer cells [15]. The inherent lower bioenergetic nature of glycolysis means that cancer cells should adopt a method to increase glucose uptake to meet their energy needs. We will now briefly summarize some of the main factors related to aerobic glycolysis promotion in cancer cells.

There are three classes of glucose transporters: GLUT 1-4 and GLUT 14 (class I), GLUT 5, 7, 9 and 11 (class II) and GLUT 6, 8, 10, 12 and 13 (class III). These transporters control the flux of glucose between intracellular and extracellular compartments to ensure that there is constant availability of glucose for cell metabolism [16]. Among GLUT proteins, GLUT 1 and GLUT 3 are the most commonly studied glucose transporters: while GLUT 1 has been found to be overexpressed in a variety of both solid and hematological malignancies, GLUT 3 has been found to be expressed predominantly in the brain and in tissues with high glucose demand, such as the placenta and testis [16-19]. In addition, poorly differentiated grade 2 and 3 endometrial and breast tumors have significantly higher GLUT1 and GLUT3 expression than well-differentiated grade tumors [20].

Hexokinases (HK) catalyze C-6 glucose phosphorylation to yield glucose-6-phosphate in the first step of glycolysis. HK2 is the most regulated isoform in human cells and is overexpressed in several cancer cells [21, 22]. The role of HK2 in pancreatic ductal adenocarcinoma revealed that this isoform is required for primary tumor growth and metastasis [23]. Interestingly, the increase in lactate levels promotes invasion, demonstrating a mechanistic link between HK2 and metastasis via the regulation of lactate production [23]. On the other hand, it has been reported that inhibition of lactate production reduces the effects of HK2 on invasion. Also documented is the fact that HK2 binds to mitochondria through the voltage-dependent anionic channel (VDAC) [23,24]. VDAC1 is the main transporter of ATP and other metabolites through the outer mitochondrial membrane. The overexpressed VDAC1 provides anchoring sites for overexpressed HK, allowing direct transport of mitochondrial ATP for phosphorylation of glucose, thus increasing the glycolytic rate. By binding to VDAC1, HK2 provides both a metabolic benefit and apoptosis-suppressive capacity that offer the cell a proliferative advantage and increased resistance to chemotherapy. Accordingly, higher VDAC1 levels were associated with sarcomatous alterations of primary malignancies of the biliary tract [24].

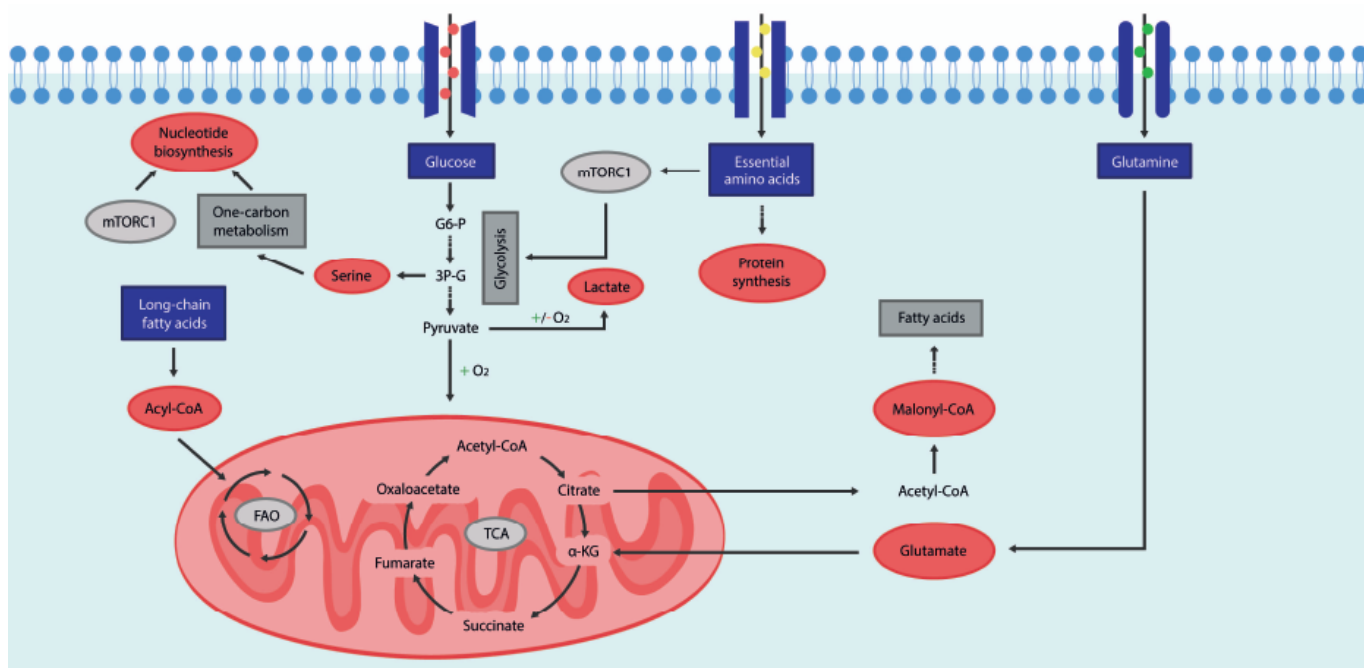


Fig. (1). Overview of cancer metabolism. The glucose molecule is firstly degraded in a process called glycolysis, which after a series of enzyme-catalyzed reactions generates two molecules of ATP, NADH and pyruvate. In non-cancer cells under aerobic conditions, pyruvate is converted into acetyl-CoA and directed to the tricarboxylic acid (TCA) cycle. Unlike normal cells, cancer cells use pyruvate for producing lactate in the presence or absence of oxygen, a process named aerobic glycolysis or Warburg effect. One-carbon metabolism provides cofactors for nucleotide biosynthesis for proliferating cancer cells. During glycolysis around 10% of 3-phosphoglycerate is oxidized by converting it into 3-phosphohydroxypyruvate, which is subsequently transaminated, forming 3-phosphoserine and dephosphorylated to yield serine. Fatty acids are synthesized from citrate and acetyl-CoA. Long-chain fatty acids are converted into acyl-CoA and enter the fatty acid oxidation where it is converted into acetyl-CoA. Essential amino acids can form new proteins or induce mTORC1 to promote glycolysis. Glutamine provides TCA cycle intermediates, glutaminase catalyzes the hydrolysis of glutamine to glutamate. G6-P: Glucose 6-phosphate; 3-PG: 3-Phosphoglycerate; α -KG: α -ketoglutarate; TCA: tricarboxylic acid cycle; FAO: Fatty acid oxidation. (*A higher resolution / color version of this figure is available in the electronic journal of the article.*)

Phosphofructokinase 1 (PFK-1), which is involved in the conversion of fructose-6-phosphate (F6P) to fructose-1,6-bisphosphate (F1,6P₂), is the main rate-limiting reaction in the glycolytic pathway and is noticeably overactive in cancer cells and primary tumor tissues [9, 25, 26]. It has been reported that Src, a proto-oncogene with kinase activity responsible for the transformation of chick-embryo fibroblasts by the Rous sarcoma virus, activates PFK-1 in immortalized cells [27]. Among the four PFK-2 isozymes (PFKFB1, PFKFB2, PFKFB3, and PFKFB4), only PFKFB3 has the highest kinase/phosphatase activity ratio and acts as a powerful activator of glycolysis [28, 29]. PFKFB3 regulates the cyclin-dependent kinase 1 and connects glycolysis to cell proliferation and survival in tumor cells. It is essential for cell cycle progression and apoptosis inhibition [30, 31]. An overexpression of PFKB3 in cancer cells maintains higher levels of fructose-2,6-bisphosphate that further activate the glycolytic enzyme, PFK-1. Since PFKFB3 displays the highest ratio of

kinase/phosphatase activity, it is hypothesized that PFKFB3 may contribute to the high glycolytic flux observed in transformed cells relative to their normal counterparts [28, 32, 33]. Moreover, several primary and aggressive human lung, breast, colon, prostatic, pancreatic and ovarian adenocarcinomas present a PFKFB3 overexpression in relation to normal tissues [33]. Also, it has been reported that HER 2 (human epidermal growth factor receptor-2) constitutive signaling increases PFKFB3 expression and glucose metabolism in breast cancer cells [34].

Pyruvate kinase (PKM2), which converts phosphoenolpyruvate (PEP) to pyruvate, regulates lactate production and glycolytic flux in cancer cells. The overexpression of PKM2 in gastric cancer cells has been outlined by many researchers and the increased activity of PKM2 is well correlated with metastasis and advanced tumor stage and size [35]. Although PKM2 seems to be related to increased aerobic glycolytic flux, the transport of pyruvate into the mitochondrial matrix

is significantly impaired in cancer cells. Mitochondrial pyruvate carrier (MPC) is a transmembrane protein complex comprised of two MPC1 and MPC2 subunits, and both isoforms are essential for pyruvate transport from the cytosol to the mitochondrial matrix [36-38]. Interestingly, depletion or low levels of the MPC1 protein have been associated with common features of multiple malignant cancer types and indicators of poor prognosis [38]. In this sense, MPC1 and MPC2 protein expression was found to be significantly down-regulated in hepatocellular carcinoma tissue [39].

Pyruvate dehydrogenase (PDH) catalyzes the conversion of pyruvate to acetyl-CoA, the entry substrate for the TCA cycle. The activity of PDH could be inhibited by overexpression of pyruvate dehydrogenase kinase (PDK). With regards to PDK, its activity is regulated by the concentration of the metabolic products such as pyruvate, NADH and acetyl-CoA [7]. Among its isoenzymes, pyruvate dehydrogenase kinase-1 (PDK1) is a key regulator of glycolysis and oxidative phosphorylation, and its expression is increased via hypoxia inducible factor-1 α (HIF-1 α) in a variety of tumors [40, 41]. In this context, the inhibition of PDK3 reverses the Warburg effect by reducing lactate concentration in the tumor microenvironment.

Lactate dehydrogenase (LDH) catalyzes the conversion of pyruvate to lactate by the simultaneous conversion of NADH to NAD⁺. LDH isoenzymes are tetramers of either heart (H) or muscle isoform (M). The M isoform predominates in the skeletal muscle and is mostly related to anaerobic metabolism and pyruvate reduction, while the H form predominates in the cardiac muscle, regulating the aerobic oxidation of pyruvate [42, 43]. Among the LDH isoforms, increased LDHA expression and activity contribute to the Warburg effect, regulation of growth and metastasis of cancer cells. However, the inhibition of LDHA negatively regulates tumor growth and metastasis in cancer cells [44-46].

Over the past decades, advances in cancer cell biology have unveiled more relevant details about the Warburg effect and aerobic glycolysis. Currently, it has been accepted that the Warburg effect is not anymore compatible with all tumors and cancer cell lines, and thus the phenomenon of aerobic glycolysis is now challenged by the knowledge of a large number of cells with mitochondrial function. In this scenario, it has been reported that ATP derived from aerobic glycolysis constitutes only a part of the total ATP present in various cancer cells [47, 48]. In fact, the ATP production by glycolysis is highly dependent on cell type and

could account for 0.31% (fibrosarcoma) or 64% (hepatoma), while the remaining ATP is derived from mitochondrial oxidative phosphorylation [47]. If the Warburg effect is not a common characteristic across all tumors, it is likely that a dynamic interplay exists between oxidative and glycolytic metabolism.

2.2. Amino Acid Metabolism

Amino acid metabolism has been a focus of cancer researchers because of its relevance to the metabolic reprogramming of proliferating cells. In addition, many enzymes related to amino acid metabolism are described as immunosuppressive in the tumor microenvironment and are therefore targets for cancer therapy [49]. Amino acid metabolism in cancer cells varies with the tissue of origin, cancer subtype, microenvironment and oncogenic driver mutations [50]. Oncogenesis relies on amino acids metabolism for protein synthesis, and also as a source of energy and metabolites [51]. Here, we will focus on some amino acids (*e.g.*, arginine, tryptophan, serine, glycine, glutamine and the branched-chain amino acids leucine, isoleucine, and valine) which are of great relevance for cancer cell proliferation and metabolic reprogramming.

Whereas arginine is a non-essential amino acid for healthy humans, it is conditionally essential for cancer cells. Although contradictory, many cancer cells lack the enzyme argininosuccinate synthetase 1 (ASS1), which catalyzes the conversion of citrulline to argininosuccinate during arginine synthesis, indicating the strong dependence of exogenous arginine for cancer cell growth [52-54]. In this context, cells such as bladder cancer cells with low ASS1 levels could not grow in arginine-free media, indicating that ASS1 behaves as a tumor suppressor [55]. Currently, five enzymes (nitric oxide synthase, glycine amidinotransferase, arginine decarboxylase, arginase and arginine deiminase) have been reported to be responsible for catabolizing free arginine [56]. Regarding arginine catabolite enzymes related to cancer promotion, it has been documented that high expression of arginase induces polyamine accumulation, which could interact with the oncogenes Myc and KRAS, thus promoting a rapid growth rate of cancer cells [57]. Arginase is a metabolizing enzyme that hydrolyzes arginine to ornithine and urea. It has been reported that arginase suppression by *n*-hydroxyarginine could reduce the intracellular polyamine content reflecting on the proliferation of cancer cells [58, 59].

Tryptophan catabolism is an important metabolic pathway for cancer cells to prevent immune responses.

Indoleamine-2,3-dioxygenase (IDO) and tryptophan-2,3-dioxygenase (TDO) are related to the conversion of tryptophan into kynurenine via the kynurenine pathway [60, 61]. While IDO is the most intensely studied enzyme associated with tryptophan catabolism and can suppress T-cell responses promoting cancer cell survival, TDO is an immunosuppressive enzyme, which is overexpressed in carcinomas and melanomas [62-64]. According to Uyttenhove *et al.* (2003), transfected mice with an IDO-negative subline of the mouse tumor model P815B overcame tumor challenge and remained alive. However, animals transfected with IDO-positive cells developed progressive tumors and died, proving the relevance of the IDO enzyme for tryptophan synthesis and tumor cell progression [63].

The metabolism of serine and glycine are interconnected via the glycine cleavage system, a major metabolic pathway in one-carbon metabolism that provides cofactors for purine and pyrimidine biosynthesis in proliferating cancer cells (Fig. 1) [65, 66]. An increased capacity for *de novo* serine synthesis via the phosphoglycerate dehydrogenase (PHGDH) pathway has been described in cancer cells. During glycolysis, PHGDH is responsible for the oxidation of approximately 10% of 3-phosphoglycerate by converting this glycolytic intermediary to 3-phosphohydroxypyruvate, which is subsequently transaminated and dephosphorylated, ultimately forming serine [67]. The marked attenuation of tumor growth and survival of pancreatic cancer cells in PHGDH-knockout mice has been reported [68]. Apart from PHGDH, serine hydroxymethyl transferase (SHMT), which converts serine into glycine, has also been implicated in tumorigenesis. The two isoforms of SHMT, cytoplasmic SHMT1 and mitochondrial SHMT2, were described as downstream effectors of c-Myc function and rescued the growth defects of c-Myc-null cells [69].

Another relevant amino acid for cell metabolism that is conditionally essential for cancer cell proliferation is glutamine. Glutamine provides TCA cycle intermediates, suppresses oxidative stress, protects mitochondrial membrane integrity and promotes cell survival and proliferation (Fig. 1) [70, 71]. Glutaminases (GLS1 and GLS2), which catalyzes the hydrolysis of glutamine to glutamate, play different roles in tumorigenesis. While GLS1 acts as a tumor promoter [72-75], GLS2 is strongly relevant to suppress tumor growth [76-79]. The effect of GLS1 on colorectal cancer cell was studied by Xiang and colleagues (2019), who showed that HIF-1 stimulates the expression of GLS1, which promoted colorectal cancer cell migra-

tion, invasion, and metastasis [75]. In addition, some studies confirmed the reduction in expression of GLS2 in hepatocellular carcinoma (HCC) [74, 76-78]. Concerning the role of GLS2 in cancer, it has been shown that GLS2 is able to inhibit the growth and colony formation of HCC cells *in vitro* as well as the growth of HCC xenograft tumors *in vivo* [76-78].

In addition to the above-mentioned amino acids, cancer cells also preferentially use branched-chain amino acids (BCAAs), such as leucine, isoleucine, and valine, to support their biosynthetic demands and nutrient signals [49, 80, 81]. Mitochondrial branched-chain aminotransferase 1 (BCAT1) and branched-chain aminotransferase 2 (BCAT2), which catalyze the conversion of BCAAs into their corresponding branched-chain α -keto acids and thereby generate glutamate, are overexpressed in many cancer cells [82, 83]. High expression of BCAT1 and BCAT2 contributes to cancer cell proliferation in acute myeloid leukemia (AML) and pancreatic ductal adenocarcinoma [82, 84]. In addition, it was shown that the expression of BCAT1 is associated with high levels of mTOR activity [83]. Taken together, these data strongly suggest that amino acid metabolism may represent an important focus for future studies into unmasking the relevance of amino acids for sustained cancer cell proliferation.

2.3. Fatty Acid Metabolism

Fatty acids (FAs) can be obtained endogenously, from the breakdown of triacylglycerols (TAG) and/or phospholipids, or exogenously, from daily meals, (Fig. 1) and are essential nutrients required for energy storage and for lipid and cell membrane synthesis. Additionally, FAs are very relevant as important precursors in the production of signaling molecules. Changes in the metabolism of FAs, lipids and cholesterol in cancer cells have already been reported with suggestions that this might play a relevant role for cancer progression [85].

In several types of cancer cells, FA catabolism is preferentially used to fuel growth, a deduction which is based on the observation that the enzymes required for FA oxidation are overexpressed in these cells [14]. Interestingly, FAs can be guided towards lipid biosynthesis (anabolism) or fatty acid oxidation (catabolism), however, the manner in which cells adapt to the distinct anabolic or catabolic pathways to channel fatty acids is currently poorly understood. Metabolism of FAs is regulated by AMP-activated protein kinase (AMPK), which is activated by the increase in the AMP:ATP ratio. AMPK negatively regulates the activity of sev-

eral enzymes and transcription factors related to anabolism of FAs and lipids, while positively mediates the activity of catabolic enzymes [86]. In this context, tumor cells use FAs as catabolic substrates, and the high contents of NADH and/or NADPH generated sustain ATP production, redox homeostasis, and biosynthetic reactions ensuring cell survival and proliferation [87]. In solid tumors, the activation of fatty acid oxidation (FAO) promotes the survival of triple-negative breast cancer cells during metabolic stress triggered by the lack of cell adhesion to the extracellular matrix [88]. In glioblastoma cells, FAO inhibition is critical for cell survival and maintenance of ATP and NADPH levels [88].

Lipid synthesis has also been recognized as another aberrant and common process related to carcinogenesis and contributes to rapid cell proliferation and decreased drug sensitivity [88, 89]. To support lipid synthesis, cancer cells are forced to find alternative routes for the preparation of acetyl-CoA, the precursor for lipid synthesis, since the shift from respiratory metabolism to aerobic glycolysis inactivates PDH by PDK1 [90, 91]. In this context, the pool of acetyl-CoA for lipid synthesis comes from the activities of ATP-driven catalysis of citrate lyase (ACLY) or acetyl-CoA synthetase (ACSS). ACLY is a cytosolic enzyme responsible for the conversion of citrate to cytosolic acetyl-CoA, and its relevance for cancer cell survival and growth has been reported [92, 93]. Under metabolic stress conditions (e.g., nutrient starvation or hypoxia), the high expression and activity of acetyl-CoA synthetase 2 (ACSS2) promote cancer cell growth due to the consumption of acetate as an alternative source of nutrient for fatty acid, cholesterol and isoprenoids biosynthesis [94, 95]. Long-chain acyl-CoA has several functions, such as serving as the backbone for the synthesis of lipids (e.g., TAGS and phospholipids) and bioactive lipids (e.g., signaling lipids). The acyl-CoA synthetase long-chain family (ACSLs) comprises an array of enzymes (ACSL1, ACSL3, ACSL4, ACSL5, and ACSL6) which are responsible for the activation of the most abundant long-chain fatty acids and are commonly deregulated in cancer cells [96]. It has been reported that different types of cancer (e.g., colorectal, breast, prostate, liver, and lung) present at least one upregulated ACSL isoform [97-104]. Thus, these studies demonstrate that ACSL overexpression could be related to changes in energy metabolism in favor of glucose consumption, increases in FAs and lipid/lipid droplets synthesis, high invasion and proliferation, survival during hypoxia and chemotherapy resistance [97, 105, 106]. Despite all the negative aspects concerning

the activity of ACSL isoforms, it seems that this family of proteins could be used for diagnosis, prognosis, and a good target for cancer therapy.

3. GENETIC INFLUENCES ON TUMOR CELL METABOLISM

Cancer is mostly caused by extrinsic or intrinsic factors, which could be prevented by tumor suppressor genes. Although the role of tumor suppressor proteins is crucial for cellular response against cell cycle deregulation, such proteins are also important for the regulation of energy metabolism. In this context, mutations in proto-oncogenes or tumor suppressor genes, such as *PI3K*, *HIF*, *MYC*, and *p53*, are closely related to changes in tumor cell metabolism [107].

Phosphatidylinositol-3-kinase (PI3K) comprises a family of proteins involved in the phosphorylation of phosphatidylinositol-4,5-bisphosphate (PIP₂) to phosphatidylinositol-3,4,5-triphosphate (PIP₃), which recruits and activates AKT (also known as PKB) via the PIP₃-PDK1 (phosphoinositide-dependent kinase 1) pathway. In this context, PI3K regulates several cellular processes, such as energy metabolism, protein synthesis, cell survival, proliferation, angiogenesis, and apoptosis [108]. It has been demonstrated that hyperactivation of PI3K also triggers other downstream kinases (e.g., mTORC1 and mTORC2) strongly related to glucose catabolism and lipidogenesis. With respect to glucose catabolism, AKT prompts aerobic glycolysis by multiple forms, such as increasing glucose uptake by the overexpression of glucose transporters (GLUT1, GLUT2 and GLUT4) and translocation of GLUT4 to the cell membrane, and stimulation of mTORC1 pathways, which activates HIF1, itself a key player for induction of *HK2* and *LDH* gene expression [109, 110]. Moreover, AKT is also related to the activation of PFK1 [111]. In lipidogenesis, AKT positively regulates the activity of ACLY and indirectly induces, via phosphorylation of the NRF2 transcription factor, the expression of 6-phosphogluconate dehydrogenase (*PGD*), glucose-6-phosphate dehydrogenase (*G6PD*) and malic enzyme 1 (*ME1*) genes, thus stimulating the synthesis of acetyl-CoA and NADPH required for FAs and lipid synthesis [112, 113]. The catalytic subunit of PI3K, p110 α , encoded by the *PIK3CA* gene, seems to be mutated in 20-40% of breast cancer instances [114]. In addition, it has been reported that PI3K E542K and E545K mutation is related to the activation of AKT/GSK3 β / β -catenin signaling, which activates glycolysis and generates the energy fuel for cancer cell proliferation [115]. Sobhani *et al.* (2018), performed a meta-

analysis study of 1,929 breast cancer cases reported in the literature in order to investigate the role of *PIK3CA* mutational status as a prognostic factor and predictor of response to anti-cancer treatments [116]. This investigation revealed that mutation in *PIK3CA* is a negative prognostic factor, thus providing a relative indication of the aggressiveness of all subtypes of breast cancer [116].

The hypoxia inducible factor (HIF) family plays a critical role in various stages of carcinogenesis and enables cells to adapt to hypoxic environments. The HIF family comprises a protein heterodimer fashioned by the interaction of one alpha (HIF-1 α , HIF-2 α , HIF-3 α) and one beta (ARNT, ARNT2) subunit which forms a functional complex which is tasked to regulate the expression of genes to preserve cell survival under hypoxic environments [117, 118]. It has been reported that hypoxia stabilizes HIF-1 α in cancerous cells, leading to changes in nutrient uptake, glycolysis, waste handling, angiogenesis, apoptosis, and cell migration, which may promote tumor survival and metastasis [117-119]. In the context of energy metabolism, adaptation to hypoxia also causes a severe reprogramming of cancer cells to shift from oxidative to fermentative metabolism. In this situation, the activation of HIF-1 α induces the expression of several genes related to glycolysis, such as *GLUT1* and *GLUT3*, *HK1* and *2*, *PFK-L*, *ALD-A*, *GAPDH*, *PGK*, *PGAM1*, *ENO1*, *PYK*, *LDH* and *PFK2* [91, 120-126]. Moreover, either aggressiveness or low prognosis is also related to the expression of some glycolytic enzymes under the positive regulation of HIF-1 α [126].

The pleiotropic transcription factor Myc plays a relevant role in cell physiology. The capacity to bind, directly or guided by other cooperative transcription factors, to promoters up- or downregulating the expression of several genes might define its oncogenic or foremost physiological behavior. Myc has been considered to be one of the most commonly amplified proto-oncogene in human cancers and it is clear that the function of Myc, like other oncogenes such as Ras, is tissue-specific and its role in regulating energy metabolism is distinct in various cancer models [127, 128]. Despite the particularity observed between cancer cells, the contribution of Myc to aerobic glycolysis (Warburg effect) operates through the upregulation of a series of glycolytic genes, such as *GLUT1*, *HK2*, *PFK*, *ENO1* and *LDH* [129-133]. Paradoxically, Myc also stimulates mitochondria biogenesis and oxygen consumption in cancer cells. However, this attributed function is related to the activation of mitochondrial glutamine me-

tabolism, which feeds the TCA cycle for α -ketoglutarate oxidation [72, 91]. The capacity of Myc to upregulate genes related to both aerobic glycolysis and mitochondrial oxidation raised the question of how Myc could contribute to the Warburg effect or mitochondrial oxidation. It is thought that Myc upregulates PDK1 expression [91], which negatively affects the conversion of glycolytic pyruvate to acetyl-CoA by phosphorylating and inhibiting pyruvate dehydrogenase, which inhibits the entrance of acetyl-CoA into the TCA cycle. Moreover, by upregulating *LDH* gene expression Myc increases the conversion of pyruvate to lactate, which redirects the flux of substrates from mitochondrial oxidation to aerobic fermentation. Regarding the activation of mitochondrial oxidation, Myc directly upregulates the expression of glutamine transporters (*ASCT2* and *SLC7A25*) and indirectly enhances glutamine oxidation in mitochondria [72]. Thus, under non-hypoxic environment, Myc can positively regulate both processes together. In this context, it has been reported that Myc-induced liver tumors displayed increased glucose uptake and catabolism to generate lactate, and glutamine oxidation, thus increasing the quantities of TCA cycle intermediates [134]. However, unlike Myc-induced liver tumors, Myc-induced lung tumors displayed elevated lactate and glutamine levels, which were suggestive of increased glucose catabolism, but not glutamine catabolism [135]. Finally, Myc is also capable of upregulating lipid metabolism (FA, cholesterol and complex lipids synthesis) by activating the sterol regulatory element-binding protein 1 (SREBP1), which directly regulates FAs and lipid synthesis [136].

The transcription factor p53, encoded by the gene *TP53*, is the master tumor suppressor and regulates nutrients (*e.g.*, glucose, lipids, and amino acids) metabolism, oxidative phosphorylation, ROS generation and growth factors. While wild-type p53 acts to reduce glucose uptake and aerobic glycolysis through downregulation of glucose transporters such as *GLUT1* and *GLUT4*, mutated forms of p53 induce cancer cells to increase expression of those transporters and consequently to increase glucose consumption [137]. Moreover, p53 has also the capacity to inhibit glycolysis by activating the fructose-2,6-bisphosphatase TIGAR (TP53-induced glycolysis and apoptosis regulator), which is responsible for converting fructose-2,6-bisphosphate, a strong allosteric regulator of PFK1, into fructose-6-phosphate [138]. The regulatory role of p53 in glycolysis also entails the reduction of the activity and expression of phosphoglycerate mutase (PGM), which is related to the conversion of 3-phospho-

glycerate into 2-phosphoglycerate [139]. To circumvent the Warburg effect, p53 also upregulates the expression of SCO2 and GLS2, key partners related to mitochondrial oxidation, and downregulates the expression of ME1 and ME2, which are related to the generation of TCA substrates for biosynthesis and NADPH [140, 141]. Once cancer cells display a gain-of-function of deregulated or mutated p53, the genetic reprogramming regulated by this protein mostly contributes to the Warburg effect. In this context, it has been reported that HK2 is upregulated by mutant p53 in a hepatoma cancer cell line [142]. Also, p53 mutation downregulates the liver-specific isoform of glutaminase (GLS2) and thus affecting the control of ROS generation and DNA oxidation, both of which are related to cancer progression [78, 79]. In this context, *GLS2* as a p53 target gene is a relevant mediator for the suppression of cancer metastasis [79]. Moreover, since *GLS2* upregulation by p53 increases the TCA cycle and oxidative phosphorylation due to the increase of carbon flux, the lack of p53 normal activity may also decrease *GSL2* expression and oxidative phosphorylation, therefore contributing to the Warburg effect. As regards lipid metabolism, p53 blocks lipogenesis by inhibiting G6PD activity and represses the expression of SREBP1, which consequently impairs NADPH synthesis and the transcription of citrate lyase and fatty acid synthase, respectively [143, 144]. On the other hand, as a mechanism to stop cancer cell proliferation, p53 activates FAO by upregulating lipin (LPIN1) and guanidinoacetate N-methyltransferase (GAMT) expression, thus stimulating FAO rather than lipogenesis [145, 146].

Taken all together, PI3K, MYC and HIF-1 proto-oncogenes have the capacity to induce aerobic glycolysis by regulating key energy metabolic enzymes. On the other hand, the tumor suppressor *p53* shows an inhibitory effect on glycolysis and directly stimulates mitochondria oxidation. In this scenario, it seems that the switch on/off of the Warburg effect is mostly due to the suppression of *p53* (e.g., deregulation or mutations) and induction of *PI3K*, *MYC* and *HIF*. To an increasing extent, cancer research has focused on these metabolic regulators which, in turn, provide potential therapeutic targets for cancer therapy.

4. ANTITUMOR THERAPY BASED ON CANCER CELL METABOLISM INTERVENTION

The growth and proliferation of cancer cells rely on energy metabolic changes. This metabolic differentiation can be used as a target for therapy since cancer

cells may be dependent on specific metabolic processes or enzymes. In (Fig. 2), we illustrate some targets for intervention on cancer cell energy metabolism.

Targeting GLUT1 activity is a promising strategy for the development of drugs to treat cancer cell growth. Since high glucose uptake is a direct consequence of altered tumor metabolism, the activity of GLUT1 and GLUT3, as well as the consumption of glucose, can be exploited by using competitive inhibitors of this nutrient. For instance, resveratrol acts as a GLUT1 inhibitor, by direct interaction with the internal face of GLUT1, thus impairing glucose uptake in the human leukemic cell line, HL-60 [19, 147]. While uptake is a result of overexpression and high affinity of GLUT1 and GLUT3 transporters, glucose entrapment depends on high-speed glucose phosphorylation by the HK2 enzyme. 2-Deoxy-D-glucose (2-DG) is a glucose analog in which the 2-hydroxyl group is replaced by a hydrogen atom, so that it cannot undergo further aerobic glycolysis. Indeed, 2-DG is phosphorylated by hexokinase to produce 2-deoxyglucose-6-phosphate which accumulates within the cell and impairs the continuation of glycolysis [148]. The Warburg effect-targeting glucose analog, 2-(2-[2-(2-aminoethoxy) ethoxy]ethoxy)-D-glucose, has been synthesized in order to facilitate drug uptake by glucose transporters, thereby promoting its cellular accumulation. This glucose analog has demonstrated inhibition of glucose phosphorylation by HK2, indicating its interaction with the enzyme and thereby confirming the potential to facilitate intracellular trapping mechanisms for its conjugates [149].

Another class of interesting molecules designed for cancer therapy is the antimetabolic agents. These compounds prevent cell division by inhibiting DNA and/or RNA metabolism. Among the main antimetabolites are the antifolates, which block the action of folic acid, a cofactor for enzymes involved in the biosynthesis of serine, threonine, thymidine and purine. In doing so, they, therefore, inhibit the synthesis of RNA/DNA and proteins [3]. It is known that drug analogs of folic acid, such as methotrexate, inhibit dihydrofolate reductase, the enzyme responsible for converting dihydrofolate into tetrahydrofolate which subsequently inhibits the production of thymidylate, which is essential for DNA replication. The success of therapies based on antagonizing the action of folic acid prompted the search for agents that interfere with the synthesis of nucleotides. From this perspective, nucleoside analogs such as 5-fluorouracil, gemcitabine and fludarabine, have been used in the treatment of different types of tumors [107].

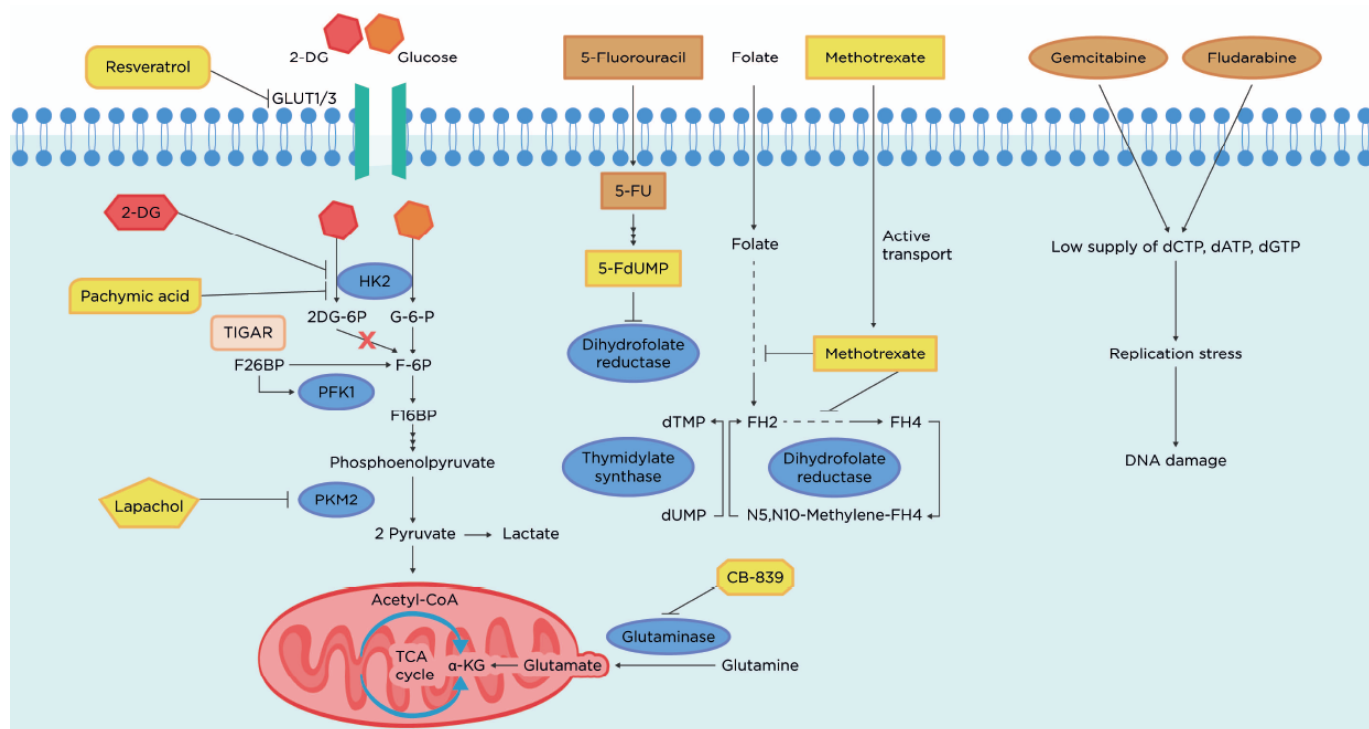


Fig. (2). Some therapeutic targets/drugs designed to intervene cancer metabolism. Resveratrol acts as GLUT1 inhibitor; inhibits the glucose uptake in human leukemic cells by a direct interaction with the internal face of GLUT1. The 2-deoxy-D-glucose (2-DG) is a glucose analog that cannot undergo further aerobic glycolysis, after phosphorylation by hexokinase to produce 2-deoxyglucose-6-phosphate; it accumulates in the cell and continues the glycolytic pathway so that the activity of HK2 is inhibited to perform the further steps of glycolysis. The triterpenoid pachymic acid (PA), can also act as HK2 inhibitor, impair glucose metabolism and down-regulate glycolysis. TIGAR reduces the activity of PFK1 by reducing the level of fructose 2,6-bisphosphate (F2,6BP) resulting in *glycolysis* inhibition, decreased proliferation and increased apoptosis. Lapachol presents an inhibitory effect on PKM2 activity, which is related to the reduction of ATP levels. Glutamine catabolism starts with the conversion of glutamine to glutamate, which is converted into α -ketoglutarate for further metabolism in the tricarboxylic acid (TCA) cycle. CB-839, as glutaminase inhibitor, significantly inhibits tumor growth. Folic acid analogue drugs, such as methotrexate and 5-fluorouracil inhibit dihydrofolate reductase, the enzyme responsible for converting dihydrofolate into tetrahydrofolate that inhibits the production of thymidylate, which is essential for DNA replication. Moreover, nucleoside analogs such as gemcitabine and fludarabine induce replicative stress followed by DNA damage. (A higher resolution / colour version of this figure is available in the electronic copy of the article).

Since the glycolytic enzymes PFK1, HKs and PKM2 are overexpressed in cancer cells and are considered as major regulators of aerobic glycolysis (the Warburg effect), these molecules became ideal potential targets for cancer therapy. Recently, it has been reported that lapachol presents an inhibitory effect on the activity of PKM2, which is related to the reduction of ATP levels and the impairment of melanoma cell proliferation [150]. In 2019, Miao and coworkers described the triterpenoid pachymic acid (PA), derived from *Poria cocos*, as delivering high anti-cancer activity [151]. Although the exact mechanism of action of PA remains to be fully elucidated, it is known to disrupt cancer cell proliferation mainly by the impairment of glucose metabolism. In this context, PKM2 and HK2 were discovered to be new targets for PA. However,

while PA showed an inhibitory effect on HK2, the triterpenoid was found to activate PKM2. Although this appears somewhat contradictory, by decreasing HK2 and activating PKM2, the levels of glycolytic intermediates can be converted into the pentose phosphate pathway intermediates, 6-PGA will be reduced, which thus impacts on NADPH production for ROS elimination [151]. Furthermore, PA affects aerobic glycolysis by decreasing glucose uptake and lactate production, causes HK2 dissociation from mitochondria, and it also induces apoptosis due to the activation of c-Jun N-terminal kinase (JNK), as well as interfering with endoplasmic reticulum (ER) stress pathways [152]. Another promising strategy to inhibit HK2 was tested in liver cancer cells and xenograft models. Shili Xu and colleagues (2018) used a doxycycline-inducible

shRNA silencing system to evaluate the consequence of HK2 knockdown [153]. Unlike HK1⁺/HK2⁺ cancer cells, HK1⁻/HK2⁺ showed increased sensitivity to HK2 silencing-induced cytostasis. Thus, the selective inhibition of the HK2 isoform appears to be a promising therapy for HK2⁺ cancer cells [153].

Investigation into amino acid (*e.g.*, tryptophan, arginine and/or glutamine) metabolism and their associated enzymes has provided valuable insights into the regulation of energy metabolism in the tumor microenvironment. Several amino acid metabolism inhibitors, which are used alone or in combination with established chemotherapy drugs, have now reached the stage of clinical trials. It has been reported that CB-839, a glutaminase inhibitor, significantly impedes tumor growth in a patient-derived xenograft model of breast cancer, which has the characteristic of higher gene/protein expressions of enzymes involved in the conversion of glutamine to proline [154].

The PI3K, Myc, HIF-1, and p53 signaling pathways are the most commonly disturbed processes encountered in cancer cells. Indeed, deregulation of these signaling pathways can be crucial for the survival, proliferation, migration, differentiation, and chemo- or radiotherapy resistance of transformed cells. Once the importance of these regulators in the control cancer progression was realized, several attempts were made to design and synthesize drug inhibitors to either target these proteins directly or interfere with any components of their signaling pathways.

As regards PI3K, several inhibitors presenting distinct mechanisms of action (*e.g.*, dual PI3K/mTOR inhibitors, pan-PI3K inhibitors and isoform-specific inhibitors) were synthesized, and they gave excellent results in preclinical investigations and also in clinical trials (phase I, II and III). Among the drugs designed to target PI3K, the dual PI3K/mTOR inhibitor, Gedatolisib, which is an efficient ATP competitor of PI3K and mTOR kinases, attenuated cell cycle progression and induced apoptosis in tumor cells [155]. Currently, Gedatolisib has reached phase III in clinical trials, and investigations are ongoing to determine the efficacy of this drug against different cancers [155]. Copanlisib, a potent inhibitor of PI3K, has been approved by the FDA and is currently the focus of several investigations regarding its efficacy, either alone or in combination with other chemotherapy drugs (undergoing clinical trials phase I, II and III) [156-158]. As regards isoform-specific inhibitors, Duvelisib (inhibitor of PI3K- δ and - γ isoforms) and Idelalisib (inhibitor of PI3K δ isoform)

have both achieved FDA approval and several clinical trials (*e.g.*, phase I, II and III) are underway [159-162].

One of the biggest challenges in cancer therapy is to successfully target cancer cells in hypoxic environments and thus circumvent the chemoresistance of these hypoxic cancer cells. Since HIF-1 is the key regulator of the response of cells to hypoxia and this environment is crucial for the development of cancer, many research groups have sought to develop therapies to block the cell signaling pathways mediated by the HIF-1 protein. After many unsuccessful attempts of preparing molecules that were selective and specific for blocking the HIF-1 signaling pathway, the strategy changed to creating non-selective compounds (*e.g.*, 17-AAG, Topotecan, CCI-779, Trastuzumab) capable of inhibiting the function of proteins that are components of HIF-1 signaling [163-167]. Indeed, the HIF-1 function can be affected by interfering with its protein expression, heterodimerization, DNA binding, and transcriptional activity [163]. During the last three decades, several studies were performed in order to demonstrate the potential application of hypoxia-activated prodrugs in cancer chemotherapy. These prodrugs were developed to circumvent the restrictive pharmacokinetics and/or cytotoxicity of drugs that had previously failed in preclinical trials [168]. These drugs are activated, either by a one or two-electron reduction or by the release of its carrier, only when in contact with a reductive environment, such as hypoxia [169]. Despite the chemical relevance of this class of drugs, the development of this area has received very little attention and has presented fewer positive feedbacks from clinical trials [163].

The Myc protein is seemingly an interesting target in the field of selective cancer drug therapy. However, until now the promising strategies encountered to block Myc activity have been based on targeting some components of Myc transcription, translation, stability or activation. Several drugs, such as roscovitine, flavopiridol and rapamycin, are inhibitors of Myc transcription and translation. Roscovitine and flavopiridol downregulate Myc expression by inhibiting the activity of the bromodomain-containing protein, BRD4, and the cyclin-dependent kinases, CDK7 and CDK9. On the other hand, rapamycin and its derivatives inhibit Myc translation by binding and inhibiting mTOR kinase activity [170-173]. The interference on Myc stability and activation is also a promising target strategy. Small nonpeptide molecules such as MLN8237, BI 6727, and 10058-F4 can bind and block the function of important proteins related to Myc activation (*e.g.*, AURKA,

PLK1 and Max) [174-176]. The heterodimerization of Myc with Max, which is crucial for Myc activation and recognition of specific promoters of genes related to energy metabolism and proliferation, can be disrupted by the small-molecule 10058-F4 [176].

The tumor suppressor protein p53 is a key player in controlling the transcription of genes related to energy metabolism, cell cycle arrest, apoptosis, and DNA repair. On the other hand, the mutant p53 protein displays a gain-of-function, which, among several other changes, promotes an increase in aerobic glycolysis (the Warburg effect). As is the case for other oncogenes, the mutant p53 protein can be a therapeutic target. In this respect, the following three main avenues have been explored to abrogate the mutant p53 function: restoration of normal p53 function, depletion of mutant p53, and inhibition of components of p53 signaling pathways [177]. Since the p53 mutant lacks transcriptional activity, several compounds such as STIMA-1, PRIMA-1 and MIRA stabilize and restore the native conformation and activity of p53 [178-180]. Moreover, numerous compounds that deplete mutant p53, including the Hsp90 inhibitors geldanamycin and ganetespib, arsenic trioxide and disulfiram, have also been reported and have reached clinical trials [177, 181, 182].

Altogether, it remains a difficult task to create compounds that selectively target and inhibit the activity of enzymes and transcriptional regulators related to energy metabolism. However, the findings that many potential drugs have achieved excellent results in clinical and preclinical trials encourage us to believe that a cure for cancer can be achieved by attacking the energy metabolism of the cancer cells.

CONCLUSION

Since the discovery of glucose metabolism reprogramming, a growing interest in understanding the metabolism of cancer cells has been pursued for the ideal of developing much better therapeutics. Seemingly, cancer cells favor the flux of energy metabolism to aerobic glycolysis (the Warburg effect). However, deregulated anabolism/catabolism of FAs and amino acids, especially glutamine, serine and glycine, have been shown to function as metabolic regulators to maintain cancer cell growth and survival. Also, changes in the expression and activity of proto-oncogenes or tumor suppressors may lead to alteration in nutrient uptake and metabolism to support several processes related to cell proliferation, differentiation, resistance to chemotherapy, and metastasis. Hence, further insights into the

biology and the energy metabolism of cancer cells could facilitate the development of metabolism-based drugs for cancer therapy. Given that the road to discover an effective therapy against different types of cancer will be long and arduous, we should learn from our past and look to the horizon to develop new strategies that are more selective and specific and also less detrimental to the patient.

LIST OF ABBREVIATIONS

2-DG	= 2-Deoxy-D-glucose
3-PG	= 3-Phosphoglycerate
5-FdUMP	= 5-Fluoro-2'-deoxyuridylate
5-FU	= 5-Fluorouracil
6-PGA	= 6-Phosphogluconic acid
6-PGD	= 6-Phosphogluconate dehydrogenase
ACLY	= Citrate lyase
ACSLs	= Acyl-CoA synthetase long-chain family
ACSS	= Acetyl-CoA synthetase
ACSS2	= Acetyl-CoA synthetase-2
ALD-A	= Aldehyde dehydrogenase-A
AML	= Acute myeloid leukemia
AMP	= Adenosine 5'-monophosphate
AMPK	= AMP-activated protein kinase
ARNT	= Aryl hydrocarbon receptor nuclear translocator
ARNT2	= Aryl hydrocarbon receptor nuclear translocator-2
ASS1	= Argininosuccinate synthetase 1
ATP	= Adenosine 5'-triphosphate
AURKA	= Aurora kinase A
BCAAs	= Branched-chain amino acids
BCAT1	= Mitochondrial branched-chain aminotransferase-1
BCAT2	= Mitochondrial branched-chain aminotransferase-2
BRD4	= Bromodomain-containing protein
CDK7	= Cyclin-dependent kinases-7
CDK9	= Cyclin-dependent kinases-9
dATP	= Deoxyadenosine triphosphate
dCTP	= Deoxycytidine triphosphate

dGTP	= Deoxyguanosine triphosphate	MPC2	= Mitochondrial pyruvate carrier-2
dTMP	= Deoxythymidine monophosphate	NADH	= Nicotinamide adenine dinucleotide
dUMP	= Deoxyuridine monophosphate	NADPH	= Nicotinamide adenine dinucleotide phosphate
ENO- α	= <i>Alpha</i> -enolase1	PA	= Pachymic acid
ER	= Endoplasmic reticulum	PDH	= Pyruvate dehydrogenase
F1,6BP	= Fructose-1,6-bisphosphate	PDK	= Pyruvate dehydrogenase kinase
F2,6BP	= Fructose-2,6-bisphosphate	PDK1	= Pyruvate dehydrogenase lipoamide kinase isozyme 1
F6P	= Fructose-6-phosphate	PDK3	= Pyruvate dehydrogenase kinase-3
FAO	= Fatty acid oxidation	PEP	= Phosphoenolpyruvate
FAs	= Fatty acids	PFK1	= Phosphofructokinase-1
FDA	= Food and drug administration	PFK-2	= Phosphofructokinase-2
FH2	= Dihydrofolate	PGAM-B	= Phosphoglycerate mutase
FH4	= Tetrahydrofolate	PGK	= Phosphoglycerate kinase
G6-P	= Glucose-6-phosphate	PGM	= Phosphoglycerate mutase
G6PD	= Glucose-6-phosphate dehydrogenase	PHGDH	= Phosphoglycerate dehydrogenase
GAMT	= Guanidinoacetate N-methyltransferase	PI3K	= Phosphoinositide-3-kinase
GAPDH	= Glyceraldehyde-3-phosphate dehydrogenase	PIP ₂	= Phosphatidylinositol-4,5-bisphosphate
GLS1	= Glutaminases-1	PIP ₃	= Phosphatidylinositol-3,4,5- triphosphate
GLS2	= Glutaminases-2	PIP ₃ -PDK1	= Phosphoinositide-dependent kinase-1
GLUT	= Glucose transporters	PKM2	= Pyruvate kinase isozymes M2
HER2	= Human epidermal growth factor receptor-2	PLK1	= Polo Like Kinase-1
HIF	= Hypoxia inducible factor	PYK	= Pyruvate kinase
HIF-1 α	= Hypoxia inducible factor-1 α	SCO2	= Synthesis of cytochrome C oxidase-2
HIF-2 α	= Hypoxia inducible factor-2 α	SHMT	= Hydroxymethyl transferase
HIF-3 α	= Hypoxia inducible factor-3 α	SHMT1	= Hydroxymethyl transferase-1
HK	= Hexokinases	SHMT2	= Hydroxymethyl transferase-2
HK2	= Hexokinases2	SREBP1	= Sterol regulatory element-binding protein-1
IDO	= Indoleamine-2,3-dioxygenase	TAG	= Triacylglycerols
JNK	= c-Jun N-terminal kinase	TCA	= Tricarboxylic acid
LDH	= Lactate dehydrogenase	TDO	= Tryptophan-2,3-dioxygenase
LDHA	= Lactate dehydrogenase-A	TIGAR	= TP53-induced glycolysis and apoptosis regulator
LPIN1	= Lipin	VDAC	= Voltage-dependent anionic channel
MAX	= MYC Associated Factor X	VDAC1	= Voltage-dependent anionic channel-1
ME1	= Malic enzyme-1	α -KG	= α -ketoglutarate
MPC	= Mitochondrial pyruvate carrier		
MPC1	= Mitochondrial pyruvate carrier-1		

CONSENT FOR PUBLICATION

Not applicable.

FUNDING

This work was financially supported by the Coordenação de Aperfeiçoamento de Pessoal de Nível Superior (CAPES n°88882.331359/2019-01 and n°88882.331336/2019-01), Conselho Nacional de Pesquisas e Desenvolvimento Tecnológico (CNPq n°313783/2018-7) and Fundação Carlos Chagas de Amparo à Pesquisa do Rio de Janeiro (FAPERJ n°E-26/010.002670/2014).

CONFLICT OF INTEREST

The authors declare no conflict of interest, financial or otherwise.

ACKNOWLEDGEMENTS

The authors would like to thank Dr. Malachy McCann (Department of Chemistry at the National University of Ireland Maynooth - NUIM, Co. Kildare, Ireland) for his valuable contribution to the critical review and editing of English.

REFERENCES

- [1] Vander Heiden, M.G.; Cantley, L.C.; Thompson, C.B. Understanding the Warburg effect: the metabolic requirements of cell proliferation. *Science*, **2009**, *324*(5930), 1029-1033. <http://dx.doi.org/10.1126/science.1160809> PMID: 19460998
- [2] Warburg, O.; Wind, F.; Negelein, E. The Metabolism of Tumors in the Body. *J. Gen. Physiol.*, **1927**, *8*(6), 519-530. <http://dx.doi.org/10.1085/jgp.8.6.519> PMID: 19872213
- [3] Cagan, R.; Meyer, P. Rethinking cancer: current challenges and opportunities in cancer research. *Dis. Model. Mech.*, **2017**, *10*(4), 349-352. <http://dx.doi.org/10.1242/dmm.030007> PMID: 28381596
- [4] Crabtree, H.G. Observations on the carbohydrate metabolism of tumours. *Biochem. J.*, **1929**, *23*(3), 536-545. <http://dx.doi.org/10.1042/bj0230536> PMID: 16744238
- [5] Wojtczak, L. The Crabtree effect: a new look at the old problem. *Acta Biochim. Pol.*, **1996**, *43*(2), 361-368. http://dx.doi.org/10.18388/abp.1996_4505 PMID: 8862181
- [6] Gatenby, R.A.; Gillies, R.J. Why do cancers have high aerobic glycolysis? *Nat. Rev. Cancer*, **2004**, *4*(11), 891-899. <http://dx.doi.org/10.1038/nrc1478> PMID: 15516961
- [7] Cairns, R.A.; Harris, I.; McCracken, S.; Mak, T.W. Cancer cell metabolism. *Cold Spring Harb. Symp. Quant. Biol.*, **2011**, *76*, 299-311. <http://dx.doi.org/10.1101/sqb.2011.76.012856> PMID: 22156302
- [8] Sussman, I.; Erecińska, M.; Wilson, D.F. Regulation of cellular energy metabolism: the Crabtree effect. *Biochim. Biophys. Acta*, **1980**, *591*(2), 209-223. [http://dx.doi.org/10.1016/0005-2728\(80\)90153-X](http://dx.doi.org/10.1016/0005-2728(80)90153-X) PMID: 7397121
- [9] Rodríguez-Enríquez, S.; Juárez, O.; Rodríguez-Zavala, J.S.; Moreno-Sánchez, R. Multisite control of the Crabtree effect in ascites hepatoma cells. *Eur. J. Biochem.*, **2001**, *268*(8), 2512-2519. <http://dx.doi.org/10.1046/j.1432-1327.2001.02140.x> PMID: 11298771
- [10] Diaz-Ruiz, R.; Rigoulet, M.; Devin, A. The Warburg and Crabtree effects: On the origin of cancer cell energy metabolism and of yeast glucose repression. *Biochim. Biophys. Acta*, **2011**, *1807*(6), 568-576. <http://dx.doi.org/10.1016/j.bbabi.2010.08.010> PMID: 20804724
- [11] Evtodienco YuV.; Teplova, V.V.; Duszyński, J.; Bogucka, K.; Wojtczak, L. The role of cytoplasmic [Ca²⁺] in glucose-induced inhibition of respiration and oxidative phosphorylation in Ehrlich ascites tumour cells: a novel mechanism of the Crabtree effect. *Cell Calcium*, **1994**, *15*(6), 439-446. [http://dx.doi.org/10.1016/0143-4160\(94\)90108-2](http://dx.doi.org/10.1016/0143-4160(94)90108-2) PMID: 8082127
- [12] Wojtczak, L.; Teplova, V.V.; Bogucka, K.; Czyz, A.; Makowska, A.; Wieckowski, M.R.; Duszyński, J.; Evtodienco, Y.V. Effect of glucose and deoxyglucose on the redistribution of calcium in ehrlich ascites tumour and Zajdela hepatoma cells and its consequences for mitochondrial energetics. Further arguments for the role of Ca²⁺ in the mechanism of the crabtree effect. *Eur. J. Biochem.*, **1999**, *263*(2), 495-501. <http://dx.doi.org/10.1046/j.1432-1327.1999.00522.x> PMID: 10406959
- [13] Maughan, R. Carbohydrate Metabolism. *Surg.*, **2009**, *27*(1), 6-10. <http://dx.doi.org/10.1016/j.mpsur.2008.12.002>
- [14] Boroughs, L.K.; DeBerardinis, R.J. Metabolic pathways promoting cancer cell survival and growth. *Nat. Cell Biol.*, **2015**, *17*(4), 351-359. <http://dx.doi.org/10.1038/ncb3124> PMID: 25774832
- [15] Moreno-Sánchez, R.; Rodríguez-Enríquez, S.; Marín-Hernández, A.; Saavedra, E. Energy metabolism in tumor cells. *FEBS J.*, **2007**, *274*(6), 1393-1418. <http://dx.doi.org/10.1111/j.1742-4658.2007.05686.x> PMID: 17302740
- [16] Augustin, R. The Protein Family of Glucose Transport Facilitators: It's Not Only about Glucose after All *IUBMB Life*, **2010**.
- [17] Frolova, A.I.; Moley, K.H. Glucose transporters in the uterus: an analysis of tissue distribution and proposed physiological roles. *Reproduction*, **2011**, *142*(2), 211-220. <http://dx.doi.org/10.1530/REP-11-0114> PMID: 21642384
- [18] Grabelus, F.; Nagarajah, J.; Bockisch, A.; Schmid, K.W.; Sheu, S-Y. Glucose transporter 1 expression, tumor proliferation, and iodine/glucose uptake in thyroid cancer with emphasis on poorly differentiated thyroid carcinoma. *Clin. Nucl. Med.*, **2012**, *37*(2), 121-127. <http://dx.doi.org/10.1097/RLU.0b013e3182393599> PMID: 22228332
- [19] Zambrano, A.; Molt, M.; Uribe, E.; Salas, M. Glut 1 in Cancer Cells and the Inhibitory Action of Resveratrol as A Potential Therapeutic Strategy. *Int. J. Mol. Sci.*, **2019**, *20*(13), 3374. <http://dx.doi.org/10.3390/ijms20133374> PMID: 31324056
- [20] Krzeslak, A.; Wojcik-Krowiranda, K.; Forma, E.; Jozwiak, P.; Romanowicz, H.; Bienkiewicz, A.; Brys, M. Expression of GLUT1 and GLUT3 glucose transporters in endometrial and breast cancers. *Pathol. Oncol. Res.*, **2012**, *18*(3), 721-728. <http://dx.doi.org/10.1007/s12253-012-9500-5> PMID: 22270867

- [21] Smith, T.A.D. Mammalian hexokinases and their abnormal expression in cancer. *Br. J. Biomed. Sci.*, **2000**, 57(2), 170-178.
PMID: 10912295
- [22] Wilson, J.E. Isozymes of mammalian hexokinase: structure, subcellular localization and metabolic function. *J. Exp. Biol.*, **2003**, 206(Pt 12), 2049-2057.
<http://dx.doi.org/10.1242/jeb.00241> PMID: 12756287
- [23] Anderson, M.; Marayati, R.; Moffitt, R.; Yeh, J.J. Hexokinase 2 promotes tumor growth and metastasis by regulating lactate production in pancreatic cancer. *Oncotarget*, **2016**, 8(34), 56081-56094.
<http://dx.doi.org/10.18632/oncotarget.9760> PMID: 28915575
- [24] Yoo, H-J.; Yun, B-R.; Kwon, J-H.; Ahn, H-S.; Seol, M-A.; Lee, M-J.; Yu, G-R.; Yu, H-C.; Hong, B.; Choi, K.; Kim, D-G. Genetic and expression alterations in association with the sarcomatous change of cholangiocarcinoma cells. *Exp. Mol. Med.*, **2009**, 41(2), 102-115.
<http://dx.doi.org/10.3858/emm.2009.41.2.013> PMID: 19287191
- [25] Hennipman, A.; Smits, J.; van Oirschot, B.; van Houwelingen, J.C.; Rijksen, G.; Neyt, J.P.; Van Unnik, J.A.M.; Staal, G.E.J. Glycolytic enzymes in breast cancer, benign breast disease and normal breast tissue. *Tumour Biol.*, **1987**, 8(5), 251-263.
<http://dx.doi.org/10.1159/000217529> PMID: 3448771
- [26] Hennipman, A.; van Oirschot, B.A.; Smits, J.; Rijksen, G.; Staal, G.E.J. Glycolytic enzyme activities in breast cancer metastases. *Tumour Biol.*, **1988**, 9(5), 241-248.
<http://dx.doi.org/10.1159/000217568> PMID: 2973647
- [27] Bosca, L.; Mojena, M.; Ghysdael, J.; Rousseau, G.G.; Hue, L. Expression of the v-src or v-fps oncogene increases fructose 2,6-bisphosphate in chick-embryo fibroblasts. Novel mechanism for the stimulation of glycolysis by retroviruses. *Biochem. J.*, **1986**, 236(2), 595-599.
<http://dx.doi.org/10.1042/bj2360595> PMID: 2944513
- [28] Sakakibara, R.; Kato, M.; Okamura, N.; Nakagawa, T.; Komada, Y.; Tominaga, N.; Shimojo, M.; Fukasawa, M. Characterization of a human placental fructose-6-phosphate, 2-kinase/fructose-2,6-bisphosphatase. *J. Biochem.*, **1997**, 122(1), 122-128.
<http://dx.doi.org/10.1093/oxfordjournals.jbchem.a021719> PMID: 9276680
- [29] Ros, S.; Schulze, A. Balancing glycolytic flux: the role of 6-phosphofructo-2-kinase/fructose 2,6-bisphosphatases in cancer metabolism. *Cancer Metab.*, **2013**, 1(1), 8.
<http://dx.doi.org/10.1186/2049-3002-1-8> PMID: 24280138
- [30] Gustafsson, N.M.S.; Färnegårdh, K.; Bonagas, N.; Ninou, A.H.; Groth, P.; Wiita, E.; Jönsson, M.; Hallberg, K.; Lehto, J.; Pennisi, R.; Martinsson, J.; Norström, C.; Hollers, J.; Schultz, J.; Andersson, M.; Markova, N.; Marttila, P.; Kim, B.; Norin, M.; Olin, T.; Helleday, T. Targeting PFKFB3 radiosensitizes cancer cells and suppresses homologous recombination. *Nat. Commun.*, **2018**, 9(1), 3872.
<http://dx.doi.org/10.1038/s41467-018-06287-x> PMID: 30250201
- [31] Rider, M.H.; Bertrand, L.; Vertommen, D.; Michels, P.A.; Rousseau, G.G.; Hue, L. 6-phosphofructo-2-kinase/fructose-2,6-bisphosphatase: head-to-head with a bifunctional enzyme that controls glycolysis. *Biochem. J.*, **2004**, 381(Pt 3), 561-579.
<http://dx.doi.org/10.1042/BJ20040752> PMID: 15170386
- [32] Chesney, J.; Mitchell, R.; Benigni, F.; Bacher, M.; Spiegel, L.; Al-Abed, Y.; Han, J.H.; Metz, C.; Bucala, R. An inducible gene product for 6-phosphofructo-2-kinase with an AU-rich instability element: role in tumor cell glycolysis and the Warburg effect. *Proc. Natl. Acad. Sci. USA*, **1999**, 96(6), 3047-3052.
<http://dx.doi.org/10.1073/pnas.96.6.3047> PMID: 10077634
- [33] Atsumi, T.; Chesney, J.; Metz, C.; Leng, L.; Donnelly, S.; Makita, Z.; Mitchell, R.; Bucala, R. High expression of inducible 6-phosphofructo-2-kinase/fructose-2,6-bisphosphatase (iPFK-2; PFKFB3) in human cancers. *Cancer Res.*, **2002**, 62(20), 5881-5887.
PMID: 12384552
- [34] O'Neal, J.; Clem, A.; Reynolds, L.; Dougherty, S.; Imbert-Fernandez, Y.; Telang, S.; Chesney, J.; Clem, B.F. Inhibition of 6-phosphofructo-2-kinase (PFKFB3) suppresses glucose metabolism and the growth of HER2+ breast cancer. *Breast Cancer Res. Treat.*, **2016**, 160(1), 29-40.
<http://dx.doi.org/10.1007/s10549-016-3968-8> PMID: 27613609
- [35] Wu, J.; Hu, L.; Chen, M.; Cao, W.; Chen, H.; He, T. Pyruvate kinase M2 overexpression and poor prognosis in solid tumors of digestive system: evidence from 16 cohort studies. *OncoTargets Ther.*, **2016**, 9, 4277-4288.
<http://dx.doi.org/10.2147/OTT.S106508> PMID: 27478385
- [36] Paradies, G.; Capuano, F.; Palombini, G.; Galeotti, T.; Papa, S. Transport of pyruvate in mitochondria from different tumor cells. *Cancer Res.*, **1983**, 43(11), 5068-5071.
PMID: 6616443
- [37] Palmieri, F.; Monné, M. Discoveries, metabolic roles and diseases of mitochondrial carriers: A review. *Biochim. Biophys. Acta*, **2016**, 1863(10), 2362-2378.
<http://dx.doi.org/10.1016/j.bbamcr.2016.03.007> PMID: 26968366
- [38] Bender, T.; Martinou, J-C. The mitochondrial pyruvate carrier in health and disease: To carry or not to carry? *Biochim. Biophys. Acta*, **2016**, 1863(10), 2436-2442.
<http://dx.doi.org/10.1016/j.bbamcr.2016.01.017> PMID: 26826034
- [39] Ma, X.; Cui, Y.; Zhou, H.; Li, Q. Function of mitochondrial pyruvate carriers in hepatocellular carcinoma patients. *Oncol. Lett.*, **2018**, 15(6), 9110-9116.
<http://dx.doi.org/10.3892/ol.2018.8466> PMID: 29805642
- [40] Lu, C-W.; Lin, S-C.; Chien, C-W.; Lin, S-C.; Lee, C-T.; Lin, B-W.; Lee, J-C.; Tsai, S-J. Overexpression of pyruvate dehydrogenase kinase 3 increases drug resistance and early recurrence in colon cancer. *Am. J. Pathol.*, **2011**, 179(3), 1405-1414.
<http://dx.doi.org/10.1016/j.ajpath.2011.05.050> PMID: 21763680
- [41] Lu, C-W.; Lin, S-C.; Chen, K-F.; Lai, Y-Y.; Tsai, S-J. Induction of pyruvate dehydrogenase kinase-3 by hypoxia-inducible factor-1 promotes metabolic switch and drug resistance. *J. Biol. Chem.*, **2008**, 283(42), 28106-28114.
<http://dx.doi.org/10.1074/jbc.M803508200> PMID: 18718909
- [42] Li, S.S.; Fitch, W.M.; Pan, Y.C.; Sharief, F.S. Evolutionary relationships of vertebrate lactate dehydrogenase isozymes A4 (muscle), B4 (heart), and C4 (testis). *J. Biol. Chem.*, **1983**, 258(11), 7029-7032.
PMID: 6853510
- [43] Baumgart, E.; Fahimi, H.D.; Stich, A.; Völkl, A. L-Lactate Dehydrogenase A- and AB Isoforms Are Bona Fide Peroxisomal Enzymes in Rat Liver. *J. Biol. Chem.*, **1996**, 271(7), 3846-3855.
<http://dx.doi.org/10.1074/jbc.271.7.3846> PMID: 8632003
- [44] Sheng, S.L.; Liu, J.J.; Dai, Y.H.; Sun, X.G.; Xiong, X.P.; Huang, G. Knockdown of lactate dehydrogenase A suppresses tumor growth and metastasis of human hepatocellular carcinoma. *FEBS J.*, **2012**, 279(20), 3898-3910.

- <http://dx.doi.org/10.1111/j.1742-4658.2012.08748.x> PMID: 22897481
- [45] Yao, F.; Zhao, T.; Zhong, C.; Zhu, J.; Zhao, H. LDHA is necessary for the tumorigenicity of esophageal squamous cell carcinoma. *Tumour Biol.*, **2013**, *34*(1), 25-31. <http://dx.doi.org/10.1007/s13277-012-0506-0> PMID: 22961700
- [46] Koukourakis, M.I.; Giatromanolaki, A.; Sivridis, E.; Gatter, K.C.; Harris, A.L. Tumour Angiogenesis Research Group. Lactate dehydrogenase 5 expression in operable colorectal cancer: strong association with survival and activated vascular endothelial growth factor pathway—a report of the Tumour Angiogenesis Research Group. *J. Clin. Oncol.*, **2006**, *24*(26), 4301-4308. <http://dx.doi.org/10.1200/JCO.2006.05.9501> PMID: 16896001
- [47] Zu, X.L.; Guppy, M. Cancer metabolism: facts, fantasy, and fiction. *Biochem. Biophys. Res. Commun.*, **2004**, *313*(3), 459-465. <http://dx.doi.org/10.1016/j.bbrc.2003.11.136> PMID: 14697210
- [48] Jose, C.; Bellance, N.; Rossignol, R. Choosing between glycolysis and oxidative phosphorylation: a tumor's dilemma? *Biochim. Biophys. Acta*, **2011**, *1807*(6), 552-561. <http://dx.doi.org/10.1016/j.bbabi.2010.10.012> PMID: 20955683
- [49] Ananieva, E. Targeting amino acid metabolism in cancer growth and anti-tumor immune response. *World J. Biol. Chem.*, **2015**, *6*(4), 281-289. <http://dx.doi.org/10.4331/wjbc.v6.i4.281> PMID: 26629311
- [50] Pavlova, N.N.; Thompson, C.B. The Emerging Hallmarks of Cancer Metabolism. *Cell Metab.*, **2016**, *23*(1), 27-47. <http://dx.doi.org/10.1016/j.cmet.2015.12.006> PMID: 26771115
- [51] Vazquez, A.; Kamphorst, J.J.; Markert, E.K.; Schug, Z.T.; Tardito, S.; Gottlieb, E. Cancer metabolism at a glance. *J. Cell Sci.*, **2016**, *129*(18), 3367-3373. <http://dx.doi.org/10.1242/jcs.181016> PMID: 27635066
- [52] Bobak, Y.P.; Vynnytska, B.O.; Kurlishchuk, Y.V.; Sibirny, A.A.; Stasyk, O.V. Cancer cell sensitivity to arginine deprivation *in vitro* is not determined by endogenous levels of arginine metabolic enzymes. *Cell Biol. Int.*, **2010**, *34*(11), 1085-1089. <http://dx.doi.org/10.1042/CBI20100451> PMID: 20653567
- [53] Dillon, B.J.; Prieto, V.G.; Curley, S.A.; Ensor, C.M.; Holtsberg, F.W.; Bomalaski, J.S.; Clark, M.A. Incidence and distribution of argininosuccinate synthetase deficiency in human cancers: a method for identifying cancers sensitive to arginine deprivation. *Cancer*, **2004**, *100*(4), 826-833. <http://dx.doi.org/10.1002/cncr.20057> PMID: 14770441
- [54] Patil, M.D.; Bhaumik, J.; Babykutty, S.; Banerjee, U.C.; Fukumura, D. Arginine dependence of tumor cells: targeting a chink in cancer's armor. *Oncogene*, **2016**, *35*(38), 4957-4972. <http://dx.doi.org/10.1038/onc.2016.37> PMID: 27109103
- [55] Allen, M.D.; Luong, P.; Hudson, C.; Leyton, J.; Delage, B.; Ghazaly, E.; Cutts, R.; Yuan, M.; Syed, N.; Lo Nigro, C.; Lattanzio, L.; Chmielewska-Kassassir, M.; Tomlinson, I.; Roylance, R.; Whitaker, H.C.; Warren, A.Y.; Neal, D.; Frezza, C.; Beltran, L.; Jones, L.J.; Chelala, C.; Wu, B.-W.; Bomalaski, J.S.; Jackson, R.C.; Lu, Y.-J.; Crook, T.; Lemoine, N.R.; Mather, S.; Foster, J.; Sosabowski, J.; Avril, N.; Li, C.-F.; Szlosarek, P.W. Prognostic and therapeutic impact of argininosuccinate synthetase 1 control in bladder cancer as monitored longitudinally by PET imaging. *Cancer Res.*, **2014**, *74*(3), 896-907. <http://dx.doi.org/10.1158/0008-5472.CAN-13-1702> PMID: 24285724
- [56] Fultang, L.; Vardon, A.; De Santo, C.; Mussai, F. Molecular basis and current strategies of therapeutic arginine depletion for cancer. *Int. J. Cancer*, **2016**, *139*(3), 501-509. <http://dx.doi.org/10.1002/ijc.30051> PMID: 26913960
- [57] Gerner, E.W.; Meyskens, F.L., Jr Polyamines and cancer: old molecules, new understanding. *Nat. Rev. Cancer*, **2004**, *4*(10), 781-792. <http://dx.doi.org/10.1038/nrc1454> PMID: 15510159
- [58] Singh, R.; Pervin, S.; Karimi, A.; Cederbaum, S.; Chaudhuri, G. Arginase activity in human breast cancer cell lines: N(omega)-hydroxy-L-arginine selectively inhibits cell proliferation and induces apoptosis in MDA-MB-468 cells. *Cancer Res.*, **2000**, *60*(12), 3305-3312. PMID: 10866325
- [59] Buga, G.M.; Wei, L.H.; Bauer, P.M.; Fukuto, J.M.; Ignarro, L.J. NG-hydroxy-L-arginine and nitric oxide inhibit Caco-2 tumor cell proliferation by distinct mechanisms. *Am. J. Physiol.*, **1998**, *275*(4), R1256-R1264. <http://dx.doi.org/10.1152/ajpregu.1998.275.4.R1256> PMID: 9756558
- [60] Mellor, A.L.; Munn, D.H. IDO expression by dendritic cells: tolerance and tryptophan catabolism. *Nat. Rev. Immunol.*, **2004**, *4*(10), 762-774. <http://dx.doi.org/10.1038/nri1457> PMID: 15459668
- [61] Huang, L.; Mellor, A.L. Metabolic control of tumour progression and antitumour immunity. *Curr. Opin. Oncol.*, **2014**, *26*(1), 92-99. <http://dx.doi.org/10.1097/CCO.000000000000035> PMID: 24305570
- [62] Godin-Ethier, J.; Hanafi, L.-A.; Piccirillo, C.A.; Lapointe, R. Indoleamine 2,3-dioxygenase expression in human cancers: clinical and immunologic perspectives. *Clin. Cancer Res.*, **2011**, *17*(22), 6985-6991. <http://dx.doi.org/10.1158/1078-0432.CCR-11-1331> PMID: 22068654
- [63] Uyttenhove, C.; Pilotte, L.; Théate, I.; Stroobant, V.; Colau, D.; Parmentier, N.; Boon, T.; Van den Eynde, B.J. Evidence for a tumoral immune resistance mechanism based on tryptophan degradation by indoleamine 2,3-dioxygenase. *Nat. Med.*, **2003**, *9*(10), 1269-1274. <http://dx.doi.org/10.1038/nm934> PMID: 14502282
- [64] Pilotte, L.; Larriue, P.; Stroobant, V.; Colau, D.; Dolusic, E.; Frédérick, R.; De Plaen, E.; Uyttenhove, C.; Wouters, J.; Masereel, B.; Van den Eynde, B.J. Reversal of tumoral immune resistance by inhibition of tryptophan 2,3-dioxygenase. *Proc. Natl. Acad. Sci. USA*, **2012**, *109*(7), 2497-2502. <http://dx.doi.org/10.1073/pnas.1113873109> PMID: 22308364
- [65] Snell, K. Liver enzymes of serine metabolism during neonatal development of the rat. *Biochem. J.*, **1980**, *190*(2), 451-455. <http://dx.doi.org/10.1042/bj1900451> PMID: 6781481
- [66] Kikuchi, G. The glycine cleavage system: composition, reaction mechanism, and physiological significance. *Mol. Cell. Biochem.*, **1973**, *1*(2), 169-187. <http://dx.doi.org/10.1007/BF01659328> PMID: 4585091
- [67] DeBerardinis, R.J. Serine metabolism: some tumors take the road less traveled. *Cell Metab.*, **2011**, *14*(3), 285-286. <http://dx.doi.org/10.1016/j.cmet.2011.08.004> PMID: 21907134
- [68] Ma, X.; Li, B.; Liu, J.; Fu, Y.; Luo, Y. Phosphoglycerate dehydrogenase promotes pancreatic cancer development by

- interacting with eIF4A1 and eIF4E. *J. Exp. Clin. Cancer Res.*, **2019**, *38*(1), 66.
<http://dx.doi.org/10.1186/s13046-019-1053-y> PMID: 30744688
- [69] Nikiforov, M.A.; Chandriani, S.; O'Connell, B.; Petrenko, O.; Kotenko, I.; Beavis, A.; Sedivy, J.M.; Cole, M.D. A functional screen for Myc-responsive genes reveals serine hydroxymethyltransferase, a major source of the one-carbon unit for cell metabolism. *Mol. Cell. Biol.*, **2002**, *22*(16), 5793-5800.
<http://dx.doi.org/10.1128/MCB.22.16.5793-5800.2002> PMID: 12138190
- [70] Lacey, J.M.; Wilmore, D.W. Is glutamine a conditionally essential amino acid? *Nutr. Rev.*, **1990**, *48*(8), 297-309.
<http://dx.doi.org/10.1111/j.1753-4887.1990.tb02967.x> PMID: 2080048
- [71] Wise, D.R.; Thompson, C.B. Glutamine addiction: a new therapeutic target in cancer. *Trends Biochem. Sci.*, **2010**, *35*(8), 427-433.
<http://dx.doi.org/10.1016/j.tibs.2010.05.003> PMID: 20570523
- [72] Gao, P.; Tchernyshyov, I.; Chang, T.-C.; Lee, Y.-S.; Kita, K.; Ochi, T.; Zeller, K.I.; De Marzo, A.M.; Van Eyk, J.E.; Mendell, J.T.; Dang, C.V. c-Myc suppression of miR-23a/b enhances mitochondrial glutaminase expression and glutamine metabolism. *Nature*, **2009**, *458*(7239), 762-765.
<http://dx.doi.org/10.1038/nature07823> PMID: 19219026
- [73] Wang, J.-B.; Erickson, J.W.; Fujii, R.; Ramachandran, S.; Gao, P.; Dinavahi, R.; Wilson, K.F.; Ambrosio, A.L.B.; Dias, S.M.G.; Dang, C.V.; Cerione, R.A. Targeting mitochondrial glutaminase activity inhibits oncogenic transformation. *Cancer Cell*, **2010**, *18*(3), 207-219.
<http://dx.doi.org/10.1016/j.ccr.2010.08.009> PMID: 20832749
- [74] Xiang, Y.; Stine, Z.E.; Xia, J.; Lu, Y.; O'Connor, R.S.; Altman, B.J.; Hsieh, A.L.; Gouw, A.M.; Thomas, A.G.; Gao, P.; Sun, L.; Song, L.; Yan, B.; Slusher, B.S.; Zhuo, J.; Ooi, L.L.; Lee, C.G.L.; Mancuso, A.; McCallion, A.S.; Le, A.; Milone, M.C.; Rayport, S.; Felsher, D.W.; Dang, C.V. Targeted inhibition of tumor-specific glutaminase diminishes cell-autonomous tumorigenesis. *J. Clin. Invest.*, **2015**, *125*(6), 2293-2306.
<http://dx.doi.org/10.1172/JCI75836> PMID: 25915584
- [75] Xiang, L.; Mou, J.; Shao, B.; Wei, Y.; Liang, H.; Takano, N.; Semenza, G.L.; Xie, G. Glutaminase 1 expression in colorectal cancer cells is induced by hypoxia and required for tumor growth, invasion, and metastatic colonization. *Cell Death Dis.*, **2019**, *10*(2), 40.
<http://dx.doi.org/10.1038/s41419-018-1291-5> PMID: 30674873
- [76] Hu, W.; Zhang, C.; Wu, R.; Sun, Y.; Levine, A.; Feng, Z. Glutaminase 2, a novel p53 target gene regulating energy metabolism and antioxidant function. *Proc. Natl. Acad. Sci. USA*, **2010**, *107*(16), 7455-7460.
<http://dx.doi.org/10.1073/pnas.1001006107> PMID: 20378837
- [77] Liu, J.; Zhang, C.; Lin, M.; Zhu, W.; Liang, Y.; Hong, X.; Zhao, Y.; Young, K.H.; Hu, W.; Feng, Z. Glutaminase 2 negatively regulates the PI3K/AKT signaling and shows tumor suppression activity in human hepatocellular carcinoma. *Oncotarget*, **2014**, *5*(9), 2635-2647.
<http://dx.doi.org/10.18632/oncotarget.1862> PMID: 24797434
- [78] Suzuki, S.; Tanaka, T.; Poyurovsky, M.V.; Nagano, H.; Mayama, T.; Ohkubo, S.; Lokshin, M.; Hosokawa, H.; Nakayama, T.; Suzuki, Y.; Sugano, S.; Sato, E.; Nagao, T.; Yokote, K.; Tatsuno, I.; Prives, C. Phosphate-activated glutaminase (GLS2), a p53-inducible regulator of glutamine metabolism and reactive oxygen species. *Proc. Natl. Acad. Sci. USA*, **2010**, *107*(16), 7461-7466.
<http://dx.doi.org/10.1073/pnas.1002459107> PMID: 20351271
- [79] Zhang, C.; Liu, J.; Zhao, Y.; Yue, X.; Zhu, Y.; Wang, X.; Wu, H.; Blanco, F.; Li, S.; Bhanot, G.; Haffty, B.G.; Hu, W.; Feng, Z. Glutaminase 2 is a novel negative regulator of small GTPase Rac1 and mediates p53 function in suppressing metastasis. *eLife*, **2016**, *5*e10727
<http://dx.doi.org/10.7554/eLife.10727> PMID: 26751560
- [80] Nicklin, P.; Bergman, P.; Zhang, B.; Triantafellow, E.; Wang, H.; Nyfeler, B.; Yang, H.; Hild, M.; Kung, C.; Wilson, C.; Myer, V.E.; MacKeigan, J.P.; Porter, J.A.; Wang, Y.K.; Cantley, L.C.; Finan, P.M.; Murphy, L.O. Bidirectional transport of amino acids regulates mTOR and autophagy. *Cell*, **2009**, *136*(3), 521-534.
<http://dx.doi.org/10.1016/j.cell.2008.11.044> PMID: 19203585
- [81] Avruch, J.; Long, X.; Ortiz-Vega, S.; Rapley, J.; Papageorgiou, A.; Dai, N. Amino acid regulation of TOR complex 1. *Am. J. Physiol. Endocrinol. Metab.*, **2009**, *296*(4), E592-E602.
<http://dx.doi.org/10.1152/ajpendo.90645.2008> PMID: 18765678
- [82] Dey, P.; Baddour, J.; Muller, F.; Wu, C.C.; Wang, H.; Liao, W.-T.; Lan, Z.; Chen, A.; Gutschner, T.; Kang, Y.; Fleming, J.; Satani, N.; Zhao, D.; Achreja, A.; Yang, L.; Lee, J.; Chang, E.; Genovese, G.; Viale, A.; Ying, H.; Draetta, G.; Maitra, A.; Wang, Y.A.; Nagrath, D.; DePinho, R.A. Genomic deletion of malic enzyme 2 confers collateral lethality in pancreatic cancer. *Nature*, **2017**, *542*(7639), 119-123.
<http://dx.doi.org/10.1038/nature21052> PMID: 28099419
- [83] Zhang, L.; Han, J. Branched-chain amino acid transaminase 1 (BCAT1) promotes the growth of breast cancer cells through improving mTOR-mediated mitochondrial biogenesis and function. *Biochem. Biophys. Res. Commun.*, **2017**, *486*(2), 224-231.
<http://dx.doi.org/10.1016/j.bbrc.2017.02.101> PMID: 28235484
- [84] Hattori, A.; Tsunoda, M.; Konuma, T.; Kobayashi, M.; Nagy, T.; Glushka, J.; Tayyari, F.; McSkimming, D.; Kannan, N.; Tojo, A.; Edison, A.S.; Ito, T. Cancer progression by reprogrammed BCAA metabolism in myeloid leukaemia. *Nature*, **2017**, *545*(7655), 500-504.
<http://dx.doi.org/10.1038/nature22314> PMID: 28514443
- [85] Chen, Y.; Li, P. Fatty Acid Metabolism and Cancer Development. *Sci. Bull. (Beijing)*, **2016**, *61*(19), 1473-1479.
<http://dx.doi.org/10.1007/s11434-016-1129-4>
- [86] Wang, Q.; Liu, S.; Zhai, A.; Zhang, B.; Tian, G. AMPK-Mediated Regulation of Lipid Metabolism by Phosphorylation. *Biol. Pharm. Bull.*, **2018**, *41*(7), 985-993.
<http://dx.doi.org/10.1248/bpb.b17-00724> PMID: 29709897
- [87] Martinez-Outschoorn, U.E.; Peiris-Pagés, M.; Pestell, R.G.; Sotgia, F.; Lisanti, M.P. Cancer metabolism: a therapeutic perspective. *Nat. Rev. Clin. Oncol.*, **2017**, *14*(1), 11-31.
<http://dx.doi.org/10.1038/nrclinonc.2016.60> PMID: 27141887
- [88] Harjes, U.; Kalucka, J.; Carmeliet, P. Targeting fatty acid metabolism in cancer and endothelial cells. *Crit. Rev. Oncol. Hematol.*, **2016**, *97*, 15-21.
<http://dx.doi.org/10.1016/j.critrevonc.2015.10.011> PMID: 26558689
- [89] Swierczynski, J.; Hebanowska, A.; Sledzinski, T. Role of abnormal lipid metabolism in development, progression, di-

- agnosis and therapy of pancreatic cancer. *World J. Gastroenterol.*, **2014**, *20*(9), 2279-2303.
<http://dx.doi.org/10.3748/wjg.v20.i9.2279> PMID: 24605027
- [90] Papandreou, I.; Cairns, R.A.; Fontana, L.; Lim, A.L.; Denko, N.C. HIF-1 mediates adaptation to hypoxia by actively downregulating mitochondrial oxygen consumption. *Cell Metab.*, **2006**, *3*(3), 187-197.
<http://dx.doi.org/10.1016/j.cmet.2006.01.012> PMID: 16517406
- [91] Kim, J.W.; Tchernyshyov, I.; Semenza, G.L.; Dang, C.V. HIF-1-mediated expression of pyruvate dehydrogenase kinase: a metabolic switch required for cellular adaptation to hypoxia. *Cell Metab.*, **2006**, *3*(3), 177-185.
<http://dx.doi.org/10.1016/j.cmet.2006.02.002> PMID: 16517405
- [92] Zu, X-Y.; Zhang, Q-H.; Liu, J-H.; Cao, R-X.; Zhong, J.; Yi, G-H.; Quan, Z-H.; Pizzorno, G. ATP citrate lyase inhibitors as novel cancer therapeutic agents. *Recent Patents Anticancer Drug Discov.*, **2012**, *7*(2), 154-167.
<http://dx.doi.org/10.2174/157489212799972954> PMID: 22339355
- [93] Hatzivassiliou, G.; Zhao, F.; Bauer, D.E.; Andreadis, C.; Shaw, A.N.; Dhanak, D.; Hingorani, S.R.; Tuveson, D.A.; Thompson, C.B. ATP citrate lyase inhibition can suppress tumor cell growth. *Cancer Cell*, **2005**, *8*(4), 311-321.
<http://dx.doi.org/10.1016/j.ccr.2005.09.008> PMID: 16226706
- [94] Schug, Z.T.; Peck, B.; Jones, D.T.; Zhang, Q.; Grosskurth, S.; Alam, I.S.; Goodwin, L.M.; Smethurst, E.; Mason, S.; Blyth, K.; McGarry, L.; James, D.; Shanks, E.; Kalna, G.; Saunders, R.E.; Jiang, M.; Howell, M.; Lassailly, F.; Thin, M.Z.; Spencer-Dene, B.; Stamp, G.; van den Broek, N.J.F.; Mackay, G.; Bulusu, V.; Kamphorst, J.J.; Tardito, S.; Strachan, D.; Harris, A.L.; Aboagye, E.O.; Critchlow, S.E.; Wakelam, M.J.O.; Schulze, A.; Gottlieb, E. Acetyl-CoA synthetase 2 promotes acetate utilization and maintains cancer cell growth under metabolic stress. *Cancer Cell*, **2015**, *27*(1), 57-71.
<http://dx.doi.org/10.1016/j.ccell.2014.12.002> PMID: 25584894
- [95] Kuo, C-Y.; Ann, D.K. When fats commit crimes: fatty acid metabolism, cancer stemness and therapeutic resistance. *Cancer Commun (Lond)*, **2018**, *38*(1), 47.
<http://dx.doi.org/10.1186/s40880-018-0317-9> PMID: 29996946
- [96] Rossi Sebastiano, M.; Konstantinidou, G. Targeting Long Chain Acyl-CoA Synthetases for Cancer Therapy. *Int. J. Mol. Sci.*, **2019**, *20*(15), 3624.
<http://dx.doi.org/10.3390/ijms20153624> PMID: 31344914
- [97] Sánchez-Martínez, R.; Cruz-Gil, S.; García-Álvarez, M.S.; Reglero, G.; Ramírez de Molina, A. Complementary ACSL isoforms contribute to a non-Warburg advantageous energetic status characterizing invasive colon cancer cells. *Sci. Rep.*, **2017**, *7*(1), 11143.
<http://dx.doi.org/10.1038/s41598-017-11612-3> PMID: 28894242
- [98] Chen, W-C.; Wang, C-Y.; Hung, Y-H.; Weng, T-Y.; Yen, M-C.; Lai, M-D. Systematic Analysis of Gene Expression Alterations and Clinical Outcomes for Long-Chain Acyl-Coenzyme A Synthetase Family in Cancer. *PLoS One*, **2016**, *11*(5)e0155660
<http://dx.doi.org/10.1371/journal.pone.0155660> PMID: 27171439
- [99] Padanad, M.S.; Konstantinidou, G.; Venkateswaran, N.; Melegari, M.; Rindhe, S.; Mitsche, M.; Yang, C.; Batten, K.; Huffman, K.E.; Liu, J.; Tang, X.; Rodriguez-Canales, J.; Kalhor, N.; Shay, J.W.; Minna, J.D.; McDonald, J.; Wistuba, I.I.; DeBerardinis, R.J.; Scagliioni, P.P. Fatty Acid Oxidation Mediated by Acyl-CoA Synthetase Long Chain 3 Is Required for Mutant KRAS Lung Tumorigenesis. *Cell Rep.*, **2016**, *16*(6), 1614-1628.
<http://dx.doi.org/10.1016/j.celrep.2016.07.009> PMID: 27477280
- [100] Yen, M-C.; Kan, J-Y.; Hsieh, C-J.; Kuo, P-L.; Hou, M-F.; Hsu, Y-L. Association of long-chain acyl-coenzyme A synthetase 5 expression in human breast cancer by estrogen receptor status and its clinical significance. *Oncol. Rep.*, **2017**, *37*(6), 3253-3260.
<http://dx.doi.org/10.3892/or.2017.5610> PMID: 28498416
- [101] Wang, Y.; Cai, X.; Zhang, S.; Cui, M.; Liu, F.; Sun, B.; Zhang, W.; Zhang, X.; Ye, L. HBXIP up-regulates ACSL1 through activating transcriptional factor Sp1 in breast cancer. *Biochem. Biophys. Res. Commun.*, **2017**, *484*(3), 565-571.
<http://dx.doi.org/10.1016/j.bbrc.2017.01.126> PMID: 28132807
- [102] Wang, J.; Scholtens, D.; Holko, M.; Ivancic, D.; Lee, O.; Hu, H.; Chatterton, R.T., Jr; Sullivan, M.E.; Hansen, N.; Bethke, K.; Zalles, C.M.; Khan, S.A. Lipid metabolism genes in contralateral unaffected breast and estrogen receptor status of breast cancer. *Cancer Prev. Res. (Phila.)*, **2013**, *6*(4), 321-330.
<http://dx.doi.org/10.1158/1940-6207.CAPR-12-0304> PMID: 23512947
- [103] Migita, T.; Takayama, K.I.; Urano, T.; Obinata, D.; Ikeda, K.; Soga, T.; Takahashi, S.; Inoue, S. ACSL3 promotes intratumoral steroidogenesis in prostate cancer cells. *Cancer Sci.*, **2017**, *108*(10), 2011-2021.
<http://dx.doi.org/10.1111/cas.13339> PMID: 28771887
- [104] Nwosu, Z.C.; Megger, D.A.; Hammad, S.; Sitek, B.; Roessler, S.; Ebert, M.P.; Meyer, C.; Dooley, S. Identification of the Consistently Altered Metabolic Targets in Human Hepatocellular Carcinoma. *Cell. Mol. Gastroenterol. Hepatol.*, **2017**, *4*(2), 303-323.e1.
<http://dx.doi.org/10.1016/j.jcmgh.2017.05.004> PMID: 28840186
- [105] Wu, X.; Li, Y.; Wang, J.; Wen, X.; Marcus, M.T.; Daniels, G.; Zhang, D.Y.; Ye, F.; Wang, L.H.; Du, X.; Adams, S.; Singh, B.; Zavadil, J.; Lee, P.; Monaco, M.E. Long chain fatty Acyl-CoA synthetase 4 is a biomarker for and mediator of hormone resistance in human breast cancer. *PLoS One*, **2013**, *8*(10)e77060
<http://dx.doi.org/10.1371/journal.pone.0077060> PMID: 24155918
- [106] Sánchez-Martínez, R.; Cruz-Gil, S.; Gómez de Cedrón, M.; Álvarez-Fernández, M.; Vargas, T.; Molina, S.; García, B.; Herranz, J.; Moreno-Rubio, J.; Reglero, G.; Pérez-Moreno, M.; Feliu, J.; Malumbres, M.; Ramírez de Molina, A. A link between lipid metabolism and epithelial-mesenchymal transition provides a target for colon cancer therapy. *Oncotarget*, **2015**, *6*(36), 38719-38736.
<http://dx.doi.org/10.18632/oncotarget.5340> PMID: 26451612
- [107] DeBerardinis, R.J.; Chandel, N.S. Fundamentals of cancer metabolism. *Sci. Adv.*, **2016**, *2*(5)e1600200
<http://dx.doi.org/10.1126/sciadv.1600200> PMID: 27386546
- [108] Engelman, J.A.; Luo, J.; Cantley, L.C. The evolution of phosphatidylinositol 3-kinases as regulators of growth and metabolism. *Nat. Rev. Genet.*, **2006**, *7*(8), 606-619.
<http://dx.doi.org/10.1038/nrg1879> PMID: 16847462
- [109] Kohn, A.D.; Summers, S.A.; Birnbaum, M.J.; Roth, R.A. Expression of a constitutively active Akt Ser/Thr kinase in 3T3-L1 adipocytes stimulates glucose uptake and glucose

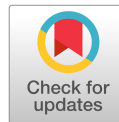
- transporter 4 translocation. *J. Biol. Chem.*, **1996**, *271*(49), 31372-31378.
<http://dx.doi.org/10.1074/jbc.271.49.31372> PMID: 8940145
- [110] Yecies, J.L.; Manning, B.D. Transcriptional control of cellular metabolism by mTOR signaling. *Cancer Res.*, **2011**, *71*(8), 2815-2820.
<http://dx.doi.org/10.1158/0008-5472.CAN-10-4158> PMID: 21487041
- [111] Deprez, J.; Vertommen, D.; Alessi, D.R.; Hue, L.; Rider, M.H. Phosphorylation and activation of heart 6-phosphofructo-2-kinase by protein kinase B and other protein kinases of the insulin signaling cascades. *J. Biol. Chem.*, **1997**, *272*(28), 17269-17275.
<http://dx.doi.org/10.1074/jbc.272.28.17269> PMID: 9211863
- [112] Berwick, D.C.; Hers, I.; Heesom, K.J.; Moule, S.K.; Tavaré, J.M. The identification of ATP-citrate lyase as a protein kinase B (Akt) substrate in primary adipocytes. *J. Biol. Chem.*, **2002**, *277*(37), 33895-33900.
<http://dx.doi.org/10.1074/jbc.M204681200> PMID: 12107176
- [113] Patra, K.C.; Hay, N. The pentose phosphate pathway and cancer. *Trends Biochem. Sci.*, **2014**, *39*(8), 347-354.
<http://dx.doi.org/10.1016/j.tibs.2014.06.005> PMID: 25037503
- [114] Saal, L.H.; Holm, K.; Maurer, M.; Memeo, L.; Su, T.; Wang, X.; Yu, J.S.; Malmström, P.-O.; Mansukhani, M.; Enoksson, J.; Hibshoosh, H.; Borg, A.; Parsons, R. PIK3CA mutations correlate with hormone receptors, node metastasis, and ERBB2, and are mutually exclusive with PTEN loss in human breast carcinoma. *Cancer Res.*, **2005**, *65*(7), 2554-2559.
<http://dx.doi.org/10.1158/0008-5472.CAN-04-3913> PMID: 15805248
- [115] Jiang, W.; He, T.; Liu, S.; Zheng, Y.; Xiang, L.; Pei, X.; Wang, Z.; Yang, H. The PIK3CA E542K and E545K mutations promote glycolysis and proliferation via induction of the β -catenin/SIRT3 signaling pathway in cervical cancer. *J. Hematol. Oncol.*, **2018**, *11*(1), 139.
<http://dx.doi.org/10.1186/s13045-018-0674-5> PMID: 30547809
- [116] Sobhani, N.; Roviello, G.; Corona, S.P.; Scaltriti, M.; Ianza, A.; Bortol, M.; Zanconati, F.; Generali, D. The prognostic value of PI3K mutational status in breast cancer: A meta-analysis. *J. Cell. Biochem.*, **2018**, *119*(6), 4287-4292.
<http://dx.doi.org/10.1002/jcb.26687> PMID: 29345357
- [117] Lisy, K.; Peet, D.J. Turn me on: regulating HIF transcriptional activity. *Cell Death Differ.*, **2008**, *15*(4), 642-649.
<http://dx.doi.org/10.1038/sj.cdd.4402315> PMID: 18202699
- [118] Hu, C.-J.; Sataur, A.; Wang, L.; Chen, H.; Simon, M.C. The N-terminal transactivation domain confers target gene specificity of hypoxia-inducible factors HIF-1 α and HIF-2 α . *Mol. Biol. Cell*, **2007**, *18*(11), 4528-4542.
<http://dx.doi.org/10.1091/mbc.e06-05-0419> PMID: 17804822
- [119] Zhao, M.; Zhang, Y.; Zhang, H.; Wang, S.; Zhang, M.; Chen, X.; Wang, H.; Zeng, G.; Chen, X.; Liu, G.; Zhou, C. Hypoxia-induced cell stemness leads to drug resistance and poor prognosis in lung adenocarcinoma. *Lung Cancer*, **2015**, *87*(2), 98-106.
<http://dx.doi.org/10.1016/j.lungcan.2014.11.017> PMID: 25512094
- [120] Semenza, G.L.; Roth, P.H.; Fang, H.M.; Wang, G.L. Transcriptional regulation of genes encoding glycolytic enzymes by hypoxia-inducible factor 1. *J. Biol. Chem.*, **1994**, *269*(38), 23757-23763.
PMID: 8089148
- [121] Semenza, G.L.; Jiang, B.-H.; Leung, S.W.; Passantino, R.; Concordet, J.-P.; Maire, P.; Giallongo, A. Hypoxia response elements in the aldolase A, enolase 1, and lactate dehydrogenase A gene promoters contain essential binding sites for hypoxia-inducible factor 1. *J. Biol. Chem.*, **1996**, *271*(51), 32529-32537.
<http://dx.doi.org/10.1074/jbc.271.51.32529> PMID: 8955077
- [122] Graven, K.K.; Yu, Q.; Pan, D.; Roncarati, J.S.; Farber, H.W. Identification of an oxygen responsive enhancer element in the glyceraldehyde-3-phosphate dehydrogenase gene. *Biochim. Biophys. Acta*, **1999**, *1447*(2-3), 208-218.
[http://dx.doi.org/10.1016/S0167-4781\(99\)00118-9](http://dx.doi.org/10.1016/S0167-4781(99)00118-9) PMID: 10542317
- [123] Firth, J.D.; Ebert, B.L.; Pugh, C.W.; Ratcliffe, P.J. Oxygen-regulated control elements in the phosphoglycerate kinase 1 and lactate dehydrogenase A genes: similarities with the erythropoietin 3' enhancer. *Proc. Natl. Acad. Sci. USA*, **1994**, *91*(14), 6496-6500.
<http://dx.doi.org/10.1073/pnas.91.14.6496> PMID: 8022811
- [124] Firth, J.D.; Ebert, B.L.; Ratcliffe, P.J. Hypoxic regulation of lactate dehydrogenase A. Interaction between hypoxia-inducible factor 1 and cAMP response elements. *J. Biol. Chem.*, **1995**, *270*(36), 21021-21027.
<http://dx.doi.org/10.1074/jbc.270.36.21021> PMID: 7673128
- [125] Ebert, B.L.; Firth, J.D.; Ratcliffe, P.J. Hypoxia and mitochondrial inhibitors regulate expression of glucose transporter-1 via distinct Cis-acting sequences. *J. Biol. Chem.*, **1995**, *270*(49), 29083-29089.
<http://dx.doi.org/10.1074/jbc.270.49.29083> PMID: 7493931
- [126] Marín-Hernández, A.; Gallardo-Pérez, J.C.; Ralph, S.J.; Rodríguez-Enriquez, S.; Moreno-Sánchez, R. HIF-1 α modulates energy metabolism in cancer cells by inducing over-expression of specific glycolytic isoforms. *Mini Rev. Med. Chem.*, **2009**, *9*(9), 1084-1101.
<http://dx.doi.org/10.2174/138955709788922610> PMID: 19689405
- [127] Meyer, N.; Penn, L.Z. Reflecting on 25 years with MYC. *Nat. Rev. Cancer*, **2008**, *8*(12), 976-990.
<http://dx.doi.org/10.1038/nrc2231> PMID: 19029958
- [128] Camarda, R.; Williams, J.; Goga, A. *In vivo* Reprogramming of Cancer Metabolism by MYC. *Front. Cell Dev. Biol.*, **2017**, *5*, 35.
<http://dx.doi.org/10.3389/fcell.2017.00035> PMID: 28443280
- [129] Kim, J.; Lee, J.H.; Iyer, V.R. Global identification of Myc target genes reveals its direct role in mitochondrial biogenesis and its E-box usage *in vivo*. *PLoS One*, **2008**, *3*(3)e1798
<http://dx.doi.org/10.1371/journal.pone.0001798> PMID: 18335064
- [130] Osthus, R.C.; Shim, H.; Kim, S.; Li, Q.; Reddy, R.; Mukherjee, M.; Xu, Y.; Wonsey, D.; Lee, L.A.; Dang, C.V. Deregulation of glucose transporter 1 and glycolytic gene expression by c-Myc. *J. Biol. Chem.*, **2000**, *275*(29), 21797-21800.
<http://dx.doi.org/10.1074/jbc.C000023200> PMID: 10823814
- [131] O'Connell, B.C.; Cheung, A.F.; Simkevich, C.P.; Tam, W.; Ren, X.; Mateyak, M.K.; Sedivy, J.M. A large scale genetic analysis of c-Myc-regulated gene expression patterns. *J. Biol. Chem.*, **2003**, *278*(14), 12563-12573.
<http://dx.doi.org/10.1074/jbc.M210462200> PMID: 12529326
- [132] Menssen, A.; Hermeking, H. Characterization of the c-MYC-regulated transcriptome by SAGE: identification and analysis of c-MYC target genes. *Proc. Natl. Acad. Sci. USA*, **2002**, *99*(9), 6274-6279.
<http://dx.doi.org/10.1073/pnas.082005599> PMID: 11983916
- [133] Kim, J.W.; Zeller, K.I.; Wang, Y.; Jegga, A.G.; Aronow, B.J.; O'Donnell, K.A.; Dang, C.V. Evaluation of myc E-box phylogenetic footprints in glycolytic genes by chromatin immunoprecipitation assays. *Mol. Cell. Biol.*, **2004**, *24*(13), 5923-5936.

- <http://dx.doi.org/10.1128/MCB.24.13.5923-5936.2004>
PMID: 15199147
- [134] Yuneva, M.O.; Fan, T.W.M.; Allen, T.D.; Higashi, R.M.; Ferraris, D.V.; Tsukamoto, T.; Matés, J.M.; Alonso, F.J.; Wang, C.; Seo, Y.; Chen, X.; Bishop, J.M. The metabolic profile of tumors depends on both the responsible genetic lesion and tissue type. *Cell Metab.*, **2012**, *15*(2), 157-170.
<http://dx.doi.org/10.1016/j.cmet.2011.12.015> PMID: 22326218
- [135] Ciribilli, Y.; Singh, P.; Inga, A.; Borlak, J. c-Myc targeted regulators of cell metabolism in a transgenic mouse model of papillary lung adenocarcinoma. *Oncotarget*, **2016**, *7*(40), 65514-65539.
<http://dx.doi.org/10.18632/oncotarget.11804> PMID: 27602772
- [136] Gouw, A.M.; Margulis, K.; Liu, N.S.; Raman, S.J.; Mancuso, A.; Toal, G.G.; Tong, L.; Mosley, A.; Hsieh, A.L.; Sullivan, D.K.; Stine, Z.E.; Altman, B.J.; Schulze, A.; Dang, C.V.; Zare, R.N.; Felsher, D.W. The MYC Oncogene Cooperates with Sterol-Regulated Element-Binding Protein to Regulate Lipogenesis Essential for Neoplastic Growth. *Cell Metab.*, **2019**, *30*(3), 556-572.e5.
<http://dx.doi.org/10.1016/j.cmet.2019.07.012> PMID: 31447321
- [137] Schwartzberg-Bar-Yoseph, F.; Armoni, M.; Karnieli, E. The tumor suppressor p53 down-regulates glucose transporters GLUT1 and GLUT4 gene expression. *Cancer Res.*, **2004**, *64*(7), 2627-2633.
<http://dx.doi.org/10.1158/0008-5472.CAN-03-0846> PMID: 15059920
- [138] Bensaad, K.; Tsuruta, A.; Selak, M.A.; Vidal, M.N.C.; Nakano, K.; Bartrons, R.; Gottlieb, E.; Vousden, K.H. TIGAR, a p53-inducible regulator of glycolysis and apoptosis. *Cell*, **2006**, *126*(1), 107-120.
<http://dx.doi.org/10.1016/j.cell.2006.05.036> PMID: 16839880
- [139] Kondoh, H.; Leonart, M.E.; Gil, J.; Wang, J.; Degan, P.; Peters, G.; Martinez, D.; Carnero, A.; Beach, D. Glycolytic enzymes can modulate cellular life span. *Cancer Res.*, **2005**, *65*(1), 177-185.
PMID: 15665293
- [140] Jiang, P.; Du, W.; Mancuso, A.; Wellen, K.E.; Yang, X. Reciprocal regulation of p53 and malic enzymes modulates metabolism and senescence. *Nature*, **2013**, *493*(7434), 689-693.
<http://dx.doi.org/10.1038/nature11776> PMID: 23334421
- [141] Matoba, S. P53 Regulates Mitochondrial Respiration *Science (80-.)*, **2006**, *312*(5780), 1650-1653.
<http://dx.doi.org/10.1126/science.1126863>
- [142] Mathupala, S.P.; Heese, C.; Pedersen, P.L. Glucose catabolism in cancer cells. The type II hexokinase promoter contains functionally active response elements for the tumor suppressor p53. *J. Biol. Chem.*, **1997**, *272*(36), 22776-22780.
<http://dx.doi.org/10.1074/jbc.272.36.22776> PMID: 9278438
- [143] Yahagi, N.; Shimano, H.; Matsuzaka, T.; Najima, Y.; Sekiya, M.; Nakagawa, Y.; Ide, T.; Tomita, S.; Okazaki, H.; Tamura, Y.; Iizuka, Y.; Ohashi, K.; Gotoda, T.; Nagai, R.; Kimura, S.; Ishibashi, S.; Osuga, J.; Yamada, N. p53 Activation in adipocytes of obese mice. *J. Biol. Chem.*, **2003**, *278*(28), 25395-25400.
<http://dx.doi.org/10.1074/jbc.M302364200> PMID: 12734185
- [144] Jiang, P.; Du, W.; Wang, X.; Mancuso, A.; Gao, X.; Wu, M.; Yang, X. p53 regulates biosynthesis through direct inactivation of glucose-6-phosphate dehydrogenase. *Nat. Cell Biol.*, **2011**, *13*(3), 310-316.
<http://dx.doi.org/10.1038/ncb2172> PMID: 21336310
- [145] Ide, T.; Brown-Endres, L.; Chu, K.; Ongusaha, P.P.; Ohtsuka, T.; El-Deiry, W.S.; Aaronson, S.A.; Lee, S.W. GAMT, a p53-inducible modulator of apoptosis, is critical for the adaptive response to nutrient stress. *Mol. Cell*, **2009**, *36*(3), 379-392.
<http://dx.doi.org/10.1016/j.molcel.2009.09.031> PMID: 19917247
- [146] Assaily, W.; Rubinger, D.A.; Wheaton, K.; Lin, Y.; Ma, W.; Xuan, W.; Brown-Endres, L.; Tsuchihara, K.; Mak, T.W.; Benchimol, S. ROS-mediated p53 induction of Lpin1 regulates fatty acid oxidation in response to nutritional stress. *Mol. Cell*, **2011**, *44*(3), 491-501.
<http://dx.doi.org/10.1016/j.molcel.2011.08.038> PMID: 22055193
- [147] Salas, M.; Obando, P.; Ojeda, L.; Ojeda, P.; Pérez, A.; Vargas-Urbe, M.; Rivas, C.I.; Vera, J.C.; Reyes, A.M. Resolution of the direct interaction with and inhibition of the human GLUT1 hexose transporter by resveratrol from its effect on glucose accumulation. *Am. J. Physiol. Cell Physiol.*, **2013**, *305*(1), C90-C99.
<http://dx.doi.org/10.1152/ajpcell.00387.2012> PMID: 23615963
- [148] Wang, L.; Wang, J.; Xiong, H.; Wu, F.; Lan, T.; Zhang, Y.; Guo, X.; Wang, H.; Saleem, M.; Jiang, C.; Lu, J.; Deng, Y. Co-targeting hexokinase 2-mediated Warburg effect and ULK1-dependent autophagy suppresses tumor growth of PTEN- and TP53-deficiency-driven castration-resistant prostate cancer. *EBioMedicine*, **2016**, *7*, 50-61.
<http://dx.doi.org/10.1016/j.ebiom.2016.03.022> PMID: 27322458
- [149] Glenister, A.; Simone, M.I.; Hambley, T.W. A Warburg effect targeting vector designed to increase the uptake of compounds by cancer cells demonstrates glucose and hypoxia dependent uptake. *PLoS One*, **2019**, *14*(7)e0217712
<http://dx.doi.org/10.1371/journal.pone.0217712> PMID: 31306426
- [150] Shankar Babu, M.; Mahanta, S.; Lakhter, A.J.; Hato, T.; Paul, S.; Naidu, S.R. Lapachol inhibits glycolysis in cancer cells by targeting pyruvate kinase M2. *PLoS One*, **2018**, *13*(2)e0191419
<http://dx.doi.org/10.1371/journal.pone.0191419> PMID: 29394289
- [151] Miao, G.; Han, J.; Zhang, J.; Wu, Y.; Tong, G. Targeting Pyruvate Kinase M2 and Hexokinase II, Pachymic Acid Impairs Glucose Metabolism and Induces Mitochondrial Apoptosis. *Biol. Pharm. Bull.*, **2019**, *42*(1), 123-129.
<http://dx.doi.org/10.1248/bpb.b18-00730> PMID: 30381614
- [152] Ma, J.; Liu, J.; Lu, C.; Cai, D. Pachymic acid induces apoptosis via activating ROS-dependent JNK and ER stress pathways in lung cancer cells. *Cancer Cell Int.*, **2015**, *15*(1), 78.
<http://dx.doi.org/10.1186/s12935-015-0230-0> PMID: 26244039
- [153] Xu, S.; Catapang, A.; Braas, D.; Stiles, L.; Doh, H.M.; Lee, J.T.; Graeber, T.G.; Damoiseaux, R.; Shirihai, O.; Herschman, H.R. A precision therapeutic strategy for hexokinase 1-null, hexokinase 2-positive cancers. *Cancer Metab.*, **2018**, *6*(1), 7.
<http://dx.doi.org/10.1186/s40170-018-0181-8> PMID: 29988332
- [154] Grinde, M.T.; Hilmarsdottir, B.; Tunset, H.M.; Henriksen, I.M.; Kim, J.; Haugen, M.H.; Rye, M.B.; Mælandsmo, G.M.; Moestue, S.A. Glutamine to proline conversion is associated with response to glutaminase inhibition in breast cancer. *Breast Cancer Res.*, **2019**, *21*(1), 61.

- <http://dx.doi.org/10.1186/s13058-019-1141-0> PMID: 31088535
- [155] Freitag, H.; Christen, F.; Lewens, F.; Grass, I.; Briest, F.; Iwaszkiewicz, S.; Siegmund, B.; Grabowski, P. Inhibition of mTOR's Catalytic Site by PKI-587 Is a Promising Therapeutic Option for Gastroenteropancreatic Neuroendocrine Tumor Disease. *Neuroendocrinology*, **2017**, *105*(1), 90-104. <http://dx.doi.org/10.1159/000448843> PMID: 27513674
- [156] Liu, N.; Rowley, B.R.; Bull, C.O.; Schneider, C.; Haegbarth, A.; Schatz, C.A.; Fracasso, P.R.; Wilkie, D.P.; Hentemann, M.; Wilhelm, S.M.; Scott, W.J.; Mumberg, D.; Ziegelbauer, K. BAY 80-6946 is a highly selective intravenous PI3K inhibitor with potent p110 α and p110 δ activities in tumor cell lines and xenograft models. *Mol. Cancer Ther.*, **2013**, *12*(11), 2319-2330. <http://dx.doi.org/10.1158/1535-7163.MCT-12-0993-T> PMID: 24170767
- [157] Kim, R.D.; Alberts, S.R.; Peña, C.; Genvresse, I.; Ajavon-Hartmann, A.; Xia, C.; Kelly, A.; Grilley-Olson, J.E.; Phase, I. Phase I dose-escalation study of copanlisib in combination with gemcitabine or cisplatin plus gemcitabine in patients with advanced cancer. *Br. J. Cancer*, **2018**, *118*(4), 462-470. <http://dx.doi.org/10.1038/bjc.2017.428> PMID: 29348486
- [158] Dreyling, M.; Morschhauser, F.; Bouabdallah, K.; Bron, D.; Cunningham, D.; Assouline, S.E.; Verhoef, G.; Linton, K.; Thieblemont, C.; Vitolo, U.; Hiemeyer, F.; Giurescu, M.; Garcia-Vargas, J.; Gorbachevsky, I.; Liu, L.; Koechert, K.; Peña, C.; Neves, M.; Childs, B.H.; Zinzani, P.L.; Phase, I.I. Phase II study of copanlisib, a PI3K inhibitor, in relapsed or refractory, indolent or aggressive lymphoma. *Ann. Oncol.*, **2017**, *28*(9), 2169-2178. <http://dx.doi.org/10.1093/annonc/mdx289> PMID: 28633365
- [159] Ma, C.X.; Luo, J.; Naughton, M.; Ademuyiwa, F.; Suresh, R.; Griffith, M.; Griffith, O.L.; Skidmore, Z.L.; Spies, N.C.; Ramu, A.; Trani, L.; Pluard, T.; Nagaraj, G.; Thomas, S.; Guo, Z.; Hoog, J.; Han, J.; Mardis, E.; Lockhart, C.; Ellis, M.J. A Phase I Trial of BKM120 (Buparlisib) in Combination with Fulvestrant in Postmenopausal Women with Estrogen Receptor-Positive Metastatic Breast Cancer. *Clin. Cancer Res.*, **2016**, *22*(7), 1583-1591. <http://dx.doi.org/10.1158/1078-0432.CCR-15-1745> PMID: 26563128
- [160] Dong, S.; Guinn, D.; Dubovsky, J.A.; Zhong, Y.; Lehman, A.; Kutok, J.; Woyach, J.A.; Byrd, J.C.; Johnson, A.J. IPI-145 antagonizes intrinsic and extrinsic survival signals in chronic lymphocytic leukemia cells. *Blood*, **2014**, *124*(24), 3583-3586. <http://dx.doi.org/10.1182/blood-2014-07-587279> PMID: 25258342
- [161] Flinn, I.W.; Hillmen, P.; Montillo, M.; Nagy, Z.; Illés, Á.; Etienne, G.; Delgado, J.; Kuss, B.J.; Tam, C.S.; Gasztonyi, Z.; Offner, F.; Lunin, S.; Bosch, F.; Davids, M.S.; Lamanna, N.; Jaeger, U.; Ghia, P.; Cymbalista, F.; Portell, C.A.; Skarbnik, A.P.; Cashen, A.F.; Weaver, D.T.; Kelly, V.M.; Turnbull, B.; Stilgenbauer, S. The phase 3 DUO trial: duvelisib vs ofatumumab in relapsed and refractory CLL/SLL. *Blood*, **2018**, *132*(23), 2446-2455. <http://dx.doi.org/10.1182/blood-2018-05-850461> PMID: 30287523
- [162] Brown, J.R.; Byrd, J.C.; Coutre, S.E.; Benson, D.M.; Flinn, I.W.; Wagner-Johnston, N.D.; Spurgeon, S.E.; Kahl, B.S.; Bello, C.; Webb, H.K.; Johnson, D.M.; Peterman, S.; Li, D.; Jahn, T.M.; Lannutti, B.J.; Ulrich, R.G.; Yu, A.S.; Miller, L.L.; Furman, R.R. Idelalisib, an inhibitor of phosphatidylinositol 3-kinase p110 δ , for relapsed/refractory chronic lymphocytic leukemia. *Blood*, **2014**, *123*(22), 3390-3397. <http://dx.doi.org/10.1182/blood-2013-11-535047> PMID: 24615777
- [163] Wigerup, C.; Pählman, S.; Bexell, D. Therapeutic targeting of hypoxia and hypoxia-inducible factors in cancer. *Pharmacol. Ther.*, **2016**, *164*, 152-169. <http://dx.doi.org/10.1016/j.pharmthera.2016.04.009> PMID: 27139518
- [164] Isaacs, J.S.; Jung, Y.-J.; Mimnaugh, E.G.; Martinez, A.; Cuttitta, F.; Neckers, L.M. Hsp90 regulates a von Hippel Lindau-independent hypoxia-inducible factor-1 α -degradative pathway. *J. Biol. Chem.*, **2002**, *277*(33), 29936-29944. <http://dx.doi.org/10.1074/jbc.M204733200> PMID: 12052835
- [165] Rapisarda, A.; Uranchimeg, B.; Scudiero, D.A.; Selby, M.; Sausville, E.A.; Shoemaker, R.H.; Melillo, G. Identification of small molecule inhibitors of hypoxia-inducible factor 1 transcriptional activation pathway. *Cancer Res.*, **2002**, *62*(15), 4316-4324. PMID: 12154035
- [166] Georger, B.; Kerr, K.; Tang, C.B.; Fung, K.M.; Powell, B.; Sutton, L.N.; Phillips, P.C.; Janss, A.J. Antitumor activity of the rapamycin analog CCI-779 in human primitive neuroectodermal tumor/medulloblastoma models as single agent and in combination chemotherapy. *Cancer Res.*, **2001**, *61*(4), 1527-1532. PMID: 11245461
- [167] Klos, K.S.; Zhou, X.; Lee, S.; Zhang, L.; Yang, W.; Nagata, Y.; Yu, D. Combined trastuzumab and paclitaxel treatment better inhibits ErbB-2-mediated angiogenesis in breast carcinoma through a more effective inhibition of Akt than either treatment alone. *Cancer*, **2003**, *98*(7), 1377-1385. <http://dx.doi.org/10.1002/ncr.11656> PMID: 14508823
- [168] Hambley, T.W. Chemistry. Metal-based therapeutics. *Science*, **2007**, *318*(5855), 1392-1393. <http://dx.doi.org/10.1126/science.1150504> PMID: 18048674
- [169] Denny, W.A. The role of hypoxia-activated prodrugs in cancer therapy. *Lancet Oncol.*, **2000**, *1*(1), 25-29. [http://dx.doi.org/10.1016/S1470-2045\(00\)00006-1](http://dx.doi.org/10.1016/S1470-2045(00)00006-1) PMID: 11905684
- [170] Chen, R.; Keating, M.J.; Gandhi, V.; Plunkett, W. Transcription inhibition by flavopiridol: mechanism of chronic lymphocytic leukemia cell death. *Blood*, **2005**, *106*(7), 2513-2519. <http://dx.doi.org/10.1182/blood-2005-04-1678> PMID: 15972445
- [171] Awan, F.T.; Jones, J.A.; Maddocks, K.; Poi, M.; Grever, M.R.; Johnson, A.; Byrd, J.C.; Andritsos, L.A. A phase I clinical trial of flavopiridol consolidation in chronic lymphocytic leukemia patients following chemoimmunotherapy. *Ann. Hematol.*, **2016**, *95*(7), 1137-1143. <http://dx.doi.org/10.1007/s00277-016-2683-1> PMID: 27118540
- [172] Cienas, J.; Kalyan, K.; Sorokinas, A.; Stankunas, E.; Levy, J.; Meskinyte, I.; Stankevicius, V.; Kaupinis, A.; Valius, M. Roscovitine in cancer and other diseases. *Ann. Transl. Med.*, **2015**, *3*(10), 135. <http://dx.doi.org/10.3978/j.issn.2305-5839.2015.03.61> PMID: 26207228
- [173] Vignot, S.; Faivre, S.; Aguirre, D.; Raymond, E. mTOR-targeted therapy of cancer with rapamycin derivatives. *Ann. Oncol.*, **2005**, *16*(4), 525-537. <http://dx.doi.org/10.1093/annonc/mdi113> PMID: 15728109
- [174] Brockmann, M.; Poon, E.; Berry, T.; Carstensen, A.; Deubzer, H.E.; Rycak, L.; Jamin, Y.; Thway, K.; Robinson, S.P.; Roels, F.; Witt, O.; Fischer, M.; Chesler, L.; Eilers, M. Small Molecule Inhibitors of Aurora-A Induce Proteasomal Degra-

- duction of N-Myc in Childhood Neuroblastoma. *Cancer Cell*, **2016**, *30*(2), 357-358.
<http://dx.doi.org/10.1016/j.ccell.2016.07.002> PMID: 27505677
- [175] Schöffski, P.; Awada, A.; Dumez, H.; Gil, T.; Bartholomeus, S.; Wolter, P.; Taton, M.; Fritsch, H.; Glomb, P.; Munzert, G. A phase I, dose-escalation study of the novel Polo-like kinase inhibitor volasertib (BI 6727) in patients with advanced solid tumours. *Eur. J. Cancer*, **2012**, *48*(2), 179-186.
<http://dx.doi.org/10.1016/j.ejca.2011.11.001> PMID: 22119200
- [176] Wang, H.; Hammoudeh, D.I.; Follis, A.V.; Reese, B.E.; Lazo, J.S.; Metallo, S.J.; Prochownik, E.V. Improved low molecular weight Myc-Max inhibitors. *Mol. Cancer Ther.*, **2007**, *6*(9), 2399-2408.
<http://dx.doi.org/10.1158/1535-7163.MCT-07-0005> PMID: 17876039
- [177] Parrales, A.; Iwakuma, T. Targeting Oncogenic Mutant p53 for Cancer Therapy. *Front. Oncol.*, **2015**, *5*, 288.
<http://dx.doi.org/10.3389/fonc.2015.00288> PMID: 26732534
- [178] Zache, N.; Lambert, J.M.R.; Rökaeus, N.; Shen, J.; Hainaut, P.; Bergman, J.; Wiman, K.G.; Bykov, V.J.N. Mutant p53 targeting by the low molecular weight compound STIMA-1. *Mol. Oncol.*, **2008**, *2*(1), 70-80.
<http://dx.doi.org/10.1016/j.molonc.2008.02.004> PMID: 19383329
- [179] Lambert, J.M.R.; Gorzov, P.; Veprintsev, D.B.; Söderqvist, M.; Segerbäck, D.; Bergman, J.; Fersht, A.R.; Hainaut, P.; Wiman, K.G.; Bykov, V.J.N. PRIMA-1 reactivates mutant p53 by covalent binding to the core domain. *Cancer Cell*, **2009**, *15*(5), 376-388.
<http://dx.doi.org/10.1016/j.ccr.2009.03.003> PMID: 19411067
- [180] Bykov, V.J.N.; Issaeva, N.; Zache, N.; Shilov, A.; Hultcrantz, M.; Bergman, J.; Selivanova, G.; Wiman, K.G. Reactivation of mutant p53 and induction of apoptosis in human tumor cells by maleimide analogs. *J. Biol. Chem.*, **2005**, *280*(34), 30384-30391.
<http://dx.doi.org/10.1074/jbc.M501664200> PMID: 15998635
- [181] Yan, W.; Jung, Y-S.; Zhang, Y.; Chen, X. Arsenic trioxide reactivates proteasome-dependent degradation of mutant p53 protein in cancer cells in part via enhanced expression of Pirh2 E3 ligase. *PLoS One*, **2014**, *9*(8)e103497
<http://dx.doi.org/10.1371/journal.pone.0103497> PMID: 25116336
- [182] Paranjpe, A.; Srivenugopal, K.S. Degradation of NF-κB, p53 and other regulatory redox-sensitive proteins by thiol-conjugating and -nitrosylating drugs in human tumor cells. *Carcinogenesis*, **2013**, *34*(5), 990-1000.
<http://dx.doi.org/10.1093/carcin/bgt032> PMID: 23354308

DISCLAIMER: The above article has been published in Epub (ahead of print) on the basis of the materials provided by the author. The Editorial Department reserves the right to make minor modifications for further improvement of the manuscript.



MS. BRUNA MARTINS DE FRANÇA (Orcid ID : 0000-0003-3754-0679)

DR. MARIA BERNADETE RIEMMA PIERRE (Orcid ID : 0000-0002-7893-3172)

Article type : Research Article

***In vitro* Studies of Antitumor Effect, Toxicity/Cytotoxicity and Skin Permeation/Retention of a Green Fluorescence Pyrene-based Dye for PDT Application**

Bruna M. de França*¹, Zeinab Ghasemishahrestani¹, Gabriel F. M. de Souza¹, Renata N. da Silva¹, Daniela D. Queiroz¹, Maria Bernadete R. Pierre², Marcos D. Pereira¹, Josué S. B. Forero¹, Rodrigo J. Corrêa¹.

¹Instituto de Química, Universidade Federal do Rio de Janeiro, Rio de Janeiro - RJ, Brazil.

²Faculdade de Farmácia, Universidade Federal do Rio de Janeiro, Rio de Janeiro - RJ, Brazil.

*Corresponding author e-mail: brunamartins.franca@gmail.com (Bruna M.de França)

This article has been accepted for publication and undergone full peer review but has not been through the copyediting, typesetting, pagination and proofreading process, which may lead to differences between this version and the [Version of Record](#). Please cite this article as [doi: 10.1111/PHP.13335](https://doi.org/10.1111/PHP.13335)

This article is protected by copyright. All rights reserved

ABSTRACT

Photosensitizers (PS) are compounds that can generate reactive oxygen species under irradiation of appropriate light and are widely used in photodynamic therapy (PDT). Currently, topical PDT is an effective treatment for several skin diseases, including bacterial infections, fungal mycoses and psoriasis. In addition, PDT is also used to treat non-melanoma skin cancer and can be a potential tool for melanoma, associated with other treatments. In this work, we evaluated the antitumor photoactivity of a new pyrene-based PS (TPPy) by using the murine melanoma cell line (B16F10). The *in vitro* permeation/retention tests in porcine ear skin were also performed in order to evaluate the potential application of the PS for topical use in skin cancer. Moreover, to determine the toxicity *in vivo*, we used the *Galleria mellonella* as an alternative animal model of study. The results showed that TPPy is a promising PS for application in PDT, with potential antitumor photoactivity (IC_{50} $6.5 \mu\text{mol L}^{-1}$), absence of toxicity in the *G. mellonella* model at higher concentration (70.0 mmol L^{-1}) and the accumulation tendency in the Epidermis plus Dermis sites ($165.20 \pm 4.12 \text{ ng/cm}^2$).

INTRODUCTION

Photodynamic therapy (PDT) is a treatment capable of inducing cell and tissue death by oxidative stress through activation of a nontoxic photosensitizer (PS) by absorption of a specific visible wavelength for the reactive oxygen species (ROS) production (1) (2). An important advantage of PDT as a treatment modality is its dual selectivity towards lesions vs normal tissues, which is achieved by preferential uptake of the photosensitizer for diseased cells and the light selective application (3). Currently, topical PDT is an effective treatment for several skin diseases, including bacterial infections (4), fungal mycoses (5) and psoriasis (6). In addition, PDT is also used to treat non-melanoma skin cancer and can be a potential tool for cutaneous metastatic melanomas with stage III/IV (7), associated with other treatments (8) (9). Despite the advances in clinical research, treatment options for malignant melanoma have been limited. Melanoma is characterized by its high metastatic potential and strong resistance to clinical therapies available (10). The tumor excision is the most common way to remove melanoma but adjuvant treatments as immunotherapy (11), gene therapy (12), chemotherapy (13), and radiotherapy (14) have been used although do not always provide significant and effective results.

The PDT has been explored for cutaneous metastatic melanomas treatment because of its noninvasiveness, fewer side effects, negligible drug resistance, and low systemic toxicity (15) (16). Traditional red or blue light source has been widely used to activate the photosensitizer for skin cancer therapy (14). Several studies have shown that PDT can be promising for melanoma treatment (10). MONGE-FUENTES et al. (2017) have used Acai oil in nanoemulsion as a novel PS in melanoma cell lines and *in vivo* experimental models. The results exhibited 85% of melanoma cell death, maintaining viability in normal cells (17). SPARSA et al. (2013) investigated the effect of 5-ALA toward amelanotic (B16G4F) and melanotic (B16F10) cells after light activation. The study showed that PDT induced cell death pathway was linked with melanin synthesis ability in melanoma cells (18). ONO et al. (2018) evaluated the PDT effect of the PS Photodithazine (a glucosamine salt of chlorine e6) in a murine melanoma cell line (B16F10) and the results showed a reduction of over 90% in the cell viability at low levels of Photodithazine (19).

The result of the PDT is dependent on the photophysical properties of the photosensitizer, as well as its uptake for the skin the precise subcellular site where this event occurs (20) and preferentially should

be taken up and/or retained by neoplastic tissues (21). A photosensitizer should ideally be a single pure compound, have good stability and low manufacturing costs (22). Moreover, the PS must have a substantial triplet quantum yield leading to a great production of ROS upon irradiation with a specific wavelength. The quantum yield of photosensitized singlet oxygen production (Φ_{Δ}) is a parameter of major importance for the optimized development of applications that uses singlet oxygen (23). It is also necessary that the PS shows no dark toxicity and rapid clearance from normal tissues, decreasing the side effects of phototoxicity (24).

In this way, the choice of a PS for application in PDT involves the evaluation of parameters like the singlet oxygen generation quantum yield, light absorption spectrum (λ_{\max}), chemical stability, toxicity in the dark, lipophilicity and *in vitro* skin retention studies (22). Such criteria can be achieved by aromatic compounds like porphyrins, which are the current choice for PDT (25) (26). Nevertheless, even porphyrins are not a perfect PDT candidate due to the photodegradation process *in vivo* (27). So, in this work, we show a recently synthesized green fluorescent pyrene-based photosensitizer, the TPPy (Fig. 1) (28), which encompasses all the above mentioned characteristics. For evaluated the application of the TPPy in PDT, we studied the antitumor photoactivity by using the murine melanoma cell line (B16F10) as a model for *in vitro* PDT. Moreover, to determine the TPPy toxicity, we used the *Galleria mellonella* as an alternative animal model of study and the *in vitro* permeation/retention skin tests were also performed as a well-established protocol in order to evaluate the potential application of the PS for topical use in skin cancer (29) (30) (31) (32).

<Figure 1>

MATERIALS AND METHODS

Chemicals. 4-(3,6,8-tris(phenylethynyl)pyren-1-yl)butanoic acid (TPPy) ($C_{44}H_{28}O_2$, M.W: 588.69; ~95%) was previously synthesized by our research group (28). 1-pyrenebutyric acid ($C_{20}H_{16}O_2$, M.W: 288.34; ~97%) phosphate buffered saline tablet and Triton™ X-100 purchased from Sigma Aldrich®. Anhydrous dimethyl sulfoxide (DMSO) was obtained from Tedia®. Polyethylene glycol 400 (PEG-400) was purchased from Vetec®. All other reagents were of analytical grade and they were used without further purification.

Equipment. *In vitro* cutaneous permeation and retention of TPPy through/on the skin were carried out using a natural membrane, porcine ear skin, in Franz diffusion cells. For extraction method of TPPy from porcine skin samples, the ultrasonic bath (Q-335D; Quimis) (40 kHz, continuous mode) and the Ultra-Turrax® homogenizer (T25 digital; IKA®, Yamato Koriyama Shi, Nara, Japan) were used. Fluorometric quantification of TPPy was performed using steady-state/time-resolved spectrofluorometer Edinburgh

Instruments FS/FL900 (λ_{exc} : 335 nm; λ_{em} : 465/495 nm). TPPy was quantified by using a calibration curve in PBS 0.1 mol L⁻¹ + Triton X-100 1% (w/v) or the PEG-400 and DMSO solvents.

Statistical analysis. For the *in vitro* skin retention studies, the results were expressed as mean \pm SD and were analyzed statistically (GraphPad Prism 5.0) using the parametric unpaired two-tailed Student's t-test to compare two experimental groups. One-way ANOVA (Tukey's multiple comparison test) was used to compare three or more groups for *in vitro* skin retention studies. The level of significance was set at $p < 0.05$. For the PDT studies using murine melanoma cell line (B16F10) as a model, the results were analyzed using GraphPad Prism 7.0 by two-way ANOVA/Tukey. The level of significance was set at $p < 0.0001$. The IC₅₀ values were calculated using the "dose-response curves – inhibition" equation and "log (inhibitor) vs. normalized response – variable slope" with the aid of GraphPad Prism 7.0 software. *Galleria mellonella* survival curves were analyzed by GraphPad Prism 7.0, which uses Kaplan-Meier survival curves (and also compares survival with the log-rank and Gehan-Wilcoxon tests) (33).

Studies of TPPy aggregation behavior and solubility. The TPPy solubility studies in different media (receptor solution or solvents DMSO and PEG-400) were required for TPPy solubilization in the *in vitro* permeation assay and TPPy extraction in porcine skin for cutaneous retention evaluation, respectively. PEG-400 and DMSO were chosen because these reagents have low toxicity and are already used in pharmaceutical formulations. The equipment used in the *in vitro* permeation studies uses a donor compartment (for laying the skin sample and drug) and a receptor compartment, generally containing an aqueous solution or receptor phase (phosphate buffer solution, PBS) that simulates the bloodstream, thus the PS must be completely solubilized in the receptor phase. However, for actives very lipophilic, a surfactant is added to PBS to enhance the solubilization process. The non-ionic surfactant Triton X-100 was added at different concentrations in the PBS solution (0.25%, 0.5% and 1.0% w/v), without altering the photochemical properties of the PS and an excessive amount of the TPPy (60 $\mu\text{g mL}^{-1}$) was added in the PBS solution. The maximum solubility of TPPy was determined ($n = 3$) in the receptor phase (PBS + Triton-X 1.0% w/v) and the pure solvents DMSO and PEG-400, after keeping this overnight under constant stirring. Subsequently, the samples were centrifuged for 10 minutes and filtrated, and the TPPy was determined spectrophotometrically in the filtrate by using an integrated spectrum area.

The extraction method of TPPy from porcine ear skin samples

Preparation of porcine ear skin samples. The *in vitro* cutaneous permeability (permeation and retention studies) of TPPy was assessed using an *in vitro* model of porcine ear skin. Full-thickness skins from porcine ears used for *in vitro* cutaneous permeability studies were obtained from a local slaughterhouse. Dorsal skin was removed from the underlying cartilage with a scalpel (hairs were not removed), wrapped in aluminum foil and stored at -20°C for a maximum of 4 weeks before use (34).

Determination of % TPPy recovery and extraction method from skin samples in stratum corneum (SC) and Epidermis plus Dermis [EP+D]. The percentage of TPPY recovery aims to evaluate the efficiency of the PS extraction method (both SC and [EP+D]). This extraction method will be used later in the *in vitro* skin retention studies of PS. The absolute recovery of TPPy from skin tissue was determined for three concentrations (2.0, 3.0, and 4.0 $\mu\text{g mL}^{-1}$). This was performed by spiking samples of adhesive tape (15 pieces) containing stratum corneum (SC), subjected to tape-stripping (35). The remaining skin sections (1.77 cm^2), referring to the epidermis (EP) plus dermis (D) tissue, were added to aliquots of appropriate volumes of TPPy stock solution in PEG-400 (46.00 $\mu\text{g mL}^{-1}$), consequently producing final concentrations of 2.0, 3.0 and 4.0 $\mu\text{g mL}^{-1}$ after the extraction procedure. The spiked skin samples ($n = 3$), SC, and [EP+D], were allowed to rest for 30 minutes before TPPy extraction. The TPPy extraction from the adhesive tapes of TPPy from SC samples was done as follows: 4.0 mL of PBS 0.1 mol L^{-1} plus Triton X-100 1% (w/v) was added, stirred in the mixer for 2 minutes and sonicated in an ultrasonic bath for 30 minutes to break the cells and release the TPPy. After SC removal from the skin sections, the [EP+D] samples were cut into small pieces, before being immersed in 4.0 mL PBS containing Triton X-100 1% (w/v) and submitted to homogenization in the Ultra-Turrax® homogenizer for 1 min after vortex stirring and before bath sonication. For both samples from SC and [EP+D] after bath sonication, filtration was carried out in qualitative filter paper and the filtrate was centrifuged for 15 minutes at 3000 rpm. The TPPy was then quantified after filtration of supernatant through 0.2 μm pore membranes (Millipore®) by spectrofluorometric assay using a standard curve. The % of TPPy recovered from SC and [EP+D] samples after extraction was calculated as following: $\% \text{ recovered} = \text{TPPy extracted } (\mu\text{g mL}^{-1}) / \text{TPPy added } (\mu\text{g mL}^{-1}) \times 100$.

In vitro skin permeation/retention studies

In vitro studies of TPPy permeability in the skin (permeation and retention) were carried out using porcine ear skin as an animal model in the Franz diffusion cell and receptor phase as PBS (0.1 mol L^{-1} , pH 7.2) containing the non-ionic surfactant Triton X-100 (1% w/v). The solubility of TPPy in this receptor phase was found as $146.3 \pm 1.18 \mu\text{g mL}^{-1}$. The skin samples were mounted on the modified Franz diffusion cell (diffusion area of 1.77 cm^2) with the dermis side in contact with the receptor compartment, filled with 50 mL receptor phase ($37 \pm 1^\circ\text{C}$), to maintain the sink conditions, and stirred using magnetic stirring bars (300 rpm). An aliquot of 300.0 μL of TPPy in PEG-400 as the vehicle ($46.00 \pm 1.49 \mu\text{g mL}^{-1}$) was added on the surface of the porcine skin samples.

TPPY permeation through the skin: At appropriate time intervals (2, 4, 8, and 24 h), aliquots (3.0 mL) were collected from the receptor phase and an equal volume of the liquid was replaced immediately. The samples were then assayed by fluorescence spectroscopic technique ($n = 3$).

TPPy retention in the SC: At the end of the *in vitro* permeation experiment, SC in the area of skin exposed to diffusion (1.77 cm²) was isolated using adhesive tape straps (Scotch Book Tape, 3M, St. Paul, MN; n = 14) and collected in test tubes, where TPPy was extracted from the material according to the method described before for the TPPy extraction in the SC skin layer.

TPPy retention in the [EP+D]: After the removal of the SC as described above, the remaining area of skin [EP+D] was cut in pieces and TPPy was extracted from skin samples according to the method described before for the TPPy extraction in the [EP+D] skin layer. The samples from SC and [EP+D] were quantified by fluorescence spectroscopic technique. The results were expressed as the amount of TPPy retained in the SC and [EP+D]/area of exposure (ng/cm²).

In vitro photodynamic therapy (PDT). Photodynamic therapy assay was carried out *in vitro* by submitting the murine melanoma cell line, B16F10, maintained in DMEM (Dulbecco's modified Eagle's medium; Invitrogen, São Paulo, SP, Brazil) supplemented with 10% (v/v) FBS (fetal bovine serum; Invitrogen) and L-glutamine, to blue light irradiation of 1h delivered by LED strip (12,3 W), λ_{max} 450-470 nm, 300 J/cm² and power density of 84 mW/cm². This LED strip was adapted around the 96-well plates to guarantee irradiation on the entire sample, minimizing light loss by scattering and inner filter effect. The photosensitizer TPPy did not show photobleaching during the irradiation time that was used in this work (See Supporting Information, Figure S1). Before PDT, cells (1.25×10^4 cells/mL) seeded in 96-well microplates were incubated at 37°C in a 5% CO₂ in DEMEM up to 24h. Then, adherent cells were washed and directly subjected to PDT in the presence and absence of increasing concentrations (0.1 to 35.0 $\mu\text{mol L}^{-1}$) of 1-pyrenebutyric acid (PBA, the precursor of the TPPy) and 4-(3, 6, 8-(tris phenylethynyl)pyren-1-yl)butanoic acid (TPPy). In order to evaluate the effect of irradiation, non-treated cells growing in DEMEM during 24h were irradiated and used as control (See Supporting Information, Figure S2). The toxicity of PBA and TPPy were also evaluated in cells maintained in the dark, not submitted to PDT. Cells submitted or not to PDT were incubated at 37°C in a 5% CO₂ for cell recovery up to 24h. The MTT assay [3-(4,5-dimethylthiazol-2-yl)-2,5-diphenyltetrazolium bromide] was used to evaluate the cytotoxic effects of PBA and TPPy under PDT condition (36).

Toxicity of TPPy in a Galleria mellonella model of study. Larvae of *Galleria mellonella* were obtained after the oviposition of the great wax moths and maintained in the dark at 21°C with artificial diet (200 g wheat flour, 200 g wheat bran, 200 g wheat germ, 120 g beer yeast, 120 g honey, 120 g brown sugar, 400 g milk powder and 120 g glycerol) and relative humidity 70% \pm 10% in an incubator without photoperiod. The maintenance of larvae was done periodically, in which all animals were removed from the old feed and placed into a clean recipient with fresh feed. Experiments were carried out by using selected larvae of *G. mellonella* from the last instar with similar size (15–20 mm), weight (approximately 200 mg), and absence

of grey pigmentation. Ten larvae were used for TPPy treatment, which 10 μL of TPPy in PBS 0.1 mol L^{-1} + Triton X-100 1% (w/v) solution at three different concentrations (7.0, 35.0, and 70.0 mmol L^{-1}) was administered by injection (25 μL Hamilton syringe) into *G. mellonella* hemocoel, via the last left pro-leg. As a control for physical injury, a group of ten larvae was injected with water (10 μL). After injection, larvae were maintained in the dark, in 90-mm glass dishes, without an artificial diet, at 28°C. The survival rate was followed daily and the larvae of *G. mellonella* were considered dead when no reaction to touch was observed. Survival curves and statistics were designed using GraphPad Prism 7.0 software. The larvae were obtained at the Laboratory of Cytotoxicity and Genotoxicity (LCG) from the Biochemistry Department, Chemistry Institute of the Federal University of Rio de Janeiro, Rio de Janeiro, Brazil.

RESULTS

TPPy solubility in receptor phase (PBS + 1% Triton X-100), PEG-400 and DMSO

TPPy solution in DMSO, Fig. 2, shows a Fluorescence emission spectrum with three emission bands centered at 467, 497, and 530 nm. This spectrum was obtained by setting the solution absorption 0.2 at 420 nm, to avoid the dye aggregation and inner filter effects. The solubility in this solvent was evaluated as $6.29 \pm 1.19 \mu\text{g mL}^{-1}$ (Table 1). When TPPy was solubilized in PBS, the emission spectrum was redshifted by 80 nm; in addition, a loss of resolution in the bands was observed. The second and the third bands are grouped in one large band centered at 566 nm. This large bathochromic shift in the fluorescence emission spectrum can be assumed as a result of TPPy aggregation in PBS (Fig. 2, dashed line). Nonetheless, as it can be seen, TPPy aggregation was eliminated after adding 1% (v/v) of Triton X-100 and the emission maxima are just 2 nm red-shifted concerning the DMSO solution. The maximum solubility of TPPy in this PBS/1% Triton X-100 (receptor phase) was found as $146.3 \pm 1.18 \mu\text{g mL}^{-1}$ (Table 1).

<Figure 2>

TPPy solubility in the solvents PEG-400 and DMSO were evaluated for *in vitro* permeability studies and the values of $46.00 \pm 1.49 \mu\text{g mL}^{-1}$ and $6.29 \pm 1.19 \mu\text{g mL}^{-1}$, were found, respectively (Table 1). DMSO has been used in similar tests, but since the solubility obtained was low compared to PBS 0.1 mol L^{-1} + Triton X-100 1% (w/v) as found the value of 146.30 ± 1.18 , this medium was selected as an extraction solvent for TPPy in the skin retention studies.

<Table 1>

TPPy recovery from porcine skin samples in SC and [EP+D] layers

Table 2 shows the results of TPPy recovery, extracted from the skin samples SC and [EP+D] after extraction with PBS containing Triton-X 100. The recovery of TPPy from SC and [EP+D] layers was respectively above 75.0% and 90.0% of the spiked dose (n = 3) using different concentrations (2.0, 3.0, and 4.0 $\mu\text{g mL}^{-1}$).

<Table 2>

***In vitro* skin permeation/retention studies**

After 24h of the post-application of TPPy, $63.96 \pm 2.27 \text{ ng/cm}^2$ (n = 3) of the dye was detected in the SC and $165.20 \pm 4.12 \text{ ng/cm}^2$ in the [EP+D] (Fig. 3). TPPy was not detected in the samples of receptor solution (PBS 0.1 mol L^{-1} + Triton X-100 1%, w/v).

<Figure 3>

The effect of PDT on the melanoma model of study

The phototoxicity of PBA (precursor) and TPPy were evaluated with murine melanoma cell line B16F10, which is used as a mouse model for human melanoma studies (37). In this study, PDT was performed in the presence or absence of PBA and TPPy (up to $35 \mu\text{g mL}^{-1}$). Exposure of cells to PDT in the presence of TPPy promoted an increase of susceptibility of B16F10 cells (Fig. 4). In this context, from a non-linear regression of survival curves, we obtained the IC_{50} values of PBA and TPPy under PDT and non-PDT conditions. The survival curve of B16F10 cells submitted to PDT in the absence of PBA and TPPy can be observed in Supporting Information (Figure S2). Thus, B16F10 treated with PBA in the absence and the presence of photoactivation showed an IC_{50} of $22.11 \pm 1.55 \mu\text{mol L}^{-1}$ and $14.30 \pm 2.34 \mu\text{mol L}^{-1}$ (Table 3), respectively. On the other hand, the cytotoxicity/phototoxicity of TPPy under non-PDT and PDT conditions presented an IC_{50} of $11.50 \pm 0.54 \mu\text{mol L}^{-1}$ and $6.5 \pm 0.68 \mu\text{mol L}^{-1}$, respectively (Table 3).

<Figure 4>

<Table 3>

Toxicity of TPPy in a *Galleria mellonella* model

The toxicity was carried out by TPPy in PBS 0.1 mol L^{-1} + Triton X-100 1% (w/v) solution at three different concentrations (7.0, 35.0, and 70.0 mmol L^{-1}). It is important to highlight that we started testing TPPy toxicity in *G. mellonella* using high concentrations. After injection, larvae survival was appraised up to 7 days in the dark. According to Figs. 5A and B, TPPy displayed weak toxicity in *G. mellonella* larvae. Analyzing a representative survival curve of *G. mellonella* larvae submitted to TPPy, it seems that only at the higher TPPy concentration (70.0 mmol L^{-1}) was possible to observe a slight decrease in the larvae survival curve (Fig. 5A). However, statistical analysis demonstrated that the reduction of the percentage of larvae survival was not statistically different in comparison to control groups (Fig. 5B). Regarding the lower concentrations, we observed an overlap of the TPPy curves with the control curves indicating that this photosensitizer in the non-PDT condition is not toxic for the *G. mellonella* experimental model (Fig. 5A and B).

DISCUSSION

The TPPy molecules aggregation in PBS solution occurs due to the low solubility of this PS (high lipophilicity, $\text{miLog } P = 8.79$) and this is the cause of the bathochromic shift of the maximum emission wavelength (~ 530 nm), Fig. 2. In fact, in a previous paper, we reported the excimer formation of TPPy in high concentrations (10^{-4} mol L^{-1} in THF) as a broad shoulder at 530 nm in conjunction with the monomer fluorescence at 490 nm (28). As can be seen in Fig. 2 the excimer can also be observed for TPPy in PBS as broadband at *c.a.* 530 nm. So, the non-ionic surfactant Triton X-100 was added to the medium in order to prevent excimer formation by trapping PS into micelles (38). The maximum solubility obtained of the receptor solution (PBS 0.1 mol L^{-1} + Triton X-100 1% w/v) was 146.30 ± 1.18 $\mu\text{g mL}^{-1}$, which is considered a satisfactory value for utilization as receptor solution to TPPy.

The solvent PEG-400 was tested as a vehicle, because this solvent is used in many *in vitro* skin permeation/retention studies, due to its low toxicity for biological applications (34) (39) (40). In the present work, the maximum solubility value obtained for TPPy in PEG-400 was 46.00 ± 1.49 $\mu\text{g mL}^{-1}$. This value is considered adequate for the use of PEG-400 as a vehicle for TPPy in the permeation/retention skin assay since primary studies obtained similar solubility for other drugs in this vehicle (41) (42).

No studies describing the recovery of TPPy (unpublished molecule) from skin samples were found in the literature. DMSO was tested as an extractor solvent to extract TPPy from porcine skin samples. However, in the solubility tests, the maximum solubility value obtained for TPPy in DMSO was low (6.29 ± 1.19 $\mu\text{g mL}^{-1}$). Therefore, this solvent was discarded as an extractor.

After extraction with receptor solution (PBS 0.1 mol L^{-1} + Triton X-100 1% w/v), the TPPy recovery percentage obtained for SC was around 73 to 86% and for [EP+D] around 84-96%. This limit is in excellent agreement with several studies focused on determining the drug recovery of the skin porcine were obtained different results varying from 82 to 90%. For example, AYUB; VIANNA-SOARES; FERREIRA (2007) found an average fluconazole recovery close to 82.0% by using the RP-HPLC method (42) and SANTOYO; JALO (2002) using the same test reached up to 94.0% recovery for cidofovir, by HPLC method (43). For the fluorimetric method, ROSSETTI et al. (2010) demonstrated a 90% recovery for PpIX (38).

At the *in vitro* permeation study, no TPPy was permeated through the porcine skin, which was observed by the absence of TPPy in receptor solution. This is probably because the PS is very lipophilic ($\text{Log } P_{\text{TPPy}} = 8.79$) and does not permeate through the skin without a proper delivery system. However, for

the application of PDT in skin cancer, the PS retention observed in the [EP+D] can be sufficient for its action. The TPPy retention profile demonstrates that this PS was less retained in the SC layer and accumulates in the [EP+D] layers, site of action of interest for PDT of cutaneous tumors. Although it is considered as an inert vehicle in topical formulations, an enhancing influence of PEG-400 was recently attributed to the physical alteration of stratum corneum lipids, beyond that the conformational and structural modifications of membrane proteins (44).

At *in vitro* [EP+D] retention studies specifically, it was observed that the amount of TPPy retained in the porcine skin increases with time (4–24 h). At 24h post-application of TPPy, 63.96 ± 2.27 ng/cm² (n = 3) of TPPy was detected in the SC, and more than the double was detected in [EP+D], 165.20 ± 4.12 ng/cm² (n = 3) (**p < 0.0005). These values may be considered high for a highly lipophilic PS as TPPy. SILVA et al. (2013) compared the skin permeation/retention of the control solution of PpIX in PEG-300 and the PpIX encapsulated in (PLGA)-based nanoparticles. PpIX is very lipophilic but possesses the smaller value of log P than TPPy (Log P_{PpIX} = 7.662 and Log P_{TPPy} = 8.79). In general, retention/accumulation of PpIX from NPs was higher in the SC layer compared to [EP + D]. For PpIX in PEG-300 solution (control), it was obtained for SC and [EP+D] retention values less than 100 ng/cm². For the encapsulated PpIX, the retention in SC was 23 times higher and in [EP+D] and 10 times higher compared to control (34). For PpIX recovery assay in porcine skin, ROSSETTI et al. (2010) obtained at 12h post-application, 130.00 ± 0.01 ng/cm² (n = 5) of PpIX detected in the SC, and 16.00 ± 0.002 ng/cm² in the [EP+D]. Furthermore, similar to our results, the PS was not detected in the samples of the receptor medium (phosphate buffer pH 7.2 + CCP) (38). PIERRE et al. (2006) proposed the use of oleic acid (OA) as a skin penetration enhancer, to optimize the permeation skin of the 5-aminolevulinic acid (5-ALA), a protoporphyrin IX (PpIX) precursor approved for PDT use for cutaneous nonmalignant tumors. The *in vitro* permeation/retention studies in porcine ear skin as a model have shown that the formulations (in propylene glycol) containing 10% OA increased the accumulation of PpIX in the skin. The amounts of 5-ALA retained in [E+D] was significantly increased (~ 4 µg/cm²) compared to the values for the controls (~ 2 µg/cm²), while the amount of 5-ALA retained in the SC was similar for both (~ 0.8 µg/cm²) (45).

PBA (1-Pyrenebutyric acid) is the precursor reagent of the TPPy molecule (4-(3,6,8-tris(phenylethynyl)pyren-1-yl) butanoic acid), synthesized by our group in order to shift the maximum absorption peak to the visible region of the electromagnetic spectrum. The maximum absorption peaks of PBA in the UV region (278 and 346 nm, in DMSO), makes it difficult to use in PDT (28). After the structural modification of the molecule, the TPPy was obtained and a redshift of the maximum absorption peaks to the visible region spectrum (335 and 451 nm, in DMSO) was observed, thus favoring the use of

visible light for PDT tests. Furthermore, the PBA molecule structural modification improves the singlet oxygen generation ($\Phi_{\Delta\text{TPPy}} = 0.40$ in CCl_4) (28) that can be observed in PDT cell line tests.

The cells B16F10 were treated with PBA and TPPy and the half-maximal inhibitory concentration (IC_{50}) values were obtained. The TPPy in the dark (IC_{50} of $11.50 \pm 0.54 \mu\text{mol L}^{-1}$) is more cytotoxic than the precursor PBA (IC_{50} of $22.11 \pm 1.55 \mu\text{mol L}^{-1}$) and similar behavior is observed in the presence of light, when TPPy shows IC_{50} of $6.5 \pm 0.68 \mu\text{mol L}^{-1}$ and PBA shows an IC_{50} of $14.30 \pm 2.34 \mu\text{mol L}^{-1}$. MITRA et al. (2014) used a series of Ferrocenyl-terpyridine platinum(II) PS complexes for evaluating the PDT cytotoxicity in HaCaT cells. They obtained IC_{50} $1.6 \pm 0.2 \mu\text{mol L}^{-1}$ to $17.6 \pm 0.1 \mu\text{mol L}^{-1}$ in light and $4.8 \pm 0.6 \mu\text{mol L}^{-1}$ to $84.9 \pm 0.1 \mu\text{mol L}^{-1}$ in the dark. The highest cytotoxicity in the dark ($\text{IC}_{50} = 4.8 \pm 0.6 \mu\text{mol L}^{-1}$) is comparable to that of cisplatin, ($\text{IC}_{50} = 3.2 \mu\text{mol L}^{-1}$), used to treat traditional cancer (46). KIM; MORRISON; MOHAMMED (2011) examined the phototoxic effect of cis-Dichlorobis (3,4,7,8-tetramethyl-1,10-phenanthroline) rhodium (III) chloride (OCTBP) on malignant melanoma cells. The OCTBP ($100 \mu\text{mol L}^{-1}$) activated with light resulted in 40% melanoma cell growth inhibition (47). SHIE YIN NG et al. (2020) evaluated the *in vitro* PDT activity of two aza-BODIPYs derivatives (IK-IK-I2-aza-BODIPY and KI-KI-I2-azaBODIPY) in B16F10 murine skin melanoma and SKMEL28 human melanoma. The results revealed that these aza-BODIPYs derivatives are promising photosensitizers with enhanced singlet oxygen generation. They obtained for the PS IK-IK-I2-aza-BODIPY IC_{50} $4.00 \pm 0.33 \mu\text{mol L}^{-1}$ (B16F10 cells) and $5.00 \pm 0.13 \mu\text{mol L}^{-1}$ (SKMEL28 cells). For the PS KI-KI-I2-azaBODIPY, they obtained IC_{50} $0.74 \pm 0.06 \mu\text{mol L}^{-1}$ (B16F10 cells) and $5.00 \pm 0.13 \mu\text{mol L}^{-1}$ (SKMEL28 cells) (48).

The light source fluence is determined to increase cancer cell growth inhibition. In our study, it was used as a light dose of 300 J/cm^2 for the satisfactory results obtained, because the LED strip used in the photoreactor possesses a low power. CHANG et al. (2018) demonstrated the therapeutic efficiency of the two photosensitizers, MPPa and NMPi; in A549 tumor-bearing mice they evaluated the use of laser irradiations (630 nm) with an output power of 400 mW/cm^2 and light dose at 200 J/cm^2 . The results suggest that large-size tumors need both higher drug and light doses to allow complete tumor eradication (49). NIKITINA et al. (2011), used boronated chlorin as an effective photosensitizer for PDT of tumor models M-1 sarcoma and B-16 melanoma. They also used a light dose of 150 and 300 J/cm^2 , with a power density of 0.25 and 0.42 W/cm^2 . The complete tumor regression was achieved with light dose at 300 J/cm^2 (50).

In vivo studies using invertebrate models are important tools that have been widely used and have become a very promising alternative for toxicity assays (51). Many authors have used the invertebrate larvae model *Galleria mellonella* in order to provide preliminary evidence about the toxicity of different classes of photosensitizers, such as phenothiazinium dyes (52), porphyrin derivatives (53) and curcumin derivatives (54). In our study, the toxicity assay using the *G. mellonella* model was carried out by injecting

the photosensitizer TPPy at three different concentrations (7.0, 35.0, and 70.0 mmol L⁻¹) in PBS 0.1 mol L⁻¹ + Triton X-100 1% (w/v) solution, high above the IC₅₀ found for cell culture. Therefore, the *G. mellonella* model of study seemed to be non-affected by TPPy in the dark, showing the absence of toxicity at higher concentrations.

CONCLUSION

In general, experimental studies showed that the TPPy is a promising photosensitizer for application in photodynamic therapy. The antitumor photoactivity of TPPy was evaluated against murine melanoma cell line (B16F10) as a model of *in vitro* study, presenting a great potential (IC₅₀ 6.5 μmol L⁻¹) and the TPPy demonstrated the absence of toxicity *in vivo*, using a *Galleria mellonella* model. Finally, the *in vitro* permeation/retention assay showed the accumulation tendency of the TPPy in the Epidermis plus Dermis (165.20 ± 4.12 ng/cm²), action sites for the topical application of PDT.

Acknowledgements - The authors acknowledge CNPq and FAPERJ for the provided financial assistance.

SUPPORTING INFORMATION

Additional supporting information may be found online in the Supporting Information section at the end of the article:

Figure S1: Photobleaching of the TPPy (DMSO solution, 35 μmol L⁻¹) under irradiation with LED strip 12,3 W for 0, 30 and 60 minutes.

Figure S2. Survival curve of B16F10 cells submitted to PDT. Cells were directly exposed to PDT in the absence of PBA and TPPy. Experiments were performed as described in Materials and Methods. Data are represented as mean ± standard deviation of at least 3 independent experiments (n = 3).

REFERENCES

1. Dolmans, D., Fukumura, D. and Jain, R. (2003) Photodynamic therapy for cancer. *Nat. Rev. Cancer* **3**, 380–387.
2. Kwiatkowski, S., Knap, B., Przystupski, D., Saczko, J., Kędzierska, E., Knap-Czop, K., Kotlińska, J., Michel, O., Kotowski, K. and Kulbacka, J. (2018) Photodynamic therapy – mechanisms, photosensitizers and combinations. *Biomed. Pharmacother.* **106**, 1098–1107.
3. Kuimova, M. K. and Phillips, D. (2013) Applied photochemistry. In *Applied Photochemistry*, pp. 331–347.

4. Hamblin, M. R. (2016) Antimicrobial photodynamic inactivation: a bright new technique to kill resistant microbes. *Curr. Opin. Microbiol.* **33**, 67–73.
5. Shen, J. J., Jemec, G. B. E., Arendrup, M. C. and Saunte, D. M. L. (2020) Photodynamic therapy treatment of superficial fungal infections: A systematic review. *Photodiagnosis Photodyn. Ther.* **31**, 101774.
6. Choi, Y. M., Adelzadeh, L. and Wu, J. J. (2015) Photodynamic therapy for psoriasis. *J. Dermatolog. Treat.* **26**, 202–207.
7. Austin, E., Mamalis, A., Ho, D. and Jagdeo, J. (2017) Laser and light-based therapy for cutaneous and soft-tissue metastases of malignant melanoma: a systematic review. *Arch. Dermatol. Res.* **309**, 229–242.
8. Yanovsky, R. L., Bartenstein, D. W., Rogers, G. S., Isakoff, S. J. and Chen, S. T. (2019) Photodynamic therapy for solid tumors: A review of the literature. *Photodermatol. Photoimmunol. Photomed.* **35**, 295–303.
9. Wen, X., Li, Y. and Hamblin, M. R. (2017) Photodynamic therapy in dermatology beyond non-melanoma cancer: An update. *Photodiagnosis Photodyn. Ther.* **19**, 140–152.
10. Domingues, B., Lopes, J. M., Soares, P. and Pópulo, H. (2018) Melanoma treatment in review. *ImmunoTargets Ther.* **7**, 35–49.
11. Gasser, S., Lim, L. H. K. and Cheung, F. S. G. (2017) The role of the tumour microenvironment in immunotherapy. *Endocr. Relat. Cancer* **24**, T283–T295.
12. Simões, M. C. F., Sousa, J. J. S. and Pais, A. A. C. C. (2015) Skin cancer and new treatment perspectives: A review. *Cancer Lett.* **357**, 8–42.
13. Li, R. H., Hou, X. Y., Yang, C. S., Liu, W. Lou, Tang, J. Q., Liu, Y. Q. and Jiang, G. (2015) Temozolomide for treating malignant melanoma. *J. Coll. Physicians Surg. Pakistan* **25**, 680–688.
14. Shi, W. (2015) Role for radiation therapy in melanoma. *Surg. Oncol. Clin. N. Am.* **24**, 323–335.
15. BALDEA, I. and FILIP, A. G. (2012) Photodynamic therapy in melanoma - an update. *J. Physiol. Pharmacol.* **63**, 109–118.
16. Naidoo, C., Kruger, C. A. and Abrahamse, H. (2019) Targeted photodynamic therapy treatment of in vitro A375 metastatic melanoma cells. *Oncotarget* **10**, 6079–6095.
17. Monge-Fuentes, V., Muehlmann, L. A., Longo, J. P. F., Silva, J. R., Fascineli, M. L., Azevedo, R. B.,

- de Souza, P., Faria, F., Degterev, I. A., Rodriguez, A., Carneiro, F. P., Lucci, C. M., Escobar, P. and Amorim, R. F. B. (2017) Photodynamic therapy mediated by acai oil (*Euterpe oleracea* Martius) in nanoemulsion: A potential treatment for melanoma. *J. Photochem. Photobiol. B Biol.* **166**, 301–310.
18. Sparsa, A., Bellaton, S., Naves, T., Jauberteau, M., Bonnetblanc, J., Sol, V., Verdier, M. and Ratinaud, M. (2013) Photodynamic treatment induces cell death by apoptosis or autophagy depending on the melanin content in two B16 melanoma cell lines. *Oncol. Rep.* **29**, 1196–1200.
19. Ono, B. A., Nogueira, M., Pires, L., Pratavieira, S. and Kurachi, C. (2018) Subcellular localization and photodynamic activity of Photodithazine (glucosamine salt of chlorin e6) in murine melanoma B16-F10: an in vitro and in vivo study. In *Optical Methods for Tumor Treatment and Detection: Mechanisms and Techniques in Photodynamic Therapy XXVII* (Edited by Kessel, D. H. and Hasan, T.), p. 1047616. SPIE.
20. Laranjo, M., Serra, A. C., Abrantes, M., Piñeiro, M., Gonçalves, A. C., Casalta-Lopes, J., Carvalho, L., Sarmiento-Ribeiro, A. B., Rocha-Gonsalves, A. and Botelho, F. (2013) 2-Bromo-5-hydroxyphenylporphyrins for photodynamic therapy: Photosensitization efficiency, subcellular localization and in vivo studies. *Photodiagnosis Photodyn. Ther.* **10**, 51–61.
21. Primo, F. L., Bentley, M. V. L. B. and Tedesco, A. C. (2008) Photophysical Studies and In Vitro Skin Permeation/Retention of Foscan® /Nanoemulsion (NE) Applicable to Photodynamic Therapy Skin Cancer Treatment. *J. Nanosci. Nanotechnol.* **8**, 340–347.
22. Abrahamse, H. and Hamblin, M. R. (2016) New photosensitizers for photodynamic therapy. *Biochem. J.* **473**, 347–364.
23. Rapozzi, V. and Jori, G. (2015) Basic and clinical aspects of photodynamic therapy. In *Resistance to Photodynamic Therapy in Cancer* Vol. Vol. 5, pp. 3–26. Springer US, Rapozzi, V. & Jori, G.
24. Allison, R. R. and Sibata, C. H. (2010) Oncologic photodynamic therapy photosensitizers: A clinical review. *Photodiagnosis Photodyn. Ther.* **7**, 61–75.
25. Baldea, I., Olteanu, D. E., Bolfa, P., Tabaran, F., Ion, R. M. and Filip, G. A. (2016) Melanogenesis and DNA damage following photodynamic therapy in melanoma with two meso-substituted porphyrins. *J. Photochem. Photobiol. B Biol.* **161**, 402–410.
26. Tahmasebi, H., Khoshgard, K., Sazgarnia, A., Mostafaie, A. and Eivazi, M. T. (2016) Enhancing the efficiency of 5-aminolevulinic acid-mediated photodynamic therapy using 5-fluorouracil on human melanoma cells. *Photodiagnosis Photodyn. Ther.* **13**, 297–302.

27. Vicente, M. (2005) Porphyrin-based Sensitizers in the Detection and Treatment of Cancer: Recent Progress. *Curr. Med. Chem. Agents* **1**, 175–194.
28. de França, B. M., Bello Forero, J. S., Garden, S. J., Ribeiro, E. S., Souza, R. da S., Teixeira, R. S. and Corrêa, R. J. (2018) Green fluorescence pyrene-based dye as a new π -extended system: Synthesis, photophysical and theoretical studies. *Dye. Pigment.* **148**, 444–451.
29. De Rosa, F. S., Tedesco, A. C., Lopez, R. F. V., Pierre, M. B. R., Lange, N., Marchetti, J. M., Rotta, J. C. G. and Lopes Badra Bentley, M. V. (2003) In vitro skin permeation and retention of 5-aminolevulinic acid ester derivatives for photodynamic therapy. *J. Control. Release* **89**, 261–269.
30. Şenyiğit, T., Sonvico, F., Barbieri, S., Özer, Ö., Santi, P. and Colombo, P. (2010) Lecithin / chitosan nanoparticles of clobetasol-17-propionate capable of accumulation in pig skin. *J. Control. Release* **142**, 368–373.
31. Shah, S. N. H., Safdar, A., Riaz, R., Shahzad, Y., Rabbani, M., Karim, S. and Murtaza, G. (2013) Effect of permeation enhancers on the release behavior and permeation kinetics of novel tramadol lotions. *Trop. J. Pharm. Res.* **12**, 27–32.
32. Matos, B. N., Reis, T. A., Gratieri, T. and Gelfuso, G. M. (2015) Chitosan nanoparticles for targeting and sustaining minoxidil sulphate delivery to hair follicles. *Int. J. Biol. Macromol.* **75**, 225–229.
33. Fernandes, C. M., Fonseca, F. L., Goldman, G. H. and Pereira, M. D. (2017) A Reliable Assay to Evaluate the Virulence of *Aspergillus nidulans* Using the Alternative Animal Model *Galleria mellonella* (Lepidoptera). *bio-protocol* **7**, 1–13.
34. Silva, C. L., Ciampo, J. O. Del, Rossetti, C., Bentley, M. V. L. B. and Pierre, M. B. R. (2013) Improved In vitro and In vivo cutaneous delivery of protoporphyrin IX from PLGA-based nanoparticles. *Photochem. Photobiol.* **89**, 1176–1184.
35. Leo, M. S. and Howard I. Maibach (2014) Percutaneous Absorption. In *Topical Drug Bioavailability, Bioequivalence, and Penetration* (Edited by Shah, V. P., Maibach, Howard, I., and Jenner, J.), pp. 3–19. Springer New York, New York.
36. Denizot, F. and Lang, R. (1986) Rapid colorimetric assay for cell growth and survival. Modifications to the tetrazolium dye procedure giving improved sensitivity and reliability. *J. Immunol. Methods* **89**, 271–277.
37. Overwijk, W. W. and Restifo, N. P. (2000) B16 as a mouse model for human melanoma. *Curr. Protoc.*

Immunol. **39**, 1–29.

38. Rossetti, F. C., Depieri, L. V., Tedesco, A. C., Vitória, M. and Badra, L. (2010) Fluorometric quantification of protoporphyrin IX in biological skin samples from in vitro penetration / permeation studies. *Brazilian J. Pharm. Sci.* **46**, 753–760.
39. Kumar, S., Malick, A. W., Meltzer, N. M., Mouskountakis, J. D. and Behl, C. R. (1992) Studies of in vitro skin permeation and retention of a leukotriene antagonist from topical vehicles with a hairless guinea pig model. *J. Pharm. Sci.* **81**, 631–634.
40. Hamishehkar, H., Khoshbakht, M., Jouyban, A. and Ghanbarzadeh, S. (2015) The Relationship between Solubility and Transdermal Absorption of Tadalafil. *Adv Pharm Bull* **5**, 411–417.
41. Nada, A. H., Zaghloul, A. A., Hedaya, M. M. and KhattaB, I. S. (2014) Development of novel formulations to enhance in vivo transdermal permeation of tocopherol. *Acta Pharm.* **64**, 299–309.
42. Ayub, A. C., Vianna-soares, C. D. and Ferreira, L. A. M. (2007) Fluconazol method validation by RP-HPLC for determination in biological skin matrices. **45**, 286–290.
43. Santoyo, S., De Jalón, E. G., Campanero, M. A. and Ygartua, P. (2002) Determination of cidofovir in both skin layers and percutaneous penetration samples by HPLC. *J. Pharm. Biomed. Anal.* **29**, 819–826.
44. Anisha, A. D. and Shegokar, R. (2016) Polyethylene glycol (PEG): a versatile polymer for pharmaceutical applications. *Expert Opin. Drug Deliv.* **13**, 1257–1275.
45. Pierre, M. B. R., Ricci, E., Tedesco, A. C. and Bentley, M. V. L. B. (2006) Oleic acid as optimizer of the skin delivery of 5-aminolevulinic acid in photodynamic therapy. *Pharm. Res.* **23**, 360–366.
46. Mitra, K., Basu, U., Khan, I., Maity, B., Kondaiah, P. and Chakravarty, A. R. (2014) Remarkable anticancer activity of ferrocenyl-terpyridine platinum(ii) complexes in visible light with low dark toxicity. *Dalt. Trans.* **43**, 751–763.
47. Kim, M. R., Morrisson, H. and Mohammed, S. I. (2011) Effect of a photoactivated rhodium complex in melanoma. *Anticancer. Drugs* **22**, 896–904.
48. Ng, S. Y., Kamkaew, A., Fu, N., Kue, C. S., Chung, L. Y., Kiew, L. V., Wittayakun, J., Burgess, K. and Lee, H. B. (2020) Active targeted ligand-aza-BODIPY conjugate for near-infrared photodynamic therapy in melanoma. *Int. J. Pharm.* **579**, 119189.
49. Chang, J. E., Liu, Y., Lee, T. H., Lee, W. K., Yoon, I. and Kim, K. (2018) Tumor size-dependent

anticancer efficacy of chlorin derivatives for photodynamic therapy. *Int. J. Mol. Sci.* **19**.

50. Nikitina, R. G., Kaplan, M. A., Olshevskaya, V. A., Rodina, J. S., Drozhzhina, V. V. and Morozova, T. G. (2011) Photodynamic therapy with boronated chlorin as a photosensitizer. *J. Cancer Sci. Ther.* **3**, 216–219.

51. Freires, I. A., Sardi, J. de C. O., de Castro, R. D. and Rosalen, P. L. (2017) Alternative animal and non-animal models for drug discovery and development: bonus or burden? *Pharm. Res.* **34**, 681–686.

52. Paziani, M. H., Tonani, L., de Menezes, H. D., Bachmann, L., Wainwright, M., Braga, G. Ú. L. and von Zeska Kress, M. R. (2019) Antimicrobial photodynamic therapy with phenothiazinium photosensitizers in non-vertebrate model *Galleria mellonella* infected with *Fusarium keratoplasticum* and *Fusarium moniliforme*. *Photodiagnosis Photodyn. Ther.* **25**, 197–203.

53. Huang, X., Xu, M., Pan, W., Wang, M., Wu, X., Dai, S., Li, L. and Zeng, K. (2020) Antimicrobial and immunomodulatory responses of photodynamic therapy in *Galleria mellonella* model. *BMC Microbiol.* **20**, 4–11.

54. Sanches, C. V. G., Sardi, J. de C. O., Terada, R. S. S., Lazarini, J. G., Freires, I. A., Polaquini, C. R., Torrezan, G. S., Regasini, L. O., Fujimaki, M. and Rosalen, P. L. (2019) Diacetylcurcumin: a new photosensitizer for antimicrobial photodynamic therapy in *Streptococcus mutans* biofilms. *Biofouling* **35**, 340–349.

FIGURE CAPTIONS

Figure 1: Chemical structure of 4-(3,6,8-tris(phenylethynyl)pyren-1-yl)butanoic acid – TPPy.

Figure 2: TPPy normalized emission spectra in PBS (0.1 mol L⁻¹) before (dashed) and after (line) addition the non-ionic surfactant Triton X-100 1% (w/v) in comparison to the TPPy in DMSO solution (abs = 0.2) (red line).

Figure 3: TPPy *in vitro* retention profiles in the SC and [E+D] at 2, 4, 8 and 24 h post-application of a PS solution in PEG-400. Each value is the mean of three different experiments ± SD for each group. Statistical analysis: T-test. Values considered significant between groups SC and [EP+D] at 2h (*p < 0.05), 4 h (**p < 0.005), 8h and 24h (**p < 0.0005).

Figure 4: Survival curve of B16F10 cells submitted to PDT with PBA or TPPy. Cells were directly exposed to PDT in the presence or absence of PBA and TPPy. Experiments were performed as described in Materials and Methods. Data are represented as mean ± standard deviation of 3 independent experiments (n = 3). All statistical analyzes were carried using GraphPad Prism 7.0 by two-way ANOVA/Tukey. *indicates statistically different results at p < 0.0001 between PBA +PDT and PBA -PDT groups. #indicates statistically different results at p < 0.0001 between TPPy +PDT and TPPy -PDT.

Figure 5: Survival of *Galleria mellonella* larvae submitted to TPPy. Survival was appraised up to 7 days post-injection with TPPy in PBS 0.1 mol L⁻¹ + Triton X-100 1% (w/v) solution at 7.0, 35.0 and 70.0 mmol L⁻¹. The control groups constituted one group harboring untreated *G. mellonella* larvae and another group that was submitted to water injection. Experimental groups were composed of 10 larvae, and the experiments were carried out in triplicates. The log-rank test was used to compare the survival rates; **p < 0.01 and *p < 0.05.

Table 1. Quantification of TPPy in PEG-400, DMSO and PBS 0.1 mol L⁻¹ + Triton X-100 1% (w/v), from the addition of PS excess (600 μg) in respective solvents. Each value is the mean of three different experiments ± SD for each group.

Solvent	Concentration found (μg mL⁻¹)
PEG-400	46.00 ± 1.49
DMSO	6.29 ± 1.19
PBS 0.1 mol L ⁻¹ + Triton X-100 1% (w/v)	146.30 ± 1.18

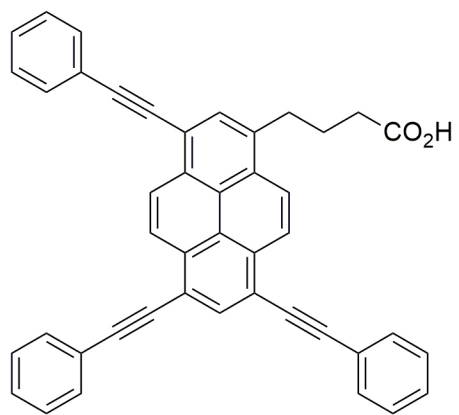
Table 2. TPPy recovery from SC and [EP+D] samples. Each value is the mean of three different experiments \pm SD for each group.

Skin layers	TPPy add ($\mu\text{g mL}^{-1}$)	TPPy extracted ($\mu\text{g mL}^{-1}$)	Recovery (%)
SC	2.0	1.50 ± 0.09	75.03 ± 4.28
	3.0	2.21 ± 0.11	73.50 ± 3.65
	4.0	3.44 ± 0.14	86.02 ± 3.58
[EP+D]	2.0	1.86 ± 0.07	93.17 ± 3.29
	3.0	2.53 ± 0.06	84.33 ± 1.91

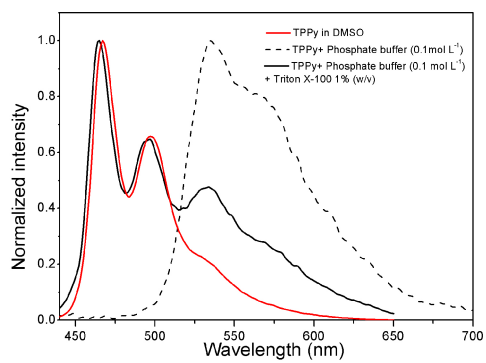
Table 3. Cytotoxicity/phototoxicity of PBA and TPPy under non-PDT and PDT conditions.

Condition	IC ₅₀ (μmol L ⁻¹)	
	PBA	TPPy
Non-PDT	22.11 ± 1.55	11.50 ^{**,*} ± 0.54
PDT	14.30 [†] ± 2.34	6.5 ^{††,*} ± 0.68

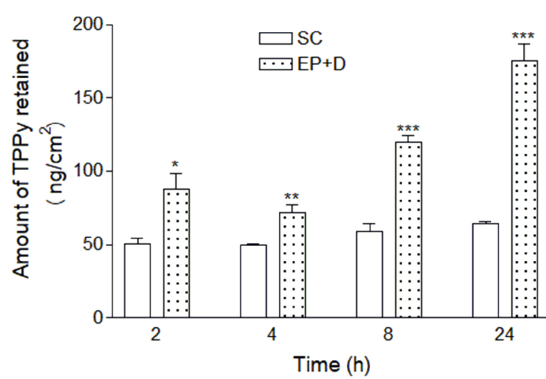
IC₅₀ values were obtained from non-linear regression of survival curves after 1h PDT condition in the presence and absence of PBA or TPPy. The statistical analyzes were carried out using GraphPad Prism 7.0 (One-way ANOVA/Tukey). [†]means different results at p < 0.0001 compared with PBA in non-PDT; ^{††}means different results at p < 0.0001 compared with PBA in PDT; * means different results at p < 0.0001 compared with PBA in PDT or non-PDT.



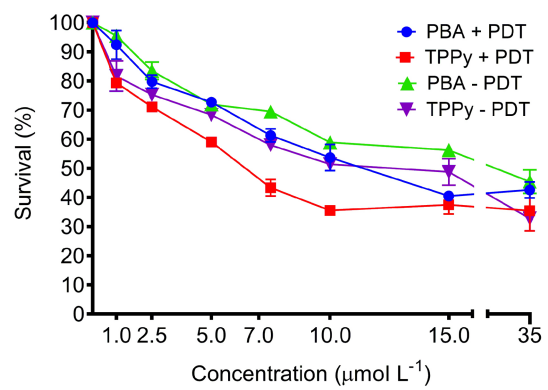
php_13335_f1.jpg



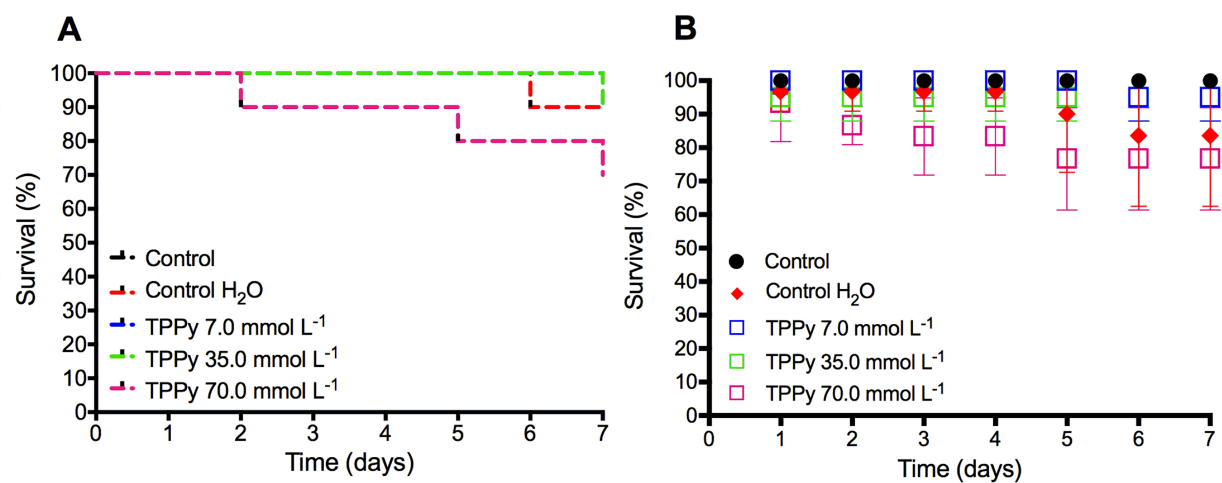
php_13335_f2.jpg



php_13335_f3.jpg



php_13335_f4.jpg



php_13335_f5.jpg